PHD THESIS

Quantum Information Processing with Quantum Optical Systems

Author:
Vincent E. ELFVING

Supervisor:
Prof. Anders S. SØRENSEN

A thesis submitted in partial fulfillment of the requirements for the degree of Doctor of Philosophy

in

Theoretical Quantum Optics

at

the Niels Bohr Institute

This thesis has been submitted to the PhD School of
the Faculty of Science, University of Copenhagen

October 1, 2018

Declaration of Authorship

I, Vincent E. ELFVING, declare that this thesis titled, "Quantum Information Processing with Quantum Optical Systems" and the work presented in it are my own. I confirm that:

- This work was done wholly or mainly while in candidature for a research degree at this University.
- Where I have consulted the published work of others, this is always clearly attributed.
- Where I have quoted from the work of others, the source is always given.
- I have acknowledged all main sources of help.
- Where the thesis is based on work done by myself jointly with others, I have made clear exactly what was done by others and what I have contributed myself.

Signed:

Date:

"*It is difficult to make predictions, especially about the future.*"

Niels Bohr

English Abstract

The topic of this thesis is quantum information processing with quantum optical devices. The development progress in this field in recent years can roughly be characterized as two-fold: experimental advances in photonics technologies have enabled the creation of strong light-matter interactions between coherent quantum two-level systems and waveguides, while theoretical quantum computing algorithm proposals have started to unlock the potential of quantum information processing architectures. In this thesis, we discuss progress in both of these directions.

Quantum photonics platforms can exhibit exciting single-photon physics with a wide range of interesting applications. To better understand the interactions and physics of single-photon scattering in waveguides, we apply a recently proposed theoretical scattering framework to specific 1D waveguide scattering problems involving one or two emitters with different level structures. We observe non-trivial interference phenomena on the single-photon level. We further discuss an application to a ground-state entanglement of an emitter with a lambda-type level structure.

We show how sub-radiant states can be engineered in multi-emitter-waveguide devices; we use this physics to our advantage in a new proposal for a quantum information transducer. Such a device can convert a signal between different energy scales. As a device implementation, we consider the transducer acting as a node in a future "quantum internet", where optical photons are the flying information carrier while the stationary qubits operate in the microwave domain. We calculate the device performance in different emitter-waveguide configurations. We show how engineering the photon-mediated interactions in photonic waveguides can significantly enhance performance and can reach highly efficient transduction and good fidelity, assuming experimentally verified component parameters.

As an alternative system, we propose a transducer based on the coupling of an emitter with an optical cavity. By electrically coupling a two-level system to an emitter-cavity system with the same energy splitting, highly efficient transduction can be achieved with good entanglement fidelity. Additionally, we investigate the entanglement fidelity dependence on node dissimilarity and on dephasing effects.

In the last part of this thesis, we discuss how a superconducting quantum computing platform operating with microwave photons can be used to simulate quantum chemistry. Quantum information processing may lead to incredible advances in many fields of science and society as a whole, as the simulation of complex systems previously untouched becomes possible by clever use of quantum resources. We use a dual plane-wave basis approach to solve a 2-dimensional uniform electron gas model on a simulated quantum computer based on superconducting hardware with tunable couplers. We combine different strategies to achieve minimal gate depth and, using a Variational Quantum Eigensolver algorithm, we converge to good fidelity to the groundstate of the problem Hamiltonian. This constitutes a realistic near-term experimental proposal for a practical quantum supremacy experiment on currently available superconducting quantum hardware.

Dansk Resumé

Emnet for denne afhandling er kvanteinformationsbehandling med kvanteoptiske enheder. Udviklingens fremskridt på dette område i de sidste år kan karakteriseres ved forbedringer på to fronter: eksperimentelle fremskridt i fotoniske teknologier har muliggjort stærke lysstof vekselvirkninger mellem kohærente kvante-niveau systemer og bølgeledere, mens teoretiske forslag af kvanteinformationsalgoritmer har begyndt at åbne for potentialet i kvanteinformationsbehandlingsarkitekturer. I denne afhandling diskuteres fremskridtet på de to områder.

Kvantefotoniske platforme kan udvise spændende enkelt-foton fysik med mange forskellige interessante applikationer. For bedre at forstå vekselvirkningerne og fysikken af enkelt-foton-spredningen i bølgeledere, anvender vi et nyligt foreslået teoretisk spredningsframework for specifikke 1D-bølgeleder spredningsproblemer, der involverer en eller to emittere med forskellige niveau strukturer. Vi observerer ikke-trivielle interferensfænomener på enkelt-foton niveauet. Vi diskuterer yderligere en anvendelse til grundtilstandssammenfiltreringen af en emitter med en lambda-type niveaustruktur.

Vi viser hvordan sub-strålende tilstande kan konstrueres i multi-emitter bølgeledere og udnytter denne fysik i et nyt forslag af en kvantuminformationstransducer. Denne enhed kan omdanne et signal mellem forskellige energiniveauer. Med hensyn til implementering af enheden betragter vi transduceren som en station i et fremtidigt "kvanteinternet", hvor optiske fotoner er flyvende informationsbærer, mens de stationære kvantebits opererer i mikrobølgeområdet. Vi beregner enhedens ydeevne i forskellige emitter-bølgeleder konfigurationer. Vi viser, hvordan justeringen af fotonmedierede interaktioner i fotoniske bølgeledere kan forbedre ydeevnen betydeligt og kan føre til meget effektiv transduktion og god kvalitet med eksperimentelt verificerede komponentparametre.

Som et alternativt system foreslår vi en transducer baseret på koblingen af en emitter med en optisk kavitet. Ved elektrisk kobling af et to-niveau system til et emitter-kavitetssystem med samme energispredning, kan en høj effektiv transduktion blive opnået med god sammenfiltreringskvalitet. Derudover undersøger vi sammenfiltreringskvalitetens afhængighed af stationsforskelle og dephasing-effekter.

I den sidste del af denne afhandling diskuteres, hvordan en superledende kvantecomputerplatform, der arbejder med mikrobølgefotoner, kan bruges til at simulere kvantekemi. Kvanteinformationsbehandling kan føre til utrolige fremskridt inden for mange områder i videnskaben og samfundet som helhed, fordi simuleringen af hidtilværende uberørte komplekse systemer bliver muliggjort ved klog brug af kvanteressourcer. Vi bruger en dual-planbølge-basis tilgang til at løse en 2-dimensionel uniform elektrongas-model på en simuleret kvantecomputer baseret på superledende hardware med indstillelige koblere. Vi kombinerer forskellige strategier for at opnå en minimal gatedybde og ved hjælp af Variational Quantum Eigensolver algoritmen konvergerer vi med god kvalitet til grundtilstanden af systemets Hamiltonian. Dette udgør et realistisk eksperimentelt forslag af et praktisk kvante-overlegenhedseksperiment med nuværende førende superledende kvante-hardware, der kan realiseres i den nærmere tid.

List of Publications

The results presented in this thesis are covered by the following articles:

- **V. E. Elfving**, S. Das, A. S. Sørensen, Enhancing quantum transduction via long-range waveguide mediated interactions between quantum emitters, arXiv submission 1810.01381, (2018). [1]
- S. Das, **V. E. Elfving**, F. Reiter, A. S. Sørensen, Photon scattering from a system of multilevel quantum emitters. II. Application to emitters coupled to a one-dimensional waveguide, Phys. Rev. A **97** (4), 043838 (2018). [2]
- **V. E. Elfving**, S. Das, A. S. Sørensen, Efficient quantum transducer based on cavity QED for long-distance quantum entanglement - performance and dephasing, *to be submitted*

Related publications by the author which are not explicitly included in this thesis:

- S. Das, **V. E. Elfving**, S. Faez, A. S. Sørensen, Interfacing superconducting qubits and single optical photons using molecules in waveguides, Phys. Rev. Let. **118** (14), 140501 (2017). [3]
- S. Das, **V. E. Elfving**, F. Reiter, A. S. Sørensen, Photon scattering from a system of multilevel quantum emitters. I. Formalism, Phys. Rev. A **97** (4), 043837 (2018). [4]

Acknowledgements

Foremost, I would like to sincerely thank my PhD academic supervisor, professor Anders S. Sørensen, for giving me the chance to work with him and to welcome me in his group. I am forever grateful to him for teaching me not only what to think but how to think and how to address problems and find solutions in a systematic way, focusing on what is really important. These skills are invaluable also in life. I appreciate his vast knowledge and intuition for physics, and his dissemination of quantum information and quantum optics will stay with me as some of the most fun and interesting experiences I had academically. I thank him also for sending me to conferences locally and abroad, learning from other experts in the field and in the process allowing me to share my ideas and work with them. In addition, without his permission and encouragement, I would not have been able to go for an external stay at Google Santa Barbara, one of my favourite periods during the PhD. I am still a bit surprised everything worked out as well as it did.

Within Anders' group, I would like to acknowledge the tremendous efforts and help I got from Sumanta Das, Assistant Professor, teacher, and truly a friend. We wrote several publications together and it was a joy to be part of some of his awesome theoretical work. Likewise, I have had the pleasure to share most of my time at the Niels Bohr Institute with Oleksandr Kyriienko, who I look up to as one of my role models (except the running part!). Luca Dellantonio is definitely the kindest and most warm-hearted person I have met; sharing these three years will be one of my fondest memories. I thank Johann Kollath-Bönig for his help with proofreading parts of the thesis. I would also like to thank Ivan Iakoupov, Iason Tsiamis, and Kenichi Maeda; not only did these people help me cultivate a mindset for research and the sharing of knowledge with academic peers, we also shared many memorable coffee breaks, lunches, dinners and barbecues together, pondering, vociferating, discussing politics, physics, philosophy and the important things in life. I would also like to thank Charlotte Hviid for always helping out in times of administrative issues or clarifying bureaucratic rules. I could always count on her to fix it or inform me.

I would like to sincerely thank John Martinis for inviting me to his group at Google Santa Barbara and giving me the opportunity to work together with experts in the field of superconducting qubits and quantum simulation algorithms. I acknowledge my day-to-day supervisor Pedram Roushan for supporting me and get settled in Santa Barbara and teaching me how to truly always be critical of what you hear or read. I thank Austin Fowler for sharing my contact information with Pedram Roushan and for letting me do some real experimental (!) work. I want to thank Yu Chen for collaborations on quantum annealing and QAOA projects; our discussion may have yielded more questions than we started with, but we also learned that it may very well be a good reason to investigate further in the topic. I want to thank Charles Neill for insightful discussions, making me feel welcome in the lab and encouraging progress. I thank Andrew Dunsworth for his taking and kind sharing of gmon data. Without the help of Rami Barends, a fellow Dutchman in the group, I would not have been able to fit into and attempt to understand the local culture, foreign to us. We shared a great deal of laughter with iconic sarcasm as the central point of humour.

Last but not least, I thank the all other group members (you know who you are!) for the fun and interesting discussions in meetings and during lunch. Without this social aspect, work is just work.

Finally, an acknowledgment of the citizens of the European Union, who have funded my PhD study through the support from the European Union Seventh Framework Programme ERC Grant QIOS, and the Danish citizens through the Danish council for independent research (Natural Sciences), and the Danish National Research Foundation (Center of Excellence "Hy-Q")

Contents

Dedicated to my parents, Anders & Suzanne, and my sister, Linnéa

Chapter 1

Introduction

QUANTUM INFORMATION PROCESSING
The theoretical, experimental and technological areas covering the use of quantum mechanics for communication and computation.

Encyclopaedia of Mathematics, Supplement III [5]

The term ‘quantum information’ is a broad term capturing all manner of operations related to information processing using quantum mechanics. In recent years, tremendous progress in this field has spurred the development of both theoretical and experimental applications in near-term devices [6]. In this Thesis, we present research on both communication and computation aspects of quantum information processing with quantum optical devices.

In the field of quantum information processing for quantum communication purposes, we propose a novel implementation of a quantum optical device dubbed a ‘quantum transducer’. Efficient transduction of electromagnetic signals between different frequency scales is an essential ingredient for modern communication technologies. An equivalent quantum transducer would be pivotal for hybrid quantum technologies, allowing the merger of existing techniques for quantum information processing, sensing and communication. One of the hallmark examples is that an efficient quantum transducer is an essential building block of the quantum internet. The essence of a quantum internet is the transfer of quantum information from a stationary quantum memory to a flying qubit. The principal quantum information carrier over long distances is optical photons in fibers or free space, but stationary qubits like superconducting qubits often operate at microwave frequencies. A quantum transducer, which can merge these different frequencies regimes, is therefore a key enabling technology for a future quantum internet.

We in this Thesis demonstrate how to exploit recent advances in waveguide photonics and cavity quantum electrodynamics to form a fully coherent efficient quantum transducer. The proposed system relies on semiconductor quantum dots integrated into a photonic waveguide and photonic crystal nanocavity respectively, with high coupling efficiency to individual photons. As such, the system can readily be integrated with existing semiconductor photonic platforms for application in a wide range of hybrid technologies.

For the waveguide-based transducer, we show how the coupling of the quantum dots to the waveguide enables efficient interaction between a single optical photon and a coherent two-level system. We furthermore show that exploiting and engineering waveguide mediated photonic interactions between distant quantum dots allows for an enhancement of the transduction process and thereby enables efficient transduction of weak signals. For the cavity-based transducer, we show how the coupling between the cavity and quantum dot opens up a resonant Raman transition pathway, greatly enhancing the transduction efficiency. We also

explore in detail and quantify detrimental effects that may occur in a practical experiment for these types of quantum transduction devices.

The key technologies required for the proposed transducer have proven qualities and fidelities, which enables the implementation of the transducer with existing technologies. To illustrate the potential of the setup for the long-term vision of a quantum internet, we describe how the proposed transducer may enable long-distance entanglement of superconducting qubits, highlighting the transducer as the key component of a 'quantum internet node'.

Our transducer proposals bring efficient coherent single-photon quantum transduction between different electromagnetic frequency regimes within practical reach. This can lead to different quantum technologies being combined together, which previously could not interact or communicate with each other.

The second topic of this Thesis concerns quantum computation (we refer to Refs. [7–12] for background reading) using quantum optical devices. Exploiting quantum mechanical effects to speed up certain types of computation has been proposed over thirty years ago [13, 14] and since then many breakthroughs have occurred. Still, practical quantum supremacy over classical computing has yet to be shown experimentally. Many different physical hardware implementations have been proposed; a physical system has to adhere to several criteria to be able to implement quantum computation. In his 2000 paper 'The Physical Implementation of Quantum Computation' [15], David P. DiVincenzo proposed the following criteria:

1. A scalable physical system with well-characterized qubits.
2. The ability to initialize the state of the qubits.
3. Long relevant decoherence times.
4. A "universal" set of quantum gates.
5. A qubit-specific measurement capability.
6. The ability to interconvert stationary and flying qubits.
7. The ability to faithfully transmit flying qubits between specified locations.

In Chapter 5 we discuss quantum chemistry algorithms and numerically implement them assuming a certain superconducting qubit architecture called 'g-mons', a quantum hardware system which satisfies the first five criteria. In Chapters 3 and 4 we focus on devices aiming to fulfill the last two criteria.

This Thesis is structured as follows. With Chapter 2, we begin with an introductory chapter on applying a scattering theory for single-photon scattering in one-dimensional waveguides. We implement an existing photon scattering formalism and solve several different scattering situations. We apply the framework to one- and two emitters in a waveguide with different energy level structures. This chapter has been adapted from a published article, Ref. [2]. In Chapter 3, we apply the scattering formalism to a quantum transducer device based on emitters in a waveguide. The results of this chapter have been compiled into a manuscript and submitted to the arXiv Ref. [1]. In Chapter 4, we investigate an alternative device architecture based on a quantum dot strongly coupled to a cavity. We detail dephasing effects on the long-distance entanglement protocol fidelity. In Chapter 5, we combine a range of near-term quantum simulation algorithm techniques to simulate the groundstate of a uniform electron gas ('jellium') on a 'g-mon' type hardware architecture. In Chapter 6, we summarize the results of this Thesis and give an outlook on future research and potential experimental implementations.

Chapter 2

Single-photon scattering problems in one-dimensional waveguides[1]

2.1 Introduction

Efficient light-matter interfaces at the few to single-photon level are crucial for quantum information processing and future quantum technologies [16–20]. Traditionally, such interfaces have been pursued with atoms coupled to a single mode of an optical cavity with a high quality factor, in the regime of cavity quantum electrodynamics (QEDs) [21]. The strong confinement of light in optical cavities, however, also poses a limitation to their integration into quantum networks, which relies on the efficient out-coupling of light [22]. As such, currently a wide variety of physical systems are being studied where one achieves good light-matter interface, which can be integrated in future with opto-electronics [23–42]. Among these, waveguides coupled to quantum emitters have turned out to be a viable alternative with coupling to both two-level and multi-level emitters been achieved [43–46]. This has lead to demonstration of several interesting effects involving light scattering in waveguide systems like, optical routing of single photons [47, 48], collective reflection [49, 50], quantum state controlled directional emission [51], and many others [52–55]

The study of photon scattering in waveguides traditionally considers an emitter either coupled to a continuous set of freely propagating waveguide modes or coupled to a discrete set of modes via an optical cavity. A key question in such system is then, how to efficiently evaluate the photon reflection and transmission amplitudes, which are due to the medium's response corresponding to different pathways of scattering. In the past decades several approaches have been introduced to solve this problem. For example, one of the early approaches uses the Lippmann-Schwinger formalism in a Schrödinger picture to evaluate the reflected and transmitted field amplitudes [56–60]. This formulation, even though exact, cannot be applied for propagating photons interacting with separated multi-level emitters. Alternatively, some studies have used the transfer matrix method which is particularly useful in the weak excitation regime, where the emitters can be considered to be linear scatterers [61, 62].

To solve the problem of photon scattering from nonlinear emitters, an input-output formalism was developed although only for a two-level emitter coupled to a 1D waveguide [63]. An analogous approach was later introduced for superconducting qubits coupled to a 1D transmission line [64]. There are several other frameworks to solve the scattering problem for nonlinear emitters coupled to 1D waveguides [31, 34, 65–71]. Recently the formalism of

[1] This Chapter is an adaptation of publication Ref. [2]. In that article, Dr. Sumanta Das has written the introduction Section 2.1, Section 2.2, Section 2.3, Section 2.4.1, Appendices A and B, and collaborated on Section 2.4.2 with Vincent Elfving. Vincent Elfving has written and performed the analytical and numerical calculations for Section 2.4.3 to Section 2.5.2 and Appendix C.

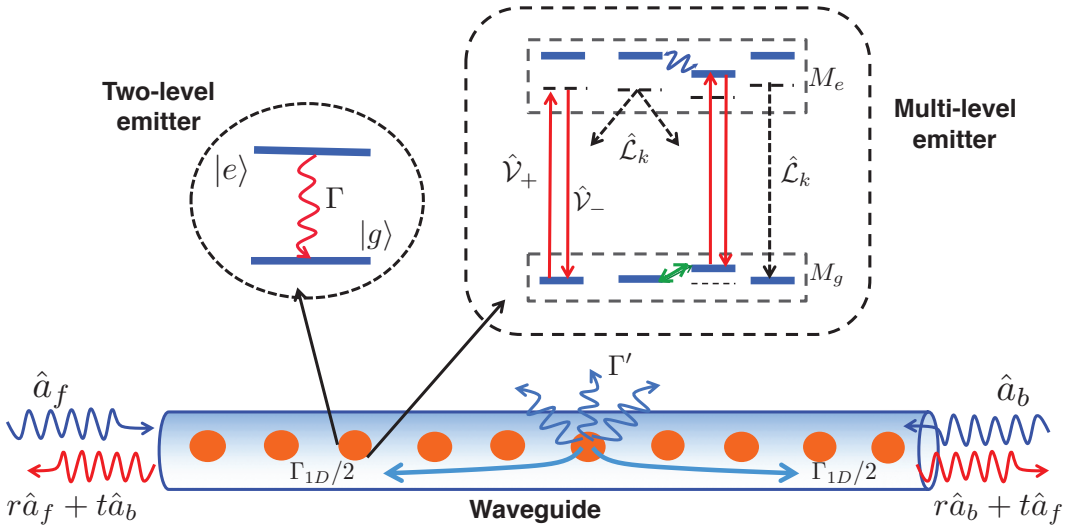

FIGURE 2.1: Schematic of photon scattering from a generic system of emitters coupled to a waveguide. The emitters can be either a simple two-level system with a decay Γ or have multiple levels. These can be separated into two subspaces: an excited-state manifold M_e and a ground-state manifold M_g. The couplings between the two manifolds $\hat{\mathcal{V}}_+(\hat{\mathcal{V}}_-)$ are assumed to be perturbative while the excited states experience decay modeled by the Lindblad operators $\hat{\mathcal{L}}_k$. The couplings within the excited and ground-state manifold are shown by the wiggly and straight arrow-headed lines respectively. The 1D waveguide supports both forward and backward propagating modes of an input photon represented by the operators a_f and a_b, respectively. Furthermore, the symbols r and t represent the reflection and transmission coefficients satisfying the relation $|r|^2 + |t|^2 = 1$. Photons scattered from the emitters can decay to outside modes and into the waveguide with decay rates of Γ' and Γ_{1D}, respectively.

Ref. [63] was generalized to multi-level emitters coupled to a 1D waveguide [72]. Furthermore, in a related work a path integral formalism-based scattering matrix was developed to study few-photon scattering dynamics in the non-Markovian regime [73]. Typically, all these approaches reduces to setting up the problem by either linearization, or by restricting the system to two-level emitters and a 1D waveguide and then numerically solving it. Even then, the solution of the full photon-scattering problem from multi-level emitters in the paradigm of waveguide QED, remains quite tedious even for a single photon.

In a preceding paper we developed a general photon-scattering relation from a system of multi-level quantum emitters embedded in a 3-dimensional dielectric medium [4]. The theoretical framework for this problem involved a set of excited and ground-state subspaces M_e and M_g respectively. Each of these subspaces are spanned by the manifold of the excited ($|e\rangle$) and ground ($|g\rangle$) states of the emitters. The theory is applicable to incident fields with a sufficiently low intensity, e.g., single-photon or weak coherent states, so that saturation effects can be ignored. In this limit, the coupling between the two subspaces can be treated perturbatively. We showed that our theory provides a solution for the amplitudes of the scattered fields, in terms of the input-photon amplitude and the dynamical response of the emitters. As a continuation of Ref. [4], in this paper we apply the formalism to the particular case of 1-dimensional waveguides and show how it can be used to solve a variety of scattering problems. Following Ref. [4], we derive a photon-scattering relation for a system of multi-level emitters coupled to a 1D waveguide in the form

$$\hat{a}_{l,\text{out}} = \hat{a}_{l,\text{in}} + i\sum_{l'}\sum_{gg'}\hat{\sigma}_{g'g}\mathcal{S}^{ll'}_{gg'}\hat{a}_{l',\text{in}}. \tag{2.1}$$

Here $\hat{a}_{l,\text{in}}$ and $\hat{a}_{l,\text{out}}$ are the input and the output field-mode operators in the waveguide, $\hat{\sigma}_{g'g}$ is an operator in the Heisenberg picture giving the dynamics within the ground-state manifold $\{|g\rangle, |g'\rangle\}$ of the emitters, while the superscripts (l, l') signify the directionality (forward, backward propagation) of photons in the waveguide. The kernel $\mathcal{S}^{ll'}_{gg'}$ is the scattering amplitude which can be evaluated once the coupling of the emitters has been determined.

In the following section we give a detailed derivation of Eq. (2.1) and discuss how to evaluate the ground-state dynamics in terms of the operator $\hat{\sigma}_{g'g}$. Furthermore, it will also be apparent that Eq. (2.1) has the following salient features (a) it provides a direct solution of the scattering problem assuming Markovian dynamics for weak input fields, (b) it can include any kind of dipole emitters coupled to the 1D mode of a waveguide and (c) it uses effective operators (EOs) to give a full solution of the emitter dynamics keeping track of all the phases and scattering component. The introduction of the EOs basically amounts to adiabatic elimination of the excited states and describing the system dynamics solely in terms of the ground-states evolution [74]. Thus, by using EOs, the complications arising from multiple emitters in the scattering problem, can be reduced to solving the dynamics for the ground-state coherences and populations.

The article is organized as follows: In Sec. II we give the detailed derivation of Eq. (2.1) starting from the photons scattering relation developed for a general dielectric medium in Ref. [4]. In Sec. III we then elaborate on the physical processes that contribute to the non-Hermitian Hamiltonian, which is the key quantity for determining the scattering relation, and explain what the different terms in this Hamiltonian correspond to. Readers primarily interested in the application of the photon scattering formalism are encouraged to visit Sec. IV directly to avoid the technical details laid out in Secs. II and III. In Sec. IV we elaborate on our results by solving different examples of photon scattering from a single emitter coupled to a one-dimensional waveguide. We start with a simple example of a two-level emitter in Sec. IV.A and continue with a more complicated example of an emitter in a V-level configuration in Sec. IV.B. In Sec. IV.C we then consider several different cases of photon scattering from a system of multiple emitters coupled to a one-dimensional waveguide. In Sec. V we then give an example that demonstrates the versality of our formalism. We consider scattering from an emitter with multiple ground-states and study several aspects including the formation of ground-state superpositions conditioned on photon scattering. Finally, in Sec. VI we summarize our results and give an outlook. Several details of our calculations are relegated to the appendices. In Appendix A we provide the derivation of the photon-scattering relation for the 1D waveguide. In Appendix B we present the derivation of the decay rate into the 1D mode of the waveguide. In Appendix C we give details of the effective detunings and decays for the two-emitter systems.

2.2 Photon-scattering relation for emitters coupled to a 1D waveguide

In this section we derive the photon-scattering relation for a system of multi-level emitters coupled to a double-sided 1D waveguide. To achieve this we first invoke the general photon-scattering relation in a dielectric medium

$$\begin{aligned}\hat{\vec{\mathcal{E}}}^{+}(\vec{r},t) &= \hat{\vec{\mathcal{E}}}_{in}(\vec{r},t)+\left(\frac{i\omega}{2\hbar}\right)\sum_{jj'}\sum_{gg'}\overleftrightarrow{\mathbf{G}}(\vec{r},\vec{r}_j,\omega-\omega_{gg'})\\ &\times \hat{\sigma}_{g'g}\sum_{ee'}\left(\vec{d}^{j}_{ge}[\tilde{\mathcal{H}}_{nh}]^{-1}_{ee'}\vec{d}^{j'}_{e'g'}\right)\hat{\vec{\mathcal{E}}}_{in}(\vec{r}_{j'},t),\end{aligned} \tag{2.2}$$

that was derived in Ref. [4]. Here $\vec{r}$ is the point of observation, while $\vec{r}_j, \vec{r}_{j'}$ corresponds to the spatial positions of emitter j and j', respectively. The dipole moments $\vec{d}^{j}_{eg}$ and $\vec{d}^{j'}_{e'g'}$ correspond to the transition $|e\rangle \leftrightarrow |g\rangle$ and $|e'\rangle \leftrightarrow |g'\rangle$ for the emitters j and j'. The Green's function, $\overleftrightarrow{\mathbf{G}}(\vec{r},\vec{r}_j,\omega-\omega_{gg'})$ gives the response of the field at the characteristic frequency $(\omega-\omega_{gg'})$ of the dielectric medium containing the emitters. Here ω is the central frequency of the input field and $\omega_{gg'}=(\omega_g-\omega_{g'})$ is the difference in frequency between states in the ground-state subspace. The input field in the above equation is defined as $\hat{\vec{\mathcal{E}}}_{in}(\vec{r},t)=i\sum_k\sqrt{\frac{\hbar\omega_k}{2}}\vec{F}_k(\vec{r})\hat{a}_k(0)e^{-i\omega_k t}$, where $\vec{F}_k(\vec{r})$ is the mode function while $\hat{a}_k$ is the mode operator for the k^{th} mode of the field. The second term in Eq. (2.2) represents the whole scattering event. It gives the scattered field including the dynamical response of the emitters. It is formulated in terms of the operator $\hat{\sigma}_{g'g}=|g\rangle\langle g'|$ and the non-Hermitian Hamiltonian $\tilde{\mathcal{H}}_{nh}$, which describes the dynamics in the excited-state subspace M_e. The non-Hermitian Hamiltonian is well known in the theory of Montecarlo wave-functions [75]. In Sec. III. we will describe in detail the meaning of this $\tilde{\mathcal{H}}_{nh}$ for our model. The states $|g\rangle$ and $|g'\rangle$ belong to the ground-state manifold M_g of the emitters as shown in Fig. (2.1). Note that our definition of the operator $\hat{\sigma}_{g'g}$ can be considered unconventional since the order is reversed. As we will see later, this definition gives us a simple relation to the density matrix $\rho_{g'g}=\langle\hat{\sigma}_{g'g}\rangle$ and simplifies the notation below.

To proceed we first rewrite Eq. (2.1) in a more convenient form. We expand $\hat{\vec{\mathcal{E}}}_{in}(\vec{r},t)$ in terms of the Green's function

$$\hat{\vec{\mathcal{E}}}_{in}(\vec{r},t)=\int d\vec{r'}\,\epsilon(\vec{r'})\overleftrightarrow{\mathbf{G}}(\vec{r},t,\vec{r'},0)\hat{\vec{\mathcal{E}}}^{+}(\vec{r'},0) \tag{2.3}$$

in Eq. (2.2) and writing the frequency-dependent $\mathbf{G}(\vec{r},\vec{r}_j,\omega-\omega_{gg'})$ as the Fourier transform of the time-dependent Green's function we get,

$$\begin{aligned}\hat{\vec{\mathcal{E}}}^{+}(\vec{r},t) &= \int d\vec{r'}\,\epsilon(\vec{r'})\overleftrightarrow{\mathbf{G}}(\vec{r},t,\vec{r'},0)\hat{\vec{\mathcal{E}}}^{+}(\vec{r'},0)+\left(\frac{i\omega}{2\hbar}\right)\\ &\times \sum_{gg'}\int_{-\infty}^{t}d\tau\,e^{i\omega_{gg'}(t-t')}\hat{\sigma}_{g'g}\overleftrightarrow{\mathbf{G}}(\vec{r},t,\vec{r}_j,t')\\ &\times \sum_{ee'}\left(\vec{d}^{j}_{ge}[\tilde{\mathcal{H}}_{nh}]^{-1}_{ee'}\vec{d}^{j'}_{e'g}\right)\int d\vec{r'}\,\epsilon(\vec{r'})\\ &\times \overleftrightarrow{\mathbf{G}}(\vec{r}_{j'},t',\vec{r'},0)\hat{\vec{\mathcal{E}}}^{+}(\vec{r'},0).\end{aligned} \tag{2.4}$$

Here $\epsilon(\vec{r})$ is the space-dependent electric permittivity of the waveguide. The first term on the right hand side of Eq. (2.4) represents the freely propagating field with the Green's function

being simply a propagator.

We want to derive the photon-scattering relation for a double-sided 1D waveguide. As such, we assume that the waveguide modes allow for the scattered photons to travel both in the forward (f) and backward (b) directions with wave-numbers (k_f) and (k_b), respectively. Furthermore, to account for the scattering into the waveguide and to the outside we divide $\hat{\mathcal{E}}^+_{k_\zeta}(\vec{r},t)$ into a waveguide and a radiative part. To treat this formally, we decompose the electric field in the form $\hat{\mathcal{E}}^+(\vec{r},t) = \sum_{k_\zeta} \hat{\mathcal{E}}^+_{k_\zeta}(\vec{r},t) + \hat{\mathcal{E}}^+_{\text{rest}}(\vec{r},t)$ with $\zeta = \{f,b\}$, such that

$$\hat{\mathcal{E}}^+_{k_\zeta}(\vec{r},t) \quad = \quad i\sum_{k_\zeta}\sqrt{\frac{\hbar\omega_{k_\zeta}}{2}}\vec{F}_{k_\zeta}(r_\perp)\hat{a}_{k_\zeta}e^{i(k_\zeta \mathrm{z}-\omega t)}, \tag{2.5}$$

represent the field in the forward and backward propagating modes of the waveguide. Here $i\sum_{k_\zeta}\sqrt{\frac{\hbar\omega_{k_\zeta}}{2}}\vec{F}_{k_\zeta}(r_\perp)e^{ik_\zeta \mathrm{z}}$ are the modes representing the field in the waveguide, z is the co-ordinate along the waveguide, while $\mathcal{E}^+_{\text{rest}}(\vec{r},t)$ are the radiative modes representing the scattered light to the outside.

Substituting Eq. (2.5) into Eq. (2.4) and decomposing the Green's function into the forward, backward and the rest of the components as

$$\overleftrightarrow{\mathbf{G}}(\vec{r},t,\vec{r'},t') \quad = \quad \sum_\zeta \overleftrightarrow{\mathbf{G}}_\zeta(\vec{r}_\perp,t,\vec{r'}_\perp,t') + \overleftrightarrow{\mathbf{G}}_{\text{rest}}(\vec{r},t,\vec{r'},t'), \tag{2.6}$$

we arrive finally (see Appendix A for details) at the photon-scattering relation in the 1D waveguide

$$\begin{aligned}\hat{a}_{\zeta,\mathrm{o}}(\mathrm{z},t) \quad &= \quad \hat{a}_{\zeta,\mathrm{in}}(\mathrm{z}\mp v_g t) + i\sum_{\zeta'}\sum_{gg'}\hat{\sigma}_{g'g}[\mathcal{S}^{\zeta\zeta'}_{gg'}]_\mp \\ &\times \quad \hat{a}_{\zeta',\mathrm{in}}(\mathrm{z}\mp v_g t) + \mathcal{F}.\end{aligned} \tag{2.7}$$

Here v_g is group velocity of the photon in the waveguide, while $\mathcal{F}$ is a noise operator that corresponds to the $\mathbf{G}_{\text{rest},\zeta}$ and $\mathcal{E}^+_{\text{rest}}$ and is associated with the loss of photons out of the waveguide. The mode operators $\hat{a}_{\mathrm{o}}$ and $\hat{a}_{\mathrm{in}}$ correspond to the output and input light field, respectively. Note that the " $-$ "$(+)$ sign stands for photons travelling in the forward (backward) direction. The scattering amplitude $[\mathcal{S}^{\zeta\zeta'}_{gg'}]_\mp$ is defined as

$$\begin{aligned}[\mathcal{S}^{\zeta\zeta'}_{gg'}]_\mp \quad &= \quad \sum_{jj'}\sum_{ee'}\mathcal{A}^{\dagger j\zeta}_{ge(1\mathrm{D})}[\tilde{\mathcal{H}}_{nh}]^{-1}_{ee'}\mathcal{A}^{j'\zeta'}_{e'g'(1\mathrm{D})} \\ &\exp \quad [\mp i((k_\zeta - k_{\zeta'})\mathrm{z}_j + \omega_{g'g}(\mathrm{z}-\mathrm{z}_j)/v_g],\end{aligned} \tag{2.8}$$

where we have defined the directional coupling of the emitters to the waveguide mode as

$$\mathcal{A}^{j\zeta}_{eg} = \sqrt{\frac{\pi\omega}{\hbar v_g}}\left[\vec{d}^{\,j}_{eg}\cdot\vec{F}_{k_\zeta}(r_{j_\perp})\right]. \tag{2.9}$$

with $\mathcal{A}^{\dagger j\zeta}_{ge(1\mathrm{D})} = \mathcal{A}^{*j\zeta}_{eg(1\mathrm{D})}$. The wave vectors in the forward and backward direction follow the relation $\Delta k = (k_\zeta - k_{\zeta'}) = 0$ and $2k_0$ for $\zeta = \zeta'$ and $\zeta \neq \zeta'$, respectively. The photon-scattering relation in Eq. (2.7) is the key result of this work and has the generic form stated in Eq. (2.1). Note that, the coupling defined in Eq. (2.9) has a directional dependence and in principle its strength can be different for the field-mode propagating along two different directions (forward or backward) in the waveguide. This leads to an interesting and

emerging question of chiral light-matter interaction [76]. Even though we do not explicitly address this, our general formalism is already equipped with such possibilities. As such the photon-scattering relation in Eq. (2.7) is applicable even to the study of chiral interactions in waveguides.

It is worth emphasizing that in the derived photon-scattering relation all the system properties are included through the non-Hermitian Hamiltonian $\tilde{\mathcal{H}}_{nh}$ while the evolution of the emitters, response is through the operator $\hat{\sigma}_{g'g}$ defined in the ground-state manifold M_g. To get the complete photon-scattering dynamics using the photon-scattering relation introduced above we need to find $\hat{\sigma}_{g'g}$. This can be quite cumbersome for complex systems involving multiple levels. However, by exploiting the formulation of EOs [74], which again involves the inverse of the non-Hermitian Hamiltonian $[\tilde{\mathcal{H}}_{nh}]$, we can solve for $\hat{\sigma}_{g'g}$ using the master equation derived explicitly in the preceding paper [4]

$$\begin{aligned}\dot{\hat{\sigma}} &= :\, i\left[\hat{\mathcal{H}}_{\text{eff}}, \hat{\sigma}\right] - \frac{1}{2}\sum_k \left(\hat{\mathcal{L}}^{k\dagger}_{\text{eff}}\hat{\mathcal{L}}^{k}_{\text{eff}}\hat{\sigma} + \hat{\sigma}\hat{\mathcal{L}}^{k\dagger}_{\text{eff}}\hat{\mathcal{L}}^{k}_{\text{eff}}\right) \\ &+ \sum_k \hat{\mathcal{L}}^{k}_{\text{eff}}\hat{\sigma}\hat{\mathcal{L}}^{k\dagger}_{\text{eff}} \,:\,. \end{aligned} \tag{2.10}$$

Here all the operators are defined in the Heisenberg picture and the subscript “eff" symbolizes EO’s. The symbol “ : ” in Eq. (2.10) stands for normal ordering, the significance of which will be discussed in details in section VI.C. Note that, Eq. (2.10) is a Heisenberg-picture generalization of the result of Ref. [74] to quantum fields. Solving the above master equation for a given system is a straightforward algebraic/numerical exercise whose complexity simply depends on the size of the Hilbert space of the emitters. Later in section IV.C we consider an example where the emitters have multiple ground-states and show how one can use the master equation in Eq. (2.10) to solve for the dynamics of the emitter’s ground-state.

It is important to point out that for the examples we discuss in Sec. IV, the noise term $\mathcal{F}$ in Eq. (2.7) is typically neglected. This is justified by the fact that in those examples we are only interested in the click probability where the vacuum noise does not contribute to any photodetector clicks. However, we would like to remind the readers that in general particular care should be taken for Heisenberg equations as the noise can play a crucial role in the system dynamics. We account for this in our formalism through the effective Lindblad operators in the master equation, which includes the noise contribution. Hence for problems where the scattering is influenced by the coherence dynamics of the ground-states, the crucial effect of noise is taken care of in the master equation. We show this in detail in the example in Sec. VI.C. Thus we discuss explicitly how to deal with the noise and treat it via the effective-operator master equation.

2.3 The non-Hermitian Hamiltonian

To be able to apply our formalism, it is important to understand the non-Hermitian Hamiltonian $[\tilde{\mathcal{H}}_{nh}]$ in Eq. (2.8). The general form of the non-Hermitian Hamiltonian from [4] is

$$[\mathcal{H}_{nh}]_{ee'} = [\mathcal{H}_{c_e}]_{ee'} - i\sum_{jj'}\sum_{g}\left(\frac{1}{2}\Gamma^{jj'e'e}_{gg} - i\Omega^{jj'e'e}_{gg}\right). \tag{2.11}$$

Note that this non-Hermitian Hamiltonian includes all possible interactions that the emitters can have within the excited-state manifold. In the following we discuss each of the terms in Eq. (2.11). The first term $\mathcal{H}_{c_e}$ is the Hamiltonian of the system defined in the single

excitation manifold M_e as shown in Fig. 2.1. Note that this term is completely general and can in principle also include effects like the long-range Rydberg interactions among emitters. The second and third term $\Gamma_{gg}^{jj'e'e}$ and $\Omega_{gg}^{jj'e'e}$ arise from the dynamics induced by the quantized field and are related to the decay from the manifold M_e to M_g, and shifts of the states in the manifold M_e due to light induced coupling between the emitters. They are defined as

$$\Gamma_{gg}^{jj',e'e} = \frac{2\omega_{eg'}^2}{\hbar c^2}\left\{\vec{d}_{e'g'}^{\,j}\cdot\mathbf{Im}\overleftrightarrow{\mathbf{G}}(\vec{r}_j,\vec{r}_{j'},\omega_{e'g})\cdot\vec{d}_{ge}^{\,j'}\right\}, \tag{2.12}$$

$$\Omega_{gg}^{jj',e'e} = \mathbf{P}\int d\omega\left(\frac{\omega^2}{\hbar\pi c^2}\right)\left\{\frac{\vec{d}_{e'g}^{\,j}\cdot\mathbf{Im}\overleftrightarrow{\mathbf{G}}\cdot\vec{d}_{ge}^{\,j'}}{(\omega-\omega_{e'g'}+i\epsilon)}\right\}, \tag{2.13}$$

where the excited $|e\rangle$, $|e'\rangle$ and ground $|g\rangle$ states belong to the excited and ground subspaces M_e and M_g, respectively. Note that to write Eq. (2.12) and Eq. (2.13) we have used the general form of these expression derived in Ref. [4].

The $\mathbf{Im}\overleftrightarrow{G}$ in the above set of equations stands for imaginary part of the Green's tensor. On expanding the Green's function using Eq. (2.6) and substituting it in Eqs. (2.12) and (2.13) we get,

$$\begin{aligned}\Gamma_{gg}^{jj',e'e} &= \frac{2\omega_{e'g'}^2}{\hbar v_g^2}\left\{\vec{d}_{e'g}^{\,j}\cdot\sum_\zeta\mathbf{Im}\overleftrightarrow{\mathbf{G}}_\zeta(\vec{r}_j,\vec{r}_{j'},\omega_{e'g})\cdot\vec{d}_{ge}^{\,j'}\right\},\\ &+ \frac{2\omega_{e'g}^2}{\hbar c^2}\left\{\vec{d}_{e'g}^{\,j}\cdot\mathbf{Im}\overleftrightarrow{\mathbf{G}}_{\text{rest}}(\vec{r}_j,\vec{r}_{j'},\omega_{e'g})\cdot\vec{d}_{ge}^{\,j'}\right\},\end{aligned} \tag{2.14}$$

$$\Omega_{gg}^{jj',e'e} = \mathbf{P}\int d\omega\left(\frac{\omega^2}{\hbar\pi v_g^2}\right)\left\{\frac{\vec{d}_{e'g}^{\,j}\cdot\sum_\zeta\mathbf{Im}\overleftrightarrow{\mathbf{G}}_\zeta\cdot\vec{d}_{ge}^{\,j'}}{(\omega-\omega_{e'g}+i\epsilon)}\right\}, \tag{2.15}$$

$$+ \mathbf{P}\int d\omega\left(\frac{\omega^2}{\hbar\pi c^2}\right)\left\{\frac{\vec{d}_{e'g}^{\,j}\cdot\mathbf{Im}\overleftrightarrow{\mathbf{G}}_{\text{rest}}\cdot\vec{d}_{ge}^{\,j'}}{(\omega-\omega_{e'g}+i\epsilon)}\right\} \tag{2.16}$$

We rewrite $\Gamma_{gg}^{jj',e'e}$ in Eq. (2.14) in the form $\Gamma_{gg}^{jj',e'e} = [\Gamma_{gg}^{jj',e'e}]_{\text{w}} + [\Gamma_{gg}^{jj',e'e}]_{\text{rest}}$. Here $[\Gamma_{gg}^{jj',e'e}]_{\text{w}}$ corresponds to the first term on the right-hand side of Eq. (2.14) and represents decay-induced coupling between the emitters mediated by the 1D waveguide mode. $[\Gamma_{gg}^{jj',e'e}]_{\text{rest}}$ represents the second term and arises due to collective decay to the non-waveguide modes (decay to the outside of the waveguide). For $j = j'$, $[\Gamma_{gg}^{jj',e'e}]_{\text{w}}$ corresponds to spontaneous decay of the emitter into the 1D waveguide mode while $[\Gamma_{gg}^{jj',e'e}]_{\text{rest}}$ gives spontaneous decay of the emitter to the outside of the waveguide. Similarly, Eq. (2.15) for $j \neq j'$ can be defined as $\Omega_{gg}^{jj',e'e} = [\Omega_{gg}^{jj',e'e}]_{\text{w}} + [\Omega_{gg}^{jj',e'e}]_{\text{rest}}$, where $[\Omega_{gg}^{jj',e'e}]_{\text{w}}$ represent the first term on the right-hand side of Eq. (2.15) and stands for waveguide-mediated coupling of the emitters while $[\Omega_{gg}^{jj',e'e}]_{\text{rest}}$ represents the second term and corresponds to coupling via other processes like dipole-dipole interactions. For $j = j'$, the coupling $\Omega_{gg}^{jj',e'e}$ gives a contribution to the Lamb shift of the excited state of a single emitter. It is worth mentioning that in general these decays and shifts in the waveguide system can be both function of frequency and alignment of the emitters [77, 78]. Note that in Ref. [4] these terms were derived within the rotating

wave approximation, which does not produce the correct form of the dipole-dipole interaction for emitters separated by less than a wavelength. Care should therefore be taken to use the correct shifts beyond the rotating wave approximation for nearby emitters.

In the following we derive an exact expression for the waveguide-mediated coupling between the emitters, by solving for the first terms on the right-hand side of Eq. (2.14) and Eq. (2.15). For this purpose we invoke the relation [79]

$$\begin{aligned}\sum_k \omega_k \vec{F}_k(\vec{r})\vec{F}_k^*(\vec{r'})\, e^{-i\omega_k(t-t')} &= 2\int d\omega\, e^{-i\omega(t-t')}\frac{\omega^2}{\pi c^2} \\ &\times \mathbf{Im}\{\overleftrightarrow{G}(\vec{r},\vec{r'},\omega)\},\end{aligned} \tag{2.17}$$

and do an inverse Fourier transform of it to get

$$\begin{aligned}\mathbf{Im}\overleftrightarrow{\mathbf{G}}_\zeta(\vec{r}_j,\vec{r}_{j'},\omega) &= \frac{\pi}{k_\zeta}F_{k_\zeta}(\vec{r}_{j\perp})F^*_{k_\zeta}(\vec{r}_{j'\perp}) \\ &\times \cos\left(k_\zeta|\mathrm{z}_j-\mathrm{z}_{j'}|\right),\end{aligned} \tag{2.18}$$

where $k_\zeta = \pm\,\omega/v_g$, with the $+(-)$ sign corresponding to the forward (backward) propagation direction. Then substituting Eq. (2.18) into the first term on the right-hand side of Eq. (2.14) and on using Eq. (2.9) we get

$$[\Gamma_{gg}^{jj',e'e}]_{\mathrm{w}} = 2\sum_\zeta \mathcal{A}^{j\zeta}_{e'g(1\mathrm{D})}\mathcal{A}^{\dagger j'\zeta}_{ge(1\mathrm{D})}\cos\left(k_\zeta|\mathrm{z}_j-\mathrm{z}_{j'}|\right). \tag{2.19}$$

Furthermore, substituting Eq. (2.18) into the first term on the right-hand side of Eq. (2.15) and then performing the principal value integral over an anticlockwise contour and invoking Cauchy's residue theorem (see Appendix B for details) gives us

$$[\Omega_{gg}^{jj',e'e}]_{\mathrm{w}} = -\sum_\zeta \mathcal{A}^{j\zeta}_{e'g(1\mathrm{D})}\mathcal{A}^{\dagger j'\zeta}_{ge(1\mathrm{D})}\sin\left(k_\zeta|\mathrm{z}_j-\mathrm{z}_{j'}|\right). \tag{2.20}$$

If we refer to the expression for the non-Hermitian Hamiltonian in Eq. (2.11) and consider the contribution to the second and the third term due to the waveguide-mediated interactions, we find, using Eq. (2.19) and Eq. (2.20), that [62, 72, 80]

$$\begin{aligned}\frac{1}{2}[\Gamma_{gg}^{jj',e'e}]_{\mathrm{w}} - i[\Omega_{gg}^{jj',e'e}]_{\mathrm{w}} &= \sum_\zeta \mathcal{A}^{j\zeta}_{e'g(1\mathrm{D})}\mathcal{A}^{\dagger j'\zeta}_{ge(1\mathrm{D})} \\ &\times e^{ik_\zeta|\mathrm{z}_j-\mathrm{z}_{j'}|}.\end{aligned} \tag{2.21}$$

Note that for the case of a single two-level emitter, $j=j'$ and $e'=e$. Eq. (2.21) becomes

$$\sum_\zeta |\mathcal{A}^\zeta_{eg(1\mathrm{D})}|^2 = \sum_\zeta \Gamma^{e,\zeta}_{g,1\mathrm{D}} = \Gamma^e_{g,1\mathrm{D}}, \tag{2.22}$$

where $\Gamma^e_{g,1\mathrm{D}}$ is the total decay of energy level $|e\rangle$ into the 1D mode of the waveguide for the emitter transition $|e\rangle \rightarrow |g'\rangle$.

We can now rewrite the non-Hermitian Hamiltonian $[\mathcal{H}_{nh}]_{ee'}$ of Eq. (2.11) as a combination of two parts, one comprising of all the interactions mediated by the waveguide (w) while the other one concerning all other processes not mediated by the waveguide (nw).

The non-Hermitian Hamiltonian then takes the form $[\tilde{\mathcal{H}}_{nh}]_{ee'} = \left[\tilde{\mathcal{H}}_c\right]_{ee'} + \left[(\tilde{\mathcal{H}}_{nh})_{\rm w}\right]_{ee'} + \left[(\tilde{\mathcal{H}}_{nh})_{\rm nw}\right]_{ee'}$, where

$$\left[(\tilde{\mathcal{H}}_{nh})_{\rm w}\right]_{ee'} = -i\sum_{jj'}\sum_{g,\zeta}\mathcal{A}^{j\zeta}_{e'g(1{\rm D})}\mathcal{A}^{\dagger j'\zeta}_{ge(1{\rm D})}e^{ik_\zeta|{\rm z}_j-{\rm z}_{j'}|} \tag{2.23}$$

$$\left[(\tilde{\mathcal{H}}_{nh})_{\rm nw}\right]_{ee'} = -\sum_{jj'}\sum_{g}\left(\frac{i}{2}[\Gamma^{jj',e'e}_{gg}]_{\rm rest} + [\Omega^{jj',e'e}_{gg}]_{\rm rest}\right). \tag{2.24}$$

Here $\tilde{\mathcal{H}}_c = \mathcal{H}_{c_e} - E_g - \hbar\omega$, with E_g being the energy of the ground-state involved in the excitation process while ω is the frequency of the incoming photon. The waveguide-mediated off-diagonal term in Eq. (2.23) can also be re-written in terms of $\Gamma_{1{\rm D}}$ as,

$$\begin{aligned}\left[(\tilde{\mathcal{H}}_{nh})_{\rm w}\right]_{ee'} &= -i\sum_{jj'}\sum_{g\zeta}\sqrt{\Gamma^{e'j\zeta}_{g,1{\rm D}}}\sqrt{\Gamma^{ej'\zeta}_{g,1{\rm D}}}e^{i\left(\phi_{e'g'}-\phi_{eg}\right)}\\ &\times\ e^{ik_\zeta|{\rm z}_j-{\rm z}_{j'}|},\end{aligned} \tag{2.25}$$

where we have used $\mathcal{A}^{j\zeta}_{eg(1{\rm D})} = |\mathcal{A}^{j\zeta}_{eg(1{\rm D})}|e^{i\phi_{eg}}$ and the definition of directional decay into the waveguide $\Gamma^{e\zeta}_{g,1{\rm D}}$ in terms of the coupling constants $\mathcal{A}$ from Eq. (2.22).

On using the general form of $[\tilde{\mathcal{H}}_{nh}]_{ee'}$ and Eq. (2.25) we find that the non-Hermitian Hamiltonian has a simple diagonal part ($j = j'$) spanned by the excited states of the emitters as

$$\left[\tilde{\mathcal{H}}_{nh}\right]_{ee} = \tilde{\Delta}_e - \frac{i}{2}\Gamma_e, \tag{2.26}$$

where $\tilde{\Delta}_e = [\tilde{\mathcal{H}}_{c_e} - E_g - \hbar\omega]_{ee}$ and $\Gamma_e = \Gamma'_e + \Gamma_{e(1{\rm D})} = \sum_g\left[\Gamma^e_{g{\rm rest}} + \sum_\zeta\Gamma^{e,\zeta}_{g,1{\rm D}}\right]$, is the natural line width of an excited state $|e\rangle$ in the single-excitation manifold M_e. Here $\Gamma'_e = \sum_g\Gamma^e_{g{\rm rest}}$ is the total decay rate to the outside of the waveguide and $\tilde{\mathcal{H}}_{c_e}$ is a redefined excited-state Hamiltonian formed by absorbing the Lamb-shift contribution in $\mathcal{H}_{c_e}$. Note that Eq. (2.26) can also be written in the standard form of a non-Hermitian Hamiltonian

$$\hat{\mathcal{H}}_{nh} = \hat{\tilde{\mathcal{H}}}_{c_e} - \frac{i}{2}\sum_k\hat{\mathcal{L}}^\dagger_k\hat{\mathcal{L}}_k, \tag{2.27}$$

where the Lindblad operators $\hat{\mathcal{L}}_k$ model decay of an excited emitter both into and outside of the waveguide.

We next discuss the contribution to the non-Hermitian Hamiltonian from the non-waveguide part $(\tilde{\mathcal{H}}_{nh})_{\rm nw}$ in Eq. (2.24). These terms can have contributions both for inter- and intra-emitter couplings. In the Dicke superradiant limit, where the separation between the emitters is less than a wavelength, the $(\tilde{\mathcal{H}}_{nh})_{\rm nw}$ gives rise to collective decay and dipole-dipole couplings. For most of this article we will ignore the $(\tilde{\mathcal{H}}_{nh})_{\rm nw}$ part of the non-Hermitian Hamiltonian. However, we do use this in two particular examples to illustrate the wide range of applicability of our formalism.

2.4 Application of the formalism to emitters with a single ground-state

In the previous sections we have introduced a formalism for photon scattering from quantum emitters in a 1D waveguide, and elaborated on the non-Hermitian Hamiltonian that is central to the response of the emitters interacting with the incoming field. In the following sub-sections IV.A - IV.C we focus on, a number of paradigmatic physical situations that demonstrates the effectiveness of our formalism for solving photon scattering problems in waveguides. In this section we restrict ourselves to examples where the emitters have a single ground-state. In the next section we consider in detail an example of emitters with multiple ground-states. It is worth emphasizing that even the simple and generic examples of scattering that we treat here are in some cases rather tedious to solve with the existing methods. However, using our formalism we can immediately provide the solution to these problems. Note that for notational convenience, in all further discussion we will label the photons incoming from the left and moving to the right with subscript (R) and the photons moving to the left as (L), such that now $\zeta = \{\mathrm{R}, \mathrm{L}\}$.

2.4.1 A two-level emitter coupled to a one-dimensional waveguide

We first analyze the simplest possible system. We consider an emitter comprising two levels with a single optical transition between a ground level $|0\rangle$ and an excited level $|1\rangle$ as shown schematically in Fig. 2.2 (a). The emitter is located at a position z_0 along the axis of a 1D waveguide. The transition is coherently coupled to a waveguide. Such a system is generally described by a Hamiltonian $\hat{\mathcal{H}} = \hat{\mathcal{H}}_0 + \hat{\mathcal{V}}$ ($\hbar = 1$), where

$$\hat{\mathcal{H}}_0 = \omega_{11}\hat{\sigma}_{11} + \omega_{00}\hat{\sigma}_{00} + \hat{\mathcal{H}}_F. \tag{2.28}$$

$$\begin{aligned}\hat{\mathcal{V}} &= \hat{\mathcal{V}}_- + \hat{\mathcal{V}}_+, \\ &= \sum_\mu \mathcal{A}^\mu_{10}\hat{a}^\dagger_\mu\hat{\sigma}_{10} + \sum_\mu \mathcal{A}^{*\mu}_{01}\hat{a}_\mu\hat{\sigma}_{01}\end{aligned} \tag{2.29}$$

with the free-energy Hamiltonian $\hat{\mathcal{H}}_0$, and the Hamiltonian of the field being given by $\hat{\mathcal{H}}_F$, while the excitation (de-excitation) is represented by $\hat{\mathcal{V}}_+$ ($\hat{\mathcal{V}}_- = [\hat{\mathcal{V}}_+]^\dagger$). Here, ω_{11} and ω_{00} are the energies of levels $|1\rangle$ and $|0\rangle$, respectively. Furthermore, as above we have used the definition of the atomic operator $\hat{\sigma}_{ij} = |j\rangle\langle i|$ such that the density matrix is given by $\rho_{ij} = \langle\hat{\sigma}_{ij}\rangle$. The coupling strength of the emitter transition $|i\rangle \leftrightarrow |j\rangle$ to the field is given by $\mathcal{A}^\mu_{ij}$, with a_μ ($a^\dagger_\mu$) being the corresponding annihilation (creation) field-mode operator and $\mu = \{\zeta, s\}$. Here, $(\mu = s)$ signifies that $\mathcal{A}^s_{ij}$ is the coupling strength of the transition to modes outside the waveguide, while $(\mu = \zeta)$ represents the directional coupling to the 1D waveguide mode with strength $\mathcal{A}^\zeta_{ij,(1\mathrm{D})}$. For the rest of this example we drop the subscripts (i, j) from the coupling constants as it involves only a single transition. We can then write the non-Hermitian Hamiltonian for this system in the form $\hat{\mathcal{H}}_{nh} = \hat{\mathcal{H}}_0 - \frac{i}{2}\sum_k \hat{\mathcal{L}}^\dagger_k\hat{\mathcal{L}}_k$, where the Lindblad operators $\mathcal{L}_k$ are given by

$$\hat{\mathcal{L}}_s = \mathcal{A}^s\,\hat{\sigma}_{10} = \sqrt{\Gamma'}\,\hat{\sigma}_{10}, \tag{2.30}$$

$$\hat{\mathcal{L}}_{\zeta_{(1\mathrm{D})}} = \mathcal{A}^\zeta_{1\mathrm{D}}\,\hat{\sigma}_{10} = \sqrt{\Gamma^\zeta_{1\mathrm{D}}}\,\hat{\sigma}_{10}, \tag{2.31}$$

corresponding to decay out of (s) and into the waveguide (ζ). Note that in writing Eq. (2.30) we have used the definition of $\Gamma^\zeta_{1\mathrm{D}}$ from Eq. (2.22), and defined the rate of decay out of the waveguide as $\Gamma' = |\mathcal{A}^s|^2$. The non-Hermitian Hamiltonian can then be written similar to that

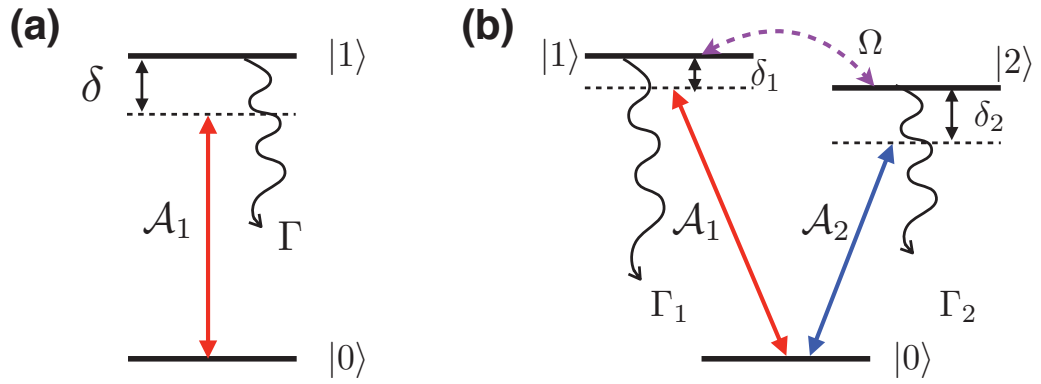

FIGURE 2.2: Schematic diagram of the energy level structure of emitters with (a) single optical transition (b) two optical transitions in V-configuration. Here $|0\rangle$ is the ground-stateand $|i = 1, 2\rangle$ the excited states of the emitter. The linewidth of the excited states is given by Γ's and the δ's are detuning of the transition with respect to the frequency of the incoming photon. The coupling strength of the transitions to the waveguide mode is given by $\mathcal{A}$'s.

in Eq. (2.26) as

$$\hat{\mathcal{H}}_{nh} = \left(\delta - \frac{i\Gamma}{2}\right)\hat{\sigma}_{11} \equiv \tilde{\delta}\hat{\sigma}_{11}, \tag{2.32}$$

where Γ is the total decay rate of the level $|1\rangle$ into $|0\rangle$ and is given by $\Gamma = \Gamma' + \sum_\zeta \Gamma^\zeta_{1D}$, while the detuning is $\delta = \omega_{11} - \omega_{00} - \omega$. Here ω is the frequency of the incoming field. Combining the decay with the detuning we then define $\tilde{\delta} = (\delta - i\Gamma/2)$ as the complex energy of the state $|1\rangle$. Inverting the $\langle 1|\hat{\mathcal{H}}_{nh}|1\rangle$ is then straightforward and we find

$$\hat{\mathcal{H}}^{-1}_{nh} = \tilde{\delta}^{-1}\hat{\sigma}_{11}, \tag{2.33}$$

For a single photon incident from left and propagating towards the right in the waveguide, Eq. (2.7) straightway gives the complete scattering dynamics of the photon from the two-level emitter. Let us write Eq. (2.7) in terms of the field-mode operators on the left and right of the emitter, after scattering of a photon as

$$\hat{a}_{\text{out,R}}(\mathrm{z}, t) = \left[1 + i\Gamma^{\mathrm{R}}_{1D}\tilde{\delta}^{-1}\hat{\sigma}_{00}\right]\hat{a}_{\text{in,R}}(\mathrm{z} - v_g t), \tag{2.34}$$

$$\hat{a}_{\text{out,L}}(\mathrm{z}', t) = i\left[\sqrt{\Gamma^{\mathrm{L}}_{1D}}\left(\tilde{\delta}^{-1}\right)\sqrt{\Gamma^{\mathrm{R}}_{1D}}\right]e^{2ik_0(\mathrm{z}_0 - \mathrm{z}')} \times \hat{\sigma}_{00}\hat{a}_{\text{in,R}}(\mathrm{z}' + v_g t), \tag{2.35}$$

where we have used that $(\hat{\mathcal{H}}_{nh})^{-1}_{11} = \tilde{\delta}^{-1}$ and $\mathrm{z}(\mathrm{z}')$ is the point of observation to the right (left) of the emitter spatially situated at z_0. Here $e^{2ik_0(\mathrm{z}_0 - \mathrm{z}')}$ is an additional phase that the reflected photon picks up as it propagates towards the left of the emitter. Note that in writing Eq. (2.34) and Eq. (2.35) we have neglected the noise term as we are mainly concerned with the photon click probability at a detector.

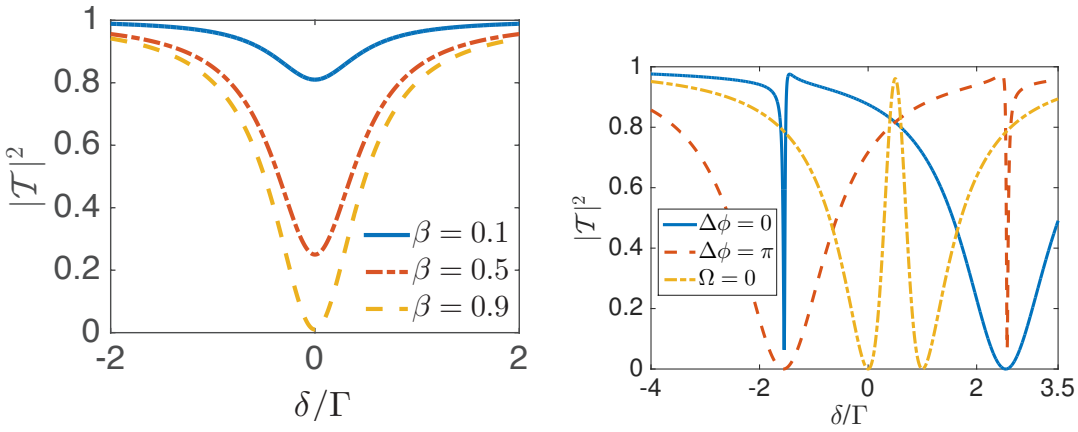

FIGURE 2.3: Transmitted intensity $|\mathcal{T}|^2 = |\langle \hat{a}^\dagger_{out,\mathrm{R}} \hat{a}_{out,\mathrm{R}} \rangle / \langle \hat{a}^\dagger_{in} \hat{a}_{in} \rangle|$ for a single (a) two-level emitter and, (b) three-level emitter in the V-configuration coupled to a 1D waveguide. For (a) we consider the parameters, $\delta = \omega_{11} - \omega_{00} - \omega$ and different values of β while for (b) we consider $\delta_1 = -\delta$, $\delta_2 = \Gamma - \delta$, $\beta = 0.99$, coupling $\Omega = 2\Gamma$ or 0, and we plot the results for $\Delta\phi = 0$ and $\Delta\phi = \pi$.

Substituting for $\tilde{\delta}$ and assuming that $\Gamma^{\mathrm{R}}_{1\mathrm{D}} = \Gamma^{\mathrm{L}}_{1\mathrm{D}} = \Gamma_{1\mathrm{D}}/2$, we get

$$\hat{a}_{\mathrm{out,R}}(\mathrm{z}, t) = \left[1 - \frac{\Gamma_{1\mathrm{D}}}{\Gamma + 2i\delta}\right] \hat{a}_{\mathrm{in,R}}(\mathrm{z} - v_g t), \tag{2.36}$$

$$\hat{a}_{\mathrm{out,L}}(\mathrm{z}', t) = -\frac{\Gamma_{1\mathrm{D}}}{\Gamma + 2i\delta} e^{2ik_0(\mathrm{z}_0 - \mathrm{z}')} \hat{a}_{\mathrm{in,R}}(\mathrm{z}' + v_g t), \tag{2.37}$$

where we have used that $\langle \hat{\sigma}_{00}(t) \rangle = \langle \hat{\sigma}_{00}(0) \rangle = 1$ for a emitter initially in the ground-state$|0\rangle$. We can do this because, once we eliminate the excited state the emitter can only be in the ground-state. For an emitter tuned into resonance ($\delta = 0$) we get the well-known results of photon scattering in waveguides, with transmission and reflection amplitudes of $(1 - \beta)$ and β, respectively [81], where $\beta = \Gamma_{1\mathrm{D}}/\Gamma$. This is illustrated in Fig. 2.3 (a) where we plot the transmitted intensity which shows a Lorentzian dip at resonance. The corresponding FWHM is found to be Γ. Thus, for a 1D waveguide with strong coupling to the emitter such that $\Gamma_{1\mathrm{D}} \sim \Gamma$, scattering leads to complete reflection of the photon with the atom behaving as a mirror [56, 81, 82].

2.4.2 A three-level emitter in V-configuration coupled to a one-dimensional waveguide

Above we considered the simplest possible situation which could also easily be solved by other means. We now consider a situation, where the result is less obvious. We choose an emitter in a V-configuration comprising a ground-state$|0\rangle$ and two excited states $|1\rangle$ and $|2\rangle$ located at some point z_0 in the waveguide (see Fig. 2.2 (b) for the schematic level structure). It is worth emphasizing that single photon scattering from such three-level emitters have been studied extensively in the past [58]. The purpose of addressing this problem here is to illustrate how the results of these previous works can be obtained directly with our method. To demonstrate the versatility of our approach, we assume that the exited states are coherently coupled by a (generally complex-valued) coupling Ω. This then corresponds to a nonzero $\left[(\tilde{\mathcal{H}}_{\mathrm{nh}})_{\mathrm{nw}}\right]_{ee'}$ contribution to the non-Hermitian Hamiltonian $\tilde{\mathcal{H}}_{\mathrm{nh}}$. Furthermore, we assume

that the transitions from $|0\rangle$ to $|1\rangle$ and $|0\rangle$ to $|2\rangle$ are coupled to the waveguide mode with strengths $\mathcal{A}^{\mu=\zeta}_{1,(1\mathrm{D})}$ and $\mathcal{A}^{\mu=\zeta}_{2,(1\mathrm{D})}$ and decay with a total decay rate of Γ_1 and Γ_2 respectively. The Hamiltonian of the system is then given by $\hat{\mathcal{H}} = \hat{\mathcal{H}}_0 + \hat{\mathcal{V}}$ ($\hbar = 1$) where,

$$\hat{\mathcal{H}}_0 = \sum_{j=0}^{2} \omega_{jj}\hat{\sigma}_{jj} + \Omega\hat{\sigma}_{12} + \Omega^*\hat{\sigma}_{21} + \hat{\mathcal{H}}_F \tag{2.38}$$

$$\hat{\mathcal{V}} = \sum_{j=1}^{2}\sum_{\mu}\left(\mathcal{A}_1^{\mu}\hat{\sigma}_{0j}\hat{a}_{\mu} + \mathcal{A}_1^{*\mu}\hat{a}_{\mu}^{\dagger}\,\hat{\sigma}_{j0}\right), \tag{2.39}$$

where as before we have defined $\hat{\sigma}_{ij} = |j\rangle\langle i|$.

The decay of the excited levels, $|1\rangle$ and $|2\rangle$ to modes other than the waveguide, is described by the Lindblad operators

$$\hat{\mathcal{L}}_{s,1} = \sqrt{\Gamma_1'}\hat{\sigma}_{10} \tag{2.40}$$

$$\hat{\mathcal{L}}_{s,2} = \sqrt{\Gamma_2'}\hat{\sigma}_{20} \tag{2.41}$$

with Γ_j' being the corresponding decay rate of the level $|j\rangle$. Note that as before, we have here used the relation $\Gamma_j' = |\mathcal{A}_j^{\mu=s}|^2$ to define the decay rates out of the waveguide. The Lindblad operator for decay into the waveguide is given by

$$\begin{aligned}\hat{\mathcal{L}}_{\zeta_{(1\mathrm{D})},1} &= e^{-i\phi_1}|\mathcal{A}^{\zeta}_{1,(1\mathrm{D})}|\,\hat{\sigma}_{10},\\ &= e^{-i\phi_1}\sqrt{\Gamma^{\zeta}_{1,1\mathrm{D}}}\,\hat{\sigma}_{10},\end{aligned} \tag{2.42}$$

$$\begin{aligned}\hat{\mathcal{L}}_{\zeta_{(1\mathrm{D})},2} &= e^{-i\phi_2}|\mathcal{A}^{\zeta}_{2,(1\mathrm{D})}|\,\hat{\sigma}_{20},\\ &= e^{-i\phi_2}\sqrt{\Gamma^{\zeta}_{2,1\mathrm{D}}}\,\hat{\sigma}_{20}\end{aligned} \tag{2.43}$$

In writing $\hat{\mathcal{L}}_{\zeta_{(1\mathrm{D})},1}$ and $\hat{\mathcal{L}}_{\zeta_{(1\mathrm{D})},2}$ in terms of the decay rates we have used the definition given in Eq. (2.22), and introduced the phases ϕ_1 and ϕ_2 of the two couplings.

Now following Eq. (2.24) - (2.25), we set up the non-Hermitian Hamiltonian

$$\hat{\mathcal{H}}_{\mathrm{nh}} = \tilde{\delta}_1\hat{\sigma}_{11} + \tilde{\delta}_2\hat{\sigma}_{22} + \mathcal{G}\hat{\sigma}_{12} + \mathcal{G}^*\hat{\sigma}_{21}, \tag{2.44}$$

where we define the complex detunings $\tilde{\delta}_j = \delta_j - i\Gamma_j/2$ with $\delta_j = \omega_{jj} - \omega_{00} - \omega$ and $\Gamma_j = \Gamma_j' + \sum_\zeta \Gamma^{\zeta}_{j,1\mathrm{D}}$, being the total line width of the excited state $|j\rangle$. Using Eq. (2.23) and Eq. (2.25) we can write a combined coupling term $\mathcal{G} = |\Omega|e^{i\theta} - i\sum_\zeta\sqrt{\Gamma^{\zeta}_{1,1\mathrm{D}}\Gamma^{\zeta}_{2,1\mathrm{D}}}e^{i(\phi_1-\phi_2)}$. Note that due to the characteristic of the $\Gamma_{1\mathrm{D}}$ coupling, the complex conjugation of the combined coupling gives $\tilde{\mathcal{G}} = |\Omega|e^{-i\theta} - i\sum_\zeta\sqrt{\Gamma^{\zeta}_{1,1\mathrm{D}}\Gamma^{\zeta}_{2,1\mathrm{D}}}e^{-i(\phi_1-\phi_2)}$. Inversion of the non-Hermitian Hamiltonian in Eq. (2.44) then yields

$$\hat{\mathcal{H}}_{\mathrm{nh}}^{-1} = \tilde{\delta}^{-1}_{1,\mathrm{eff}}\hat{\sigma}_{11} + \tilde{\delta}^{-1}_{2,\mathrm{eff}}\hat{\sigma}_{22} + \tilde{\mathcal{G}}^{-1}_{\mathrm{eff}}\hat{\sigma}_{12} + \tilde{\mathcal{G}}'_{\mathrm{eff}}\hat{\sigma}_{21}, \tag{2.45}$$

Here, we have written the inverse non-Hermitian Hamiltonian in terms of "effective" detunings and couplings

$$\tilde{\delta}_{j,\mathrm{eff}} = \tilde{\delta}_j - \frac{\mathcal{G}\tilde{\mathcal{G}}}{\tilde{\delta}_k} \tag{2.46}$$

$$\tilde{\mathcal{G}}_{\mathrm{eff}} = \frac{\mathcal{G}\tilde{\mathcal{G}} - \tilde{\delta}_1\tilde{\delta}_2}{\mathcal{G}}, \tag{2.47}$$

$$\tilde{\mathcal{G}}'_{\mathrm{eff}} = \frac{\tilde{\mathcal{G}}\mathcal{G} - \tilde{\delta}_1^*\tilde{\delta}_2^*}{\tilde{\mathcal{G}}}, \tag{2.48}$$

which depend both on the complex detunings of the excited states and on their couplings. The implications of these assignments will become more clear in the following.

We first determine the output field using Eq. (2.7) at some spatial location z to the right of the emitter,

$$\begin{aligned}\hat{a}_{\mathrm{out,R}}(\mathrm{z},t) = \Bigg[1 + i\Bigg\{ &\left(\Gamma^{\mathrm{R}}_{1,1\mathrm{D}}\right)\tilde{\delta}^{-1}_{1,\mathrm{eff}} + \left(\Gamma^{\mathrm{R}}_{2,1\mathrm{D}}\right)\tilde{\delta}^{-1}_{2,\mathrm{eff}} \\ &+ \sqrt{\Gamma^{\mathrm{R}}_{1,1\mathrm{D}}}(\tilde{\mathcal{G}}^{-1}_{\mathrm{eff}})\sqrt{\Gamma^{\mathrm{R}}_{2,1\mathrm{D}}}e^{-i(\phi_1-\phi_2)} \\ &+ \sqrt{\Gamma^{\mathrm{R}}_{2,1\mathrm{D}}}(\tilde{\mathcal{G}}'^{-1}_{\mathrm{eff}})\sqrt{\Gamma^{\mathrm{R}}_{1,1\mathrm{D}}}e^{i(\phi_1-\phi_2)}\Bigg\}\hat{\sigma}_{00}\Bigg] \\ &\times \hat{a}_{\mathrm{in,R}}(\mathrm{z} - v_{\mathrm{R}}t),\end{aligned} \tag{2.49}$$

while the output field to the left of the emitter at some spatial location z′ is

$$\begin{aligned}\hat{a}_{\mathrm{out,L}}(\mathrm{z}',t) = i\Bigg[&\sqrt{\Gamma^{\mathrm{L}}_{1,1\mathrm{D}}}\tilde{\delta}^{-1}_{1,\mathrm{eff}}\sqrt{\Gamma^{\mathrm{R}}_{1,1\mathrm{D}}} + \sqrt{\Gamma^{\mathrm{L}}_{2,1\mathrm{D}}} \\ &\times \tilde{\delta}^{-1}_{2,\mathrm{eff}}\sqrt{\Gamma^{\mathrm{R}}_{2,1\mathrm{D}}} + \sqrt{\Gamma^{\mathrm{L}}_{1,1\mathrm{D}}}(\tilde{\mathcal{G}}^{-1}_{\mathrm{eff}})\sqrt{\Gamma^{\mathrm{R}}_{2,1\mathrm{D}}} \\ &\times e^{-i(\phi_1-\phi_2)} + \sqrt{\Gamma^{\mathrm{L}}_{2,1\mathrm{D}}}(\tilde{\mathcal{G}}'^{-1}_{\mathrm{eff}})\sqrt{\Gamma^{\mathrm{R}}_{1,1\mathrm{D}}}e^{i(\phi_1-\phi_2)}\Bigg] \\ &\times \hat{\sigma}_{00}e^{2ik_0(\mathrm{z}_0-\mathrm{z}')}\hat{a}_{\mathrm{in,R}}(\mathrm{z}' + v_{\mathrm{L}}t).\end{aligned} \tag{2.50}$$

Finding the photon scattering dynamics from even this relatively simple multi-level system is quite cumbersome, due to the complicated interplay of detunings and couplings. However, as can be seen from Eqs. (2.49) and (2.50), using the developed photon scattering formalism, we can straightaway provide a solution to even the general case in the limit of a single-photon/weak-field inputs. This is the key advantage of our formalism compared to many of the existing approaches [31, 34, 61–63, 65–67, 72].

From the above expressions we can see that the scattering amplitude strongly depends on the effective detunings $\tilde{\delta}_{\mathrm{eff}}$ and the coupling $\tilde{\mathcal{G}}_{\mathrm{eff}}$. Hence adjusting the quantities that appear in it, e.g., the coupling strength $\mathcal{G}$ between the excited states, it is possible to engineer this term to yield qualitatively different results. Thus one can invoke several different situations involving the emitter-waveguide coupling and the coupling between the excited states to analyze the behaviour of the output field further. To illustrate the dynamics, we restrict ourselves to the situation where the coupling is the same in both directions and the two-levels have the same decay rate. Thus, we consider $\Gamma^{\mathrm{R/L}}_{1,1\mathrm{D}} = \Gamma^{\mathrm{R/L}}_{2,1\mathrm{D}} = \Gamma_{1\mathrm{D}}/2$ in Eqs. (2.49) and (2.50). On eliminating the excited states the emitter can only be in the ground-state and hence for all later time $\langle\sigma_{00}\rangle = 1$. The output field at the right and left of the emitter is then given

by

$$\begin{aligned}\hat{a}_{\text{out,R}}(\mathrm{z},t) &= \left[1+\frac{i\Gamma_{1\mathrm{D}}}{2}\left(\frac{\tilde{\delta}+i\Gamma_{1\mathrm{D}}-2|\Omega|\cos\Delta\phi}{\tilde{\delta}_1\tilde{\delta}_2-\mathcal{G}\tilde{\mathcal{G}}}\right)\right]\\ &\times\ \hat{a}_{\text{in,R}},\\ \hat{a}_{\text{out,L}}(\mathrm{z}',t) &= \frac{i|\Gamma_{1\mathrm{D}}|}{2}\left(\frac{\tilde{\delta}+i\Gamma_{1\mathrm{D}}-2|\Omega|\cos\Delta\phi}{\tilde{\delta}_1\tilde{\delta}_2-\mathcal{G}\tilde{\mathcal{G}}}\right)\\ &\times\ e^{2ik(\mathrm{z}_0-\mathrm{z}')}\hat{a}_{\text{in,R}}(\mathrm{z}'+v_g t),\end{aligned} \tag{2.51}$$

where $\tilde{\delta}=\tilde{\delta}_1+\tilde{\delta}_2$ and, $\Delta\phi=\theta-(\phi_1-\phi_2)$. We note here that the appearance of $\Delta\phi$ in these equations is a consequence of interferences between the different paths in Fig. 2.2 (b). For instance level $|2\rangle$ can be reached by two different paths: either from direct excitation or through excitation to level $|1\rangle$ followed by transfer to level $|2\rangle$ by the coupling Ω. These two paths interfere leading to the expressions above.

From Eqs. (2.51) we see that by satisfying the condition $\tilde{\delta}=i\Gamma_{1\mathrm{D}}-2|\Omega|\cos\Delta\phi$, the emitter can be made transparent to the incoming photon. This can be achieved by varying the phase and amplitude of the coherent coupling Ω which for example can be a magnetic field. We illustrate this in Fig. 2.3 (b), where we vary the drive phase ϕ and coupling Ω for fixed emitter parameters. Note that for the plot in Fig. 2.3 (b), we have assumed that the coupling strength of both the optical transitions are real. We also find that complete reflection from the emitter can occur under the condition $\delta_1=\delta_2=0$, provided there is no loss to the outside of the waveguide and $\Gamma_{1\mathrm{D}}\gg\Omega$. Thus we see that a three-level V system can be made to selectively transmit or reflect a single photon thereby operating as a single-photon switch as required for transistors [83–86].

2.4.3 Scattering from multiple emitters coupled to a one-dimensional waveguide

We next discuss the application of our photon scattering formalism to the case of multiple emitters coupled via the waveguide mode. We assume multi-level emitters to illustrate the full potential of our formalism. This problem is much more complicated in comparison to the ones we have discussed in the previous subsections. It however also contains rich physics due to quantum interference among various pathways of excitation and de-excitation. Additionally, it is also a prominent test bed for various interesting problems in quantum information sciences based on waveguide QED [44]. As an example one can consider generation of entanglement between emitters over long distances via waveguide-mediated photons [87]. Presently, established methods for solving such photon-scattering problem in multi-emitters system requires, setting up of a reduced master equation for the system and then performing numerical simulation to achieve the scattering amplitudes. In comparison, as will be shown in the following, one can find the scattering amplitudes directly using our photon scattering formalism.

We begin our discussion with an example of two emitters coupled to a 1D mode of an optical waveguide. We label the two emitters as $\{A,B\}$ and consider them to be located at the spatial positions z_A and z_B respectively along the waveguide as shown schematically in Fig. 2.4. The waveguide is assumed to be double-sided and we consider the input field (incident single-photon/weak coherent pulse) to be incident from the left and propagating to the right in the waveguide. We assume emitter A to be a two-level system while emitter B is a three-level V-type system, spaced $\Delta\mathrm{z}=\mathrm{z}_B-\mathrm{z}_A$ apart. Emitter A has ground-state$|g_A\rangle$ and excited state $|e_A\rangle$, whereas the three-level system B consists of a single ground-state $|g_B\rangle$ and two excited states $|e_{1B}\rangle$ and $|e_{2B}\rangle$, coherently coupled at a rate Ω (for example with

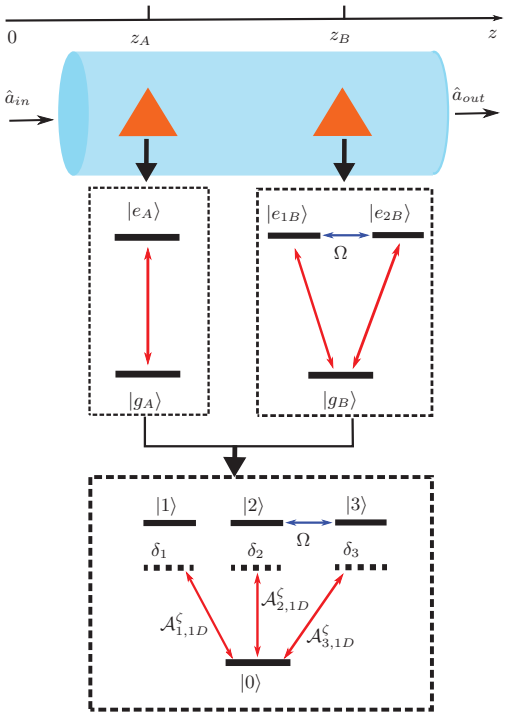

FIGURE 2.4: Two emitters in a waveguide (top) with individual level structures (center), and combined level structure in the single-excitation limit (bottom).

a magnetic field. For simplicity, we assume from now on that $\Omega = |\Omega|$ is real). The free Hamiltonian of this two-emitter system can be described as ($\hbar = 1$)

$$\begin{aligned}
\hat{\mathcal{H}}_0 &= \hat{\mathcal{H}}_{A_0} + \hat{\mathcal{H}}_{B_0} + \hat{\mathcal{H}}_F && (2.52)\\
\hat{\mathcal{H}}_{A_0} &= \omega_{e,A}\hat{\sigma}^A_{ee} + \omega_{g,A}\hat{\sigma}^A_{gg} && (2.53)\\
\hat{\mathcal{H}}_{B_0} &= \omega_{g,B}\hat{\sigma}^B_{gg} + \omega_{e1,B}\hat{\sigma}^B_{e_1e_1} + \omega_{e2,B}\hat{\sigma}^B_{e_2e_2}\\
&+ \Omega\left(\hat{\sigma}^B_{e_1e_2} + \hat{\sigma}^B_{e_2e_1}\right), && (2.54)
\end{aligned}$$

where ω_i's are the free energies of the corresponding levels, $\hat{\mathcal{H}}_F$ is the standard free-field Hamiltonian and the atomic operators as before are defined by $\sigma_{ij} = |j\rangle\langle i|$.

Our procedure is formulated in terms of the combined level structure of the emitters with one ground-state$|0\rangle \equiv |g_A, g_B\rangle$ and three excited states $|1\rangle \equiv |e_A, g_B\rangle$, $|2\rangle \equiv |g_A, e_{1B}\rangle$ and $|3\rangle \equiv |g_A, e_{2B}\rangle$ corresponding to a single excitation in either of the emitters as shown in Fig. 2.4. In the combined basis we assume that the transitions from the ground levels to the excited levels $|1\rangle$, $|2\rangle$ and $|3\rangle$ are detuned from the incoming photon's frequency ω by δ_1, δ_2, and δ_3 respectively.

The interaction Hamiltonian $\hat{\mathcal{V}}$ describing the interaction of emitters with the photons in the combined basis $\{|0\rangle, |1\rangle, |2\rangle, |3\rangle\}$ is given by

$$\begin{aligned}
\hat{\mathcal{V}} &= \sum_{\mu} \mathcal{A}^{\mu}_{1,(1D)} e^{ik_\mu z_A}(\hat{a}^\dagger_\mu|0\rangle\langle 1| + |1\rangle\langle 0|\hat{a}_\mu)\\
&+ \sum_{j=2}^{3}\sum_{\mu} e^{ik_\mu z_B}\mathcal{A}^{\mu}_{j,(1D)}(\hat{\sigma}_{0j}\hat{a}_\mu + \hat{a}^\dagger_\mu\hat{\sigma}_{j0}) && (2.55)
\end{aligned}$$

where the dipole transitions between the states $|j\rangle (j = 1, 2, 3)$ and $|0\rangle$ are coupled to the waveguide mode with strengths $\mathcal{A}^{\zeta}_{j,(1\mathrm{D})}$ respectively. We assume these couplings have no additional phase (such that $\mathcal{A}^{\zeta}_{j,(1\mathrm{D})}$ is real-valued) apart from the phase contribution originating from the distinct positions of the emitters in the waveguide, $e^{ik_0 z_{A/B}}$. As a result of these phases the incoming field couples to emitter B with an additional phase $e^{ik_0(\mathrm{z}_B - \mathrm{z}_A)}$ relative to the field at position z_A. Ignoring an overall phase, we from this point assume emitter A as the reference point $\mathrm{z}_A = 0$ and as such $\mathrm{z}_B = \Delta\mathrm{z}$. Note that, in writing Eq. (2.55) we have assumed that the spatial separation of the emitters $\Delta\mathrm{z}$ is much larger than the wavelength λ of the incoming photon. We have therefore ignored the possibility of any direct interaction (like dipole-dipole) between the emitters and focus only on the waveguide-mediated interaction. We do, however, explicitly include such direct interaction and discuss their influence on the emitter dynamics towards the end of this section.

The Hamiltonian of the combined system can then be written as $\hat{\mathcal{H}} = \hat{\mathcal{H}}_0 + \hat{\mathcal{V}}$, where now

$$\hat{\mathcal{H}}_0 = \sum_{i=0}^{3} \omega_{ii} |i\rangle\langle i| + \Omega \left(\hat{\sigma}_{23} + \hat{\sigma}_{32}\right) + \hat{\mathcal{H}}_F. \tag{2.56}$$

Based on this full Hamiltonian $\mathcal{H}$, we next wish to construct the excited-subspace Hamiltonian $\tilde{\mathcal{H}}_{\mathrm{nh}}$ similar to Eq. (2.25) in the basis $(|1\rangle, |2\rangle, |3\rangle)$. For this purpose we need to consider the decays of the excited state, which in this case is represented by the Lindblad operators

$$\hat{\mathcal{L}}_{s_j} = \sqrt{\Gamma'_j}\, \hat{\sigma}_{j0} \tag{2.57}$$

$$\hat{\mathcal{L}}_{\zeta_{(1\mathrm{D})},j} = \sqrt{\Gamma^{\zeta}_{j,1\mathrm{D}}}\, \hat{\sigma}_{j0}, \tag{2.58}$$

where as before Γ'_j is the decay rate of state $|j\rangle$ out of the waveguide, while $\Gamma^{\zeta}_{j,1\mathrm{D}}$ is the decay rate into the waveguide along the direction ζ. Note that, in writing the expression of $\hat{\mathcal{L}}_{\zeta_{(1\mathrm{D})},j}$ we have used the definition in Eq. (2.22).

Taking into consideration all of these terms the diagonal part of the non-Hermitian Hamiltonian becomes

$$(\hat{\tilde{\mathcal{H}}}_{\mathrm{nh}})_d = \sum_{j=1}^{3} \tilde{\delta}_j \hat{\sigma}_{jj} \tag{2.59}$$

where the complex detuning $\tilde{\delta}_j = \delta_j - \frac{i\Gamma_j}{2}$, with $\Gamma_j = \Gamma_{j,1\mathrm{D}} + \Gamma'_j$ being the total decay rate of transition $|j\rangle \to |0\rangle$. Here the decay into the waveguide is defined as before $\Gamma_{j,1\mathrm{D}} = \sum_{\zeta} \Gamma^{\zeta}_{j,1\mathrm{D}}$. The detuning is defined as $\delta_j = (\omega_{jj} - \omega_{00} - \omega)$, where ω is the central frequency of the incoming photon.

We next construct the off-diagonal part of the non-Hermitian Hamiltonian of the combined system $\hat{\tilde{\mathcal{H}}}_{\mathrm{nh}}$. To simplify this Hamiltonian we make an assumption about the nature of coupling between the emitters and the waveguide mode. We assume that the coupling strengths are the same along both the propagation directions, i.e., $\mathcal{A}^{(R)}_{j,(1\mathrm{D})} = \mathcal{A}^{(L)}_{j,(1\mathrm{D})} = \mathcal{A}_{j,(1\mathrm{D})}$. Using Eq. (2.23) and Eq. (2.25) we then find that the off-diagonal elements of

$\hat{\tilde{\mathcal{H}}}_{\rm nh}$ consist of the waveguide-mediated interaction terms of the form,

$$\begin{aligned}(\hat{\tilde{\mathcal{H}}}_{\rm nh})_{\rm w} &= -\frac{i}{2}\sqrt{\Gamma_{1,1D}\Gamma_{2,1D}}e^{ik\Delta z}(\hat{\sigma}_{21}+\hat{\sigma}_{12}) \\ &\quad -\frac{i}{2}\sqrt{\Gamma_{1,1D}\Gamma_{3,1D}}e^{ik\Delta z}(\hat{\sigma}_{31}+\hat{\sigma}_{13}) \\ &\quad -\frac{i}{2}\sqrt{\Gamma_{2,1D}\Gamma_{3,1D}}(\hat{\sigma}_{32}+\hat{\sigma}_{23}) \end{aligned} \tag{2.60}$$

and the non-waveguide couplings, which in this case is just the coherent coupling Ω

$$(\hat{\tilde{\mathcal{H}}}_{\rm nh})_{\rm nw} = \frac{\Omega}{2}\left(\hat{\sigma}_{23}+\hat{\sigma}_{32}\right). \tag{2.61}$$

Note that in writing Eq. (2.60) we have used the definition of $\Gamma_{j,1D}$ in terms of the coupling strengths from Eq. (2.22). Finally, we arrive at the non-Hermitian Hamiltonian

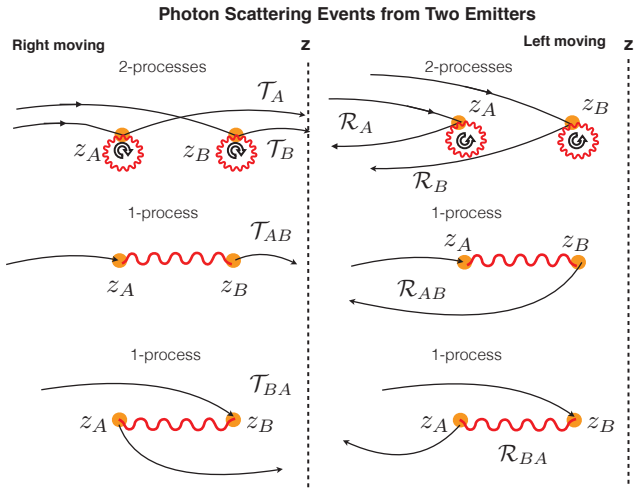

FIGURE 2.5: Schematic of light scattering from two generic emitters located at the position z_A and z_B in a double-sided waveguide with a right-going input photon pulse . Here $\mathcal{T}_i$ and $\mathcal{R}_i$ signifies the single emitter transmitted and reflected amplitudes respectively. Amplitude for transmitted and reflected light for scattering involving two emitters are on the other hand given by $\mathcal{T}_{ij}$ and $\mathcal{R}_{ij}$, respectively. The wiggly lines signify field-mediated interactions between the emitters in terms of the non-Hermitian Hamiltonian $\tilde{\mathcal{H}}_{\rm nh}$ as discussed in the text. The wiggly circles with arrows inside symbolizes the scattering event.

$$\tilde{\mathcal{H}}_{\rm nh} = \begin{pmatrix} \tilde{\delta}_1 & -\frac{i}{2}\Gamma_{12} & -\frac{i}{2}\Gamma_{13} \\ -\frac{i}{2}\Gamma_{12} & \tilde{\delta}_2 & (\frac{\Omega}{2}-\frac{i}{2}\Gamma_{23}) \\ -\frac{i}{2}\Gamma_{13} & (\frac{\Omega}{2}-\frac{i}{2}\Gamma_{23}) & \tilde{\delta}_3 \end{pmatrix}, \tag{2.62}$$

in the excited subspace defined by the basis $(|1\rangle, |2\rangle, |3\rangle)$. Here we have defined complex couplings $\Gamma_{12} = \sqrt{\Gamma_{1,1D}\Gamma_{2,1D}}e^{ik\Delta z}$, $\Gamma_{13} = \sqrt{\Gamma_{1,1D}\Gamma_{3,1D}}e^{ik\Delta z}$ and $\Gamma_{23} = \sqrt{\Gamma_{2,1D}\Gamma_{3,1D}}$. Next, on taking inverse of Eq. (2.62) we get

$$[\tilde{\mathcal{H}}_{\rm nh}]^{-1} = \begin{pmatrix} \delta^{-1}_{1,\rm eff} & \Gamma^{-1}_{12,\rm eff} & \Gamma^{-1}_{13,\rm eff} \\ \Gamma^{-1}_{12,\rm eff} & \delta^{-1}_{2,\rm eff} & \Gamma^{-1}_{23,\rm eff} \\ \Gamma^{-1}_{13,\rm eff} & \Gamma^{-1}_{23,\rm eff} & \delta^{-1}_{3,\rm eff} \end{pmatrix} \tag{2.63}$$

where the effective detunings and couplings are defined in Appendix C.

We next study the scattering of a single-photon pulse. In Fig. 2.5 we sketch the different possible scattering processes involved for a two-emitter system. As can be seen from Fig. 2.5 there are several processes to account for. Our formalism, however, is well equipped to handle such complications and the photon-scattering relation stated in Eq. (2.7) can straightaway give the solution to this scattering problem. Conveniently the multiple scattering pathways can be simply written as a matrix multiplication between the vectors $\mathcal{V}_{\pm}$ and the matrix $\tilde{\mathcal{H}}_{\rm nh}^{-1}$. If we come with a right-going input field from the left, the total outgoing field to the right of the emitters is then following Eq. (2.7), given by

$$\begin{aligned}\hat{a}_{out,\mathrm{R}}(\mathrm{z},t) &= \Big[1+i\Big(\mathcal{T}_A+\mathcal{T}_B+\mathcal{T}_{AB,12}+\mathcal{T}_{BA,12}\\ &+ \mathcal{T}_{AB,13}+\mathcal{T}_{BA,13}\Big)\hat{\sigma}_{00}\Big]\hat{a}_{in,R}(\mathrm{z}-v_g t),\end{aligned} \tag{2.64}$$

where we have divided all possible scattering pathways into separate parts with their respective transition amplitudes $\mathcal{T}$. These are expressed using the elements of the non-Hermitian Hamiltonian in Eq. (2.63), and are given by

$$\begin{aligned}\mathcal{T}_A &= \frac{\Gamma_{1,1\mathrm{D}}}{2\delta_{1,\mathrm{eff}}},\\ \mathcal{T}_B &= \frac{\Gamma_{2,1\mathrm{D}}}{2\delta_{2,\mathrm{eff}}}+\frac{\Gamma_{3,1\mathrm{D}}}{2\delta_{3,\mathrm{eff}}}+\frac{\sqrt{\Gamma_{2,1\mathrm{D}}\Gamma_{3,1\mathrm{D}}}}{\Gamma_{23,\mathrm{eff}}},\\ \mathcal{T}_{AB,12}+\mathcal{T}_{BA,12} &= \frac{\sqrt{\Gamma_{1,1\mathrm{D}}\Gamma_{2,1\mathrm{D}}}}{\Gamma_{12,\mathrm{eff}}}\cos(k_0\Delta\mathrm{z}),\\ \mathcal{T}_{AB,13}+\mathcal{T}_{BA,13} &= \frac{\sqrt{\Gamma_{1,1\mathrm{D}}\Gamma_{3,1\mathrm{D}}}}{\Gamma_{13,\mathrm{eff}}}\cos(k_0\Delta\mathrm{z}).\end{aligned} \tag{2.65}$$

Note that in writing Eq. (2.64) we have neglected the noise as the photon at output is typically detected in photodetectors where the noise owing to vacuum does not contribute. From Eqs. (2.64) and (2.65), we find that owing to the scattering from the two emitters the amplitudes now contain some interference terms $\cos(k_0\Delta\mathrm{z})$ depending on the emitter separation.

To investigate the characteristic of the outgoing field further, we below consider some specific cases with respect to the emitter configurations and couplings. We assume that initially both the emitters are in their ground-states. Similar to above we can then replace the ground-state operator $\hat{\sigma}_{00}$ by $\langle\hat{\sigma}_{00}\rangle = 1$, since the combined system only has a single ground-state after elimination of the excited states.

Two Two-Level emitters

As a first example let us consider emitter B to behave effectively as a two-level system. This can happen if the transition $|3\rangle \to |0\rangle$ does not couple to the waveguide mode such that $\Gamma_{3,1\mathrm{D}} = 0$ and $|3\rangle$ also does not couple coherently to any other level of emitter B, i.e., $\Omega = 0$. Then, the total right-going output field for a single right-going input field coming from the left is reduced to

$$\hat{a}_{out,\mathrm{R}}(\mathrm{z},t) = \Big[1+i\Big(\frac{\Gamma_{1,1\mathrm{D}}}{2\delta_{1,\mathrm{eff}}}+\frac{\Gamma_{2,1\mathrm{D}}}{2\delta_{2,\mathrm{eff}}}+\frac{\sqrt{\Gamma_{1,1\mathrm{D}}\Gamma_{2,1\mathrm{D}}}}{\Gamma_{12,\mathrm{eff}}}\cos(k\Delta\mathrm{z})\Big)\Big]\hat{a}_{in,\mathrm{R}}(\mathrm{z}-v_g t), \tag{2.66}$$

while the reflected field is given by

$$\hat{a}_{out,\mathrm{L}}(\mathrm{z}',t) = i\Big[\frac{\Gamma_{1,1\mathrm{D}}}{2\delta_{1,\mathrm{eff}}}e^{2ik(\mathrm{z}_A-\mathrm{z})} + \frac{\Gamma_{2,1\mathrm{D}}}{2\delta_{2,\mathrm{eff}}}e^{2ik(\mathrm{z}_B-\mathrm{z})} + \frac{\sqrt{\Gamma_{1,1\mathrm{D}}\Gamma_{2,1\mathrm{D}}}}{\Gamma_{12,\mathrm{eff}}}\cos(k\Delta\mathrm{z})\Big]\hat{a}_{in,\mathrm{R}}(\mathrm{z}'+v_g t). \quad (2.67)$$

If we next assume that the emitters are identical, i.e., $\Gamma_{i,1\mathrm{D}} = \Gamma_{1\mathrm{D}}$, $\Gamma_1 = \Gamma_2 \equiv \Gamma_{1\mathrm{D}} + \Gamma'$ and $\delta_1 = \delta_2 \equiv \delta$, we can after some simplifications find the transmitted output field to be,

$$\begin{aligned}\hat{a}_{out,\mathrm{R}} &= \left[1 - \frac{2\Gamma_{1\mathrm{D}} + (1-e^{2ik\Delta\mathrm{z}})\frac{\Gamma_{1\mathrm{D}}^2}{(\Gamma'+2i\delta)}}{(\Gamma'+2\Gamma_{1\mathrm{D}}+2i\delta) + (1-e^{2ik\Delta\mathrm{z}})\frac{\Gamma_{1\mathrm{D}}^2}{(\Gamma'+2i\delta)}}\right] \\ &\quad\times\hat{a}_{in,\mathrm{R}}(\mathrm{z}-v_g t). \end{aligned} \quad (2.68)$$

The transmission spectrum evaluated from Eq. (2.68) can be shown to be similar to that of a cavity of length $L = \Delta\mathrm{z} = (\mathrm{z}_B - \mathrm{z}_A)$. Furthermore, for $\Delta\mathrm{z} = q\lambda/2$, where λ is the wavelength of the incoming photon and q is an integer, the transmitted amplitude is given by

$$\hat{a}_{out,\mathrm{R}} = \left[1 - \frac{2\Gamma_{1\mathrm{D}}}{\Gamma'+2\Gamma_{1\mathrm{D}}+2i\delta}\right]\hat{a}_{in,\mathrm{R}} \quad (2.69)$$

From the above expression it is clearly visible that the system of two emitters become perfectly reflective at resonance and for $\Gamma' = 0$. The transmission spectrum then has a Lorentzian window with a width twice that of a single two-level system, due to the effective enhancement of $\Gamma_{1\mathrm{D}}$ as compared to Eq. (2.36) for a single two-level emitter. We find that the emitter system thus behaves as an 'atomic mirror' with $N_A = 2$. This problem was also investigated both in the Markovian and non-Markovian regime in Ref. [62, 88] where the phenomenon of an atomic mirror was reported for multiple emitters. We immediately obtain the same result as [62] by our formalism, thus exhibiting the strength and simplicity of it.

Additionally, one finds that for emitter spacings close to $\sin(k\Delta\mathrm{z}) \approx 0$, the spectrum contains an ultra-narrow transparency window at $\delta \approx \frac{\Gamma_{1\mathrm{D}}}{2}\sin(k\Delta\mathrm{z})$. Thus, the system moves away from behaving like a mirror with minor change in $\Delta\mathrm{z}$ about $\Delta\mathrm{z} = n\lambda/2$. This can be understood from the fact that the dark state, which was in resonance with the bright state, gets shifted by δ and starts to couple to light. We find that the FWHM of the resonance line due to the dark state is now given by $\Gamma_{1\mathrm{D}}\sin^2(k\Delta z)/2$. Note that in principle this could be used to transform the waveguide-emitter system into a narrow frequency filter that selectively allow photons to pass through for suitable separation distance between the emitters. The change in the separation can be introduced via external control, for example by moving atoms trapped near a waveguide.

Alternatively, for $\Delta\mathrm{z} = (2q+1)\lambda/4$, the transmitted amplitude becomes

$$\begin{aligned}\hat{a}_{out,\mathrm{R}} &= \frac{(\Gamma'+2i\delta)^2}{(\Gamma'+2i\delta)^2 + 2\Gamma_{1\mathrm{D}}(\Gamma'+2i\delta+\Gamma_{1\mathrm{D}})} \\ &\times \hat{a}_{in,\mathrm{R}}(\mathrm{z}-v_g t). \end{aligned} \quad (2.70)$$

In this case one finds that the transmission spectrum for $\Gamma' = 0$ has a window at resonance with a width $\sqrt{2}\Gamma_{1\mathrm{D}}$.

In Fig. 2.6 (a) using Eq. (2.68) we show the transmitted intensity for the two-emitter system as a function of the detuning. In Fig. 2.6 (b) we show the transmitted intensity for the two-emitter system for varying spacings of the emitters. The transmission resonances arise from the fact that the dark state starts to resonantly couple to the light field.

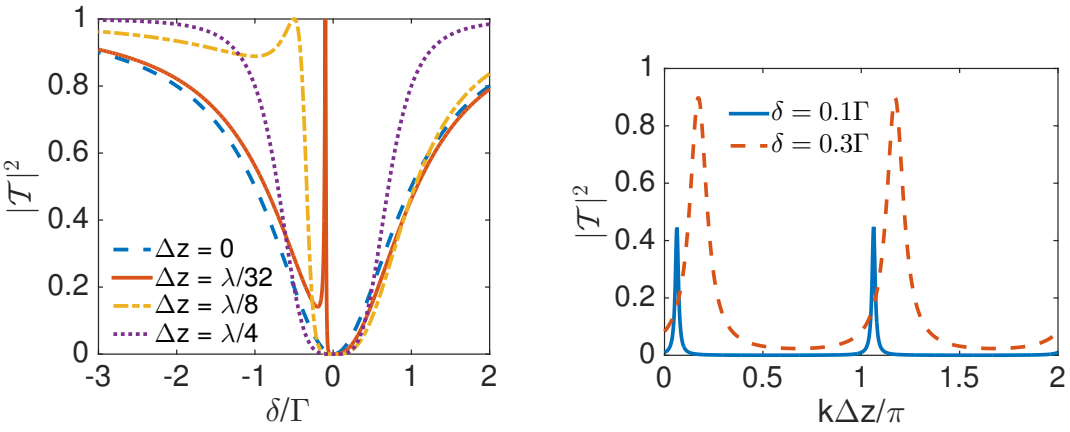

FIGURE 2.6: Transmission $|\mathcal{T}|^2 = |\langle \hat{a}^\dagger_{out,R}\hat{a}_{out,R}\rangle / \langle \hat{a}^\dagger_{in}\hat{a}_{in}\rangle|$ for two two-level emitters coupled to a 1D waveguide. The parameters used for the plots are (a) $\beta = 1$ and comparing four different values of the phase distance $k\Delta z$, (b) transmission as a function of the phase distance $k\Delta z$ for $\delta_1 = \delta_2 = \delta = 0.1\Gamma$ and 0.3Γ, $\beta = 0.99$..

In the above discussion, we have only considered interactions between the emitters mediated by the waveguide. In the following, we address the question of closely spaced emitters interacting with each other via their dipolar fields. For $\Delta z \leq \lambda$, there is strong dipole-dipole interaction between the emitters [55, 89–93] and the off-diagonal term in the non-Hermitian Hamiltonian of Eq. (2.63) is thus modified. In addition to the waveguide-mediated coupling, these terms will have contributions from the direct dipole-dipole interactions $\mathcal{V}_{AB}(\mathcal{V}_{BA})$ between the optical transitions of the emitters along with collective decays Γ'_c to the outside. In the limit of very small separation, where we can neglect the phase difference from propagation, the two-emitter system in the single-excitation regime effectively reduces to a single three-level system with dynamics similar to that discussed before in Sec. IV.A. Here the effective V-configuration is realized by defining a symmetric and anti-symmetric state which are the eigen-basis of the dipole-coupling Hamiltonian. Here we shall consider how this situation emerges from the single excitation subspace spanned by the basis $\{|e_A, g_B\rangle, |g_A, e_B\rangle\}$ of the emitters A and B. As such, the subscripts 1 and 2 in Eq. (2.62) in the previous case are now replaced with A and B respectively. The non-Hermitian Hamiltonian then becomes

$$\mathcal{H}_{\text{nh}} = \begin{bmatrix} \tilde{\delta}_A & \mathcal{V}_{AB} - \frac{i}{2}\sqrt{\Gamma_{A,1D}\Gamma_{B,1D}} \\ \mathcal{V}_{BA} - \frac{i}{2}\sqrt{\Gamma_{A,1D}\Gamma_{B,1D}} & \tilde{\delta}_B \end{bmatrix} \tag{2.71}$$

where compared to Eq. (2.62) we now have an extra off-diagonal elements describing the direct dipole-dipole interaction between the two closely separated emitters. As before we define the complex detuning $\tilde{\delta}_j = (\delta_j - \frac{i}{2}\Gamma_j)$ with $(j = A, B)$ and the total decay rate of each emitter given by $\Gamma_j = \Gamma'_j + \Gamma_{j,1D}$. Furthermore, in this case we consider the limit $k\Delta z \to 0$ for waveguide-mediated coupling. Using this we find the transmitted field to be

$$\hat{a}_{out,\text{R}} = \Bigg\{1 + \Big[4i\sqrt{\Gamma_{A,1D}\Gamma_{B,1D}}|\mathcal{V}|\cos\phi + 2\Gamma_{A,1D}\Gamma_{B,1D} - \Gamma_{A,1D}(\Gamma_B + 2i\delta_B) - \Gamma_{B,1D}(\Gamma_A + 2i\delta_A)\Big] \Big/ \Big[(\Gamma_A + 2i\delta_A)(\Gamma_B + 2i\delta_B) - \Gamma_{A,1D}\Gamma_{B,1D} - 4i\sqrt{\Gamma_{A,1D}\Gamma_{B,1D}}|\mathcal{V}|\cos\phi + 4|\mathcal{V}|^2)\Big]\Bigg\}\hat{a}_{in}(\text{z} - v_g t). \tag{2.72}$$

Here we have assumed that the dipole interaction between the emitters has the form $\mathcal{V}_{AB} = (\mathcal{V}_{BA})^* = |\mathcal{V}|e^{i\phi}$.

A two-level and a three-level emitter

Let us now investigate how the coherent coupling between level $|2\rangle$ and $|3\rangle$ of the second emitter influences the scattering dynamics. The effect of interference due to such coherent coupling is different than that due to the waveguide mediated coupling. To elaborate further, let us compare the two two-level emitter case with the present situation where the coherent coupling is non-zero, $\Omega \neq 0$. Following two two-level emitter example we now assume $\delta_2 = \delta_3 = \delta_B$, $\delta_1 = \delta_A$, $\Gamma_{1,1\mathrm{D}} = \Gamma_{2,1\mathrm{D}} = \Gamma_{3,1\mathrm{D}} = \Gamma_{1\mathrm{D}}$ and all $\Gamma_i' = 0$. The transmitted field is then given by

$$\begin{aligned} \hat{a}_{out,\mathrm{R}}(\mathrm{z},t) &= \frac{2\delta_A(\Omega+\delta_B)}{e^{2ik\Delta z}\Gamma_{1\mathrm{D}}^2 - (\Gamma_{1\mathrm{D}}+2i\delta_A)[\Gamma_{1\mathrm{D}}+i(\Omega+\delta_B)]} \\ &\times \hat{a}_{in,\mathrm{R}}(\mathrm{z}-v_g t). \end{aligned} \tag{2.73}$$

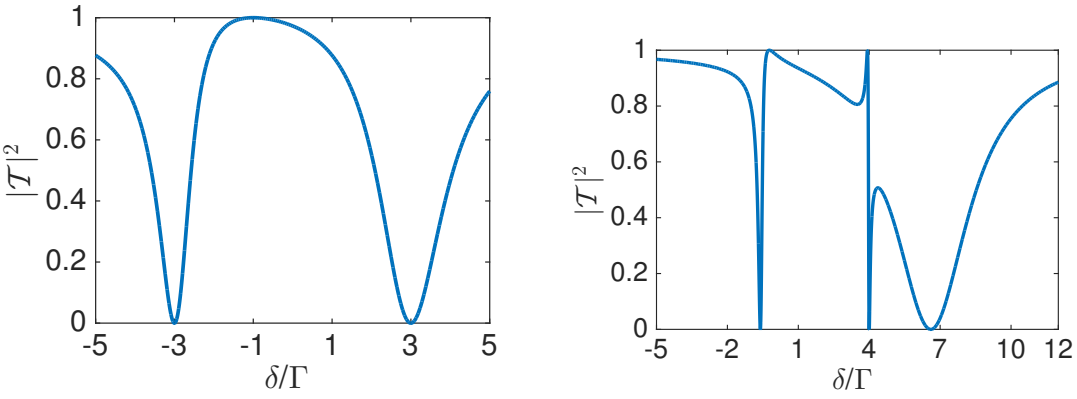

FIGURE 2.7: Transmission $|\mathcal{T}|^2 = |\langle \hat{a}^\dagger_{out,R}\hat{a}_{out,R}\rangle / \langle \hat{a}^\dagger_{in}\hat{a}_{in}\rangle|$ from a two-emitter system. Here we consider a combination of a two-level emitter and a three-level emitter in the V-configuration coupled to a 1D waveguide. The parameters used for the plots are as follows, for (a) $\delta_A = -3\Gamma - \delta$. $\delta_B = -2\Gamma - \delta$ and $\beta = 1$, $k\Delta z = 2\pi$ and $\Omega = 5$ while for (b) $\delta_1 = 4\Gamma - \delta$, $\delta_2 = -\delta$, $\delta_3 = 6\Gamma - \delta$, $\Gamma_{1,1\mathrm{D}} = 0.1\Gamma$, $\Gamma_{2,1\mathrm{D}} = \Gamma$, $\Gamma_{3,1\mathrm{D}} = 3\Gamma$, $k\Delta z = 1$ and $\Omega = 2$.

We show the transmission spectrum evaluated using Eq. (2.73) in Fig. 2.7 (a) . We find that the transmission spectrum has two points of total reflection: at resonance with emitter A, i.e., $\delta_A = 0$ and at $\delta_B = -\Omega$. At $\delta_A = 0$, the input photon is completely reflected off the emitter A which behaves as a perfect mirror and thus emitter B does not 'see' any input field. The scattered output field from the two-emitter system thus has characteristics reminiscent of total reflection off a single two-level emitter. The width of this resonance is Γ. At $\delta_B = -\Omega$, the incoming field is in resonance with the symmetric state, an eigenstate of emitter B's excited-subspace Hamiltonian. From Eq. (2.73) we find the width of this resonance to be 2Γ.

Finally, our method allows evaluating the scattering dynamics for a general emitter system. We give an example of this in Fig. 2.7 (b) which displays a complex interplay between various processes.

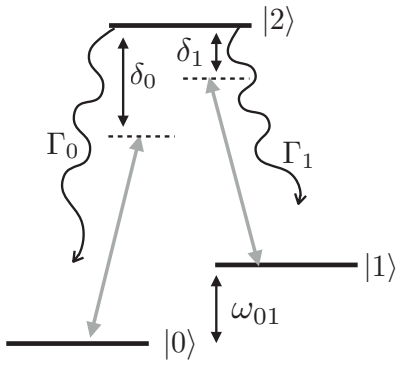

FIGURE 2.8: Three-level emitter with a Λ-type level structure consisting of two groundstates ($|0\rangle$, $|1\rangle$) and one excited state ($|2\rangle$).

2.5 Application of the photon scattering formalism to emitters with two or more ground-states

Until now we have discussed examples that involve only a single ground-state. Thus, we have not yet needed the effective operator master equation. To illustrate the full use of our formalism, in this section we solve a scattering problem involving an emitter with multiple ground-states. We will first introduce the model system in Sec. V.A and discuss the relevant Hamiltonian and equation of motions. Then in Sec. V.B and in the subsequent subsections, we discuss in detail the scattering dynamics of a single photon and a weak coherent pulse.

2.5.1 The Model System and Hamiltonian

For this purpose we consider a single three-level Λ-type emitter coherently coupled to a waveguide as shown schematically in Fig. 2.8. Such a system is generally described by a Hamiltonian $\hat{\mathcal{H}} = \hat{\mathcal{H}}_0 + \hat{\mathcal{V}}(\hbar = 1)$ where,

$$\hat{\mathcal{H}}_0 = \sum_{j=0}^{2} \omega_{jj}\hat{\sigma}_{jj} + \hat{\mathcal{H}}_F \tag{2.74a}$$

$$\hat{\mathcal{V}} = \sum_{\mu} \mathcal{A}_0^{\mu}\hat{a}_{\mu}^{\dagger}\hat{\sigma}_{20} + \sum_{\mu} \mathcal{A}_1^{\mu}\hat{a}_{\mu}^{\dagger}\hat{\sigma}_{21} + H.c. \tag{2.74b}$$

Here $\hat{\mathcal{H}}_0$ and $\hat{\mathcal{H}}_F$ are the free-energy and free-field Hamiltonian, respectively, while the excitation (de-excitation) operators are defined by $\hat{\mathcal{V}}_+ (\hat{\mathcal{V}}_- = [\hat{\mathcal{V}}_+]^\dagger)$. The frequencies ω_{jj} correspond to the energies of levels $|j\rangle$. We assume that the emitter transitions $|2\rangle \to |j\rangle$ couples to the 1D waveguide mode with a coupling strengths $\mathcal{A}_{j,(1\mathrm{D})}^{\mu=\zeta}$ and $\hat{a}_{\mu=\zeta}$ ($\hat{a}_{\mu=\zeta}^{\dagger}$) represent the corresponding annihilation (creation) operator of the waveguide mode. Considering the coupling strengths to be real we can then, following Eq. (2.22), write the decay from $|j\rangle$ into the waveguide as $\Gamma_{j,1\mathrm{D}}^{\zeta} = (\mathcal{A}_{j,(1\mathrm{D})}^{\zeta})^2$. Furthermore, the decay to the outside of the waveguide is as before, given by $\Gamma_j^{'} = (\mathcal{A}_j^{\mu=s})^2$.

In order to solve for the emitter dynamics and the scattering of such a system in a waveguide, we invoke the photon-scattering relation of Eq. (2.7). As part of the effective operator method [74], we can write the Hamiltonian in standard notation according to Eq. (2.26). In Eq. (2.27), $\tilde{\Delta}_e = \Delta_e - E_g/\hbar$, with $\Delta_e = \mathcal{H}_0 - \omega$. Here ω is the central frequency of the incoming light field and E_g is the energy of the ground-state we excite out from. From here we see that the non-Hermitian Hamiltonian is initial-state (ini) dependent. When writing

$\hat{\mathcal{H}}_{\rm nh} = \hat{\mathcal{H}}_e^{(\rm ini)} - \frac{i}{2}\sum_k \hat{\mathcal{L}}_k^\dagger \hat{\mathcal{L}}_k$ with

$$\hat{\mathcal{L}}_{1,j} = \hat{\mathcal{L}}'_j = \sqrt{\Gamma'_j}\,\hat{\sigma}_{2j}, \tag{2.75}$$

$$\hat{\mathcal{L}}_{2,j} = \hat{\mathcal{L}}^R_j = \sqrt{\Gamma^R_{j,\rm 1D}}\,\hat{\sigma}_{2j}, \tag{2.76}$$

$$\hat{\mathcal{L}}_{3,j} = \hat{\mathcal{L}}^L_j = \sqrt{\Gamma^L_{j,\rm 1D}}\,\hat{\sigma}_{2j}, \tag{2.77}$$

two initial-state dependent Hamiltonians emerge:

$$\hat{\mathcal{H}}^{(0)}_{\rm nh} = \left(\delta_0 - \frac{i\Gamma}{2}\right)\hat{\sigma}_{22} \equiv \tilde{\delta}_0\hat{\sigma}_{22}, \tag{2.78a}$$

$$\hat{\mathcal{H}}^{(1)}_{\rm nh} = \left(\delta_1 - \frac{i\Gamma}{2}\right)\hat{\sigma}_{22} \equiv \tilde{\delta}_1\hat{\sigma}_{22}, \tag{2.78b}$$

which describe the excited-subspace energies and decay rates corresponding to excitation out of the two different ground-states. Here, we have changed to a rotating frame where $\delta_0 = (\omega_{22} - \omega_{00} - \omega)$ and $\delta_1 = (\omega_{22} - \omega_{11} - \omega)$. The total decay rate of the excited state $|2\rangle$ is defined as $\Gamma = \Gamma_{0,\rm 1D} + \Gamma_{1,\rm 1D} + \Gamma'_0 + \Gamma'_1$, where $\Gamma_{j,\rm 1D} = \sum_\zeta \Gamma^\zeta_{j,\rm 1D}$ is the total decay rate for all transitions out of $|2\rangle$ into the state $|j\rangle$ by emitting into the 1D waveguide mode.

Now, let us assume that the energy separation between the ground-states is much larger than the linewidths of all states, such that the incoming field only drives a single transition. We pick the exciting transition to be from $|0\rangle$ to $|2\rangle$, which can subsequently decay to either ground-state. From here on, we therefore omit the indices on $\hat{\mathcal{H}}^{(j)}_{\rm nh}$ and δ_j. Inverting the non-Hermitian Hamiltonian in Eq. (2.78) is straightforward and yields

$$\hat{\mathcal{H}}^{-1}_{\rm nh} = \tilde{\delta}^{-1}\hat{\sigma}_{22} \tag{2.79}$$

where $\tilde{\delta}^{-1} \equiv (\delta - \frac{i}{2}\Gamma)^{-1}$. For an incoming photon incident from the left end of the double-sided waveguide and travelling towards the right, we can write Eq. (2.7) in terms of the electric field on the left and right after scattering from the Λ-system emitter as:

$$\hat{a}_{out,\rm R}(\mathrm{z},t) = \left[1 + i\left(\Gamma^{\rm R}_{0,\rm 1D}\tilde{\delta}^{-1}\hat{\sigma}_{00} + \tilde{\delta}^{-1}\sqrt{\Gamma^{\rm R}_{0,\rm 1D}\Gamma^{\rm R}_{1,\rm 1D}}\right.\right.$$
$$\left.\left.\times\hat{\sigma}_{01}e^{-i\omega_{01}\frac{(\mathrm{z}-\mathrm{z}_0)}{v_g}}\right)\right]\hat{a}_{in,\rm R}(\mathrm{z}-v_gt), \tag{2.80}$$

$$\hat{a}_{out,\rm L}(\mathrm{z}',t) = i\left(\sqrt{\Gamma^{\rm L}_{0,\rm 1D}\Gamma^{\rm R}_{0,\rm 1D}}\tilde{\delta}^{-1}\hat{\sigma}_{00} + \tilde{\delta}^{-1}\sqrt{\Gamma^{\rm L}_{1,\rm 1D}}\right.$$
$$\left.\times\sqrt{\Gamma^{\rm R}_{0,\rm 1D}}\hat{\sigma}_{01}e^{-i\omega_{01}\frac{(\mathrm{z}_0-\mathrm{z}')}{v_g}}\right)e^{2ik_0(\mathrm{z}_0-\mathrm{z}')}\hat{a}_{in,\rm R}(\mathrm{z}'+v_gt), \tag{2.81}$$

where z_0 is the position of the emitter, $\hat{\sigma}_{00} = |0\rangle\langle 0|$ and $\hat{\sigma}_{01} = |1\rangle\langle 0|$, while z is some point to the right of the emitter and $\mathrm{z}' < \mathrm{z}_0$ is to the left of the emitter.

From Eqs. (2.80) and (2.81) we see that, unlike the earlier discussed cases involving only the population of a single ground-state, the scattered field now involves the response of the emitter in terms of both the population and coherence of the ground-states. Furthermore, compared to the previous examples now the populations of the ground-states $|0\rangle$ and $|1\rangle$ evolve with time. Hence we now need to invoke the effective-operator master equation (2.10) to solve for the dynamics of the emitter. To use the master equation we first define a basis

$\{|0\rangle, |1\rangle\}$ with $\hat{\sigma}_{ij} = |j\rangle\langle i|$. The *effective* Hamiltonian governing the coherent dynamics of the ground-state density matrix is given by

$$\hat{\mathcal{H}}_{\text{eff}} = -\frac{1}{2}\hat{\mathcal{V}}_{-}[\hat{\mathcal{H}}_{\text{nh}}^{-1} + (\hat{\mathcal{H}}_{\text{nh}}^{-1})^{\dagger}]\hat{\mathcal{V}}_{+} + \hat{\mathcal{H}}_{g}, \tag{2.82}$$

where the excitation and de-excitation operators are defined respectively by $\hat{\mathcal{V}}_{+} = \sum_{\mu} \mathcal{A}_{0}^{\mu}\hat{a}_{\mu}\hat{\sigma}_{02} + \sum_{\mu} \mathcal{A}_{1}^{\mu}\hat{a}_{\mu}^{'}\hat{\sigma}_{12}$ and $\hat{\mathcal{V}}_{-} = \sum_{\mu} \mathcal{A}_{0}^{\mu}\hat{a}_{\mu}^{\dagger}\hat{\sigma}_{20} + \sum_{\mu} \mathcal{A}_{1}^{\mu}\hat{a}_{\mu}^{'\dagger}\hat{\sigma}_{21}$ while $\hat{\mathcal{H}}_{g} = \omega_{01}\hat{\sigma}_{11}$. Here the prime on the mode operator reflects that the field needs to have different frequencies to be resonant with the two different transition. As in this work we are mainly interested in the regime where the splitting between the ground states is large compared to the optical line width, the corresponding mode operators can essentially be considered to represent two different baths. Recall that $\mathcal{A}_{j,(1\text{D})}^{\zeta} = \sqrt{\Gamma_{j,1\text{D}}^{\zeta}}$. Note that as opposed to the previous examples we will here need to be careful about the noise terms in the $\hat{\mathcal{H}}_{\text{eff}}$. Such noise terms arise due to contribution from modes outside of the waveguide in $\hat{\mathcal{V}}_{\pm}$. Using the above expressions for $\hat{\mathcal{V}}_{\pm}$ and Eq. (2.79) we then evaluate $\mathcal{H}_{\text{eff}}$ to be

$$\mathcal{H}_{\text{eff}} = \begin{bmatrix} -(\sum_{\zeta\zeta'} \sqrt{\Gamma_{0,1\text{D}}^{\zeta}}\sqrt{\Gamma_{0,1\text{D}}^{\zeta'}}\hat{a}_{\zeta}^{\dagger}\hat{a}_{\zeta'})\frac{\delta}{|\tilde{\delta}|^2} + \mathcal{F} & \mathcal{F}' \\ \mathcal{F}'^{\dagger} & \omega_{01} \end{bmatrix}. \tag{2.83}$$

Here the noise terms $\mathcal{F}$ and $\mathcal{F}'$ are given respectively by $\mathcal{F} = -[\sum_{\zeta} \sqrt{\Gamma_{0,1\text{D}}^{\zeta}}\sqrt{\Gamma_{0}^{'}}\ \hat{a}_{\zeta}^{\dagger}\hat{a}_{s} + \sum_{\zeta} \sqrt{\Gamma_{0,1\text{D}}^{\zeta}}\sqrt{\Gamma_{0}^{'}}\ \hat{a}_{s}^{\dagger}\hat{a}_{\zeta} + \Gamma_{0}^{'}\ \hat{a}_{s}^{\dagger}\hat{a}_{s}]\delta/|\tilde{\delta}|^2$ and $\mathcal{F}' = -\sum_{\mu}\sum_{\mu'} \mathcal{A}_{0}^{\mu}\mathcal{A}_{1}^{\mu'}\hat{a}_{\mu}^{\dagger}\hat{a}_{\mu'}^{'}(\delta/|\tilde{\delta}|^2)$. Furthermore, in writing the $|1\rangle\langle 1|$ element of the matrix $\mathcal{H}_{\text{eff}}$, we have neglected the terms $\sum_{\mu}\sum_{\mu'} \mathcal{A}_{1}^{\mu}\mathcal{A}_{1}^{\mu'}\hat{a}_{\mu}^{'\dagger}\hat{a}_{\mu'}^{'}$. This is because there are no photons at the frequency corresponding to the primed reservoir since we assume that the incoming field is resonant with the transition $|0\rangle \rightarrow |2\rangle$. Also, we define *effective* Lindblad decay operators in the form

$$\hat{\mathcal{L}}_{\text{eff}}^{k} = \hat{\mathcal{L}}_{k}\hat{\mathcal{H}}_{\text{nh}}^{-1}\hat{\mathcal{V}}_{+}, \tag{2.84}$$

for each decay channel k. Recall that as $\hat{\mathcal{V}}_{\pm}$ includes modes outside the waveguide, $\hat{\mathcal{L}}_{\text{eff}}^{k}$ also has contribution from the noise in the system dynamics. In the Λ-system, we drive only the transition from $|0\rangle$ to $|2\rangle$, which can decay to either $|0\rangle$ or $|1\rangle$. We then only have two effective decoherence channels: *population transfer* described by $|1\rangle\langle 0|$ and a driving-induced *dephasing* term (shift) described by $|0\rangle\langle 0|$. Plugging Eq. (2.74b), Eqs. (2.75)-(2.77), and Eq. (2.79) into Eq. (2.84), we find the following effective Lindblad operators:

$$\begin{aligned} \hat{\mathcal{L}}_{\text{eff}}^{'} &= \tilde{\delta}^{-1}\sum_{j=0}^{1}\sqrt{\Gamma_{j}^{'}}\sum_{\zeta'}\sqrt{\Gamma_{0,1\text{D}}^{\zeta'}}\ \hat{\sigma}_{0j}\hat{a}_{\zeta'}, \\ &+ \tilde{\delta}^{-1}\sum_{j=0}^{1}\sqrt{\Gamma_{j}^{'}}\sqrt{\Gamma_{0}^{'}}\ \hat{\sigma}_{0j}\hat{a}_{s}, \end{aligned} \tag{2.85}$$

$$\begin{aligned} \hat{\mathcal{L}}_{\text{eff}}^{\zeta} &= \tilde{\delta}^{-1}\sum_{j=0}^{1}\sqrt{\Gamma_{j,1\text{D}}^{\zeta}}\sum_{\zeta'}\sqrt{\Gamma_{0,(1\text{D})}^{\zeta'}}\hat{\sigma}_{0j}\hat{a}_{\zeta'} \\ &+ \tilde{\delta}^{-1}\sum_{j=0}^{1}\sqrt{\Gamma_{j,1\text{D}}^{\zeta}}\sqrt{\Gamma_{0}^{'}}\ \hat{\sigma}_{0j}\hat{a}_{s}. \end{aligned} \tag{2.86}$$

We next assume that the coupling of the photon to the right and left travelling mode in the

waveguide have the same strength such that $\Gamma^{\rm R}_{j,1D} = \Gamma^{\rm L}_{j,1D} = \Gamma_{j,1D}/2$. Also, we consider the incoming field only to be only in the right-propagating mode, such that $\hat{a}_{{\rm L},in}|\Psi_{ini}\rangle = 0$. Hence, for all further discussions the scattered field-mode will depend only on $\hat{a}_{{\rm R},in}$ with the other modes $\hat{a}_s$ and $\hat{a}_{\rm L}$ contributing to the losses and noise. For notational simplicity we will represent $\hat{a}_{{\rm R},in}$ by $\hat{a}$, while all terms containing $\hat{a}_s$ and $\hat{a}_{\rm L}$ will be called noise.

Combining the above considerations with Eq. (2.82) and Eq. (2.85), we evaluate the effective master equation Eq. (2.10) for each element in the ground-state density matrix. This gives a series of coupled-component differential equations,

$$\dot{\hat{\sigma}}_{00} =: -{\rm P}_R\hat{a}^\dagger\hat{a}\hat{\sigma}_{00}: + \text{Noise} \tag{2.87a}$$

$$\dot{\hat{\sigma}}_{11} =: +{\rm P}_R\hat{a}^\dagger\hat{a}\hat{\sigma}_{00}: + \text{Noise}, \tag{2.87b}$$

$$\begin{aligned}\dot{\hat{\sigma}}_{01} =:& +i\hat{\sigma}_{01}(\mathcal{H}_{\text{eff},22} - \mathcal{H}_{\text{eff},11}) \\ &- \frac{1}{2}\left({\rm P}_R + {\rm P}_d\right)\hat{a}^\dagger\hat{a}\hat{\sigma}_{01}: + \text{Noise},\end{aligned} \tag{2.87c}$$

$$\begin{aligned}\dot{\hat{\sigma}}_{10} =:& -i\hat{\sigma}_{10}(\mathcal{H}_{\text{eff},22} - \mathcal{H}_{\text{eff},11}) \\ &- \frac{1}{2}\left({\rm P}_R + {\rm P}_d\right)\hat{a}^\dagger\hat{a}\hat{\sigma}_{10}: + \text{Noise},\end{aligned} \tag{2.87d}$$

where $\mathcal{H}_{\text{eff},jj} = \langle j|\mathcal{H}_{\text{eff}}|j\rangle$ in Eq. (2.82) and the effective *probabilities* corresponding to the amplitudes of the operators in the above equations. These are given by

$${\rm P}_d = \frac{\Gamma_0\Gamma^R_{0,1D}}{|\tilde{\delta}|^2}, \tag{2.88}$$

$${\rm P}_R = \frac{\Gamma_1\Gamma^R_{0,1D}}{|\tilde{\delta}|^2}, \tag{2.89}$$

where ${\rm P}_d$ represents the photon induced dephasing of level $|0\rangle$ while ${\rm P}_R$ represents the total Raman scattering probability, i.e., the probability for a single photon to scatter $|0\rangle \to |2\rangle \to |1\rangle$, either emitting into the waveguide in either direction, or to the side. To find these probabilities we have evaluated quantities like ${\rm P}_d\hat{a}^\dagger\hat{a} = \sum_{k=',{\rm R},{\rm L}}\langle 0|\hat{\mathcal{L}}^{k\dagger}_{\text{eff}}|0\rangle\langle 0|\hat{\mathcal{L}}^{k}_{\text{eff}}|0\rangle$ and ${\rm P}_R\hat{a}^\dagger\hat{a} = \sum_{k=',{\rm R},{\rm L}}\langle 0|\hat{\mathcal{L}}^{k\dagger}_{\text{eff}}|1\rangle\langle 1|\hat{\mathcal{L}}^{k}_{\text{eff}}|0\rangle$.

The solution of the above set of equations is straightforward. In particular, we find the solution of the ground-state occupations to be

$$\hat{\sigma}_{00}(t) =: \hat{\sigma}_{00}(0)e^{-{\rm P}_R\int_0^t\hat{a}^\dagger\hat{a}dt'}: + \text{Noise}, \tag{2.90a}$$

$$\hat{\sigma}_{11}(t) =: (1 - \hat{\sigma}_{00}(0)e^{-{\rm P}_R\int_0^t\hat{a}^\dagger\hat{a}dt'}): + \text{Noise}. \tag{2.90b}$$

Thus we see from the solution of the master equation that the input field drives the population from $|0\rangle$ to $|1\rangle$ at a rate ${\rm P}_R\hat{a}^\dagger\hat{a}$, that is proportional to the input-field operators appearing in the excitation terms $\hat{\mathcal{V}}_+$ in the effective decay channels $\hat{\mathcal{L}}^k_{\text{eff}}$ in Eq. (2.85).

2.5.2 The Photon Scattering Dynamics

Now that we have the knowledge of all the relevant dynamics, let us investigate light scattering into the waveguide from the emitter. To elucidate the scattering problem further, we in the following subsections consider three specific cases: (1) single-photon scattering and the probability of photo-detection after separating the two frequency components in the scattered field via a filter, (2) coherent pulse scattering followed by intensity measurement of unfiltered output, and lastly (3) generation of a ground-state superposition conditioned on photodetection (click of the detector). For all the cases discussed below, we assume that the coupling

to both the right-propagating and the left-propagating modes in the waveguide are equal i.e., $\Gamma^{R}_{j,1\mathrm{D}} = \Gamma^{L}_{j,1\mathrm{D}} = \Gamma_{j,1\mathrm{D}}/2$.

Frequency filtering of scattered single photon

Let us assume that the input field has a single near resonant photon only. The photon can excite the $|0\rangle$ to $|2\rangle$ transition, and a photon comes out either at the input photon frequency $\omega = (\omega_{22} - \omega_{00}) - \delta_0$ (blue) or at $\omega_{12} = (\omega_{22} - \omega_{11}) - \delta_1$ (red). In labelling the photon as red and blue we have assumed $\omega_{11} > \omega_{00}$. If the emitter starts in one ground-state, the outgoing photon becomes entangled with the emitter ground-state $|0\rangle$ or $|1\rangle$. By removing for example blue photons from the output using a filter, we can condition the experiment on a click in a detector to say that the emitter has flipped from state $|0\rangle$ to $|1\rangle$. Mathematically, the frequency shift is, in our formalism, contained in the time evolution of the $\hat{\sigma}_{01}$ operator in Eq. (2.80) and Eq. (2.81). The action of the frequency filter thus amounts to only retaining the term containing $\hat{\sigma}_{01}$ in Eqs. (2.80) and (2.81). We name the filtered $\hat{a}_{out,\mathrm{R}}$ as $\hat{a}_{out,\mathrm{R},red}$ and henceforth use it to denote the filtered output.

If we consider a single right-going photon input, the probability of getting a right-going red photon coming out is given by

$$\begin{aligned} \mathrm{P}^{R}_{red} &\sim \frac{\int \langle \Psi_{ini}|\hat{a}^{\dagger}_{out,\mathrm{R},red}(t)\hat{a}_{out,\mathrm{R},red}(t)|\Psi_{ini}\rangle dt}{\int \langle \Psi_{ini}|\hat{a}^{\dagger}_{in,\mathrm{R}}(t)\hat{a}_{in,\mathrm{R}}(t)|\Psi_{ini}\rangle dt} \\ &= \left|\frac{\sqrt{\Gamma^{\mathrm{R}}_{0,1\mathrm{D}}\Gamma^{\mathrm{R}}_{1,1\mathrm{D}}}}{\tilde{\delta}}\right|^2 \\ &\times \int \langle \Psi_{ini}|\hat{a}^{\dagger}_{in,\mathrm{R}}\hat{\sigma}_{01}(t)\hat{\sigma}_{10}(t)\hat{a}_{in,\mathrm{R}}|\Psi_{ini}\rangle dt, \end{aligned} \tag{2.91}$$

where, $|\Psi_{ini}\rangle \equiv \hat{a}^{\dagger}_{0}|0,\varnothing\rangle$ is the initial state of the total system with the emitter in state $|0\rangle$ and incoming right-going single-photon creation operator $\hat{a}^{\dagger}_{0} = \int dk F^{\dagger}_{R,k}\hat{a}^{\dagger}_{k}$, for some suitable mode function $F_{R,k}$ such that $\int \langle \Psi_{ini}|\hat{a}^{\dagger}_{in,\mathrm{R}}(t)\hat{a}_{in,\mathrm{R}}(t)|\Psi_{ini}\rangle dt = 1$. Using $e^x = \sum_{k=0}^{\infty} x^k/k!$ and normal ordering the solution in Eq. (2.90a), the evaluation of the integral $\int \langle \Psi_{ini}|\hat{a}^{\dagger}_{in,\mathrm{R}}\hat{\sigma}_{01}(t)\hat{\sigma}_{10}(t)\hat{a}_{in,\mathrm{R}}|\Psi_{ini}\rangle dt$ yields $\langle 0,\emptyset_R|\hat{\sigma}_{00}(0)|0,\emptyset_R\rangle$, where we have used that all noise operators vanish for a vacuum input state.

Now, as the Λ-system is assumed to be initially prepared in the ground-state $|0\rangle$, we have $\langle \hat{\sigma}_{00}(0)\rangle = 1$. Thus, on substituting this in Eq. (2.91) we find

$$\mathrm{P}^{R}_{red} = \frac{\beta_0\beta_1}{\left(1 + \frac{4\delta^2}{\Gamma^2}\right)}, \tag{2.92}$$

where $\Gamma = \Gamma_{0,1\mathrm{D}} + \Gamma_{1,1\mathrm{D}} + \Gamma'_0 + \Gamma'_1$ is the total decay rate while $\beta_0 = \Gamma_{0,1\mathrm{D}}/\Gamma$ and $\beta_1 = \Gamma_{1,1\mathrm{D}}/\Gamma$. As we assumed equal rates of decay to the left and right, $\mathrm{P}^{R}_{red} = \mathrm{P}^{L}_{red}$ and the scattering probability is maximal for $\Gamma_{0,1\mathrm{D}} = \Gamma_{1,1\mathrm{D}}$ with $\Gamma' = 0$ and on resonance $\delta = 0$. For these parameters, a single photon has a 50% chance to flip the emitter, and a red photon is emitted left or right with equal probabilities to yield a total probability of 25% for detecting the photon. Note that here the normal ordering of the operators in Eqs. (2.90a) and (2.90b) is essential for getting the right results. Without normal ordering the result in Eq. (2.92) would contain higher-order terms in the probability, which should not be there for a single incident photon. Likewise, we can perform filtered detection of a *blue* photon, yielding $\mathrm{P}^{R}_{blue} = 1 - (2 - \beta_0)\beta_0/\left(1 + \frac{4\delta^2}{\Gamma^2}\right)$.

Unfiltered total intensity output for a coherent pulse input

Instead of a single photon, if we use a weak coherent pulse as an input field, the scattering dynamics is different. In this situation, a coherent pulse input can drive the emitter from the ground-state $|0\rangle$ to $|1\rangle$ before the detection time that we consider, since now the incoming pulse may contain more than one photon. To study the characteristic of the transmitted field, we again use Eq. (2.80). Typically, in experiments one measures the intensity of the output field using photo-detectors, so we calculate the expectation value of the square of the output-field operator (without any filtering) as

$$I_{out} = \langle \hat{a}^\dagger_{out} \hat{a}_{out} \rangle = \langle \Psi_{ini} | \hat{a}^\dagger_{out} \hat{a}_{out} | \Psi_{ini} \rangle, \tag{2.93}$$

where $|\Psi_{ini}\rangle$ is the initial state of the emitter-field system. If we as before choose the emitter to be prepared initially in the state $|0\rangle$ while the field is in the coherent state $|\alpha\rangle$ such that $|\Psi_{ini}\rangle = |\Psi_\alpha\rangle = |0, \alpha\rangle$, we get the intensity

$$I_{out} = \langle \Psi_\alpha | \hat{a}^\dagger \Big[1 - \frac{(2-\beta_0-\beta_1)\beta_0}{\left(1+\frac{4\delta^2}{\Gamma^2}\right)} \hat{\sigma}_{00}(t) \Big] \hat{a} | \Psi_\alpha \rangle \tag{2.94}$$

where Γ is the total decay rate of the excited level, $\Gamma = \Gamma_{0,1\mathrm{D}} + \Gamma_{1,1\mathrm{D}} + \Gamma'_0 + \Gamma'_1$. In this calculation we evaluate the time-dependent density matrix element $|0\rangle\langle 0|$ decaying with the probability $\mathrm{P}_R = \frac{\Gamma_1 \Gamma_{0,1\mathrm{D}}}{2|\tilde{\delta}|^2}$ per incident photon.

Let us now evaluate the term $\langle \Psi_\alpha | \hat{a}^\dagger \hat{\sigma}_{00}(t) \hat{a} | \Psi_\alpha \rangle$. Note that $\hat{a}^\dagger \hat{a}$ is in the exponential in the solution given in Eq. (2.90a) which in turn can be written as a power series $e^x = \sum_{k=0}^{\infty} x^k/k!$. Also, recall that the solution to the master equation assumes normal ordering of the field-mode operators, such that $\langle \alpha | \colon \hat{a}^\dagger (\sum_{k=0}^{\infty} (\hat{a}^\dagger \hat{a})^k / k!) \hat{a} \colon | \alpha \rangle = \sum_{k=1}^{\infty} (\alpha^* \alpha)^k / (k-1)!$. Using this we then get, $\langle \alpha | \colon \hat{a}^\dagger e^{-\mathrm{P}_R \int_0^t \hat{a}^\dagger \hat{a} dt'} \hat{a} \colon | \alpha \rangle = |\alpha(t)|^2 e^{-\mathrm{P}_R |\alpha(t)|^2 t}$, where $|\alpha(t)|^2$ is the intensity of the coherent state $|\Psi_\alpha\rangle$. Also, as before we then choose the initial state such that $\langle 0 | \hat{\sigma}_{00}(t=0) | 0 \rangle = 1$. We can then write

$$I_{out}(t) = |\alpha(t)|^2 \left(1 - \mathrm{P}_{sc} e^{-\mathrm{P}_R \int_0^t |\alpha(t')|^2 dt'} \right), \tag{2.95}$$

where the time $t = 0$ is defined as the moment the incident pulse reaches the emitter, and

$$\mathrm{P}_{sc} = \frac{(2-\beta_0-\beta_1)\beta_0}{\left(1+\frac{4\delta^2}{\Gamma^2}\right)} \tag{2.96}$$

is the probability for a single photon to scatter into other directions than the right-going guided mode.

Let us now consider the probability of a click (photo-detection event) at a detector placed to the right of the emitter. If the input was a single photon, the probability of detecting a (any colour) right going photon would be

$$\mathrm{P}^{(1)}_{click} = \eta \left(1 - P_{sc}\right) = \eta (\mathrm{P}^R_{red} + \mathrm{P}^R_{blue}). \tag{2.97}$$

This, e.g., reduces to η, the detection efficiency, for $\Gamma_{0,1\mathrm{D}} = 0$, where there is no interaction with the emitter, and goes to zero for $\Gamma_{1,1\mathrm{D}} = \Gamma' = \delta = 0$ which is a perfectly reflecting two-level system. If we have a resonant field with no decay to the side, $\Gamma' = \delta = 0$, and equal decay rates $\Gamma_{0,1\mathrm{D}} = \Gamma_{1,1\mathrm{D}} = \Gamma_{1\mathrm{D}}$, there will be a 50% chance of passing through to the right.

If, instead, the input is a weak coherent pulse, we need to integrate the output intensity

over the pulse duration T of the input to find the total number of photons in the output. We consider a weak pulse, such that the integration yields the *probability* of detecting even a single photon. For a coherent pulse of duration T, we can define a total input photon number $\bar{n} = \int_0^T |\alpha(t)|^2 dt$. Thus, using Eq. (2.95) we get the detection probability for $\mathrm{P}^{(c)}_{click} \ll 1$ as

$$\begin{aligned}\mathrm{P}^{(c)}_{click} &= \eta \int_0^T I_{out}(t)dt \\ &= \eta \left[\bar{n} - \frac{\mathrm{P}_{sc}}{\mathrm{P}_R}\left[1 - e^{-\mathrm{P}_R \bar{n}}\right]\right] \\ &\approx \eta\bar{n}(1-\mathrm{P}_{sc}) = \bar{n}\mathrm{P}^{(1)}_{click},\end{aligned} \tag{2.98a}$$

where the last approximation is valid in the limit $\mathrm{P}_R\bar{n} \ll 1$; In this limit, the number of detected photons is to first order proportional to $\mathrm{P}^{(1)}_{click}$, the probability of transmitting a single photon to the right.

Conditional generation of ground-state superposition

In this example, we demonstrate how our formalism can be used to describe conditional state preparation in a Λ type emitter. In particular, our objective is to create a superposition state of the emitter's ground levels of the form $|\Psi^-\rangle = (|0\rangle - |1\rangle)/\sqrt{2}$. The physics of this state creation process is as follows. Due to the two transition pathways in a Λ system, a photon-scattering process leads to an entangled state of light and matter of the form $|\Psi_{\text{ent}}\rangle = \frac{1}{\sqrt{2}}(|\omega_{\text{blue}}\rangle|0\rangle - |\omega_{\text{red}}\rangle|1\rangle)$, where $(\omega_{\text{blue}} - \omega_{\text{red}}) = \omega_{01}$, and where $|\omega\rangle$ refers to a single photon state with frequency ω. Without filtering, the frequency difference between the two ground-states encoded in the outgoing photon will remain unresolved. A click in the photo-detector at a certain time t will erase the 'which path' information of the scattering, thereby creating the superposition state $|\Psi^-\rangle$.

Let us next evaluate the fidelity of being in state $|\Psi^-\rangle = (|0\rangle - |1\rangle)/\sqrt{2}$:

$$F = \langle\Psi^-|\hat{\rho}^{(c)}|\Psi^-\rangle = \frac{1}{2}(\rho^{(c)}_{00} - \rho^{(c)}_{01} - \rho^{(c)}_{10} + \rho^{(c)}_{11}), \tag{2.99}$$

where the elements $\rho^{(c)}_{ij}$ of the conditional density matrix $\rho^{(c)}$ can be evaluated from Eq. (2.100) below. Note that, due to normalisation, $\rho^{(c)}_{11} + \rho^{(c)}_{00} = \mathrm{Tr}(\hat{\rho}^{(c)}) = 1$ and we only need to evaluate the coherence $\rho^{(c)}_{01}$.

We next lay down a mathematical treatment for the state creation process. We begin by considering the evolution of the density matrix elements under the influence of an incoming coherent pulse. Recall that the output-field operator is also a function of the emitter operators. To find the total system evolution, we write the density matrix conditioned on a click in a detector at time t_c

$$\rho^{(c)}_{ij}(t_c, T) = \frac{\langle\Psi_{ini}|\hat{a}^\dagger_{out}(t_c)\hat{\sigma}_{ij}(T)\hat{a}_{out}(t_c)|\Psi_{ini}\rangle}{\langle\Psi_{ini}|\hat{a}^\dagger_{out}(t_c)\hat{a}_{out}(t_c)|\Psi_{ini}\rangle}. \tag{2.100}$$

In Eq. (2.100), we condition on having a click at a certain time t_c, represented by the operators $\hat{a}_{out}$. Experimentally one would however, only consider the first click which arrives at the detector. This makes no difference if the incident field only contains a single photon since in this case one cannot have two clicks. With an incident coherent state a more correct description would be to include in Eq. (2.100) the requirement that there is no photon detected before the time t_c. Since we mainly consider the limit where the probability of a detection event is small, the probability of having two detection events in the time interval is

negligible and the simple description in Eq. (2.100) is sufficient. Furthermore, we wish to calculate the time evolution of $\rho_{01}^{(c)}$ until a point T, i.e., the full duration of the incoming pulse sequence. After that, we know that the free evolution of the coherence will simply oscillate with the energy difference between the ground-states. Recall that t_c is the time after the start of the pulse, at which a photon was detected by click in the photo-detector and hence in this experiment we have $t_c \leq T$.

In evaluating Eq. (2.100) we have to be extra careful as now the vacuum noise operators, which until now we have neglected play a crucial role in the dynamics of $\rho_{ij}^{(c)}$. In particular for coherence term like $\rho_{01}^{(c)}$, one has to evaluate quantities like $\hat{a}_{out}^{\dagger}(t_c)\sigma_{01}(T)\hat{a}_{out}(t_c)$. From Eq. (2.80) and Eq. (2.87) we see that this will then involve terms like $\hat{\sigma}_{01}(t_c)\hat{\sigma}_{01}(T)\hat{\sigma}_{00}(t_c)$. Here we need to evaluate a product of operators at different times. With the normal ordered operators from in Eq. (2.90a) we have ensured that the noise operators for each of the terms vanish. This is, however, no longer the case once we have the product of three normal ordered terms and in principle we need to evaluate the noise terms. To avoid this complication we instead first calculate $\rho^{(c)}(t_c, t_c)$. In this case the three operators obey the relation $\hat{\sigma}_{10}(t_c)\hat{\sigma}_{01}(t_c)\hat{\sigma}_{00}(t_c) = \hat{\sigma}_{00}(t_c)$ since now all time arguments are equal (recall here the definition $\hat{\sigma}_{ij} = |j\rangle\langle i|$, which leads to unconventional rules for the indices in products of operators). With this relation we have reduced the product of three operators to a single operator. We can then simply use Eq. (2.90a) for a single time and all noise operators are normal ordered such that they vanish for initial vacuum states. To find the final density matrix $\rho^{(c)}(t_c, T)$, we then evolve the density matrix $\rho^{(c)}$ from t_c to T. Using Eq. (2.87) this gives us

$$\rho_{01}^{(c)}(t_c, T) = \rho_{01}^{(c)}(t_c, t_c)e^{\int_{t_c}^{T} i\omega'_{01} - \frac{1}{2}(\mathrm{P}_R + \mathrm{P}_d)|\alpha(t)|^2 dt}, \tag{2.101}$$

which essentially says that the coherence decays at a rate $\frac{1}{2}(\mathrm{P}_R + \mathrm{P}_d)|\alpha(t)|^2$ over a time $(T - t_c)$, due to both the Raman transfer rate and the photon-induced dephasing rate. Also, its phase rotates at a frequency ω'_{01} equal to the splitting between the two ground-states $|0\rangle$ and $|1\rangle$, ω_{01}, plus some AC-Stark shift $\delta\omega = (\omega'_{01} - \omega_{01})$ induced by the weak coherent drive of the $|0\rangle$ ground-state, given by $\delta\omega = \langle \mathcal{H}_{11}^{\mathrm{eff}} \rangle = \Gamma_{0,1\mathrm{D}}|\alpha(t)|^2\delta/|\tilde{\delta}|^2$.

Now we find the time evolution from $t = 0$ to the time of the click t_c at the detector. Inserting the output field $\hat{a}_{out}$ in Eq. (2.100) yields the elements as follows:

$$\rho_{01}^{(c)}(t_c, t_c) = \frac{\langle \Psi_{ini}|\hat{a}_{out}^{\dagger}(t_c)\hat{\sigma}_{01}(t_c)\hat{a}_{out}(t_c)|\Psi_{ini}\rangle}{\langle \Psi_{ini}|\hat{a}_{out}^{\dagger}\hat{a}_{out}|\Psi_{ini}\rangle}. \tag{2.102}$$

The denominator of Eq (2.102), can be recognized as the intensity of the output, given by $I_{out}(t) = |\alpha(t)|^2\left(1 - \mathrm{P}_{sc}e^{-\mathrm{P}_R\int_0^t |\alpha(t')|^2 dt'}\right)$.

Next, for notational convenience, let us write the output field $\hat{a}_{out}$ in Eq. (2.80) in the form

$$\hat{a}_{out} = \left[1 + i\left(A\hat{\sigma}_{00} + B\hat{\sigma}_{01}\right)\right]\hat{a}_{in}, \tag{2.103}$$

where we define $A = \Gamma_{0,1\mathrm{D}}/2\tilde{\delta}$ and $B = \sqrt{\Gamma_{0,1\mathrm{D}}\Gamma_{1,1\mathrm{D}}}/2\tilde{\delta}\ \exp[-i\omega_{01}(\mathrm{z} - \mathrm{z}_0)/v_{\mathrm{R}}]$. Substituting Eq. (2.103) into Eq. (2.102) we then get

$$\begin{aligned}\rho_{01}^{(c)}(t_c, t_c) &= \langle \Psi_{ini}|\hat{a}_{in}^{\dagger}\left[1 - i\left(A^*\hat{\sigma}_{00} + B^*\hat{\sigma}_{10}\right)\right]\hat{\sigma}_{01}(t_c) \\ &\times \left[1 + i\Big(A\hat{\sigma}_{00} + B\hat{\sigma}_{01}\Big)\right]\hat{a}_{in}|\Psi_{ini}\rangle / I_{out}(t_c).\end{aligned} \tag{2.104}$$

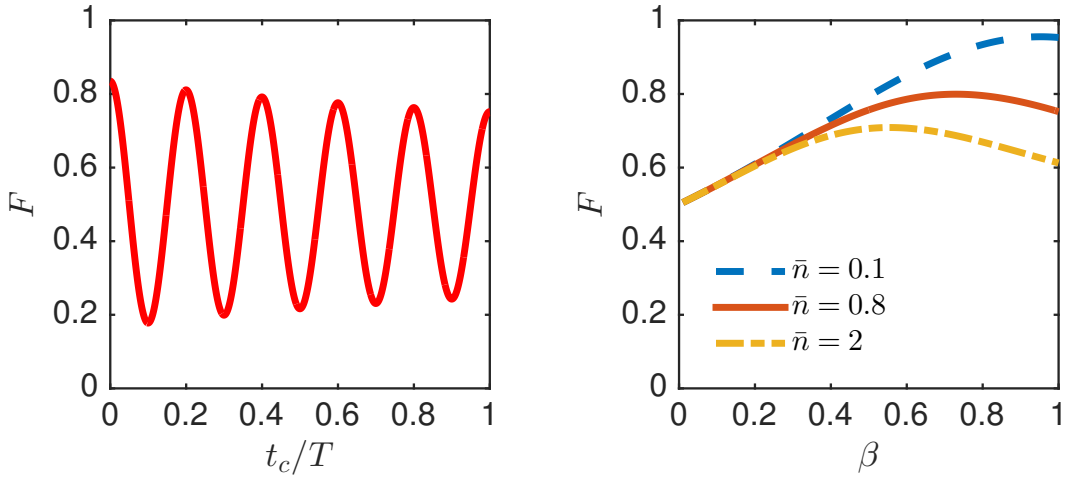

FIGURE 2.9: (a) Fidelity of the antisymmetric superposition state $|\Psi^-\rangle$ as a function of the detection time t_c normalized with the pulse duration T. We plot here for $\Gamma_{0,1D} = \Gamma_{1,1D}$, $\delta = 0$, $\phi_z = 0$, $\beta = 1$, $\omega_{01} = 5\frac{2\pi}{T}$, and an average number of photons $\bar{n} = 0.8$. Resolving the detection time determines the phase of the generated state. The detection time has an arbitrary offset determined by the spatial position of the detectors. (b) Fidelity of superposition-state generation as a function of the β-factor for different values of $\bar{n}$, the average photon number in the coherent pulse.

Considering only the relevant terms in Eq. (2.104) we get

$$\begin{aligned}\rho_{01}^{(c)}(t_c,t_c) &= |\alpha(t_c)|^2\langle\Psi_{ini}|\left[1-i\left(A^*\hat{\sigma}_{00}+B^*\hat{\sigma}_{10}\right)\right]\\ &\times \hat{\sigma}_{01}(t_c)\Big[1+i\left(A\hat{\sigma}_{00}+B\hat{\sigma}_{01}\right)\Big]|\Psi_{ini}\rangle/I_{out}(t_c).\end{aligned} \tag{2.105}$$

Now evaluating the expectation values of the operators $\langle\Psi_{ini}|\hat{\sigma}_{10}(t_c)\hat{\sigma}_{01}(t_c)\hat{\sigma}_{00}(t_c)|\Psi_{ini}\rangle = \langle\Psi_{ini}|\hat{\sigma}_{10}(t_c)\hat{\sigma}_{01}(t_c)|\Psi_{ini}\rangle$, we get $\langle\Psi_{ini}|\hat{\sigma}_{00}(t=0)\colon e^{-\mathrm{P}_R\int_0^{t_c}\hat{a}^\dagger\hat{a}dt}\colon|\Psi_{ini}\rangle = e^{-\mathrm{P}_R\int_0^{t_c}|\alpha(t)|^2dt}$. Inserting the solution for $\rho_{01}^{(c)}(t_c,t_c)$ into Eq. (2.101) gives us

$$\begin{aligned}\rho_{01}^{(c)}(t_c,T) &= |\alpha(t_c)|^2(1+iA)(-iB^*)\\ &\times (e^{-\gamma(t_c,T)+\int_{t_c}^{T}i\omega'_{01}(t)dt})/I_{out}(t_c),\end{aligned} \tag{2.106}$$

where for notational convenience we have introduced a total 'coherence-decay' term

$$\gamma(t_c,T) = \mathrm{P}_R\int_0^{t_c}|\alpha(t)|^2dt + \int_{t_c}^{T}\frac{1}{2}(\mathrm{P}_R+\mathrm{P}_d)|\alpha(t)|^2dt. \tag{2.107}$$

We consider a square pulse of length T and constant intensity $|\alpha|^2$ such that $|\alpha|^2T = \bar{n}$. Combining all these results and using Eq. (2.99) and $\rho_{10}^{(c)}(t_c) = \rho_{01}^{(c)*}(t_c)$ gives us a (t_c,T)-dependent fidelity:

$$F(t_c,T) = \frac{1}{2}+\frac{1}{2}e^{-\gamma(t_c,T)}\frac{\sqrt{\mathcal{N}}}{\mathcal{D}(t_c)}\cos\phi(t_c,T) \tag{2.108}$$

where we have defined

$$\frac{\mathcal{N}}{\Gamma^4} = \left(\frac{4\delta^2}{\Gamma^2} + (1-\beta_0)^2\right)\beta_0\beta_1, \tag{2.109}$$

$$\mathcal{D}(t_c) = (1/2)(4\delta^2+\Gamma^2)(1-\mathrm{P}_{sc}e^{-\mathrm{P}_R|\alpha|^2 t_c}) \tag{2.110}$$

$$\phi(t_c,T) = \phi_z + \omega'_{01}(T-t_c) + \arctan\left[\frac{2\delta/\Gamma}{(1-\beta_0)}\right] \tag{2.111}$$

with $\phi_z = \omega_{01}(\mathrm{z}-\mathrm{z}_0)/v_\mathrm{R}$, $\omega'_{01} = \omega_{01} + 4\beta_0|\alpha|^2\delta/\Gamma/(\delta^2/(\Gamma/2)^2+1)$ and $\gamma(t_c,T) = |\alpha|^2(\mathrm{P}_R(t_c+T)/2 + \mathrm{P}_d(T-t_c)/2)$

To elucidate the physics contained in the expression for the fidelity let us consider a specific case where $\Gamma_{0,1\mathrm{D}} = \Gamma_{1,1\mathrm{D}}$, $\Gamma' = 0$, $\delta = 0$, $\phi_z = \omega_{01}(\mathrm{z}-\mathrm{z}_\mathrm{R})/v_\mathrm{R} = q\times 2\pi$ with q being an integer. On using these conditions in Eq. (2.108) we get

$$F(t_c,T) = \frac{1}{2} + \frac{1}{2}\left(\frac{e^{-\bar{n}/2}}{2-e^{-\frac{\bar{n}}{2}t_c/T}}\right)\cos\left(\omega_{01}T\left[1-\frac{t_c}{T}\right]\right). \tag{2.112}$$

Note that in deriving the expression for fidelity, we have assumed the detector efficiency η to be small so that the probability of detecting a photon is small. We plot the fidelity derived in Eq. (2.112) for $T|\alpha|^2 = \bar{n} = 0.8$ and $\omega_{01} = 5\frac{2\pi}{T}$, as a function of t_c/T, in Fig. 2.9 (a). We find that the fidelity oscillates depending on the time of the click (detection of a photon) and that, for the given conditions, the amplitude decays with time. This is because, at later detection times, there is a larger probability that the emitter has already decayed, and hence the transmission is dominated by the direct transmission (the unity term in Eq. (2.80)). This does not create a superposition and hence the fidelity becomes lower.

In Fig. 2.9 (b) we plot the fidelity as a function of β, ($\beta = \beta_0+\beta_1$) assuming $\beta_0 = \beta_1$ for different coherent-pulse average photon numbers. Note that $F_+ = 1-F_-$ where $F_\pm = |\langle\Psi^\pm|\Psi\rangle|^2$, so the fidelity for the symmetric superposition state $|\Psi^+\rangle = (|0\rangle+|1\rangle)/\sqrt{2}$ is equal to the fidelity with respect to the antisymmetric state $|\Psi^-\rangle$ mirrored about $F = 1/2$. In an experiment, the time of detection t_c is randomly distributed according to the intensity (2.95), and as such doing many of these experiments would on average yield a fidelity $\bar{F} = \int_0^T I_{out}(t_c)F(t_c,T)dt_c/\int_0^T I_{out}(t_c)dt_c$, if we do not condition on a particular detection time. Taking the average results in

$$\bar{F} = \frac{1}{2} + \frac{1}{2}\frac{\sin(\omega_{01}T)}{\omega_{01}T}\frac{e^{-\bar{n}/2}}{2-e^{-\bar{n}/2}}. \tag{2.113}$$

For suitable limits this can be simplified to

$$\bar{F} \approx \frac{1}{2-e^{-\bar{n}/2}} \quad \text{for} \quad \omega_{01} \ll \frac{2\pi}{T} \tag{2.114}$$

$$\bar{F} \approx \frac{1}{2} + \frac{1}{2}\frac{\sin(\omega_{01}T)}{\omega_{01}T} \quad \text{for} \quad \bar{n} \ll 1. \tag{2.115}$$

From this we find, e.g., for $\omega_{01} \ll \frac{2\pi}{T}$, $\bar{F} \approx 0.7$ for $\bar{n} = 1$ and $\bar{F} \approx (1-\bar{n}/2)$ for $\bar{n} \ll 1$. In the limit of $\omega_{01} \gg \frac{2\pi}{T}$ the fidelity reaches a value for a completely mixed state of $F = 1/2$. This result is an instance of Heisenberg's 'energy-time' uncertainty of the Λ-system state. If the detection-time interval is sufficiently short we cannot resolve the frequency resulting in a superposition of the possible outcomes. Furthermore, the fidelity decreases with a larger number of photons in the input coherent pulse because the state will have a larger decoherence due to scattering of additional photons.

2.6 Summary

We have here explicitly demonstrated how to apply the scattering formalism [4] to single-photon/weak-coherent pulse scattering in a 1D waveguide. Our formalism conveniently employs the method of the effective operators to solve the possibly complicated dynamics of the emitters arising from the interaction with the incoming photons. Our approach is applicable to both single and double-sided waveguides and can also include chirality in the coupling. We have shown with several generic examples how one can apply the developed photon-scattering relation to experimentally viable physical systems. In particular, we show how our photon scattering formalism gives a direct solution to the nontrivial problem of generation of a superposition state based on detection of scattered photons.

It is worth emphasizing that this is a general framework that can be applied in many different contexts. The examples are therefore mainly meant as an illustration of how to apply the technique to achieve non-trivial results with limited calculations. In particular, we have applied the formalism to describe entanglement generation between distant emitters in Ref. [3] and [1]. Such protocols may play an important role in future emerging quantum technologies. In this context, waveguides are particular useful for distributing information and we see wide application of our formalism both for optical and microwave qubits.

2.7 Appendix A: Detailed derivation of the photon-scattering relation

In this appendix we provide a detailed derivation of the photon-scattering relation Eq. (2.7) between the amplitudes of the incoming and outgoing photons. We start by substituting Eq. (2.5) into Eq. (2.4) and then comparing the RHS and LHS of Eq. (2.4) to get

$$
\begin{aligned}
& i\sum_{k_f}\sqrt{\frac{\hbar\omega_{k_f}}{2}}\vec{F}_{k_f}(\vec{r}_\perp)\hat{a}_{k_f}e^{i(k_f z-\omega_{k_f}t)} = i\int d\vec{r'}_\perp \mathbf{G}_f(\vec{r}_\perp,t,\vec{r'}_\perp,0)\epsilon(\vec{r'}_\perp)\sum_{k_f}\sqrt{\frac{\hbar\omega_{k_f}}{2}}\vec{F}_{k_f}(\vec{r'}_\perp)\hat{a}_{k_f}e^{ik_f z} \\
+ & \left(\frac{i\omega}{2\hbar}\right)\sum_{jj'}\sum_{gg'}\int_0^\infty d\tau' e^{i\omega_{gg'}\tau}\hat{\sigma}_{g'g}\mathbf{G}_f(\vec{r}_\perp,t,\vec{r}_{j\perp},t')\sum_{ee'}\left[\vec{d}^{\,j}_{ge}(\tilde{\mathcal{H}}_{\rm nh})^{-1}_{ee'}\vec{d}^{\,j'}_{e'g}\right] \\
\times & \int d\vec{r'}_\perp\Bigg[\mathbf{G}_f(\vec{r}_{j'\perp},t',\vec{r'}_\perp,0)\epsilon(\vec{r'}_\perp)i\sum_{k_f}\sqrt{\frac{\hbar\omega_{k_f}}{2}}\vec{F}_{k_f}(\vec{r'}_\perp)\hat{a}_{k_f}e^{ik_f z}+\mathbf{G}_b(\vec{r}_{j'\perp},t',\vec{r'}_\perp,0)\epsilon(\vec{r'}_\perp) \\
& i\sum_{k_b}\sqrt{\frac{\hbar\omega_{k_b}}{2}}\vec{F}_{k_b}(\vec{r'}_\perp)\hat{a}_{k_b}e^{ik_b z}\Bigg]+\mathcal{F}
\end{aligned}
\tag{2.116}
$$

$$
\begin{aligned}
& i\sum_{k_b}\sqrt{\frac{\hbar\omega_{k_b}}{2}}\vec{F}_{k_b}(\vec{r}_\perp)\hat{a}_{k_b}e^{i(k_b z-\omega_{k_b}t)} = i\int d\vec{r'}_\perp \mathbf{G}_b(\vec{r}_\perp,t,\vec{r'}_\perp,0)\epsilon(\vec{r'}_\perp)\sum_{k_b}\sqrt{\frac{\hbar\omega_{k_b}}{2}}\vec{F}_{k_b}(\vec{r'}_\perp)\hat{a}_{k_b}e^{ik_b z} \\
+ & \left(\frac{i\omega}{2\hbar}\right)\sum_{jj'}\sum_{gg'}\int_0^\infty d\tau' e^{i\omega_{gg'}\tau}\hat{\sigma}_{g'g}\mathbf{G}_b(\vec{r}_\perp,t,\vec{r}_{j\perp},t')\sum_{ee'}\left[\vec{d}^{\,j}_{ge}(\tilde{\mathcal{H}}_{\rm nh})^{-1}_{ee'}\vec{d}^{\,j'}_{e'g}\right] \\
\times & \int d\vec{r'}_\perp\Bigg[\mathbf{G}_f(\vec{r}_{j'\perp},t',\vec{r'}_\perp,0)\epsilon(\vec{r'}_\perp)i\sum_{k_f}\sqrt{\frac{\hbar\omega_{k_f}}{2}}\vec{F}_{k_f}(\vec{r'}_\perp)\hat{a}_{k_f}e^{ik_f z}+\mathbf{G}_b(\vec{r}_{j'\perp},t',\vec{r'}_\perp,0)\epsilon(\vec{r'}_\perp) \\
& i\sum_{k_b}\sqrt{\frac{\hbar\omega_{k_b}}{2}}\vec{F}_{k_b}(\vec{r'}_\perp)\hat{a}_{k_b}e^{ik_b z}\Bigg]+\mathcal{F}
\end{aligned}
\tag{2.117}
$$

The symbol $\mathcal{F}$ here stands for noise which corresponds to the field not into the waveguide mode and can be expressed in terms of $\mathcal{E}_{\text{rest},\zeta}(\vec{r},t)$ and the Green's function $\mathbf{G}_{\text{rest},\zeta}(\vec{r},t,\vec{r'},t')$. We next solve the space and time integrals in Eq. (2.116) and (2.117) and convert the sum to an integral $\sum_k \to \frac{1}{\sqrt{2\pi}}\int dk$. Finally after multiplying both sides with the mode function $\epsilon\vec{F}^*_{k_\zeta}(\vec{r}_\perp)$, integrating over the transverse plane and on comparing the terms on the RHS and LHS, we arrive at an input-output formalism between the incoming and scattered photons represented respectively by the mode operators, $a_{o,f}$ and $a_{in,f}$

$$\begin{aligned} a_{o,f}\left(t-\frac{\mathrm{z}}{v_g}\right) &= a_{in,f}\left(t-\frac{\mathrm{z}}{v_g}\right)+\left(\frac{i\omega_0\pi}{\hbar v_g}\right)\sum_{jj'}\sum_{gg'}e^{-i\omega_{gg'}|\mathrm{z}-\mathrm{z}_j|/v_g}\hat{\sigma}_{g'g}\sum_{ee'}\Bigg[\left(\mathcal{A}^{*jf}_{ge}(H_{\text{nh}})^{-1}_{jj'}\mathcal{A}^{j'f}_{e'g}\right) \\ &\quad a_{in,f}(0)+\left(\mathcal{A}^{*jf}_{ge}(H_{\text{nh}})^{-1}_{ee'}\mathcal{A}^{j'b}_{e'g}\right)e^{-2i\vec{k}_0\mathrm{z}_j}a_{in,b}(0)\Bigg]+\mathcal{F} \end{aligned} \tag{2.118}$$

$$\begin{aligned} a_{o,b}\left(t+\frac{\mathrm{z}}{v_g}\right) &= a_{in,b}\left(t+\frac{\mathrm{z}}{v_g}\right)+\left(\frac{i\omega_0\pi}{\hbar v_g}\right)\sum_{jj'}\sum_{gg'}e^{-i\omega_{gg'}|\mathrm{z}-\mathrm{z}_j|/v_g}\hat{\sigma}_{g'g}\sum_{ee'}\Bigg[\left(\mathcal{A}^{*jf}_{ge}(H_{\text{nh}})^{-1}_{ee'}\mathcal{A}^{j'f}_{e'g}\right) \\ &\quad a_{in,b}(0)+\left(\mathcal{A}^{*jf}_{ge}(H_{\text{nh}})^{-1}_{jj'}\mathcal{A}^{j'b}_{e'g}\right)e^{2i\vec{k}_0\mathrm{z}_j}a_{in,f}(0)\Bigg]+\mathcal{F} \end{aligned} \tag{2.119}$$

Here $f(b)$ signifies the forward (backward) direction of propagation for the incoming and scattered photons. Note that we consider both the forward and backward contributions to the input field as well as the scattered fields as we assume a double-sided waveguide with input possible from both ends. In deriving the above set of equations, we have expanded $\omega_{k,f/b} = \omega_0 + v_{g_{f/b}}(k_{f/b}-k_0)$ with $k_{f/b} = \pm k$. Furthermore, we have written the Green's function in terms of the mode function and assumed that the transverse field into the waveguide have the mode functions of the form $\vec{F}_{k_f}(\vec{r}_\perp) = \vec{F}_{k_f}(\vec{r}_\perp)e^{i\vec{k}_f\mathrm{z}}$, $\vec{F}_{k_b}(\vec{r}_\perp) = \vec{F}_{k_b}(\vec{r}_\perp)e^{i\vec{k}_b\mathrm{z}}$. The coupling strength $\mathcal{A}^{j,(f/b)}_{eg}$ in the above photon-scattering relation is defined as a product of the emitter's dipole moments and the field-mode function in the form $\mathcal{A}^{j(f/b)}_{eg} = \sqrt{\frac{\pi\omega}{\hbar v_g}}\left[\vec{d}^{j}_{eg}\cdot\vec{F}_{k_\zeta}(r_{j_\perp})\right]$. Finally we have also defined different forward and backward mode operators of the incoming and scattered field as

$$\hat{a}_{o,f/b}\left(t-\frac{\mathrm{z}}{v_g}\right) = \sqrt{\frac{v_g}{2\pi}}\int dk_{f/b}e^{-i\delta k_{f/b}v_g(t-\frac{\mathrm{z}}{v_g})}\hat{a}_{k_{f/b}} \tag{2.120}$$

$$\hat{a}_{in,f/b}(t) = \sqrt{\frac{v_g}{2\pi}}\int dk_{f/b}e^{-i\delta k_{f/b}v_g t}\hat{a}_{k_{f/b}} \tag{2.121}$$

$$\tag{2.122}$$

Eq. (2.7) and Eq. (2.8) then follows from Eq. (2.118) and Eq. (2.119) with the decay into the forward and backward modes of the waveguide $\Gamma^{(f/b)}_{eg}$, defined in terms of the coupling strengths $\mathcal{A}^{(f/b)}_{eg}$ and their complex conjugate.

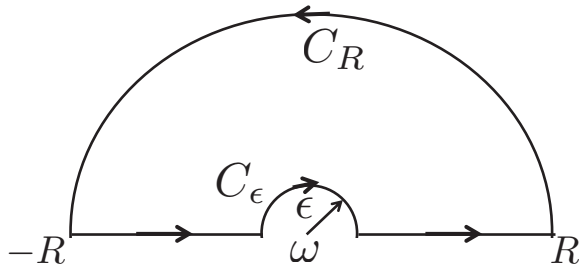

FIGURE 2.10: Contour for evaluating the principal-value integral

2.8 Appendix B: Derivation of the waveguide-mediated coupling between emitters

The waveguide-mediated decay and shifts of the emitter's excited state are given by,

$$\Gamma_{gg'}^{jj',e'e} = \frac{2\omega_{e'g'}^2}{\hbar v_g^2}\left\{\vec{d}_{e'g}^{\,\jmath}\cdot\mathbf{Im}\overleftrightarrow{\mathbf{G}}_\zeta(\vec{r}_j,\vec{r}_{j'},\omega_{e'g'})\cdot\vec{d}_{g'e}^{\,\jmath'}\right\}, \tag{2.123}$$

$$\Omega_{gg'}^{jj',e'e} = \mathbf{P}\int d\omega\left(\frac{\omega^2}{\hbar\pi v_g^2}\right)\left\{\frac{\vec{d}_{e'g}^{\,\jmath}\cdot\mathbf{Im}\overleftrightarrow{\mathbf{G}}_\zeta\cdot\vec{d}_{g'e}^{\,\jmath'}}{(\omega-\omega_{e'g'}+i\epsilon)}\right\}. \tag{2.124}$$

Now considering the expression for $\mathbf{Im}\overleftrightarrow{\mathbf{G}}_\zeta(\vec{r}_j,\vec{r}_{j'},\omega_{e'g'})$ in Eq. (2.18) and substituting it into the above Eqs. (2.123) and (2.124) we get,

$$\Gamma_{gg'}^{jj',e'e} = 2\sum_\zeta \mathcal{A}_k^{j\zeta}\mathcal{A}_k^{*j'\zeta}\cos\left(k_\zeta|\mathrm{z}_j-\mathrm{z}_{j'}|\right), \tag{2.125}$$

$$\Omega_{gg'}^{jj',e'e} = \frac{1}{2\hbar v_g}\sum_\zeta \mathbf{P}\int_{-\infty}^{\infty} d\omega'\,\omega'(g_{\omega'/v_g}^{j\zeta}g_{\omega'/v_g}^{*j'\zeta})\left[\frac{\cos\left(\omega'|\mathrm{z}_j-\mathrm{z}_{j'}|/v_g\right)}{(\omega'-\omega+i\epsilon)}\right] \tag{2.126}$$

where $g_{\omega'/v_g}^{j\zeta}=\vec{d}_{eg}^{\,\jmath}\cdot\vec{F}_{\omega'/v_g}(\vec{r}_{j\perp})$. We next expand the cosine term in the above integral as $[\exp(i\omega'|\mathrm{z}_j-\mathrm{z}_{j'}|/v_g)+\exp(-i\omega'|\mathrm{z}_j-\mathrm{z}_{j'}|/v_g)]/2$ and write Eq. (2.126) as sum of two integrals. We then solve the integral with the positive frequency integrand by the method of Cauchy's principal value over the contour shown in Fig. (2.10). It can be seen clearly that the integral does not have a pole inside the big contour C_R. Hence from the residue theorem, we find that the total integral $\left[\int_{C_R}+\int_{-R}^{\omega-\epsilon}+\int_{C_\epsilon}+\int_{\omega+\epsilon}^{R}\right]d\omega\ f(\omega)=0$. However, this can be rewritten as $\left[\int_{C_R}+\int_{-R}^{\omega-\epsilon}+\int_{\omega+\epsilon}^{R}\right]d\omega\ f(\omega)=-\int_{C_\epsilon}d\omega\ f(\omega)$. Thus, in the limit of $R\to\infty$ the right hand side can be evaluated in terms of the value of the analytical function $f(\omega)$ for the small contour C_ϵ. On evaluating the small contour C_ϵ we get $\int_{-\infty}^{\infty}d\omega f(\omega')=-i\pi f(\omega)$, where $f(\omega')=\omega'(g_{\omega'/v_g}^{j\zeta}g_{\omega'/v_g}^{*j'\zeta})e^{i\omega'|z_j-z_{j'}|/v_g}$. The integral for the negative frequency integrand $\exp(-i\omega'|\mathrm{z}_j-\mathrm{z}_{j'}|/v_g)/2$ can be solved similarly by choosing a contour that is mirror reflection of Fig. (2.10) about the real axis. This then gives for the small contour C_ϵ, that goes counter-clockwise $\int_{-\infty}^{\infty}d\omega f(\omega')=i\pi f(\omega)$, where now $f(\omega')=\omega'(g_{\omega'/v_g}^{j\zeta}g_{\omega'/v_g}^{*j'\zeta})e^{-i\omega'|z_j-z_{j'}|/v_g}$. Finally, on substituting the evaluated integral into

Eq. (2.126) we find the principal-value integral to be

$$\Omega_{gg'}^{jj',e'e} = -\sum_{\zeta} \mathcal{A}_k^{j\zeta} \mathcal{A}_k^{*j'\zeta} \sin\left(k_\zeta |z_j - z_{j'}|\right), \tag{2.127}$$

where we have used the definition of $\mathcal{A}_k^{j\zeta}$ from Sec. III. The evaluated integral thus gives Eq. (2.19) and Eq. (2.20) of Sec. III.

2.9 Appendix C: Definition of the effective detuning and rates for the two-emitter system

In this appendix we define the effective detunings and decay rates introduced as a part of the non-Hermitian Hamiltonian in Eq. (2.63) for the two-emitter system with one being a two-level system while the other system is a three-level in V-configuration.

$$\delta_{1,\text{eff}}^{-1} \equiv \left[\tilde{\delta}_1 + \frac{\Gamma_{12}^2}{4\tilde{\delta}_2} + \frac{\Gamma_{13}^2}{4\tilde{\delta}_3} - \frac{(\Omega - i\Gamma_{23})(\frac{\Gamma_{12}^2}{4\tilde{\delta}_2} + \frac{\Gamma_{13}^2}{4\tilde{\delta}_3}) - \Gamma_{12}\Gamma_{13}}{(\Omega - i\Gamma_{23}) - \frac{4\tilde{\delta}_2\tilde{\delta}_3}{\Omega - i\Gamma_{23}}}\right]^{-1} \tag{2.128a}$$

$$\delta_{2,\text{eff}}^{-1} \equiv \left[\tilde{\delta}_2 + \frac{\Gamma_{12}^2}{4\tilde{\delta}_1} - \frac{(\Omega - i\Gamma_{23})^2}{4\tilde{\delta}_3} - \frac{\Gamma_{13}(\frac{\Gamma_{12}^2}{4\tilde{\delta}_1} - \frac{(\Omega - i\Gamma_{23})^2}{4\tilde{\delta}_3}) + \Gamma_{12}(\Omega - i\Gamma_{23})}{\Gamma_{13} - \frac{4\tilde{\delta}_1\tilde{\delta}_3}{\Gamma_{13}}}\right]^{-1} \tag{2.128b}$$

$$\delta_{3,\text{eff}}^{-1} \equiv \left[\tilde{\delta}_3 + \frac{\Gamma_{13}^2}{4\tilde{\delta}_1} - \frac{(\Omega - i\Gamma_{23})^2}{4\tilde{\delta}_2} - \frac{\Gamma_{12}(\frac{\Gamma_{13}^2}{4\tilde{\delta}_1} - \frac{(\Omega - i\Gamma_{23})^2}{4\tilde{\delta}_2}) + \Gamma_{13}(\Omega - i\Gamma_{23})}{\Gamma_{12} - \frac{4\tilde{\delta}_1\tilde{\delta}_2}{\Gamma_{12}}}\right]^{-1} \tag{2.128c}$$

$$\Gamma_{12,\text{eff}}^{-1} \equiv \left[-\frac{i}{2}\left(\Gamma_{12} + \frac{4\tilde{\delta}_1\tilde{\delta}_2}{\Gamma_{12}} + \frac{\frac{\Gamma_{13}^2}{\Gamma_{12}}\tilde{\delta}_2 - 4\frac{(\Omega/2 - i\Gamma_{23}/2)^2}{\Gamma_{12}}\tilde{\delta}_1 - (\Omega/2 - i\Gamma_{23}/2)\Gamma_{13}(1 - 4\frac{\tilde{\delta}_1\tilde{\delta}_2}{\Gamma_{12}^2})}{\tilde{\delta}_3 - \frac{(\Omega/2 - i\Gamma_{23}/2)\Gamma_{13}}{\Gamma_{12}}}\right)\right]^{-1} \tag{2.129a}$$

$$\Gamma_{13,\text{eff}}^{-1} \equiv \left[-\frac{i}{2}\left(\Gamma_{13} + \frac{4\tilde{\delta}_1\tilde{\delta}_3}{\Gamma_{13}} + \frac{\frac{\Gamma_{12}^2}{\Gamma_{13}}\tilde{\delta}_3 - 4\frac{(\Omega/2 - i\Gamma_{23}/2)^2}{\Gamma_{13}}\tilde{\delta}_1 - (\Omega/2 - i\Gamma_{23}/2)\Gamma_{12}(1 + \frac{\tilde{\delta}_1\tilde{\delta}_3}{\Gamma_{13}^2})}{\tilde{\delta}_2 - \frac{(\Omega/2 - i\Gamma_{23}/2)\Gamma_{12}}{\Gamma_{13}}}\right)\right]^{-1} \tag{2.129b}$$

$$\Gamma_{23,\text{eff}}^{-1} \equiv \left[(\Omega/2 - i\Gamma_{23}/2) - \frac{\tilde{\delta}_2\tilde{\delta}_3}{\Omega/2 - i\Gamma_{23}/2} + \frac{1}{4}\frac{\left(\Gamma_{12} - \frac{\Gamma_{13}\tilde{\delta}_2}{\Omega/2 - i\Gamma_{23}/2}\right)\left(\Gamma_{13} - \frac{\Gamma_{12}\tilde{\delta}_3}{\Omega/2 - i\Gamma_{23}/2}\right)}{\tilde{\delta}_1 + \frac{1}{4}\frac{\Gamma_{12}\Gamma_{13}}{\Omega/2 - i\Gamma_{23}/2}}\right]^{-1}. \tag{2.129c}$$

Chapter 3

Enhancing quantum transduction via long-range waveguide mediated interactions between quantum emitters[1]

3.1 Introduction

Efficient transduction of electromagnetic signals between different frequency scales is an essential ingredient for modern communication technologies as well as for the emergent field of quantum information processing. Recent advances in waveguide photonics have enabled a breakthrough in light-matter coupling, where individual two-level emitters are strongly coupled to individual photons. Here we propose a scheme which exploits this coupling to boost the performance of transducers between low-frequency signals and optical fields operating at the level of individual photons. Specifically, we demonstrate how to engineer the interaction between quantum dots in waveguides to enable efficient transduction of electric fields coupled to quantum dots. Owing to the scalability and integrability of the solid-state platform, our transducer can potentially become a key building block of a quantum internet node. To demonstrate this, we show how it can be used as a coherent quantum interface between optical photons and a two-level system like a superconducting qubit.

Transduction of information between physical systems operating at different energy scales is of immense technological importance. In telecommunication in particular, efficient transduction of signals from the microwave to the optical domain and back is an essential requirement for both today's and future global networks. For future communication technologies based on the principles of quantum mechanics, analogous transduction devices capable of coherent information transfer at the few-photon level are a necessity. Possible applications of such devices range from a quantum internet [16, 94–97] and distributed quantum computing [98, 99], to sensing weak fields in quantum metrology [100–102].

Due to the large range applications, several different methods for implementing coherent quantum transducers have been investigated. A large class of these rely on the use of nanomechanical systems [103–107] or direct electro-optical coupling [108, 109]. Other proposals exploit quantum emitters with both microwave and optical transitions [97, 110–114]. Many of these rely on magnetic interactions which typically results in weak interactions to single emitters but strong coupling to ensembles of emitters (see however [112, 115] for exceptions). Despite these efforts, however, coherent state transfer from systems with only low-frequency excitations to the optical regime remains elusive.

[1] This Chapter is an adaptation of publication Ref. [1]. In that article, Dr. Sumanta Das and Professor Anders S. Sørensen are co-authors and helped revising the final draft. Vincent Elfving has written and performed the analytical and numerical calculations for both the main text and the Supplementary Information.

Common to these approaches is the use of strong optical driving fields to enhance the transduction. This can pose a major source of light-induced decoherence [116] since the energy of optical photons is much larger than typical energies in cryogenic environments. The absorption of even a single optical photon is thus a major disturbance. Furthermore the use of strong light fields poses a filtering problem since weak quantum fields, e.g. single photons, have to be distinguished from a strong background signal.

Here, we propose a scheme for an electrically coupled quantum transducer that works at very low light levels, e.g. a few photons. The principal elements of our transducer are semiconductor quantum dots (QDs) which can be grown in a photonic crystal waveguide with transform-limited linewidth [117] and very high mode coupling efficiency β, experimentally demonstrated up to 98% [118]. We show that the high coupling efficiency enables a high conversion efficiency due to the strongly suppressed loss rate out of the waveguide. A key feature of our transducer is that, by engineering the waveguide interactions between multiple QDs, it can work efficiently even when only a single optical photon is involved in the transduction. This minimizes the probability of light-induced decoherence of the quantum systems, as well as ensuring only a negligible contribution of background light in the transduced signal.

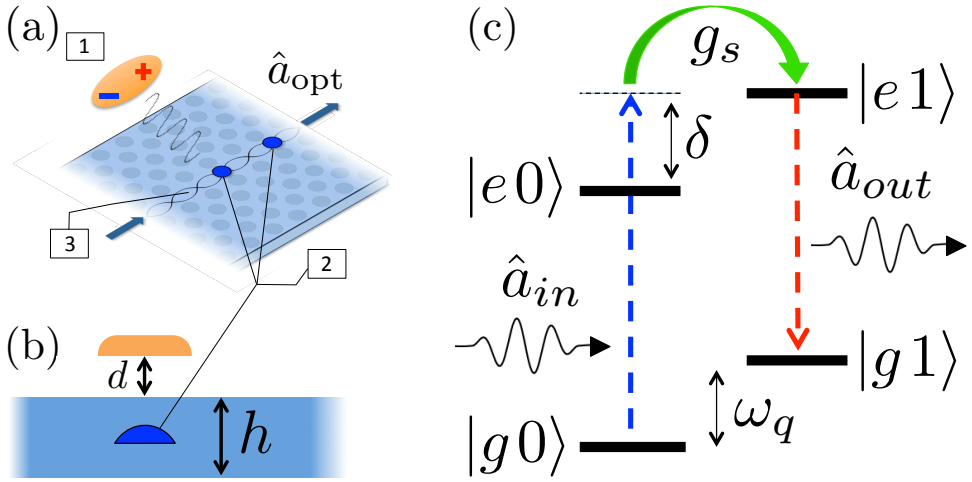

FIGURE 3.1: (a) Schematic of the transducer. A two-level system (TLS) represented by an oscillating electric dipole (1) is electrically coupled to a semiconductor QD (2) grown inside a photonic waveguide (3) to provide a highly efficient interaction with optical photons ($\hat{a}_{\rm opt}$). We consider different numbers of QDs and configurations for the transducer. (b) side view of the transducer. The TLS (orange) is a distance d away from the photonic crystal of thickness $h = 140$nm, with a QD grown in the center. (c) Energy level diagram of a single-QD transducer, with $|e\rangle/|g\rangle$ being the QD excited/ground state respectively. The electrical coupling g_s enables a Raman transfer process between internal states $|0\rangle$ and $|1\rangle$ of the coherent TLS, separated by a frequency difference ω_q. Transduction happens through the Raman path indicated by green arrows. Here an incoming photon resonant with the transition from $|g\,0\rangle$ to $|e\,1\rangle$ mediated by the virtual level $|e\,0\rangle$, results in the emission of a low frequency photon entangled with the internal state of the coherent TLS.

As a particular application we show how to exploit the proposed transducer as a quantum interface between optical photons and superconducting qubits. Related approaches were recently proposed using two nearby dipole-coupled molecules [3] or a double QD molecule [119]. As opposed to these systems, however, experimental demonstrations of QD-waveguide interfaces have shown efficient coherent coupling to traveling light fields,

which in turn strongly enhances the transduction efficiency in our scheme. Furthermore we show that the strong coupling of multiple QDs to waveguides allows engineering the photonic interactions to further enhance the transduction. In particular the long-range waveguide mediated interactions can be utilized to create super- and sub-radiant states (akin to similar states in atomic systems [55, 89, 120–122]) between distant QDs, which enhances the transduction. These photonic interactions can thus be exploited to leverage the transduction and reduce the requirements for engineering complicated near-field interactions.

3.2 Results

In Figure 3.1a, we show schematically our proposed quantum transducer. It essentially consists of three components; a 1D waveguide for efficient confinement of the optical mode; one or more QDs coupled to the photonic mode with high efficiency; and finally a nearby oscillating electric dipole, which electrically couples to a QD exciton via the Stark effect. For specificity, we focus on transduction with a coherent two level system (TLS) with a dipole allowed transition at a non-optical frequency, e.g. in the GHz regime. Examples of such coherent (effective) TLS's include superconducting qubits [123–125], crystal defect states [126], and singlet-triplet states in double-QD structures [127–129].

3.2.1 Single-QD Transducer

To begin with we consider a transducer with a single QD situated in the photonic waveguide and coupled electrically to an external oscillating dipole that represents a coherent TLS (see Figure 3.1a). The total Hamiltonian $\mathcal{H}$ describing this system can be written as $\mathcal{H} = \mathcal{H}_0 + \mathcal{V}_1 + \mathcal{V}_2$ where $\mathcal{H}_0$ is the sum of bare energies written as $\omega_d\hat{\sigma}^\dagger\hat{\sigma} + \sum_k \omega_k \hat{a}_k^\dagger \hat{a}_k + \omega_q\hat{\eta}_z$ ($\hbar = 1$). The TLS transition frequency is ω_q, the QD transition frequency ω_d, and the photonic mode frequencies ω_k. The term $\mathcal{V}_1$ represents the interaction between the QD and drive fields and is written as $\mathcal{V}_1 = \sum_k g_k(\hat{\sigma}\hat{a}_k^\dagger + \hat{\sigma}^\dagger\hat{a}_k)$, where g_k is the coupling of the 2-level QD to the k'th mode with annihilation operator $\hat{a}_k$, and $\hat{\sigma} = |g\rangle\langle e|$ is the standard lowering operator of the QD. The TLS is represented by the Pauli-X and Z operators, where $\hat{\eta}_x = |1\rangle\langle 0| + |0\rangle\langle 1|$ and $\hat{\eta}_z = (|1\rangle\langle 1| - |0\rangle\langle 0|)/2$ with $|0\rangle$ and $|1\rangle$ as the internal states. As we assume that the TLS has a dipole allowed transition between the energy levels, there will be an associated electric field of the form $\hat{E} = \vec{E}(r)\eta_x$. A QD is known to exhibit a sizable stark shift of their excited levels, corresponding to a dipole moment up to $|\vec{p}| \approx 0.4\,\mathrm{e}\cdot\mathrm{nm}$ [130], for an In(Ga)As QD. The proximity to the TLS thus leads to an interaction of the form $\mathcal{V}_2 = g_s\hat{\eta}_x\hat{\sigma}^\dagger\hat{\sigma}$ with $g_s \equiv \vec{p}\cdot\vec{E}/\hbar$. As we show in Section 3.3 this interaction can be sizable, $g_s = 2\pi \times (0.4 - 1)$GHz. For typical QDs in a waveguide, this coupling is larger than their total decay rate $\Gamma \approx 2\pi \times 150$MHz. The system is thus in a strong coupling regime $g_s > \Gamma$ allowing for the engineering of an efficient transducer

The combined TLS-QD system constitutes an effective 4-level system in which we consider a Raman transition (see Figure 3.1c) between the TLS states via a single incoming optical photon. This realizes a frequency conversion and effectively entangles the frequency of a scattered weak photon pulse with the internal state of the TLS, hereby achieving a coherent interface between the two systems.

To study the dynamics of the transducer, we apply the formalism of Ref. [4, 74] to eliminate the excited states of the system and include their effective dynamics through a non-Hermitian Hamiltonian $\mathcal{H}_{nh} = \mathcal{H}_e - \frac{i}{2}\sum_k \mathcal{L}_k^\dagger\mathcal{L}_k$ with $\mathcal{H}_e = \delta_p + \omega_q\hat{\eta}_z + g_s\hat{\eta}_x$ based on the excited subspace of the Hamiltonian $\mathcal{H}$, with $\delta_p = \omega_d - \omega_p$ being the photon-QD detuning. The operators representing the decay dynamics of the system are defined as $\mathcal{L}_k = \Gamma_k|g\rangle\langle e|$ with Γ_k being the QD decay into and out of the waveguide with rates Γ_{1D} and γ' respectively.

We calculate Section 3.3 the single-photon Raman scattering probability into a single-sided waveguide, and find $P_R = \Gamma_{1D}^2 |\langle e1|\mathcal{H}_{nh}^{-1}|e0\rangle|^2$. This is the probability of detecting a photon from the outgoing light field after frequency filtering for red (Raman scattered) photons only. Calculating the maximum transition probability as a function of the detuning between input field and QD yields the resonance conditions $\delta_\pm = (\omega_q \pm \sqrt{\omega_q^2 + g_s^2 - \Gamma^2})/2$. At these resonances we find the Raman scattering probability to be $P_R^{(1QD)} = \beta^2 g_s^2/(g_s^2 + \omega_q^2)$, and in the strong/weak coupling limits we find

$$P_R^{(1QD)} \approx \beta^2 \quad \text{for} \quad g_s \gg \omega_q, \tag{3.1}$$

$$P_R^{(1QD)} \approx \beta^2 \frac{g_s^2}{\omega_q^2} \quad \text{for} \quad g_s \ll \omega_q, \tag{3.2}$$

where $\beta = \Gamma_{1D}/(\Gamma_{1D}+\gamma')$ describes the probability of emitting a photon into the waveguide.

Eq. 3.1 expresses the striking advantage that can be obtained by exploiting strong coupling of emitters with a waveguide. For β approaching unity an extremely efficient transducer can be constructed, operating in the quantum regime where each incoming optical photon corresponds to an excitation transduced from low frequencies to optical photons. This is in contrast to most other proposals where strong classical driving fields are assumed. The efficient transduction discussed here is mainly applicable to low frequency fields in the MHz regime. Many of the qubit systems relevant for this transduction scheme are, however, in the microwave (GHz) regime, which is larger than the maximal estimated coupling $g_s \lesssim 2\pi \times 1\text{GHz}$. This strongly diminishes the efficiency in Eq. 3.2. This reduction arises because the electric dipole moment of the TLS is linked to a transition between two energy levels so that the field felt by the QD is an oscillating field, which tends to average out the coupling. To counter this effect, we here propose engineering the excited subspace using multiple QDs in the waveguide. We make use of the high β-factor achievable for QDs in a photonic crystal waveguide to get strong waveguide mediated interactions between QDs. With two QDs we show that we can suppress the magnitude of the decay into the waveguide and enhance the effective coupling by increasing the interaction time. Furthermore by using four QDs we can engineer the exchange of excitations between QDs to be resonant with the TLS transition and thereby avoid the averaging effect.

3.2.2 Two-QD Transducer

To illustrate this waveguide-mediated enhancement, we first consider two QDs placed in a 1D waveguide (see Figure 3.2a). The photonic field in the waveguide then induces long-range interactions between the two. This can be described by a non-Hermitian Hamiltonian of the single-excitation subspace for a bare two-emitter system, which can be written as $\mathcal{H}_{nh} = \Delta|eg\rangle\langle eg| + \Omega(|eg\rangle\langle ge| + |ge\rangle\langle eg|)$ (see Section 3.3), where $|eg\rangle = |e\rangle_1 \otimes |g\rangle_2$, Δ is the detuning between the emitters' transition frequencies, and the collective complex coupling Ω consists of waveguide-mediated coherent coupling between emitters ($\text{Re}(\Omega) = \sqrt{\Gamma_{1D}^{(1)}\Gamma_{1D}^{(2)}}\sin k\Delta z$) and collective decay ($\text{Im}(\Omega) = -\sqrt{\Gamma_{1D}^{(1)}\Gamma_{1D}^{(2)}}\cos k\Delta z$) (see for example Ref. [72]) where $\Gamma_{1D}^{(j)}$ is the coupling rate, $\Delta z = |z_2 - z_1|$ and z_j is the position of emitter j.

We diagonalize the bare two-emitter Hamiltonian (see Section 3.3), for simplicity assuming that the QDs have equal bare decay rates into and and out of the waveguide, at a rate $\Gamma_{1D}^{(1)} = \Gamma_{1D}^{(2)} \equiv \Gamma_{1D}$ and $\gamma_1^{'} = \gamma_2^{'} \equiv \gamma'$ respectively. We find (anti-)symmetric eigenstates $|(A)S\rangle = \xi_1|eg\rangle \pm \xi_2|ge\rangle$ of the Hamiltonian. Here $\xi_{1,2}$ are complex numbers that denote the weighted mixture of the bare states of the two emitters, including the phase arising from the collective coupling Ω and detuning Δ between the emitters. For general spacings $k\Delta z$

and detunings Δ, we find the decay rates of the (anti-)symmetric states into the waveguide

$$\Gamma_{S,1D} = (1+\alpha_2)\Gamma_{1D} \tag{3.3}$$
$$\Gamma_{A,1D} = (1-\alpha_2)\Gamma_{1D} \tag{3.4}$$

where $\alpha_2 \equiv \left[1-\Delta^2/\Gamma_{1D}^2\right]\cos(k\Delta z)$ for small mutual detuning $\Delta \ll \Gamma_{1D}$. For emitter spacings $k\Delta z = n\pi$, with mutual detuning $\Delta = 0$, we find $\xi_1 = \xi_2 = 1/\sqrt{2}$ and $\alpha_2 = 1$ such that $|A\rangle$ is a subradiant state with total decay rate $\Gamma_A = \gamma'$ while $|S\rangle$ is a superradiant state with total decay rate $\Gamma_S = 2\Gamma_{1D} + \gamma'$. For $\beta \approx 1$, the two-QD system displays strong suppression of the anti-symmetric state decay rate, effectively increasing the lifetime of the matter-excitation.

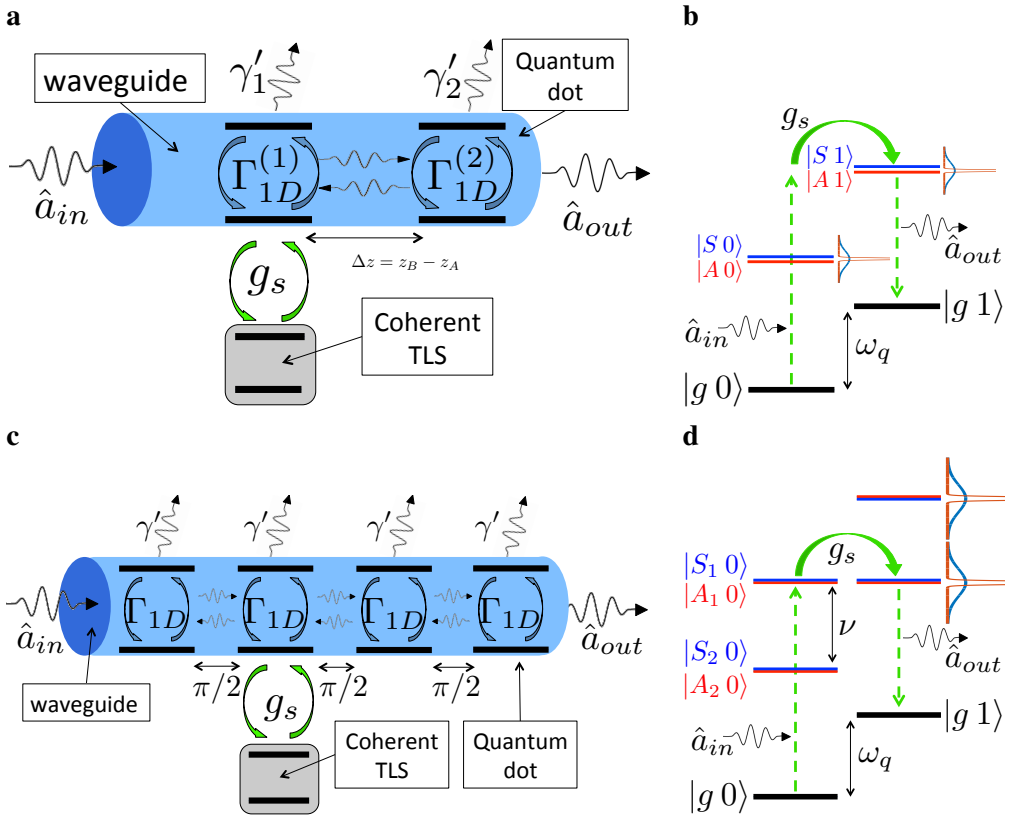

FIGURE 3.2: (a) Device architecture for coupling an optical photon pulse to a TLS via a quantum transducer comprising two QDs in a waveguide. One of the QDs is electrically coupled to the TLS. Using strong waveguide-mediated photonic coupling with a second QD, the matter-excitation lifetime can be increased and thereby the coupling to the TLS. (b) Energy level diagram of the combined QD-TLS system. $\{|0\rangle, |1\rangle\}$ represent the TLS internal states. $\{|A\rangle, |S\rangle\}$ represent the (anti-)symmetric states of the two-QD coupled system, respectively. The incoming photon is tuned in resonance with the narrow linewidth state $|A\,1\rangle$. (c) Four QDs in a waveguide are spaced equidistantly such that $k\Delta z = \pi/2$. One of the central QDs is coupled to a coherent two-level system. (d) Energy level diagram of the combined QD-TLS system for 4 QDs; In the diagonalized basis, two sets of (anti-)symmetric eigenstates of the Hamiltonian are identified, spaced by $\nu \approx 1.27\Gamma_{1D}$ and decaying at an enhanced(reduced) decay rates.

We now show that this engineered QD-QD interaction can enhance the efficiency of

our proposed quantum transducer. We assume that the TLS couples to a single QD. As described above the excited states of the two QDs couple and hybridize into (anti-)symmetric eigenstates as shown in Figure 3.2(b). The transition pathway, indicated in Figure 3.2(b), consists of 4 effective decay paths which together contribute to the output field amplitude. These contributions can be conveniently summed using the formalism of Ref. [4].

If we tune the incoming photon to be in resonance with the antisymmetric state $|A\,1\rangle$ the Raman transition rate will be dominated by a single path, $|g\,0\rangle \rightarrow |S\,0\rangle \rightarrow |A\,1\rangle \rightarrow |g\,1\rangle$. The probability for this Raman scattering for a single photon can be written Section 3.3 in the form

$$P_R^{(2QD)} \approx \left(\frac{\Gamma_{S,1D}}{\Gamma_A}\right)\left(\frac{\Gamma_{A,1D}}{\Gamma_A}\right)\left(\frac{g_s^2}{\omega_q^2}\right), \tag{3.5}$$

where $\Gamma_A = \Gamma_{A,1D} + \gamma'$ is the total decay rate of the anti-symmetric state $|A\rangle$. Eq. 3.5 illustrates the benefit from a strong waveguide mediated QD-QD interaction; one can engineer the super/sub-radiant state contrasts. Making state $|A\rangle$ longer-lived by reducing its decay into the waveguide, increases the interaction strength to the TLS and ultimately enhances the Raman probability as seen by the first factor in Eq. 3.5, $\Gamma_{S,1D}/\Gamma_A$. Because γ' is typically hard to suppress, there exists an optimal value for $\Gamma_{A,1D}$ which results in an overall improvement of the success probability. For emitters with a coupling described by a certain β-factor, the optimal sub/superradiant state decay rate occurs at $\alpha_2 = \Gamma_{1D}/(\Gamma_{1D}+\gamma')$, where $\Gamma_{A,1D} = \Gamma_{1D}(1-\beta)$ ($\Gamma_{S,1D} = \Gamma_{1D}(1+\beta)$). This condition can be met for any emitter spacing fulfilling $\cos(k\Delta z) \geq \beta$. Optimal performance can thus be reached by constructing the waveguide-emitter system such that $\cos(k\Delta z) \approx 1$, and increasing the mutual detuning between QD until $\alpha_2 = \beta$ is met (see Section 3.3 for details). For those conditions, we find

$$P_R^{(2QD),opt} \approx \frac{\beta^2}{1-\beta^2}\left(\frac{g_s}{\omega_q}\right)^2. \tag{3.6}$$

Comparing Eq. 3.5 to Eq. 3.6 there is a factor $1/(1-\beta^2)$ better transduction efficiency. For $\beta = 0.9$, this is a factor 5 improvement over Eq. 3.2. For $\beta = 0.98$, as demonstrated in ref. [118], this is a factor 25 improvement. In Figure 3.3 we compare the results of Eq. 3.2 and Eq. 3.6 for the 1 and 2 QD transducers respectively as a function of the coupling strength for $\beta = 0.9$. In the figure we also compare these approximate results with numerical simulations which include all four pathways of the transition.

3.2.3 Four-QD Transducer

The results above show that adding a second QD in the waveguide enhances the *effective* coupling to the TLS by exploiting subradiant behaviour to increase the interaction time. The main limitation of this scheme is that the relevant transition is still far off-resonant, resulting in the factor $(g_s/\omega_q)^2$ suppressing the efficiency of the Raman process. We will now show that with *four* QDs in the waveguide we can engineer the level spacing to have an even more efficient Raman transfer. Concretely, we wish to tune a set of eigenstates of the emitter-system to have an energy difference close to the TLS energy ω_q, since in a Raman scheme this brings the desired transition into resonance. In addition, we again make these states long-lived compared to the coupling g_s, such that the *effective* coupling to the TLS is enhanced.

To this end, we consider 4 QDs placed such that their mutual separations are $k\Delta z = \pi/2$ (see Figure 3.2c). At zero mutual detuning between the emitters and assuming equal decay rates, we find the spectrum of the bare excited subspace Hamiltonian and identify two bright

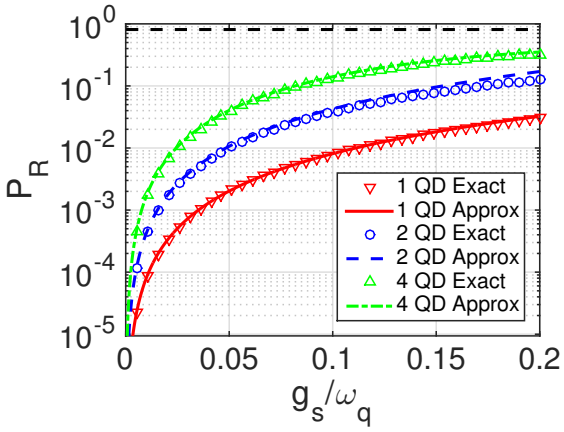

FIGURE 3.3: Raman transition probability as a function of coupling g_s. The exact forms (markers) include all transition pathways, while approximate forms (lines) include only the most significant scattering pathway transition, as given by Eqs. (3.2), (3.6) and (3.9). For the 1-QD (red) and 2-QD (blue) cases, we set $\omega_q = 2\pi \times 5$ GHz, $\Gamma_{1D} = 1$ ns^{-1}, $\beta = 0.9$, and $\alpha_2 = \beta$ in order to optimize the dark state lifetime in the 2-QD case. In the 4-QD case (green), we assume Purcell enhanced emitter decay rates into the waveguide by a factor 4 such that $1/\Gamma_{1D} = 1.27/\omega_q \approx 250$ ps while keeping $\beta = 0.9$ for comparison. The QDs are spaced such that they get a $\pi/2$ phase difference between them. In all cases we consider zero mutual detuning between emitters. For small coupling g_s, we find an order of magnitude improvement between the single-QD and the 4-QD cases. The dashed black line represents a fundamental limit of β^2 for mediation via a QD with finite waveguide-coupling efficiency β for both excitation and decay.

states and two dark states, with an energy splitting between them amounting to

$$\nu = \sqrt{\frac{1}{2}(\sqrt{5}+1)}\Gamma_{1D} \approx 1.27\,\Gamma_{1D}. \tag{3.7}$$

The dark states exhibit suppressed decay rates

$$\Gamma_{1,1D} = \Gamma_{2,1D} = (1-\alpha_4)\Gamma_{1D} \tag{3.8}$$

into the 1D waveguide with $\alpha_4 = \sqrt{\frac{1}{2}(\sqrt{5}-1)} \approx 0.79$. The resonance condition in the excited state manifold for a Raman process $|0\rangle \rightarrow |1\rangle$ is met for $\omega_q = \nu = 1.27\Gamma_{1D}$ (see Figure 3.2d). This condition can be met either by choosing a TLS with matching transition energy and/or Purcell enhancing the waveguide decay rate [78, 131, 132].

The resulting Raman process (see Figure 3.2d) probability can be calculated Section 3.3 as before, and we find

$$P_R^{(4QD)} \approx \frac{0.18(g_s/\omega_q)^2}{((g_s/\omega_q)^2 + (\beta^{-1} - 0.79)^2)^2}. \tag{3.9}$$

which we also plot in Figure 3.3 and compare with an exact expression involving all pathways.

In the limit of very weak coupling, we find $P_R \approx 64(g_s/\omega_q)^2$ for $\beta = 0.98$, and $P_R \approx 17(g_s/\omega_q)^2$ for $\beta = 0.9$. Compared to the single-QD interface, this is more than an order-of-magnitude improvement; it represents a three-fold improvement compared to the two-QD case.

3.2.4 Interfacing superconducting qubits with optical photons

We have thus far proposed an efficient quantum transducer between optical photons and a coherent two-level system at a different frequency. In the following, we discuss an important application of such a transducer as an interface between an optical photon and a microwave superconducting qubit. In a recent proposal [3], a dipole coupled organic dye molecule in an optical waveguide was considered as a transducer. However, that proposal relied on a direct dipole-dipole (proximity) interaction between molecules that is difficult to engineer and implement. Additionally, the coupling efficiency of molecules to light is typically rather low, $\beta \approx 10\%$, thereby lowering the overall Raman scattering probability. In Ref. [119], a double QD coupling was proposed to mediate the interaction; however, control of this coupling could be difficult in practice. Additionally, good coherence properties and efficient coupling to light have not yet been demonstrated for these systems. In comparison, our protocol relies on waveguide mediated long-range dipole-dipole interaction that can more easily be engineered and we exploit the high coupling efficiency of QDs to a nanophotonic waveguide.

To get an estimate for the magnitude of the Stark coupling g_s for a system with a superconducting qubit and a QD, we numerically simulate a realistic device Section 3.3 with a similar geometry as in [3]. We here assume a Cooper pair box (CPB) island of size $700\times200\times20$nm, placed above a photonic crystal waveguide of height 140nm. From the simulated electric field strength, the Stark shift coupling $g_s = \vec{p}\cdot\vec{E}/\hbar$ is calculated, where $\hbar$ is the Planck constant and $|\vec{E}|$ is the electric field strength difference between having and not having a Cooper pair on the island. $\vec{p}$ is the static dipole moment of the QD and in this context represents the Stark coefficient. Self-assembled In(Ga)As QDs with transform-limited linewidths [117] and near-unity β [118] have been reported to exhibit a Stark coefficient $|\vec{p}| = 2\pi \times 100$ MHz/(kV/m) [130]. We find that the coupling ranges from $g_s = 2\pi \times 0.4 - 1$GHz for a separation of $d = 0 - 100$nm between the qubit and the waveguide with the QD 70 nm below the top of the waveguide (see Figure 3.1b). We also numerically simulate the optical mode in this configuration and find the absorption of the light-field into the qubit to be less than 1% for the lower electrical coupling rates, and slightly higher when we consider different configurations or closer separation between qubit and waveguide Section 3.3. For coupling in the low end of our estimate $g_s = 2\pi \times 400$ MHz, a CPB qubit with $\omega_q = 2\pi \times 5$ GHz, and $\beta = 0.98$ we find a Raman success probability of $P_R \approx 0.6\%$, 13% and 31% for the single-QD, 2-QD and 4-QD interfaces, respectively. For the strongest coupling of $g_s = 2\pi \times 1000$ MHz we find $P_R \approx 4\%$, 40% and 78% respectively.

3.2.5 Long-Distance Entanglement Protocol

The quantum transducer that we have discussed is an ideal platform for long-distance entanglement schemes between remotely located qubits. Using the interference protocol proposed in [133], we consider two qubit transducers placed in either arm of a Mach-Zehnder interferometer (see inset in Figure 3.4), with fibres coupling to the waveguides containing the interfaces. Photon scattering creates entanglement between the photon frequency and the SC qubit state. Mixing the red sideband fields on a BS and detecting a photon performs an entanglement swap and creates entanglement between the qubits. For a single-photon input, the protocol has no intrinsic errors and produces an ideal state of fidelity $F = 1$ provided that no other sources of errors are present.

It is experimentally less challenging to use a weak coherent pulse with an average photon number $\bar{n}$ instead of a single-photon source. This reduces the fidelity, because the pulse may dephase or flip both qubits simultaneously. In Figure 3.4, we show the fidelity and success

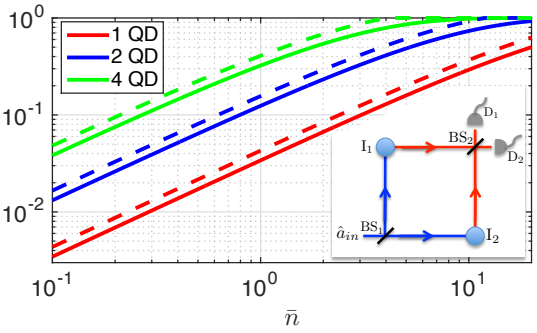

FIGURE 3.4: Infidelity ($1-F$, solid lines) and success probability (dashed lines) of entanglement generation by measurement, for a coherent pulse input, as a function of average photon number. We choose $\beta = 0.9$, detection efficiency $\eta = 0.7$, coupling $g_s = 2\pi \times 1$ GHz, and TLS transition frequency $\omega_q = 2\pi \times 5$ GHz. $\Gamma_{1D} = 1$ ns^{-1} for the 1- and 2-QD transducers and $\Gamma_{1D} = 0.25$ ns^{-1} for the 4-QD transducer. In the 4-QD case we fulfill the excited subspace resonance condition $\nu = \omega_q$ Section 3.3. Inset: schematic of entanglement generation setup, comprising a coherent input pulse labeled $\hat{a}_{in}$, two quantum interfaces I_1 and I_2, beam splitters BS_1 and BS_2 and photo-detectors D_1 and D_2.

probability for a coherent input pulse calculated using the approach of Ref. [3]. The considered Raman protocol for coherent inputs has an intrinsic requirement $1 - F \geq 1 - P_{\text{suc}}/\eta$. Our result is close to this limit, but has a slightly lower fidelity due to elastic (Rayleigh) scattering. As shown in the figure, multiple QDs enables the generation of high quality entanglement for much lower mean photons numbers. Exploiting the waveguide mediated interactions for the transduction thus reduces the possible detrimental decoherence of the SC qubit induced by the light, and allows for a near deterministic interface between photons and SC qubits. The input pulse duration is mainly limited by the linewidth of the transitions and can be in the range of 50-100 ns, reducing the effect of decoherence. For comparison, superconducting qubits of the type considered here have demonstrated coherence times exceeding a microsecond [134].

3.3 Methods

In this section, we detail the calculations which led to the above results. First, we consider the Raman scattering scheme, in the single QD situation

3.3.1 Raman Scattering Scheme

We employ the photon scattering formalism developed in Ref. [2, 4] to describe the Raman scattering of a photon in a one-dimensional waveguide from the combined system of quantum dots and a coherent two-level system (TLS). Given a right-going input field $\hat{a}_{in}$ the scattered output field to the right is given by

$$\hat{a}_{out}(z,t) = \hat{a}_{in}(z - v_g t) + i \sum_{GG'} \hat{\sigma}_{G'G} \mathcal{S}_{GG'} \hat{a}_{in}(z - v_g t) + \mathcal{F}, \tag{3.10}$$

where z is the position in the 1D waveguide, t is a time variable and v_g is the group velocity in the waveguide. $\hat{\sigma}_{G'G} = |G\rangle\langle G'|$ is an operator describing the coherence of states $|G\rangle$ and $|G'\rangle$ of the combined emitters' groundstate manifold in the Heisenberg picture, $\mathcal{F}$ is a noise

operator and

$$\mathcal{S}_{GG'} = \sum_{jj'} \sum_{EE'} \mathcal{A}^{\dagger j}_{GE(1D)} \left[\mathcal{H}_{nh}\right]^{-1}_{EE'} \mathcal{A}^{j}_{E'G'(1D)} \exp[-i\omega_{G'G}(z - z_j)/v_g] \tag{3.11}$$

is a scattering element describing the total contribution of all excited manifold dynamics to the scattering of the input field. Here, $\mathcal{A}^{\dagger j}_{GE(1D)}$ is the complex coupling constant of emitter j's transition from the excited state $|E\rangle$ to the ground state $|G\rangle$ by emitting a photon into the right-going mode of the waveguide. z_j is the position of emitter j, and $\omega_{G'G}$ is the energy difference between the scattered ground states. The scattering dynamics of the excited subspace of the system are fully absorbed into an effective non-Hermitian Hamiltonian

$$\mathcal{H}_{nh} = \mathcal{H}_e - \frac{i}{2} \sum_j \mathcal{L}^\dagger_j \mathcal{L}_j, \tag{3.12}$$

where $\mathcal{H}_e$ describes the energies and couplings in the excited subspace of the total Hamiltonian, and $\mathcal{L}_j$ are the Lindblad decay operators associated with interactions with the environment of the system.

Raman Scattering Entanglement Scheme We consider entanglement generation between an optical photon and the internal states of a coherent TLS with eigenstates $|0\rangle$ and $|1\rangle$ (the qubit). We initialise the TLS in state $|0\rangle$, the lowest energy state. In the Raman scattering scheme, inelastically scattered (red-detuned) photons signal a successful transition of the TLS to state $|1\rangle$.

We apply the photon-scattering formalism (3.10) to the scattering off groundstates $|0\rangle \otimes |g\rangle$ and $|1\rangle \otimes |g\rangle$ of a combined system consisting of a TLS and a transducer comprised of a waveguide and 1 to 4 quantum dots (QDs). Here $|g\rangle$ denotes the overall state where all quantum dots are in the groundstate. The quantum dots can be modelled as 2-level emitters using the formalism described above.

The total right-going output field for a right-going input field for a TLS initialized in $|0\rangle$ is then given by

$$\hat{a}_{out} = \left[1 + i\hat{\sigma}_{00}\mathcal{S}_{00} + i\hat{\sigma}_{01}\mathcal{S}_{10}\right] \hat{a}_{in} + \mathcal{F}. \tag{3.13}$$

We assume that the ground states are sufficiently separated in energy compared to the width of the incoming photon pulse; this means that scattered photons can be filtered spectrally and the only contribution to 'red' photons comes from the term $i\hat{\sigma}_{01}\mathcal{S}_{10}\hat{a}_{in}(z - v_g t) + \mathcal{F}$. Detection of such a red-detuned photon heralds a flip of the TLS; the Raman scattering detection probability P_R for a single-photon input can be found by the expectation value of the photon-number operator of the red field

$$P_R = \int_0^T \langle \hat{a}^\dagger_{out} \hat{a}_{out} \rangle_{\text{red}} \, dt = |\mathcal{S}_{10}|^2, \tag{3.14}$$

where we have normalized the incoming pulse of duration T to contain a single photon. Note that the quantum vacuum noise operator $\mathcal{F}$ does not contribute to the photon number expectation value. The scattering coefficient $\mathcal{S}_{10}$ contains contributions from all scattering paths going from state $|0\rangle$ to $|1\rangle$, and will be evaluated below for each of the considered cases.

3.3.2 Single-QD Transducer

We first consider a single QD-waveguide transducer, electrically coupled to a TLS situated nearby the QD, and interacting with a single photon propagating through the waveguide. To

calculate the efficiency of this transducer, we first calculate the scattering coefficient $\mathcal{S}_{10}$ in (3.14); from (3.11), this requires knowledge of the excited space Hamiltonian. We can write the *total* Hamiltonian of the combined system under consideration as $\mathcal{H} = \mathcal{H}_{qd} + \mathcal{H}_{photon} + \mathcal{H}_{TLS} + \mathcal{H}_I$. The interaction term $\mathcal{H}_I$ consists of two parts: the interaction between the optical mode and the quantum dot $\mathcal{H}_{qd-photon}$, and the interaction between the quantum dot and the TLS, $\mathcal{H}_{qd-TLS}$. For the considered model we have

$$\begin{aligned}
\mathcal{H}_{qd} &= \omega_d \hat{\sigma}^\dagger \hat{\sigma} && (3.15)\\
\mathcal{H}_{photon} &= \sum_k \omega_k \hat{a}_k^\dagger \hat{a}_k && (3.16)\\
\mathcal{H}_{TLS} &= \omega_q |1\rangle\langle 1| && (3.17)\\
\mathcal{H}_I &= \mathcal{H}_{qd-photon} + \mathcal{H}_{qd-TLS} && (3.18)\\
\mathcal{H}_{qd-photon} &= \sum_k (\mathcal{A}_{k,1D}^\dagger \hat{a}_k^\dagger \hat{\sigma} + \mathcal{A}_{k,1D} \hat{a}_k \hat{\sigma}^\dagger) && (3.19)\\
\mathcal{H}_{qd-TLS} &= \frac{g_s}{2} \hat{\sigma}^\dagger \hat{\sigma} \Big(|1\rangle\langle 0| + |0\rangle\langle 1| \Big). && (3.20)
\end{aligned}$$

The operators, frequencies ω_q, ω_k and ω_d and coupling strength g_s are as described before. The total system's state-space with zero or single excitations in the QD is depicted schematically in Figure 3.5. We next consider the QD to couple with equal strengths to the left and right propagating modes given by the coupling rates $|\mathcal{A}_{L,1D}|^2 = |\mathcal{A}_{R,1D}|^2 = \Gamma_{1D}/2$ and assume the QD to decay into non-waveguide modes at a rate γ', such that the total decay rate of the QD is $\Gamma = \Gamma_{1D} + \gamma'$. We eliminate the photon field and consider coupling into or out of the waveguide as a Markovian decay process. Additionally, we go to a rotating frame where the photon energy is zero and describe the QD energy through the photon detuning $\delta = \omega_k - \omega_d$. We can then write the effective non-Hermitian Hamiltonian $\mathcal{H}_{nh}$ in (3.12) as

$$\mathcal{H}_{nh} = \begin{pmatrix} -\delta - \frac{i\Gamma}{2} & g_s \\ g_s & \omega_q - \delta - \frac{i\Gamma}{2} \end{pmatrix}, \tag{3.21}$$

where these excited energy levels are schematically represented in the upper part of Figure 3.5. The scattering coefficient $\mathcal{S}_{10}$ can now be expressed using (3.11) as

$$\mathcal{S}_{10} = \frac{\Gamma_{1D}}{2} \langle e1 | \hat{\mathcal{H}}_{nh}^{-1} | e0 \rangle. \tag{3.22}$$

We ignore here an accumulated phase $\exp[-i\omega_q(z - z_j)/v_g]$ because it does not contribute to the magnitude $|\mathcal{S}_{10}|$. Note that this coefficient is for the right-going mode (transmission) but it is equal in magnitude to the left-going mode (reflection). Experimentally, this coefficient can therefore be twice enhanced by combining both modes on a beamsplitter [19], or using a single-sided waveguide [58], corresponding to a factor of 4 in the success probability. Including this enhancement we then find the total Raman scattering probability

$$\begin{aligned}
P_R &= |2\mathcal{S}_{10}|^2 = \Gamma_{1D}^2 |\langle e1 | \mathcal{H}_{nh}^{-1} | e0 \rangle|^2 \\
&= \frac{\Gamma_{1D}^2 g_s^2}{g_s^4/4 + \frac{1}{2} g_s^2 \left(\Gamma^2 - 4\delta(\delta + \omega_q)\right) + \frac{1}{4}\left(\Gamma^2 + 4\delta^2\right)\left(\Gamma^2 + 4(\delta + \omega_q)^2\right)}. && (3.23)
\end{aligned}$$

The couplings between waveguide, quantum dot and TLS all hybridize the excited state leading to a shift of the resonance condition; optimizing the Raman scattering probability with respect to the photon detuning δ yields the new resonance conditions $\delta = (\omega_q \pm$

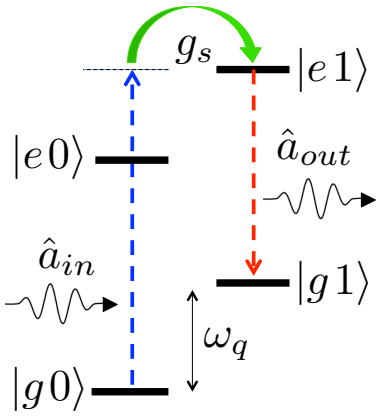

FIGURE 3.5: Energy level schematic of the combined single QD-TLS system, where $|g\rangle$ ($|e\rangle$) refers to the ground (excited) state of the quantum dot. $|0\rangle(|1\rangle)$ refer to the ground (excited) state of the TLS. The blue, green, red arrows depict the path described by the scattering coefficient S_{01} in (3.22).

$\sqrt{\omega_q^2 + g_s^2 - \Gamma^2})/2$. At this detuning we find

$$P_R^{(1QD)} = \beta^2 \frac{g_s^2}{g_s^2 + \omega_q^2} \tag{3.24}$$

where $\beta = \Gamma_{1D}/\Gamma$ is the coupling efficiency (β-factor) of the QD. This yields $P_R \approx \beta^2(g_s/\omega_q)^2$ in the low-coupling limit $g_s \ll \omega_q$, whereas the probability approaches the fundamental upper limit $P_R \approx \beta^2$ in the strong-coupling regime $g_s \gg \omega_q$.

3.3.3 Two-QD Transducer

In this section we discuss the enhancement of the transduction including one more QD in the interaction. Here we harness the interplay between coupling of the two QDs mediated via the waveguide mode and the QD-TLS coupling. We engineer the excited subspace of the two-QD system such that one of the excited states that couple to the TLS is long-lived (a subradiant state). We achieve this via the waveguide mediated QD-QD coupling that exhibits superradiant and sub-radiant emission characteristics depending on detuning, coupling strength and QD-QD spacing in the waveguide.

For two emitters in a waveguide, with mutual detuning Δ, the single-excitation Hamiltonian can be written in the basis $\{|e_1 g_2\rangle, |g_1 e_2\rangle\}$

$$\mathcal{H}_2 = \begin{pmatrix} \Delta/2 & \frac{\Omega}{2} \\ \frac{\Omega}{2} & -\Delta/2 \end{pmatrix} \tag{3.25}$$

where Ω is a coupling term between the excited states of the two QDs, for QDs spaced far apart and optically coupled to the same waveguide mode. We here exclude the diagonal part and assume the decay rates of the emitters do not differ significantly, but we will include it below. The interaction is photon-mediated and of the form

$$\Omega = -ie^{ik\Delta z}\sqrt{\Gamma_{1D}^{(1)}\Gamma_{1D}^{(2)}}, \tag{3.26}$$

where $\Delta z = z_2 - z_1$ is the QD-QD separation, $z_2 > z_1$, and $\Gamma_{1D}^{(i)}$ is the decay rate of emitter i into the 1D waveguide. Note that the complex-valued coupling Ω appears on both sides of

the diagonal of the Hamiltonian, which breaks the Hermicity. For details on the derivation of this interaction, see for example Ref. [2]

As we will now show, in the right parameter-regime and for the right resonance conditions, exploiting the super/sub radiant state dynamics we achieve an effective Raman transfer of population between the states $|g_1g_2 0\rangle$ and $|g_1g_2 1\rangle$. Here $|g_1g_2\rangle$ refers to the ground state of both QDs, and $|0\rangle$ and $|1\rangle$ are the TLS states with energy difference ω_q. In order to derive the Raman transfer rate for a multi-QD system, we again employ the photon scattering formalism as described in Ref. [4]. In this formalism, we absorb the excited state dynamics of the combined system into the non-Hermitian Hamiltonian which we write (with a single-excitation assumption) in the basis $\{|e_1g_2 0\rangle, |g_1e_2 0\rangle, |e_1g_2 1\rangle, |g_1e_2 1\rangle\}$ such that

$$\mathcal{H}_{nh} = \begin{pmatrix} \Delta/2 - \delta - \frac{i\Gamma_1}{2} & \frac{\Omega}{2} & g_s^{(1)} & 0 \\ \frac{\Omega}{2} & -\Delta/2 - \delta - \frac{i\Gamma_2}{2} & 0 & g_s^{(2)} \\ g_s^{(1)} & 0 & \omega_q + \Delta/2 - \delta - \frac{i\Gamma_1}{2} & \frac{\Omega}{2} \\ 0 & g_s^{(2)} & \frac{\Omega}{2} & \omega_q - \Delta/2 - \delta - \frac{i\Gamma_2}{2} \end{pmatrix} \tag{3.27}$$

where δ is the detuning of the incoming photon compared to the central frequency between the two QDs. The two QDs are detuned relative to each other by Δ, and each QD can emit into or out of the waveguide, with decay rates $\Gamma_{1D}^{(i)}$ and $\gamma_i^{'}$, respectively, yielding a total decay rate $\Gamma_i = \Gamma_{1D}^{(i)} + \gamma_i^{'}$. The TLS internal states are coupled to the QD states with coupling constants $g_s^{(i)}$ proportional to the Stark shift of the QD excited state.

In principle, using the above Hamiltonian we can calculate all scattering paths that contribute to the Raman scattering transition. However, it is convenient to change basis such that we can exploit the physics of subradiance: we introduce a basis-transformation $\mathcal{H}'_{nh} = \mathcal{U}\mathcal{H}_{nh}\mathcal{U}^{-1}$ to a basis in which $\mathcal{H}_2$, the bare QD-QD Hamiltonian, is diagonal. The (non-unitary) transformation matrix $\mathcal{U}$ is constructed from the eigenvectors of $\mathcal{H}_2$ such that

$$\mathcal{U}\mathcal{H}_2\mathcal{U}^{-1} = \begin{pmatrix} \nu/2 & 0 \\ 0 & -\nu/2 \end{pmatrix}. \tag{3.28}$$

The columns of the transformation matrix $\mathcal{U}$ are the (anti-)symmetric eigenstates of $\mathcal{H}_2$, $|S\rangle = \xi_1|eg\rangle + \xi_2|ge\rangle$ ($|A\rangle = \xi_1'|eg\rangle - \xi_2'|ge\rangle$) with

$$\xi_1 \equiv \frac{\Omega}{2\sqrt{\Omega^2+\Delta^2}}\sqrt{1+\left|\frac{\sqrt{\Omega^2+\Delta^2}+\Delta}{\Omega}\right|^2} \tag{3.29}$$

$$\xi_2 \equiv \frac{\sqrt{\Omega^2+\Delta^2}-\Delta}{2\sqrt{\Omega^2+\Delta^2}}\sqrt{1+\left|\frac{\sqrt{\Omega^2+\Delta^2}+\Delta}{\Omega}\right|^2} \tag{3.30}$$

$$\xi_1' \equiv \frac{\Omega}{2\sqrt{\Omega^2+\Delta^2}}\sqrt{1+\left|\frac{\sqrt{\Omega^2+\Delta^2}-\Delta}{\Omega}\right|^2} \tag{3.31}$$

$$\xi_2' \equiv \frac{\sqrt{\Omega^2+\Delta^2}+\Delta}{2\sqrt{\Omega^2+\Delta^2}}\sqrt{1+\left|\frac{\sqrt{\Omega^2+\Delta^2}-\Delta}{\Omega}\right|^2}. \tag{3.32}$$

States $|A\rangle$ and $|S\rangle$ are separated by a (generally complex) energy $\nu = \sqrt{\Delta^2+\Omega^2}$ which can be interpreted as combining detuning and decay of the states. In the basis $\{|S1\rangle, |S0\rangle, |A1\rangle, |A0\rangle\}$

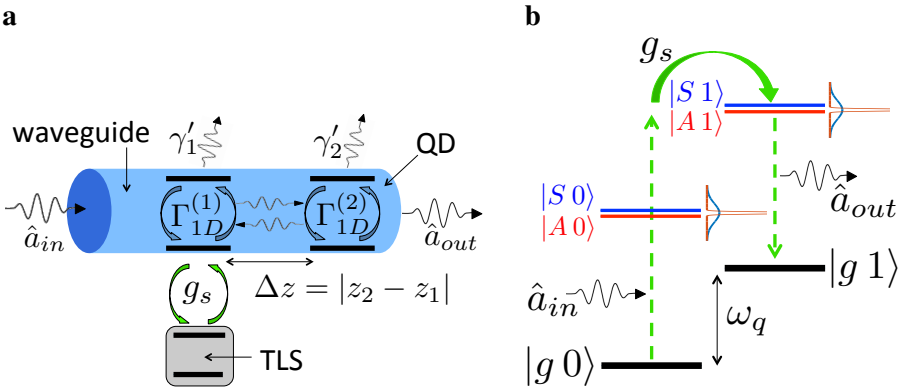

FIGURE 3.6: (a) Efficient transduction of a single microwave excitation in a coherent TLS to an incoming single optical photon via a QD electrically coupled to the TLS and embedded in a photonic waveguide for efficient light-matter interaction. An additional QD is also embedded in the waveguide, and couples to the first QD through a common photonic mode. (b) Energy level diagram of the combined QDs-TLS system. $\{|0\rangle, |1\rangle\}$ represent the TLS internal states. $\{|A\rangle, |S\rangle\}$ represent the (anti-)symmetric states of the two-QD waveguide coupled system, respectively. The incoming photon is set off-resonantly with the $|g0\rangle \rightarrow |S0\rangle$ transition and is tuned into resonance with $|A1\rangle$.

the Hamiltonian is transformed such that

$$\mathcal{H}'_{nh} = \begin{pmatrix} \omega_q + \nu/2 - \delta - \frac{i\Gamma'_S}{2} & G_1/2 & -i\frac{\Gamma_{AS}}{2} & G \\ G_1/2 & \nu/2 - \delta - \frac{i\Gamma'_S}{2} & G & -i\frac{\Gamma_{AS}}{2} \\ -i\frac{\Gamma_{AS}}{2} & G & \omega_q - \nu/2 - \delta - \frac{i\Gamma'_A}{2} & G_2/2 \\ G & -i\frac{\Gamma_{AS}}{2} & G_2/2 & -\nu/2 - \delta - \frac{i\Gamma'_A}{2} \end{pmatrix}. \tag{3.33}$$

Generally, explicit expressions for the variables in this Hamiltonian are very involved. We are mainly interested in the parameter regime which gives the largest Raman probability; we find that this happens when the detuning between the QDs is small compared to the magnitude of the total coupling between them. In this regime, where $\Delta \ll |\Omega|$, we can approximate the quantities in the Hamiltonian (3.33) as

$$\begin{aligned} \nu &\approx \Omega + \frac{\Delta^2}{\Omega} \\ G &\approx \frac{1}{2}(g_s^{(2)} - g_s^{(1)}) \\ G_1 &\approx \frac{1}{2}\left[(g_s^{(1)} + g_s^{(2)}) + \frac{\Delta}{\Omega}(g_s^{(1)} - g_s^{(2)})\right] \\ G_2 &\approx \frac{1}{2}\left[(g_s^{(1)} + g_s^{(2)}) - \frac{\Delta}{\Omega}(g_s^{(1)} - g_s^{(2)})\right] \\ \Gamma'_A &\approx \frac{\Gamma_1 + \Gamma_2}{2} - \frac{\Delta}{\Omega}\frac{\Gamma_1 - \Gamma_2}{2} \\ \Gamma'_S &\approx \frac{\Gamma_1 + \Gamma_2}{2} + \frac{\Delta}{\Omega}\frac{\Gamma_1 - \Gamma_2}{2} \\ \Gamma_{AS} &\approx \Gamma_2 - \Gamma_1. \end{aligned} \tag{3.34}$$

The enhanced transduction scheme, schematically shown in Figure 3.6(b), is based on super- and sub-radiant states: if the two 2-level QDs are tuned into resonance and their

(phase) distance $k\Delta z$ is a multiple of 2π, emission from the QDs add up destructively for the anti-symmetric state (subradiant emission) and the state therefore decays only at a reduced rate γ' to modes outside the waveguide. Meanwhile, their emissions into the waveguide add up constructively for the symmetric state (superradiant emission). To couple an incoming photon pulse to the dark state, however, we need to admix some of the symmetric state into it by choosing either the detuning or the separation slightly different from the point of maximal super- and subradiance.

To describe this we assume that the QDs have equal decay rates $\Gamma_1 = \Gamma_2$ (and $\Gamma_{1D}^{(1)} = \Gamma_{1D}^{(2)}$), and write the Hamiltonian in terms of the energy shifts and decays of the symmetric states such that

$$\mathcal{H}'_{nh} = \begin{pmatrix} \omega_q + \Delta_S - \delta - \frac{i\Gamma_S}{2} & G_1/2 & 0 & G \\ G_1/2 & \Delta_S - \delta - \frac{i\Gamma_S}{2} & G & 0 \\ 0 & G & \omega_q + \Delta_A - \delta - \frac{i\Gamma_A}{2} & G_2/2 \\ G & 0 & G_2/2 & \Delta_A - \delta - \frac{i\Gamma_A}{2} \end{pmatrix} \tag{3.35}$$

in the basis $\{|S1\rangle, |S0\rangle, |A1\rangle, |A0\rangle\}$, with $|S\rangle = \xi_1|eg\rangle + \xi_2|ge\rangle$ and $|A\rangle = \xi_3|eg\rangle - \xi_4|ge\rangle$ where we approximate $\xi_1 \approx 1/\sqrt{2}, \xi_2 \approx (1 - \Delta/\Omega)/\sqrt{2}, \xi_3 \approx 1/\sqrt{2}$ and $\xi_4 \approx (1 + \Delta/\Omega)/\sqrt{2}$ in the limit $\Delta \ll |\Omega|$. The QD-QD photon mediated interaction term is $\Omega = -i\Gamma_{1D}e^{ik\Delta z}$. We assume only one of the QD's couples to the qubit, such that $g_s^{(1)} \to g_s$, $g_s^{(2)} = 0$, and $G = g_s/2$. Then, for $\Delta \ll \Gamma_{1D}$, we find

$$\begin{aligned} \Delta_S &\approx \frac{\Gamma_{1D}}{2}\sin(k\Delta z) + \frac{\Delta^2}{\Gamma_{1D}}\sin(k\Delta z) \\ \Delta_A &\approx -\frac{\Gamma_{1D}}{2}\sin(k\Delta z) - \frac{\Delta^2}{\Gamma_{1D}}\sin(k\Delta z) \\ G &\approx -g_s/2 \\ G_1 &\approx 0 \\ G_2 &\approx 0 \\ \Gamma_A &\approx \gamma' + \Gamma_{1D} - \left[\Gamma_{1D} - \frac{\Delta^2}{\Gamma_{1D}}\right]\cos(k\Delta z) \\ \Gamma_S &\approx \gamma' + \Gamma_{1D} + \left[\Gamma_{1D} - \frac{\Delta^2}{\Gamma_{1D}}\right]\cos(k\Delta z). \end{aligned} \tag{3.36}$$

To solve for the total red-sideband Raman transfer, we calculate the contribution of each path: $|g0\rangle \to |S0\rangle \to |A1\rangle \to |g1\rangle$, $|g0\rangle \to |S0\rangle \to |S1\rangle \to |g1\rangle$, $|g0\rangle \to |A0\rangle \to |A1\rangle \to |g1\rangle$, and $|g0\rangle \to |A0\rangle \to |S1\rangle \to |g1\rangle$. For example, the transition amplitude $|S0\rangle \to |A1\rangle$ is given by the matrix element $\langle A1|\mathcal{H}_{nh}^{-1}|S0\rangle$, and so forth. Inverting the Hamiltonian (3.35) yields the amplitudes for each of the four paths given. We find that for small detuning and $g_s \ll \omega_q$, the only significant contribution to the total red-detuned scattering amplitude is given by the path $|g0\rangle \to |S0\rangle \to |A1\rangle \to |g1\rangle$, which exploits the large coupling of $|S0\rangle$ to couple the incoming photon to the long lived state state $|A1\rangle$. The scattering amplitude for this transition is

$$\hat{a}_{out} = i\Gamma_{1D}e^{-ik\Delta z}(\xi_3^* e^{ik\Delta z} - \xi_4^*)\langle A1|\mathcal{H}_{nh}^{-1}|S0\rangle(\xi_1 + \xi_2 e^{ik\Delta z})e^{i\omega_q t}\hat{\sigma}_{01}\hat{a}_{in}, \tag{3.37}$$

where we set $\Gamma_{1D}^{(1)} = \Gamma_{1D}^{(2)} = \Gamma_{1D}$ and applied the basis transform to $|S\rangle$ and $|A\rangle$ to obtain effective decay rates of these states as a function of the bare QD decay rates $\Gamma_{1D}^{(i)}$ and the relative phase originating from locations z_i in the waveguide.

We assume that the scattering is near resonance with the narrow $|A1\rangle$ state. We can then

approximate the matrix element $\langle A1|\mathcal{H}_{nh}^{-1}|S0\rangle$ by instead setting up a 2x2 non-Hermitian Hamiltonian in the basis $\{|S0\rangle, |A1\rangle\}$ as

$$\mathcal{H}'_{nh} = \begin{pmatrix} \Delta_S - \delta - \frac{i\Gamma_S}{2} & G \\ G & \omega_q + \Delta_A - \delta - \frac{i\Gamma_A}{2} \end{pmatrix}. \tag{3.38}$$

From the field amplitude we calculate the single-photon Raman probability, for zero QD-QD detuning $\Delta = 0$ and a single-sided waveguide, to be

$$P_R = \Gamma_{1D}^{(A)}\Gamma_{1D}^{(S)}|\langle A1|\mathcal{H}_{nh}^{-1}|S0\rangle|^2. \tag{3.39}$$

where we defined $\Gamma_{1D}^{(A)} \equiv \Gamma_{1D}|\xi_3^* e^{ik\Delta z} - \xi_4^*|^2$ and $\Gamma_{1D}^{(S)} \equiv \Gamma_{1D}|\xi_1 + \xi_2 e^{ik\Delta z}|^2$. Evaluating (3.39) with the inverse Hamiltonian element yields

$$P_R = \frac{16\Gamma_{1D}^{(A)}\Gamma_{1D}^{(S)}G^2}{4(\Gamma_S(\omega_q + \Delta_A - \delta) + \Gamma_A(\Delta_S - \delta))^2 + (4G^2 + \Gamma_A\Gamma_S - 4(\omega_q + \Delta_A - \delta)(\Delta_S - \delta))^2}. \tag{3.40}$$

Diagonalisation of Hamiltonian (3.38) reveals a resonance condition for $\delta = \omega_q + \Delta_A + G^2/\omega_q$ (this is in the first-order correction of the splitting due to a coupling G much smaller than the TLS frequency, $G \ll \omega_q$). Choosing this resonance condition and noting that $\Delta_S = -\Delta_A$ yields

$$P_R = \frac{16\Gamma_{1D}^{(A)}\Gamma_{1D}^{(S)}G^2\omega_q^4}{4\omega_q^2(G^2(\Gamma_A + \Gamma_S) + \omega_q\Gamma_A(\omega_q + 2\Delta_A))^2 + (4G^4 - \omega_q^2\Gamma_A\Gamma_S + 8G^2\omega_q\Delta_A)^2}. \tag{3.41}$$

When we take the limit of very weak coupling, such that the dressing by G is small compared to the linewidths, we find that we can write (3.41) as

$$P_R \approx \Gamma_{1D}^{(A)}\Gamma_{1D}^{(S)}\frac{1}{\Gamma_A^2}\frac{4G^2}{\omega_q^2}. \tag{3.42}$$

Defining $\alpha_2 \equiv \left[1 - \Delta^2/\Gamma_{1D}^2\right]\cos(k\Delta z)$, we can write $\Gamma_{1D}^{(A)}/\Gamma_{1D} = 1 - \alpha_2$, $\Gamma_{1D}^{(S)}/\Gamma_{1D} = 1 + \alpha_2$ and $\Gamma_A/\Gamma_{1D} = 1/\beta - \alpha_2$ where $\beta \equiv \frac{\Gamma_{1D}}{\gamma' + \Gamma_{1D}}$. Substituting $G = -g_s/2$ we find

$$P_R = \frac{1 - \alpha_2^2}{(\beta^{-1} - \alpha_2)^2}\left(\frac{g_s}{\omega_q}\right)^2. \tag{3.43}$$

The maximum of (3.43) w.r.t. α_2 occurs at $\alpha_2 = \beta$, where

$$P_R^{(2QD)} \approx \frac{\beta^2}{1 - \beta^2}\left(\frac{g_s}{\omega_q}\right)^2, \tag{3.44}$$

which shows a factor $1/(1 - \beta^2) \approx \Gamma_{1D}/2\gamma$ improvement versus using a single two-level system. The condition to be met for this improvement is $\left[1 - \Delta^2/\Gamma_{1D}^2\right]\cos(k\Delta z) = \beta$. An experimental strategy would be to place the 2 QDs such that $\cos(k\Delta z) \approx 1$ and adjust the detuning between QDs by a local or gradient electric field, until the condition above is met and the output amplitude is maximal. This is always possible for $\cos(k\Delta z) \geq \beta$

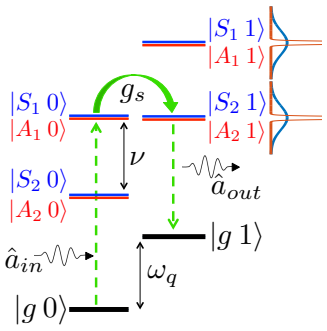

FIGURE 3.7: Level scheme of the hybridized states in a four-QD transducer model. Red and blue indicate narrow and broad states respectively, while the green arrows indicate the considered Raman scattering path.

3.3.4 Four-QD Transducer

We now consider four QDs coupled to a single waveguide mode. A TLS is placed nearby one of the QDs. Under the right conditions, the single-excitation subspace of the four 2-level systems hybridize due to the photon-mediated QD-QD interactions and exhibits a level structure with long-lived states that are also separated in energy. We show below that this effectively enhances the Raman scheme efficiency as compared to the single- and two-QD systems, because we can simultaneously obtain resonance between the involved levels and that states decay slowly such that the TLS-QD interaction time is enhanced.

Let us consider four QDs in a 1D waveguide, all with equal decay rates into the same left- and right-propagating modes $\Gamma_{1D,R,j} = \Gamma_{1D,L,j} = \Gamma_{1D}/2$. We consider the transition energies of these QDs to be equal. The photon-mediated coupling terms between QD i and j are given by $-(i/2)\Gamma_{1D}e^{ik|z_i - z_j|}$. For resonant QDs, the maximum transducer effectiveness that we have been able to identify numerically is attained at an equal QD-QD spacing Δz between nearest neighbors fulfilling $k\Delta z = \pi/2$. For this geometry, the bare effective non-Hermitian Hamiltonian for the single-excitation space, in the basis $\{|eggg\rangle, |gegg\rangle, |ggeg\rangle, |ggge\rangle\}$, is

$$\mathcal{H}_{nh} = -\frac{i}{2}\Gamma_{1D}\begin{pmatrix} 1 & i & -1 & -i \\ i & 1 & i & -1 \\ -1 & i & 1 & i \\ -i & -1 & i & 1 \end{pmatrix} \tag{3.45}$$

Diagonalisation of this Hamiltonian yields a spectrum of four eigenstates: $\{|S_1\rangle, |A_1\rangle, |S_2\rangle, |A_2\rangle\}$ with eigenvalues
$\{\lambda_{S_1}, \lambda_{A_1}, \lambda_{S_2}, \lambda_{A_2}\}$. We identify two slowly decaying states $|A_1\rangle$ and $|A_2\rangle$ with real energies $\pm\nu/2$, where
$\nu = \sqrt{\frac{1}{2}(\sqrt{5}+1)}\Gamma_{1D} \approx 1.27\Gamma_{1D}$, and equal suppressed decay rate $\Gamma_{1D}^{(A)}/\Gamma_{1D} = (1-\alpha_4)$ where $\alpha_4 = \sqrt{\frac{1}{2}(\sqrt{5}-1)} \approx 0.79$. Also, there are two rapidly decaying states, $|S_1\rangle$ and $|S_2\rangle$, with real energies $\pm\nu/2$ and equal enhanced decay rate $\Gamma_{1D}^{(S)}/\Gamma_{1D} = (1+\alpha_4) \approx 1.79$.

Coupling to a TLS The eigenstates $|A_1\rangle$ and $|A_2\rangle$ are superpositions of a single excitation in either of the four QDs; however, the central two QDs have the largest weight to the wavefunction of the long lived states $|A_1\rangle$ and $|A_2\rangle$ and from its magnitude we calculate the largest coupling constant $G \approx 0.40 g_s$. Again, because of the narrow linewidths we can approximate the scattering amplitude $\mathcal{S}_{01}$ by a single scattering path $|g0\rangle \to |A_1 0\rangle \to |A_2 1\rangle \to |g1\rangle$ via a 2x2 effective non-Hermitian Hamiltonian. In the basis $\{|A_1 0\rangle, |A_2 1\rangle\}$, this Hamiltonian

reads

$$\mathcal{H}'_{nh} = \begin{pmatrix} \nu/2 - \delta - \frac{i\Gamma_A}{2} & G \\ G & \omega_q - \nu/2 - \delta - \frac{i\Gamma_A}{2} \end{pmatrix} \tag{3.46}$$

where ν is the energy splitting between states $|A_1\rangle$ and $|A_2\rangle$, while $\Gamma_A = \Gamma_{1D}^{(A)} + \gamma' = [(1/\beta) - \alpha_4]\Gamma_{1D}$ is the total modified decay rate of the hybridized states $|A_1\rangle$ and $|A_2\rangle$. In the hybridized basis, we can write the total Raman scattering probability $P_R = |\mathcal{S}_{10}|^2$ as

$$P_R = (\Gamma_{1D}^{(A)})^2 |\langle A_2 1|\mathcal{H}_{nh}^{-1}|A_1 0\rangle|^2 = \frac{G^2(\Gamma_{1D}^{(A)})^2}{(\Gamma_A^2/4 + G^2)^2 + 2(\Gamma_A^2/4 - G^2)\delta'^2 + \delta'^4} \tag{3.47}$$

where we have defined $\delta' \equiv \nu/2 - \delta$ and we choose to meet the resonance condition $\omega_q = \nu = \sqrt{\frac{1}{2}(\sqrt{5}+1)}\Gamma_{1D} \approx 1.27\Gamma_{1D}$. This is possible either by choosing the TLS such that it has the right transition energy ω_q or, if required, by Purcell-engineering the decay rates of the QDs to match the resonance frequency of the TLS.

For the parameters considered here $G \leq \Gamma_A/2$ and the optimal choice for the photon-detuning is at $\delta' = 0$ where $\delta = \nu/2$. At this detuning we have

$$P_R = \frac{G^2(\Gamma_{1D}^{(A)})^2}{(\Gamma_A^2/4 + G^2)^2} \tag{3.48}$$

Then, substituting $\Gamma_A = [(1/\beta) - \alpha_4]\Gamma_{1D}$, $\Gamma_{1D}^{(A)} = [1 - \alpha_4]\Gamma_{1D}$, $G = -g_s$, $\Gamma_{1D} = \omega_q/1.27$ and $\alpha = 0.79$ in (3.48) gives the expression from the main results,

$$P_R^{(4QD)} \approx \frac{0.11(g_s/\omega_q)^2}{((g_s/\omega_q)^2 + (0.79/\beta - 0.62)^2)^2}. \tag{3.49}$$

For very large coupling $g_s \gtrapprox \omega_q$ more scattering paths need to be considered and (3.49) is no longer a valid approximation.

3.3.5 Coupling factor estimation

To calculate the coupling factor g_s between the oscillating dipole and the QD through the Stark effect, one needs to know the dipole field strength and the system geometry. We here focus on the specific case of a superconducting qubit where a single cooper pair, oscillating on and off a superconducting island, is responsible for the interaction with the QD.

The geometry we consider is depicted in Figure 3.8(a). In this configuration, we model the photonic crystal as a semi-infinite GaAs slab of 140 nm in thickness, surrounded by air on both sides. The superconducting island, with dimensions $20 \times 200 \times 700$ nm, is positioned a distance d from the top of the slab, for example by a flip-switch bonding technique or by bringing the superconducting circuit substructure close to the transducing QD using piezo-actuators. The QD is positioned in the middle of the slab at a height $h/2 = 70$ nm from the top and bottom. We consider four different relative positions of the QD compared to the corners of the island, labeled according to definitions given in Figure 3.8(b). In a different geometry, depicted schematically in Figure 3.8(c), we position the qubit at a 90 degrees angle to the waveguide substrate. In this configuration, a minimum amount of optical light is expected to hit the superconducting island. Using COMSOL's Electrostatics solver, we simulate the steady-state electric field resulting from a single Cooper pair of charge 2e on the island. Assuming an intrinsic dipole of $e \cdot 0.4$ nm for InAs QDs in a GaAs structure [130] gives a stark shift coefficient of 0.4 μeV/(kV/m). After converting to frequency we plot the resulting coupling factor g_s as a function of the qubit-slab separation d in Figure 3.8(d).

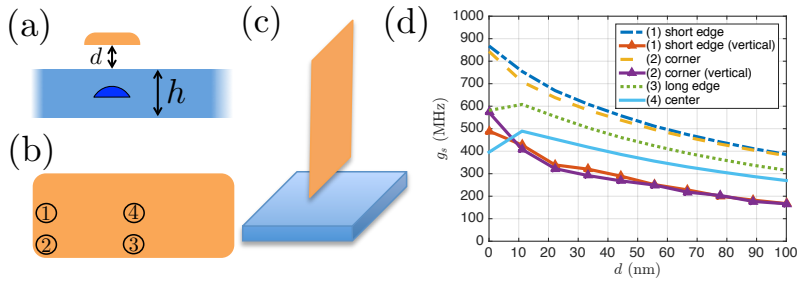

FIGURE 3.8: (a) Horizontal geometry. The qubit (orange) is positioned a distance d away from the waveguide (blue) of thickness $h = 140$ nm with a quantum dot in the middle. (b) Top view of the qubit, with numbers labeling the relative position of the QD underneath the qubit. Assumed dimension are: short edge 200 nm, long edge 700 nm, and thickness 20 nm. (c) Vertical geometry, with the qubit island orthogonal to the waveguide. (d) Coupling g_s derived from a electrostatic simulation of the device. Different relative positioning of the QD underneath the qubit is labeled with indices defined in (b). ('Vertical' in the legend refers to configuration (c), otherwise the island is positioned as shown in Figure 3.9(a))

3.3.6 Optical Photon Absorption

The absorption of a single optical photon destroys the superconducting properties and heats up the sample locally. It is therefore necessary to consider the optical absorption probability. We assume an optical wavelength of $\lambda = 980$ nm (in air). For simplicity we model the system as a nano-beam waveguide made of GaAs suspended in air, with refractive indices $n_{GaAs} = 3.456$ [135] and $n_{air} = 1$ respectively. We assume negligible absorption in these media, while for the aluminum we assume th real part of the refractive index $n_{Al} = 1.47$ and an extinction coefficient (imaginary part of the refractive index) $\kappa = 9.22$ [136]. Again, we consider the aluminum island to have dimensions $20 \times 200 \times 700$ nm, and the nanobeam waveguide is assumed to be 140 nm thick and 300 nm wide. A full 3D COMSOL simulation

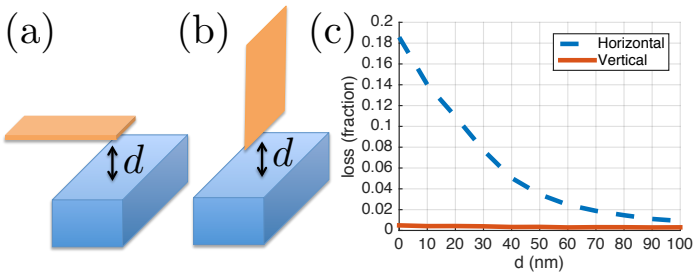

FIGURE 3.9: (a) Horizontal geometry of the qubit (orange), a distance d away from the waveguide (blue). We assume the short edge of the qubit to align with the center of the waveguide to maximize electrical coupling and minimize optical interference. (b) Vertical geometry of the qubit (orange), a distance d away from the waveguide (blue). (c) COMSOL simulation of optical absorption as a function of distance d, for the two different configurations (a) and (b).

is executed as follows; first, the input- and output-port fundamental mode is calculated and 1W of power is inserted into the fundamental mode at the input port with a frequency $c/980$ nm where c is the speed of light. We consider scattering boundary conditions on the borders of the simulation box. Next, a 3D 'Electromagnetic Waves, Frequency Domain' numerical intergration of Maxwell's equations is performed. We analyze the optical absorption by

integrating the total power flow over the surface of the island. This allows us to find the total absorbed fraction of the power, which directly translates into the photon absorption probability. The resulting probability is shown in Figure 3.9

Depending on how the island is oriented, we find a large difference in optical absorption. For the vertical geometry in Figure 3.9(b), the absorption is always less than 1%. For the horizontal configuration in Figure 3.9(a), the absorption is significantly larger at short separations but less than 1% for separations larger than $d = 90$ nm.

3.4 Summary & Outlook

In summary we have shown that long-range waveguide mediated interactions can be exploited to boost the efficiency of quantum transducers. As a direct application, the proposed device can be used to provide an on-chip interface between SC qubits and optical photons. This could facilitate a breakthrough in long-distance quantum communication via a quantum repeater network [16, 94–97] and scaling of SC quantum computers by connecting them optically [98, 99]. Alternatively the proposed transducers can have applications for quantum limited sensing by exploiting efficient optical detection of low frequency fields [100–102].

Chapter 4

Quantum transduction with a single quantum dot coupled to a cavity

4.1 Introduction

In Chapter 3, we have introduced the concept of a quantum transducer and detailed its use-cases and properties [1]. We refer the interested reader to Section 3.1 for a brief introduction and to Section 3.2.1 for the model basics, for a transducer based on quantum dots in an optical waveguide. We found good performance of the device for the two- and four-QD cases. The requirements for constructing such devices are relatively low and engineering the interactions via the waveguide is practically feasible. However, as an experimental alternative to that transducer architecture, we in this chapter introduce a cavity-QD architecture transducer, exploiting the strong cavity-QD coupling being on the same order as the coherent TLS one couples to. We also extend in more detail the long-distance entanglement scheme we mentioned in Chapter 3. Finally, we investigate the effects of dephasing on entanglement fidelity.

Optical cavity technology is improving at a rapid pace [137]. Single photon optical cavity quantum electrodynamics [138, 139] has introduced a display of interesting physics. One of those platforms, single-quantum dot coupled to a high-quality factor (Q) cavity (see for example Ref. [140]) is the system we will focus on here. It is an ideal candidate for integration with photonic circuits and we show how it can serve as a platform for optical photon-to-superconducting qubit transduction below.

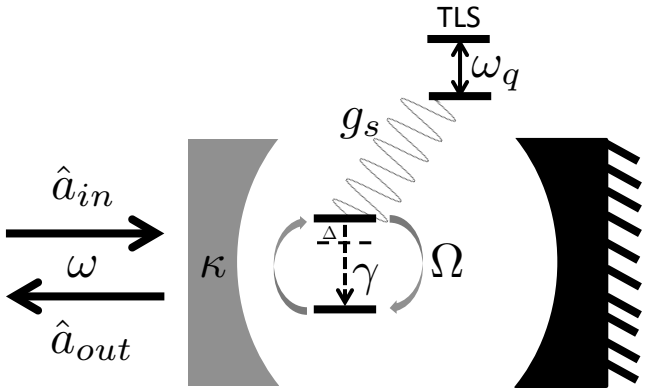

FIGURE 4.1: Schematic diagram of cavity transducer. A single quantum dot (QD) is electrically coupled to a TLS. A single-photon pulse is scattered off the cavity-QED system and the output field is frequency-filtered such that the photon frequency becomes entangled with the TLS internal state.

4.2 Cavity transducer analysis

We are interested in calculating the transduction efficiency of quantum information being transferred from a stationary qubit to a flying qubit. For this, we will use the photon scattering formalism detailed in Ref. [4]. More specifically, we in this case consider a 1D-mode scattering of a single emitter system which is the combined cavity-QD system. Thus, we employ the scattering relation derived in Ref. [2]. The scattering situation is schematically shown in Figure 4.1. For a single input field $\hat{a}_{in}$, the output field (ignoring the noise, which will not contribute since we perform photon measurement of the $\hat{a}^\dagger\hat{a}$ operator) is given by

$$\hat{a}_{out} = \hat{a}_{in}\left(1 + i\sum_{gg'}\hat{\sigma}_{gg'}\sum_{ee'}\mathcal{S}_{ee'}\right) \tag{4.1}$$

$$\mathcal{S}_{ee'} = \mathcal{A}^\dagger_{ge}\left[\tilde{\mathcal{H}}_{nh}\right]^{-1}_{ee'}\mathcal{A}_{e'g'}. \tag{4.2}$$

In the specific scattering situation we consider, $\mathcal{A}_{e'g'} = \sqrt{\kappa/2}$ is the cavity de-excitation rate, and the groundstate manifold consists of two states, $|-\rangle$ and $|+\rangle$, such that $\hat{\sigma}_{+-} = |+\rangle\langle -|$ is the TLS excitation operator.

The cavity transducer system shown schematically in Figure 4.1 consists of the following components. A quantum dot (QD) with detuning Δ is coupled at a rate Ω to a cavity where one side has decay rate κ and the other is a perfect reflector. The QD electrically couples to a nearby two-level system with transition frequency ω_q, through the Stark effect with a rate g_s. The total system Hamiltonian excluding photonic modes and up to a single excitation in the cavity-QED system is schematically depicted in Figure 4.2

With these definitions, we can now write the non-Hermitian Hamiltonian describing the excited state subspace of the cavity-qd-qubit system, in the basis $\{|g1-\rangle, |e0-\rangle, |g1+\rangle, |e0+\rangle\}$, as follows:

$$\mathcal{H}_{nh} = \begin{pmatrix} \Delta/2 - \delta - \frac{i\kappa}{2} & \Omega/2 & 0 & 0 \\ \Omega/2 & -\Delta/2 - \delta - \frac{i\gamma'}{2} & 0 & g_s \\ 0 & 0 & \omega_q + \Delta/2 - \delta - \frac{i\kappa}{2} & \Omega/2 \\ 0 & g_s & \Omega/2 & \omega_q - \Delta/2 - \delta - \frac{i\gamma'}{2} \end{pmatrix}. \tag{4.3}$$

Due to the strong cavity-QD interaction, states $|g1\rangle$ and $|e0\rangle$ hybridize as shown in Figure 4.2(a), and it is convenient to go to a rotating frame, $\mathcal{H}'_{nh} = \mathcal{U}\mathcal{H}_{nh}\mathcal{U}^{-1}$, such that (anti-)symmetric states $|A\rangle$ and $|S\rangle$ are eigenstates of the bare cavity-QD Hamiltonian. The transformation matrix $\mathcal{U}$ is constructed from the eigenvectors of

$$\mathcal{H}_2 = \begin{pmatrix} \Delta/2 & \frac{\Omega}{2} \\ \frac{\Omega}{2} & -\Delta/2 \end{pmatrix} \qquad \text{such that} \qquad \mathcal{U}\mathcal{H}_2\mathcal{U}^{-1} = \begin{pmatrix} \nu/2 & 0 \\ 0 & -\nu/2 \end{pmatrix}. \tag{4.4}$$

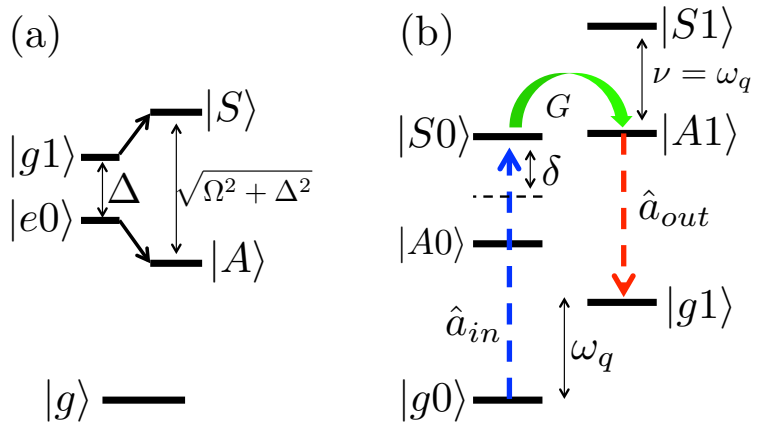

FIGURE 4.2: Schematic diagram of the energy levels in the cavity transducer, up to a single excitation subspace. (a) coupling between cavity and QD causes hybridization and symmetric- and anti-symmetric states $|S\rangle$ and $|A\rangle$ can be defined. (b) Raman scattering path in the hybridized basis.

The eigenstates of this Hamiltonian are the (anti-)symmetric states $|S\rangle = \xi_1|g1\rangle + \xi_2|e0\rangle$ ($|A\rangle = \xi_1'|g1\rangle - \xi_2'|e0\rangle$). We define basis rotation matrix $\mathcal{U}$ through these eigenvectors with

$$\xi_1 = \frac{\Omega}{2\sqrt{\Omega^2+\Delta^2}}\sqrt{1+\left|\frac{\sqrt{\Omega^2+\Delta^2}+\Delta}{\Omega}\right|^2} \tag{4.5}$$

$$\xi_2 = \frac{\sqrt{\Omega^2+\Delta^2}-\Delta}{2\sqrt{\Omega^2+\Delta^2}}\sqrt{1+\left|\frac{\sqrt{\Omega^2+\Delta^2}+\Delta}{\Omega}\right|^2} \tag{4.6}$$

$$\xi_1' = \frac{\Omega}{2\sqrt{\Omega^2+\Delta^2}}\sqrt{1+\left|\frac{\sqrt{\Omega^2+\Delta^2}-\Delta}{\Omega}\right|^2} \tag{4.7}$$

$$\xi_2' = \frac{\sqrt{\Omega^2+\Delta^2}+\Delta}{2\sqrt{\Omega^2+\Delta^2}}\sqrt{1+\left|\frac{\sqrt{\Omega^2+\Delta^2}-\Delta}{\Omega}\right|^2}. \tag{4.8}$$

States $|A\rangle$ and $|S\rangle$ are separated by a (generally complex) energy $\nu = \sqrt{\Delta^2+\Omega^2}$ which can be interpreted as combining detuning and decay of the states. In the basis $\{|A-\rangle, |S-\rangle, |A+\rangle|S+\rangle\}$ the Hamiltonian is rotated such that

$$\mathcal{H}_{nh}' = \begin{pmatrix} -\nu/2-\delta-\frac{i\Gamma_A}{2} & -i\frac{\Gamma_{AS}}{2} & G_+ & G \\ -i\frac{\Gamma_{AS}}{2} & \nu/2-\delta-\frac{i\Gamma_S}{2} & G & G_- \\ G_+ & G & \omega_q-\nu/2-\delta-\frac{i\Gamma_A}{2} & -i\frac{\Gamma_{AS}}{2} \\ G & G_- & -i\frac{\Gamma_{AS}}{2} & \omega_q+\nu/2-\delta-\frac{i\Gamma_S}{2} \end{pmatrix}. \tag{4.9}$$

If the splitting ν is close to the qubit transition frequency ω_q, i.e. $\nu \approx \omega_q$, scattering path $|g-\rangle \to |S-\rangle \to |A+\rangle \to |g+\rangle$ dominates the red-scattered part of the total output amplitude. This path is depicted in Figure 4.2(b), and the output field after filtering for red photons, absorbing irrelevant phases, is then given by

$$\hat{a}_{red} = \hat{a}_{in}|+\rangle\langle-|\mathcal{S}_{+-} \tag{4.10}$$

where we expect the scattering coefficient $\mathcal{S}_{+-}$ to be approximately

$$\mathcal{S}_{+-} \approx \xi_1' \sqrt{\kappa} \langle A+ | \left[\mathcal{H}_{nh}^{-1}\right] |S-\rangle \sqrt{\kappa} \xi_1 \tag{4.11}$$

where we approximate the 4x4 inverse non-Hermitian Hamiltonian $\mathcal{H}_{nh}^{-1}$ by the 2x2

$$\mathcal{H}_{nh}' = \begin{pmatrix} \nu/2 - \delta - \frac{i\Gamma_S}{2} & G \\ G & \omega_q - \nu/2 - \delta - \frac{i\Gamma_A}{2} \end{pmatrix}, \tag{4.12}$$

such that the single-photon Raman transfer probability is given by

$$\begin{aligned} P_R &= |\mathcal{S}_{+-}|^2 \\ &= \frac{16|\xi_1|^2|\xi_1'|^2\kappa^2 G^2}{16G^4 + 8G^2(\Gamma_A\Gamma_S + 4(\omega_q - 2\delta)\delta - 2\omega_q\nu + \nu^2) + (\Gamma_A^2 + (2\omega_q - \nu - 2\delta)^2)(\Gamma_S^2 + (\nu - 2\delta)^2)} \end{aligned} \tag{4.13}$$

From Eq. 4.13 we can identify two tunable parameters, which make the denominator minimal: the Rabi splitting ν and the photon detuning δ. For the purpose of maximizing Raman transfer, in Chapter 3 we recall it is optimal to align states $|S0\rangle$ and $|A1\rangle$ in energies. This is achieved by setting $\nu = \omega_q$.

Generally, explicit expressions for the variables defined in this Hamiltonian are very involved. Let us therefore separately consider different regimes; first, we assume that the detuning between cavity and quantum dot is zero, i.e. $\Delta = 0$. There, $\nu = \Omega = \omega_q$ is the resonant coupling condition, and the basis change becomes $\xi_1 = \xi_2 = \xi_1' = \xi_2' = 1/\sqrt{2}$. We find $\Gamma_A = \Gamma_S = (\kappa + \gamma')/2$ and $G = -g_s/2$. If we now take the derivative with respect to the photon detuning δ, we find two optimal solutions depending on coupling strength g_s:

• For weak coupling g_s compared to the linewidths, $g_s < (\kappa + \gamma')/2$, the photon resonance condition is $\delta \to \omega_q/2$. There, the single-photon Raman scattering probability is

$$P_R = \left(\frac{g_s\kappa}{gs^2 + (\kappa + \gamma')^2/4}\right)^2 \tag{4.14}$$

• For strong coupling g_s compared to the linewidths $g_s > (\kappa+\gamma')/2$, the states hybridize further due to coupling g_s and a new photon resonance condition is identified as $\delta \to \omega_q/2 + \frac{1}{4}\sqrt{4g_s^2 - (\kappa + \gamma')^2}$. There, the single-photon Raman scattering probability is

$$P_R = \left(\frac{\kappa}{\kappa + \gamma'}\right)^2 \tag{4.15}$$

This result for the strong-coupling condition is optimal and can reach high values for a quantum dot decay rate to the side that is lower than the cavity decay rate.

In practice in an experiment, it is unlikely to manage resonance condition $\nu = \omega_q$ without any detuning Δ between the cavity mode and quantum dot. We now generalize above expressions for non-zero detunings; first, we assume that the coupling between quantum dot and cavity is much larger than the detuning. In this regime, where $\Delta \ll |\Omega|$, we can approximate $\xi_1 \approx (1+\Delta/2\Omega)/\sqrt{2}, \xi_2 \approx (1-\Delta/2\Omega)/\sqrt{2}, \xi_1' \approx (1-\Delta/2\Omega)/\sqrt{2}, \xi_2' \approx (1+\Delta/2\Omega)/\sqrt{2}$

and the quantities in the Hamiltonian (4.9) as

$$\begin{aligned}
\nu &\approx \sqrt{\Omega^2+\Delta^2} \\
G &\approx -\frac{g_s}{2} \\
G_+ &\approx \frac{g_s}{2}\left[1+\frac{\Delta}{\Omega}\right] \\
G_- &\approx \frac{g_s}{2}\left[1-\frac{\Delta}{\Omega}\right] \\
\Gamma_A &\approx (\kappa+\gamma')/2 - \frac{\Delta}{2\Omega}(\kappa-\gamma') \\
\Gamma_S &\approx (\kappa+\gamma')/2 + \frac{\Delta}{2\Omega}(\kappa-\gamma') \\
\Gamma_{AS} &\approx (\kappa-\gamma')/2 - \left(\frac{\Delta}{2\Omega}\right)^2(\kappa-\gamma')
\end{aligned} \tag{4.16}$$

When we calculate the Raman scattering probability for this non-zero detuning case, we find the following expansion in Δ/ω_q:

$$P_R \approx A\left[1+2B\left(\frac{\Delta}{\omega_q}\right)-\left(\frac{1}{2}-3B^2\right)\left(\frac{\Delta}{\omega_q}\right)^2\right] \tag{4.17}$$

For weak coupling g_s compared to the linewidths and detuning, $4g_s^2 < (\kappa+\gamma')^2 + (\kappa-\gamma')^2\Delta^2/\Omega^2$, the photon resonance condition is $\delta \to \omega_q/2$. There,

$$A \equiv \left(\frac{g_s\kappa}{gs^2+(\kappa+\gamma')^2/4}\right)^2 \quad , \quad B \equiv \frac{(\kappa^2-\gamma'^2)/4}{gs^2+(\kappa+\gamma')^2/4} \tag{4.18}$$

For strong coupling g_s compared to the linewidths and detuning, $4g_s^2 > (\kappa+\gamma')^2 + (\kappa-\gamma')^2\Delta^2/\Omega^2$, the photon resonance condition is $\delta \to \omega_q/2 + \frac{1}{4}\sqrt{4g_s^2-(\kappa+\gamma')^2-(\kappa-\gamma')^2\Delta^2/\Omega^2}$. There,

$$A \equiv \left(\frac{\kappa}{\kappa+\gamma'}\right)^2 \quad , \quad B \equiv \left(\frac{\kappa-\gamma'}{2(\kappa+\gamma')}\right) \tag{4.19}$$

4.3 Interferomety using two distant transducers: Fidelity of Bell state generation

In this section, we consider long-distance entanglement generation between two stationary qubits through measurements of flying photons. In this scheme, a single photon incident on a beamsplitter is directed to two separated transducer-qubit systems. The scattered output is mixed on a second beamsplitter to remove which-way information and entanglement of the two stationary qubits is achieved, conditioned on a click at one of the detectors. If no click is observed, the qubits are to be reset and the single-photon shot experiment is repeated until success. See for example Refs. [133, 141, 142] for more background on this type of entanglement generation.

Because the probability amplitudes for each qubit changing their internal state differ, the achieved fidelity of the Bell state produced can not be guaranteed at 1. For example, if we block one qubit from flipping, the resulting state will be a certain $|10\rangle$ (conditioned on a click) instead of a desired Bell state $(|10\rangle + |01\rangle)/\sqrt{2}$. Then the fidelity is equal to the first beam splitter's branching ratio, which is the best one can hope to achieve classically.

Let us formally quantify this effect for arbitrary Raman transition scattering amplitudes r^A and r^B for transducer-qubit systems A and B. The input of the interferometer setup is a single photon pulse, and as such we can ignore all two-photon processes. Also, we condition the experiment on a click at one of the detectors. The total state before the second beam splitter, ignoring the zero-photon states, is then given by

$$|\Psi\rangle = \chi e^{i\phi} r^A |1^A 0^B\rangle|10\rangle + \sqrt{1-\chi^2} r^B |0^A 1^B\rangle|01\rangle \tag{4.20}$$

where $|0^A 1^B\rangle$ refers to a photon coming into the beamsplitter from transducer A and no photon coming from transducer B. As such, entanglement has been generated between the photon beams and the qubit states. We have ignored normalization for now. χ^2 is the branching ratio of the first beamsplitter, between 0 and 1. For example, for a $50/50$ beamsplitter, $\chi^2 = 0.5$. $e^{i\phi}$ can be tweaked by adjusting the phase between the two outputs of the beamsplitter.
The success probability of a Bell-state generation in the qubits is then simply $P = \eta(\chi^2 P_{suc,A} + (1-\chi^2)P_{suc,B})$, where the indices refer to each transducer-qubit system respectively. η is the single-photon detector efficiency. Also, this result depends on the choice of the beam splitter parameters, and can be optimized by balancing.
Now, we will remove which-way information using a second beamsplitter with the following transformation:

$$|0^A 1^B\rangle \rightarrow |0^+ 1^-\rangle + |1^+ 0^-\rangle \tag{4.21}$$

$$|1^A 0^B\rangle \rightarrow |0^+ 1^-\rangle - |1^+ 0^-\rangle \tag{4.22}$$

where $|1^+ 0^-\rangle$ denotes a click in detector $+$ but not in $-$.
For now, let us select $\chi^2 = 1/2$ and generalize later. Then, after the second beamsplitter, we perform a measurement on the state

$$|\Psi\rangle = (r^B|-+\rangle + r^A|+-\rangle)|0^+ 1^-\rangle + (r^B|-+\rangle - r^A|+-\rangle)|1^+ 0^-\rangle \tag{4.23}$$

by observing the clicks in detectors $+$ and $-$, we prepare a Bell state and the Fidelity in this case is given by

$$F = |\langle\Psi|(|-+\rangle + |+-\rangle)/\sqrt{2}|^2 \tag{4.24}$$

For example, if our detector D^- clicks, the fidelity is

$$F = |\left(\frac{r^B\langle -+| + r^A\langle +-|}{\sqrt{(r^A)^2+(r^B)^2}}\right)\left(\frac{|-+\rangle + |+-\rangle)}{\sqrt{2}}\right)|^2 = \left|\frac{r^A + r^B}{\sqrt{2}\sqrt{(r^A)^2+(r^B)^2}}\right|^2 \tag{4.25}$$

$$F = 1 - \frac{1}{2}\frac{|r_A - r_B|^2}{|r_A|^2 + |r_B|^2} \tag{4.26}$$

Note that, for the *magnitude* of the amplitudes r_A and r_B being equal, but with a random relative *phase* in each experiment, we find an average fidelity of 0.5, which is also the best correlation fidelity you can get classically.
To maximize the fidelity of an experiment which has some degree of phase-correlation to it, we can tune the beamsplitter parameters χ and ϕ. Expression (4.26) then generalizes to

$$F = 1 - \left(\frac{1}{2}\right)\frac{|\chi e^{i\phi} r_A - \sqrt{1-\chi^2} r_B|^2}{\chi^2|r_A|^2 + (1-\chi^2)|r_B|^2} \tag{4.27}$$

We see that χ and ϕ can together always fully compensate for a discrepancy between r_A and r_B, but only as long as we have exact knowledge about these scattering amplitudes and they do not drift between or during experiments. Any additional unknown drifting of the parameters will not be possible to be compensated for just by statically tuning the initial

beamsplitter, and is likely to introduce dephasing. We will come back to this topic later in this chapter.

4.4 Coherent Pulse input

In this section, we investigate how the Bell state generation probability changes when we use a coherent pulse as input. Often, it is difficult in practice to create a perfect single-photon source. Instead, experiments use a weak coherent pulse with low average photon number to avoid having a two-photon incidence (see for example Ref. [16, 143]).
Recall that the output field operator according to the input-output formalism, after filtering for the right frequency $(\omega_{in} - \omega_q)$, is given by

$$\hat{a}_{out}(t) = \left(\sqrt{\kappa/2}\left[H_{NH}^{-1}\right]_{c_-c_+}\sqrt{\kappa/2}\right)\hat{\rho}_{g_-g_+}(t)\hat{a}_{in}(t) \tag{4.28}$$

where we have omitted phase factors. Here, we define $\zeta_{-+} = \sqrt{\kappa/2}\left[H_{NH}^{-1}\right]_{c_-c_+}\sqrt{\kappa/2}$ as the matrix element for the transition of the qubit while a single photon is in the cavity and the QD is in the ground state. $\hat{\rho}_{g_-g_+}(t)$ denotes the density operator $\rho|g_+\rangle\langle g_-|$ characterizing the coherence between the ground states of the transducer-qubit system for the qubit being in state $|-\rangle$ and $|+\rangle$ respectively.

Let's apply this operator to a coherent state $|\alpha\rangle$ and find the intensity (scattering transition probability) as:

$$I_R(t) = \left|\sqrt{\kappa/2}\left[H_{NH}^{-1}\right]_{c_-c_+}\sqrt{\kappa/2}\right|^2 \langle\alpha|\hat{a}^\dagger : \hat{\rho}_{g_-g_-}(t) : \hat{a}|\alpha\rangle \tag{4.29}$$

where the ':' denotes normal ordering of the photon annihilation operators.We now solve for the density operator element $\hat{\rho}_{g_-g_-}(t)$ using the effective operator formalism and find an effective decay of the population as $\hat{\rho}_{g_-g_-}(t) = \hat{\rho}_{g_-g_-}(0)e^{-|L_{-+}^{\kappa}|^2(t)-|L_{-+}^{\gamma}|^2(t)}$, where

$$L_{-+}^{\kappa}(t) = \sqrt{\kappa}\left[H_{NH}^{-1}\right]_{c_-c_+}\Omega(t) \tag{4.30}$$

and

$$L_{-+}^{\gamma}(t) = \sqrt{\gamma}\left[H_{NH}^{-1}\right]_{c_-c_+}\Omega(t) \tag{4.31}$$

with a weak coherent drive $\Omega(t) = \sqrt{\kappa}\hat{a}^\dagger$.
Now, for a system initialized as $\hat{\rho}_{g_-g_-}(0) = 1$, Eq. 4.29 reduces to

$$I_R(t) = |\left[H_{NH}^{-1}\right]_{c_-c_+}|^2\kappa^2/4\langle\alpha|\hat{a}^\dagger : e^{-\hat{a}^\dagger\hat{a}P_{\gamma,\kappa}t} : \hat{a}|\alpha\rangle \tag{4.32}$$

where

$$P_{\gamma,\kappa} = \kappa^2|\left[H_{NH}^{-1}\right]_{c_-c_+}|^2 + \gamma'\kappa|\left[H_{NH}^{-1}\right]_{c_-c_+}|^2 = P_R + P_{RO} \tag{4.33}$$

is the total probability for a single photon to induce a transition from ground states $|-\rangle$ to $|+\rangle$, found by applying above methods to a single-photon fock state, making all terms in the exponential drop away except the base $e^0 = 1$.

For a single photon input, the succes probability is simply

$$P_{suc}^{(1)} = \eta P_R \tag{4.34}$$

For a coherent state input, due to the normal ordering of the photon operators, we replace $\langle\alpha|\hat{a}^\dagger : e^{-\hat{a}^\dagger\hat{a}P_{\gamma,\kappa}t} : \hat{a}|\alpha\rangle$ by $|\alpha|^2e^{-|\alpha|^2P_{\gamma,\kappa}t}$. Let us integrate the intensity Eq. 4.29 for a coherent state input, over the course of the pulse, to find the total success *probability*, for a

detection efficiency η:

$$P_{suc}^{(c)} = P_{suc}^{(1)} \int_0^T |\alpha|^2 e^{-|\alpha|^2 P_{\gamma,\kappa} t} dt = \frac{P_{suc}^{(1)}}{P_R + P_{RO}} (1 - e^{-(P_R + P_{RO})\bar{n}}) \tag{4.35}$$

The strategy here is to turn on the input for a time until the detector detects a click at time T (relative to the start of the pulse). Then, the input is immediately turned off, and we call $\bar{n}$ the number of photons in that pulse. For weak pulses compared to the transition probabilities, i.e. $\bar{n}(P_R + P_{RO}) \ll 1$, we can approximate

$$P_{suc}^{(c)} \approx \bar{n} P_{suc}^{(1)} \tag{4.36}$$

One can immediately see the following: if P_R of the transducer is very low, one may increase the overall success probability by using a stronger photon pulse. We will now show, however, that this method will also degrade the fidelity.

4.5 Fidelity for a Coherent pulse

To generalize the fidelity calculation to a coherent pulse, let us consider a general input operator instead of a single photon. To calculate the fidelity after a click has been observed at the detectors, we need to project the density matrix of the two-hybrid system onto the photonic state and detector state as follows. We denote the components of the detector state density matrix as $\hat{\rho}^{AB}_{\pm(\mu)}(t,T)$.

$$\hat{\rho}^{AB}_{\pm(\mu)}(t,T) = \langle \Psi_{ini,\alpha} | \hat{d}^{\dagger}_{out,\pm} \hat{\rho}^{AB}_{\mu}(t,T) \hat{d}_{out,\pm} | \Psi_{ini}, \alpha \rangle / \operatorname{Tr}[\hat{\rho}^{AB}_{\mu}(t,T)], \tag{4.37}$$

where $\mu = \{i, j, i', j'\}$ and $\hat{\rho}^{AB}_{\mu}(t,T)$ is a component $|i\rangle\langle j| \otimes |i'\rangle\langle j'|$ of the density matrix of the 2-hybrid system written in the Heisenberg picture as a function of times t (time of the click) and T (duration of the coherent pulse). We only consider iterations of the experiment where a click was registered before a time T, i.e. $t < T$.
From the above expression it is clear we mix the two interferometry beams through photonic operator

$$\hat{d}_{out,\pm} = \eta(\chi e^{i\phi} \hat{a}_A \pm \sqrt{1-\chi^2} \hat{a}_B) \tag{4.38}$$

where $\pm$ indicates the operator for detector D_+ or D_- respectively, while $\hat{a}_{A/B}$ are the annihilation operators of the photonic modes in beams coming from hybrid A and B respectively. χ is the branching ratio of the first beamsplitter, enabling us to send more of the light to hybrid A or B.

From the previous section, we found through input-output formalism an expression for the photonic operators $\hat{a}_{A/B}$, after filtering for the right frequency:

$$\hat{a}_{out,i}(t) = \zeta_{i,-+} \hat{\rho}^{i}_{-+}(t) \hat{a}_{in,i}(t) \tag{4.39}$$

From now on, let us assume all $\zeta_{i,-+}$ are transitions from $|-\rangle$ to $|+\rangle$, so we drop these subscripts. Combining all of these terms, leads to 2 contributions of arm A and B respectivey, and 2 interference terms:

$$\begin{aligned}\hat{\rho}^{AB}_{\pm(\mu)}(t,T) = \frac{\eta|\alpha|^2}{2} \langle \Psi_{ini,\alpha} | \chi e^{-i\phi} \sqrt{1-\chi^2} \zeta_A^{\dagger} \zeta_B (\hat{\rho}^{A}_{-+})^{\dagger} \hat{\rho}^{AB}_{\mu}(t,T) \hat{\rho}^{B}_{-+} \\ + \chi e^{i\phi} \sqrt{1-\chi^2} \zeta_B^{\dagger} \zeta_A (\hat{\rho}^{B}_{-+})^{\dagger} \hat{\rho}^{AB}_{\mu}(t,T) \hat{\rho}^{A}_{-+} + \chi^2 \zeta_A^{\dagger} \zeta_A (\hat{\rho}^{A}_{-+})^{\dagger} \hat{\rho}^{AB}_{\mu}(t,T) \hat{\rho}^{A}_{-+} \\ + (1-\chi^2) \zeta_B^{\dagger} \zeta_B (\hat{\rho}^{B}_{-+})^{\dagger} \hat{\rho}^{AB}_{\mu}(t,T) \hat{\rho}^{B}_{-+} | \Psi_{ini}, \alpha \rangle / \operatorname{Tr}[\hat{\rho}^{AB}_{\mu}(t,T)],\end{aligned} \tag{4.40}$$

where we have used $\hat{a}|\alpha\rangle = \alpha|\alpha\rangle$ for a coherent state.
The purpose of finding these elements of the density matrix of the detector, is so we can find the *fidelity* conditioned on a click at a detector D_- or D_+:

$$F(t,T) = \langle\Psi^+|\hat{\rho}^{AB}_+(t,T)|\Psi^+\rangle = \frac{1}{2}\left[\hat{\rho}^{AB}_{++--} + \hat{\rho}^{AB}_{--++} + \hat{\rho}^{AB}_{+--+} + \hat{\rho}^{AB}_{-++-}\right] \tag{4.41}$$

Let us look at these 4 terms separately.
In the next steps, we will consider a photon-induced dephasing of the coherences as

$$\hat{\rho}^{AB}_{--++}(t,T) = \hat{\rho}^{AB}_{--++}(t)e^{-\Gamma_{R,A}\chi^2|\alpha|^2(T-t)} \tag{4.42}$$

$$\hat{\rho}^{AB}_{++--}(t,T) = \hat{\rho}^{AB}_{++--}(t)e^{-\Gamma_{R,B}(1-\chi^2)|\alpha|^2(T-t)} \tag{4.43}$$

Here, $\Gamma_{R,A/B}$ is the total Raman transition rate, and χ is the input pulse branching ratio to beam A and B. After a click has been registered at time t, we note that the state of the other qubit can still be flipped by the remaining photons in the pulse, giving rise in the decay of the state towards $\hat{\rho}^{AB}_{++++}$.
Furthermore, the coherences are affected as:

$$\hat{\rho}^{AB}_{-++-}(t,T) = \hat{\rho}^{AB}_{-++-}(t)e^{-(\Gamma_{R,B}+\Gamma_{D,B})(1-\chi^2)|\alpha|^2(T-t)} \tag{4.44}$$

$$\hat{\rho}^{AB}_{+--+}(t,T) = \hat{\rho}^{AB}_{+--+}(t)e^{-(\Gamma_{R,A}+\Gamma_{D,A})\chi^2|\alpha|^2(T-t)} \tag{4.45}$$

Where Γ_D is the photon-induced dephasing probability. Consider that each subsequent photon after t has a probability to dephase the coherence between the states.
Let us evaluate these 4 terms using Eq. 4.40 and we get

$$\hat{\rho}^{AB}_{+(--++)} = (1-\chi^2)\eta\frac{|\alpha|^2}{2}\langle\Psi_{ini,\alpha}|\zeta^\dagger_B\zeta_B(\hat{\rho}^B_{-+})^\dagger\hat{\rho}^{AB}_{--++}(t,T)\hat{\rho}^B_{-+}|\Psi_{ini},\alpha\rangle/\operatorname{Tr}[\hat{\rho}^{AB}_\mu(t,T)] \tag{4.46}$$

and, on using $(\hat{\rho}^B_{-+})^\dagger\hat{\rho}^{AB}_{--++}(t)\hat{\rho}^B_{-+} = \hat{\rho}^A_{--}(t)\otimes\hat{\rho}^B_{--}(t)$ we get

$$\hat{\rho}^{AB}_{+(--++)} = (1-\chi^2)\eta\frac{|\alpha|^2}{2}\zeta^\dagger_B\zeta_B\langle\Psi_{ini,\alpha}|\hat{\rho}^A_{--}\otimes\hat{\rho}^B_{--}|\Psi_{ini},\alpha\rangle e^{-\Gamma_{R,A}\chi^2|\alpha|^2(T-t)}/\operatorname{Tr}[\hat{\rho}^{AB}_\mu(t,T)] \tag{4.47}$$

Then, for an initial state of both qubits in $|-\rangle$, we find that element $\hat{\rho}^A$ decays as $e^{-\Gamma_{R,A}\chi^2|\alpha|^2t}$ and element $\hat{\rho}^B$ decays as $e^{-\Gamma_{R,B}\sqrt{1-\chi^2}|\alpha|^2t}$, such that

$$\hat{\rho}^{AB}_{+(--++)} = (1-\chi^2)\eta\frac{|\alpha|^2}{2}\zeta^\dagger_B\zeta_B e^{-(\Gamma_{R,A}\chi^2+\Gamma_{R,B}(1-\chi^2))|\alpha|^2t}e^{-\Gamma_{R,A}\chi^2|\alpha|^2(T-t)}/\operatorname{Tr}[\hat{\rho}^{AB}_\mu(t,T)] \tag{4.48}$$

Similarly, we find for $\hat{\rho}^{AB}_{+(++--)}$

$$\hat{\rho}^{AB}_{+(++--)} = \chi^2\eta\frac{|\alpha|^2}{2}\zeta^\dagger_A\zeta_A e^{-(\Gamma_{R,A}\chi^2+\Gamma_{R,B}(1-\chi^2))|\alpha|^2t}e^{-\Gamma_{R,B}(1-\chi^2)|\alpha|^2(T-t)}/\operatorname{Tr}[\hat{\rho}^{AB}_\mu(t,T)] \tag{4.49}$$

Now for the coherences between the two hybrids, using similar methods, we find:

$$\hat{\rho}^{AB}_{+(+--+)} = \chi e^{i\phi}\sqrt{1-\chi^2}\eta\frac{|\alpha|^2}{2}\zeta^\dagger_B\zeta_A e^{-(\Gamma_{R,A}\chi^2+\Gamma_{R,B}(1-\chi^2))|\alpha|^2t}e^{-(\Gamma_{R,A}+\Gamma_{D,A})\chi^2|\alpha|^2(T-t)} \tag{4.50}$$

and

$$\hat{\rho}^{AB}_{+(-++-)} = \chi e^{-i\phi}\sqrt{1-\chi^2}\eta\frac{|\alpha|^2}{2}\zeta_A^\dagger\zeta_B e^{-(\Gamma_{R,A}\chi^2+\Gamma_{R,B}(1-\chi^2))|\alpha|^2 t}e^{-(\Gamma_{R,B}+\Gamma_{D,B})(1-\chi^2)|\alpha|^2(T-t)} \tag{4.51}$$

Finally, we have all terms to complete the expression Eq. 4.41, the time-dependent Fidelity. To find the average fidelity over all experiments, we must integrate as:

$$\bar{F}(T) = \frac{\int_0^T F(t,T)p(t)dt}{\int_0^T p(t)dt} \tag{4.52}$$

This equation says we average over all possible values of F depending on the time t at which we detect a click. The probability for a click at each time point is given by the probability function $p(t)$, which is also simply the trace $\mathrm{Tr}[\hat{\rho}^{AB}]$ in the denominator of $F(t,T)$, (all events which result in a click at the detectors):

$$p(t) = \mathrm{Tr}[\hat{\rho}^{AB}] = \eta\frac{|\alpha|^2}{2}\left(\chi^2\zeta_A^\dagger\zeta_A e^{-\chi^2\Gamma_{R,A}|\alpha|^2 t} + (1-\chi^2)\zeta_B^\dagger\zeta_B e^{-(1-\chi^2)\Gamma_{R,B}|\alpha|^2 t}\right) \tag{4.53}$$

The integral of $p(t)$ from 0 to T we define as a total $P^{(c)}_{suc}$ (see Eq. 4.35):

$$\begin{aligned}\int_0^T p(t)dt = P^{(c)}_{suc} = \frac{\eta}{2}(\zeta_A^\dagger\zeta_A(1-e^{-\chi^2\Gamma_{R,A}|\alpha|^2 T})/\Gamma_{R,A} \\ + \zeta_B^\dagger\zeta_B(1-e^{-(1-\chi^2)\Gamma_{R,B}|\alpha|^2 T})/\Gamma_{R,B})\end{aligned} \tag{4.54}$$

and,

$$\begin{aligned}F(t)p(t) = \frac{\eta}{2}\frac{|\alpha|^2}{2}\Big[&\chi^2\zeta_A^\dagger\zeta_A e^{-\Gamma_{R,A}\chi^2|\alpha|^2 t}e^{-\Gamma_{R,B}(1-\chi^2)|\alpha|^2 T} \\ &+ (1-\chi^2)\zeta_B^\dagger\zeta_B e^{-\Gamma_{R,B}(1-\chi^2)|\alpha|^2 t}e^{-\Gamma_{R,A}\chi^2|\alpha|^2 T} \\ &+ \chi\sqrt{1-\chi^2}e^{-i\phi}\zeta_A^\dagger\zeta_B e^{-\left[\Gamma_{R,A}\chi^2-\Gamma_{D,B}(1-\chi^2)\right]|\alpha|^2 t}e^{-(\Gamma_{R,B}+\Gamma_{D,B})(1-\chi^2)|\alpha|^2 T} \\ &+ \chi\sqrt{1-\chi^2}e^{+i\phi}\zeta_B^\dagger\zeta_A e^{-\left[\Gamma_{R,B}(1-\chi^2)-\Gamma_{D,A}\chi^2\right]|\alpha|^2 t}e^{-(\Gamma_{R,A}+\Gamma_{D,A})\chi^2|\alpha|^2 T}\Big]\end{aligned} \tag{4.55}$$

In the special case where we have equal hybrids and balanced arms, i.e. $\zeta_A = \zeta_B \equiv \zeta$, $\chi^2 = 1/2$, $\Gamma_{R,A} = \Gamma_{R,B} \equiv \Gamma_R$ and $\Gamma_{D_A} = \Gamma_{D_B} \equiv \Gamma_D$, we can combine terms and evaluate Eq. 4.52 as

$$\bar{F}_{eq} = \frac{\Gamma_R\frac{\eta}{2}\zeta^\dagger\zeta e^{-\Gamma_R\frac{|\alpha|^2}{2}T}}{\eta\zeta^\dagger\zeta(1-e^{-\Gamma_R\frac{|\alpha|^2}{2}T})}\left[\frac{1-e^{-\Gamma_R\frac{|\alpha|^2}{2}T}}{\Gamma_R} + \cos(\phi)\frac{1-e^{-(\Gamma_R-\Gamma_D)\frac{|\alpha|^2}{2}T}}{\Gamma_R+\Gamma_D}e^{-\Gamma_D\frac{|\alpha|^2}{2}T}\right] \tag{4.56}$$

cleaning up, and replacing $|\alpha|^2 T \to \bar{n}$ to denote the average photon number in the coherent pulse:

$$\bar{F}_{eq} = \frac{1}{2}e^{-\Gamma_R\frac{\bar{n}}{2}}\left[1+\cos(\phi)\frac{\Gamma_R}{\Gamma_R-\Gamma_D}\frac{e^{-\Gamma_D\frac{\bar{n}}{2}}-e^{\Gamma_R\frac{\bar{n}}{2}}}{1-e^{-\Gamma_R\frac{\bar{n}}{2}}}\right] \tag{4.57}$$

Taking the limit where $\Gamma_R\bar{n} \ll 1$ and $\Gamma_D\bar{n} \ll 1$, we find a first order correction to a fidelity of unity as:

$$\bar{F}_{eq} \approx 1 - \frac{1}{2}(\Gamma_R + \frac{\Gamma_D}{4})\bar{n} \tag{4.58}$$

This result consists of two terms reducing the fidelity of a Bell state generation. The $\Gamma_R\bar{n}/2$ stems from a photon flipping the second qubit after the first one resulted in a click at the

detector already. On average, the click happened halfway between time 0 and T, and thus only half of the coherent pulse is left to cause this process of flipping the second qubit.
The second contribution, $\Gamma_D\bar{n}/4$, comes from the photon induced dephasing; the remaining photons in the pulse can distort the phase coherence between the qubit states, but only through one of the qubits (the one that has *not* flipped).

If we consider the hybrids to have different properties, we can first maximize the fidelity by balancing the arms such that $\chi^2\Gamma_{R,A} = (1-\chi^2)\Gamma_{R,B}$, by looking at the Raman transfer probability by coherent pulses at each hybrid and do state readout of the SC qubits separately. Next, we can ensure the phases are balanced by tuning the relative phase ϕ until we maximize the intensity at detectors $D-$ and $D+$. This ensures that coherences $\zeta_A^\dagger\zeta_B = \zeta_B^\dagger\zeta_A e^{+2i\phi}$ match. Solving for the fidelity and taking the limit where the rates are small, we find

$$\bar{F} \approx 1 - \frac{1}{2}(1-Z) - \Big[\frac{(1+Z)}{2}\chi^2\Gamma_{R,A} + \frac{Z}{4}(\chi^2\Gamma_{D,A} + (1-\chi^2)\Gamma_{D,B}\Big]\bar{n} \tag{4.59}$$

or

$$\bar{F} \approx 1 - \frac{1}{2}(1-Z) - \chi^2\Big[\frac{(1+Z)}{2}\Gamma_{R,A} + \frac{Z}{2}Q\Gamma_{D,A}\Big]\bar{n} \tag{4.60}$$

where we have an imbalance Z as

$$Z = \frac{2\sqrt{1-\chi^2}}{\chi}\frac{\sqrt{\frac{P_{R,B}}{P_{R,A}}}}{1+\frac{1-\chi^2}{\chi^2}\left(\frac{P_{R,B}}{P_{R,A}}\right)} \tag{4.61}$$

and an imbalance Q as

$$Q = \frac{1}{2}\Big[1 + \frac{1-\chi^2}{\chi^2}\frac{\Gamma_{D,B}}{\Gamma_{D,A}}\Big] \tag{4.62}$$

with χ^2 the beamsplitter ratio, and $P_{R,A/B}$ the single photon Raman transition success probability for hybrid A/B respectively.

Eq. 4.60 then reduces to the same expression for the fidelity for $\chi^2 = 0.5$ and equal system properties.

In the next section, we investigate the effects of dephasing of the QD. We can consider two limits of dephasing rates: fast or slowly varying.

4.6 'Slow' dephasing

In this limit, we consider dephasing due to the QD energy levels drifting slowly throughout time, as a reaction to an inherently random environment with charges and fields floating around. We here consider drifting slow compared to the timescale of the photon-hybrid interaction (i.e. it varies more slowly than the rate of transfer from qubit state $|-\rangle$ to $|+\rangle$).

By assuming the QD transition energy changes more slowly than the other system parameters, we calculate the impact of this slow dephasing on the success probability of the transducer as follows: consider the success probability P_{suc} of a Raman transition that created qubit-photon entanglement. In general, this success will depend on the detuning of the QD. As the detuning Δ is not constant between different shots of the experiment, we average over a distribution with a central expectation value of the detuning in addition to some characteristic distribution parameter.

Let us consider the detuning to be a stochastic variable with a Normal (Gaussian) distribution f_{norm} governed by the (normalized) probability density function

$$f_{norm}(x|\mu,\sigma) = \frac{1}{\sqrt{2\sigma^2\pi}}e^{-(x-\mu)^2/(2\sigma^2)}, \tag{4.63}$$

where x is the stochastic variable, μ is the expectation value of x, and σ is the standard deviation of x.
We can then calculate the expectation value of P_{suc}, averaged over many experiments, as a function of the distribution parameters by

$$P_{suc,avg} = \int_{-\infty}^{+\infty} d\Delta f_{norm}(\Delta|0,\sigma)P_{suc} = \int_{-\infty}^{+\infty} \frac{1}{\sqrt{2\sigma^2\pi}} e^{-(\Delta-\Delta_0)^2/(2\sigma^2)} P_{suc}(\Delta)d\Delta \tag{4.64}$$

Repeating the procedure many times results in sampling the detuning distribution many times, resulting in an average $P_{suc,avg}$.
Note that the resonance condition of the Raman process we are interested in is given by

$$\omega_q = \sqrt{\Omega^2 + \Delta^2} \tag{4.65}$$

Additionally, depending on the parameter regime, the optimal *photon* detuning one should pick is a function of the cavity-QD detuning Δ. Therefore there exists a base Δ_0 which is optimal in the sense that it maximizes the Raman transition amplitude in an experiment. However, due to external random field effects, the QD energy will drift around this Δ_0 and on average gives rise to a dephasing effect. In the above equations, we should therefore replace Δ by Δ_0 and the original equations of motion contain $\Delta_0 + \Delta_{drift}$. In the rest of this paper, we will set Δ_0 to zero for simplicity, and refer to Δ_{drift} as the 'cavity-QD detuning'.

With this insight, we can in principle numerically solve for the statistically averaged success probability of the Raman transition process. However, in order to gain some insight into the dependency of the various parameters, we calculate an analytical solution to Eq. 4.64 under some approximations.

Let us consider the following approximation: we assume that we can tune the cavity into resonance with the QD so the average QD detuning over time can in principle be set to zero. In addition, we assume the coupling Ω is equal to the qubit energy ω_q. This means Δ_0 is zero in Eq. 4.64.

For arbitrary σ, Eq. 4.64 will not yield a converging integral. However, if we assume the QD drifting σ to be smaller than the line widths of the QD-cavity system (so, typically $\Delta < \kappa, \gamma...$), we can expand P_R in Δ/ω_q and we found in Section 4.2 that

$$P_R \approx A\left[1 + 2B\left(\frac{\Delta}{\omega_q}\right) - \left(\frac{1}{2} - 3B^2\right)\left(\frac{\Delta}{\omega_q}\right)^2\right] \tag{4.66}$$

. We now solve Eq. 4.64 analytically and the result is

$$P_{R,avg} \approx \int_{-\infty}^{+\infty} d\Delta \frac{1}{\sqrt{2\sigma^2\pi}} e^{-\Delta^2/(2\sigma^2)} P_R(\Delta) = A\left(1 - \left(\frac{1}{2} - 3B^2\right)\left(\frac{\sigma}{\omega_q}\right)^2\right). \tag{4.67}$$

We find that the term linear in Δ in Eq. 4.66 vanishes on average, as we average over a zero-mean random variable.

For weak coupling g_s compared to the linewidths and detuning, $4g_s^2 < (\kappa+\gamma')^2 + (\kappa-\gamma')^2\Delta^2/\Omega^2$, the photon resonance condition is $\delta \to \omega_q/2$. There,

$$A \equiv \left(\frac{g_s\kappa}{gs^2 + (\kappa+\gamma')^2/4}\right)^2 \quad , \quad B \equiv \frac{(\kappa^2 - \gamma'^2)/4}{gs^2 + (\kappa+\gamma')^2/4} \tag{4.68}$$

For strong coupling g_s compared to the linewidths and detuning, $4g_s^2 > (\kappa+\gamma')^2 + (\kappa-\gamma')^2\Delta^2/\Omega^2$, the photon resonance condition is $\delta \to \omega_q/2 + \frac{1}{4}\sqrt{4g_s^2 - (\kappa+\gamma')^2 - (\kappa-\gamma')^2\Delta^2/\Omega^2}$.

There,

$$A \equiv \left(\frac{\kappa}{\kappa+\gamma'}\right)^2 \quad , \quad B \equiv \left(\frac{\kappa-\gamma'}{2(\kappa+\gamma')}\right) \tag{4.69}$$

Average Fidelity - Slowly varying random detuning For each experiment, hybrids A and B will in general have different detunings (between QD and cavity) and other parameters. We can calculate an *average* fidelity over many experiments with successful entanglement creations, by integrating the fidelity of entanglement generation over a Gaussian distribution for Δ with a variance σ^2 for each transducer A and B.
To find the average effect of a drifting detuning in experimental setups, we can now integrate the fidelity Eq. 4.26 over normally distributed detunings of both transducers. Recall that the fidelity for two differing transducers reads

$$F = 1 - \frac{1}{2}\frac{|r_1 - r_2|^2}{|r_1|^2 + |r_2|^2} \tag{4.70}$$

To calculate the fidelity from r_1 and r_2 and therefore scattering amplitudes $\mathcal{S}_{+-}$, we again make the approximation where σ is considered small compared to linewidths, such that Δ is small on average too. We consider two regimes, weak coupling and strong coupling compared to the linewidths. The expression for scattering coefficient $\mathcal{S}_{+-}$ is approximated by

$$\mathcal{S}_{+-} \approx A\left[1 + B\left(\frac{\Delta}{\omega_q}\right) - \left(\frac{1}{4} - B^2\right)\left(\frac{\Delta}{\omega_q}\right)^2\right] \tag{4.71}$$

for small Δ. For weak coupling $g_s < (\kappa + \Gamma')/2$, approximate expressions for A and B are

$$A \approx \frac{-ig_s\kappa}{gs^2 + (\kappa+\gamma')^2/4} \quad , \quad B \approx \frac{(\kappa^2 - \gamma'^2)/4}{gs^2 + (\kappa+\gamma')^2/4} \tag{4.72}$$

Conversely, for strong coupling g_s compared to the linewidths and detuning, $4g_s^2 \gg (\kappa + \gamma')^2 + (\kappa-\gamma')^2\Delta^2/\Omega^2$, the photon resonance condition is $\delta \to \omega_q/2 + \frac{1}{4}\sqrt{4g_s^2 - (\kappa+\gamma')^2}$. There, the scattering amplitude is also of the form Eq. 4.71 and now

$$A \approx \left(\frac{\kappa}{\kappa+\gamma'}\right) \quad , \quad B \approx \left(\frac{\kappa-\gamma'}{2(\kappa+\gamma')}\right) \tag{4.73}$$

Then, we find for the fidelity of a single experiment with single-photon input, for small $\Delta \ll \omega_q$:

$$F \approx 1 - \frac{1}{4}\left[B\left(\frac{\Delta_1 - \Delta_2}{\omega_q}\right) - \left(\frac{1}{4} - B^2\right)\left(\frac{\Delta_1^2 - \Delta_2^2}{\omega_q}\right)\right]^2 \tag{4.74}$$

We integrate this Fidelity for each experiment over many experiments where Δ_A and Δ_B are normally distributed with variance σ_1 and σ_2, respectively:

$$F_{\text{SD}} = \int_{-\infty}^{+\infty}\int_{-\infty}^{+\infty} d\Delta_1 d\Delta_2 F(\Delta_1, \Delta_2)\frac{1}{2\pi\sigma_1\sigma_2} e^{-\frac{\Delta_1^2}{2\sigma_1^2}} e^{-\frac{\Delta_2^2}{2\sigma_2^2}} \tag{4.75}$$

$$F_{\text{SD}} \approx 1 - \frac{B^2}{4\omega_q^2}\left(\sigma_1^2 + \sigma_2^2\right) - \frac{(1-4B^2)^2}{64\omega_q^4}\left(2\sigma_1^4 + 2\sigma_2^4 + (\sigma_1^2 - \sigma_2^2)^2\right) \tag{4.76}$$

where subscript SD indicates Slow Dephasing, and 'weak' refers to the weak coupling g_s compared to linewidths.

4.7 Conclusion

We in this Chapter presented a novel quantum transducer device architecture comprising an optical cavity and a quantum dot coupled electrically to a coherent TLS. We calculated for different parameter regimes the Raman scattering probability. This quantity describes the probability of entanglement generation between an inelastically scattered photon and the TLS internal state. We also investigate the application of said transducers in a long-distance quantum entanglement protocol. The fidelity of the output wavefunction with a maximally entangled state was found. For a single photon input, the fidelity can always reach unity by calibrating the experimental setup: we showed how tuning the beamsplitter and beam phase can compensate for transducer parameter differences. We also show the fidelity of entanglement when the input is a weak coherent pulse. Although a stronger pulse is shown to give a higher probability of entanglement generation per shot, the fidelity goes down linearly with the average photon number, in part due to light-induced dephasing.

Although beamsplitters can be tuned to maximize entanglement fidelity, in practice there are parameters which are not constant over time and one-time calibration will not be able to prevent the environment from affecting the success probability nor the entanglement fidelity. As a specific example, we quantitatively investigated the effect of fluctuations of the QD-cavity detuning on the success probability and entanglement fidelity. We there average over many experiments with the transducer detunings as normally distributed random variables. We find how the expected fidelity degrades as we increase the distribution width of the detuning drift. In other words, the stronger the environment couples to the quantum dot energy level, the lower the average fidelity will be.

The system we presented here has great potential to be experimentally implemented in the near future. One of the striking advantages is that the Raman scattering can be made resonant when the TLS transition frequency is close to the coupling strength between the cavity and QD. This enable highly efficient transduction, requiring only a single photon or weak coherent pulse to operate. This opens up possibilities to use this transducer device as a node in a future quantum internet [16, 54].

Chapter 5

Simulating Quantum Chemistry on a Quantum Computer

> Nature isn't classical, dammit, and if you want to make a simulation of nature, you'd better make it quantum mechanical, and by golly it's a wonderful problem, because it doesn't look so easy.
>
> *Richard Feynman [14]*

Natural reality is currently best understood using theories of quantum physics. In particular on the micro- to nanoscale behaviour of reality, tremendous progress in understanding by applying quantum theory has been made, enabling technological advancement to rapidly evolve us as a species. As an example of direct technological application, all of modern chemistry has its origin in quantum theory. In fact, large parts of quantum theory in use today were developed through the study of atoms, to explain observations which could not be reconciled with classical physics.

Being able to simulate the nature of reality, humans have now become able to construct their own, virtual, reality. In this reality, objects typically still obey the laws we know govern our own universe, as long as we wish it so. This enables rapid iterations over possible outcomes of events and product quality depending on minute differences in starting conditions. More possible combinations can be tested than can ever be tested in our reality. Using this concept, many new pharmaceutical drugs have been developed and new materials have changed the way we build our tools and objects to improve our daily lives. Is this it? Have we then already reached complete enlightenment and understanding of chemical processes down to the nuclear level?

The short answer is no. Sure, one might easily imagine that we can use quantum theory to predict the behaviour of any chemical compound. While true in theory, in practice this becomes quickly intractable for larger systems. The exact application of the laws of quantum mechanics to molecules with more than a few tens of electrons leads to equations much too complicated to be soluble even on our most powerful computers. The so-called wavefunction of a quantum system grows exponentially with the problem size, while the increase in computing speed of our fastest supercomputers does not grow as fast. In essence, this means we will likely never be able to simulate exactly very large molecules, materials and chemical processes using even our most powerful computers. This is a fundamental roadblock to the advancement of chemistry; is there any way to solve this problem?

In this chapter, we first introduce the basics of quantum chemistry and how to simulate this on a classical computer. Next, we introduce quantum information and computing concepts and explain how these may help to overcome the challenge of exact quantum chemistry

simulation. Lastly, we present results on quantum computational chemistry research performed at Google Santa Barbara, California, USA, over the course of 6 months as part of the PhD program of the Author.

5.1 Intro to Quantum Chemistry

Quantum chemistry is the study of electronic structure and nuclei like atoms and molecules, in addition to a broader field of material studies and chemical reactions. We here focus on the electronic structure problem and finding the ground state energy of molecular and material Hamiltonians.

The Hamiltonian for a molecule consisting of nuclei and electrons contains terms for the kinetic energies and the coulomb attraction/repulsion potentials between the electrons, between the nuclei and between electrons and nuclei. As the nuclei of a molecule are over a thousand times heavier than electrons, one can apply the Born-Oppenheimer approximation [144], treating nuclei as stationary classical point charges and only solving for the electron dynamics. The electronic Hamiltonian in dimensionless units then reads [145]

$$-\sum_i \frac{\nabla_i^2}{2} - \sum_{i,I} \frac{Z_I}{|\mathbf{r}_i - \mathbf{R}_I|} + \frac{1}{2}\sum_{i \neq j} \frac{1}{|\mathbf{r}_i - \mathbf{r}_j|} \tag{5.1}$$

where r_i, R_I and Z_I represent the position of an electron i, the position of a nucleus I, and the charge of nucleus I respectively. The aim of quantum chemistry is to find the energy eigenstate $|\Psi_g\rangle$ and corresponding energy eigenvalue E_g of Hamiltonian Eq. 5.1. In general, finding all eigenstates and eigenvalues can give useful information to a chemist; in this work, we focus on finding the groundstate energy for a specific configuration of the problem. The same techniques we use are applicable to higher excited states.

5.2 Quantum chemistry simulation on a quantum computer

Generally speaking, simulating quantum dynamics of a system described by a (generally time-dependent) Hamiltonian $\hat{\mathcal{H}}(t)$ involves solving the Schroedinger equation for a quantum wavefunction $|\Psi(t)\rangle$ given some initial state $|\Psi(0)\rangle$. The Schroedinger equation [146] reads

$$i\hbar \frac{\mathrm{d}}{\mathrm{d}t}|\Psi(t)\rangle = \hat{\mathcal{H}}|\Psi(t)\rangle \tag{5.2}$$

where i is the imaginary unit, and $\hbar$ is the reduced Planck constant. The general solution to this first-order differential equation can be written as

$$|\Psi(t)\rangle = e^{-i\int_0^t \hat{\mathcal{H}}(t')/\hbar \mathrm{d}t'}|\Psi(0)\rangle \tag{5.3}$$

One may ask the valid question: "Wait, that's the solution right there, is it not? Then what is the issue?" Well, typically one is interested in the entries of final wavefunction $|\Psi(t)\rangle$; but in order to calculate those, matrix multiplication of $e^{-i\int_0^t \hat{\mathcal{H}}(t')/\hbar dt'}$ with vector $|\Psi(0)\rangle$ requires evaluation of matrix exponentiation, which is very costly computationally as a function of matrix size. In turn, the matrix size is proportional to the size of Hamiltonian $\hat{\mathcal{H}}(t')$ which covers the entire Hilbert space of the problem. For example for simulating N interacting two-level systems or N-orbital chemistry problems, the Hilbert space is proportional to 2^N. Direct evaluation of Eq. 5.3 is therefore impossible for anything but small problems.

Quantum simulation aims to circumvent the problem by meticulously constructing an analogous system to the problem system, which behaves alike but can be analyzed and probed

in a controlled environment. Let's say a particular problem can be described by a Hamiltonian $\mathcal{H}$. We now construct a controlled environment which is governed by a Hamiltonian $\mathcal{H}$. If the structure of the interactions and energies is equivalent between the two, finding the solution to the dynamics of the simulator system amounts to *solving* the problem system.

In addition, ideally such a quantum simulator should be programmable, in order to simulate different instances of the problem. It can then be used as a design-tool, much like we run classical simulations on computers in use today. The ability to simulate systems millions of times for different configurations and parameters in order to synthesize optimal solutions or strategies have transformed all aspects of modern society. It is therefore highly desirable to construct simulators which, even if they specialize in for example chemistry, are reconfigurable between experiments.

5.3 Gate-based quantum computing

In analogy with classical computation, *gate-based quantum computing* maps problems to quantum data structures called 'qubits' (see for instance Ref. [7] for a detailed introduction). These qubits can be in a quantum state $|0\rangle$ or $|1\rangle$, or any superposition of the two:

$$|\Psi_{\text{qubit}}\rangle = c_0|0\rangle + c_1|1\rangle \tag{5.4}$$

with c_0 and c_1 complex numbers and $|c_0|^2 + |c_1|^2$ such that normalization $\langle\Psi_{\text{qubit}}|\Psi_{\text{qubit}}\rangle = 1$ is ensured. When we measure the state of this qubit, we get either the result 0, with probability $|c_0|^2$, or 1, with probability $|c_1|^2$.

There are several criteria for a physical system to be able to implement universal gate-based quantum computation. In his 2000 paper 'The Physical Implementation of Quantum Computation' [15], David P. DiVincenzo proposed the following criteria:

1. A scalable physical system with well-characterized qubits.
2. The ability to initialize the state of the qubits.
3. Long relevant decoherence times.
4. A "universal" set of quantum gates.
5. A qubit-specific measurement capability.
6. The ability to interconvert stationary and flying qubits.
7. The ability to faithfully transmit flying qubits between specified locations.

Many different physical systems can be used to realize qubits. To list a few: the two different polarizations of a photon [147], the alignment of a nuclear spin in a magnetic field [148], two states of an electron orbiting a single atom or confined to an artificial atom (quantum dot) [149], and three types of superconducting qubit [150] archetypes: the phase, charge and flux qubits. Common to all these systems is that the logical quantum states $|0\rangle$ and $|1\rangle$ are mapped to two states of the system, typically their discrete energy levels or quantum superpositions thereof.

In addition to the physical realization of qubits (1), the possibility to initialize them (2) and their remaining coherent for a sufficiently long time (3), it is essential for gate-based quantum computing to have access to a universal set of quantum gates (4). Quantum gates are the quantum equivalent of classical computing logic gate operations like `NOT`, `CNOT`, `XOR` etc. A set of gates is said to be universal for quantum computation if any unitary operation may be approximated to arbitrary accuracy by a quantum circuit involving only those

gates [7]. The catch is that there exist unitary transforms which require exponentially many gates to approximate! In practice, we would like to devise algorithms which can be performed efficiently as compared to using classical computing.

We here refer the reader to other excellent works for a background and origins of quantum computing [7–14]. We from this point assume a certain degree of familiarity with the topic.

5.3.1 Suzuki-Trotter Expansion

It is technologically very challenging to construct multi-qubit gates with high fidelity. Typically, Hamiltonian evolution is instead decomposed into a circuit consisting only of single- and two-qubit gates of high fidelity. However, multiple two-qubit gates can not involve the same qubits at the same time. This means not all terms in the Hamiltonian can be applied simultaneously; if there are terms in the Hamiltonian which do not commute with each other, it is non-trivial whether we can apply the corresponding gates in series instead. A rigorous decomposition of the Hamiltonian into partial evolutions is therefore required. One of these, the Suzuki-Trotter expansion, expands the exponential operator in Eq. 5.3 as

$$e^{(A+B)} = \lim_{n\to\infty} \left(e^{\frac{A}{n}} e^{\frac{B}{n}}\right)^n \tag{5.5}$$

where, in the limit of the number of Trotter steps n, the two operators are equivalent. In other words, instead of applying the whole Hamiltonian evolution at once, the different parts A and B are alternated n times with interaction strengths reduced by a factor n. If we choose some finite n, the Suzuki-Trotter incurs truncation errors we will refer to as 'Trotter errors'. Depending on the accuracy required for the simulation, one may need a few or many Trotter steps to simulate the total Hamiltonian dynamics.

In this way, a gate-based quantum circuit employing a Trotterization scheme applies copies of alternating gate sequences for n Trotter steps to approximate the real Hamiltonian evolution.

5.4 Quantum Annealing

Quantum annealing, formulated in its present form by Ref. [151], consists of the following strategy; start a system in a superposition of all possible configurations with equal weights. Allow the system to evolve with a Hamiltonian which encapsulates the problem one wishes to solve. If the rate of increasing the strength of this Hamiltonian is low enough, one stays close to the ground state of the instantaneous Hamiltonian according to the adiabatic theorem [152], eventually ending up in the groundstate of the problem Hamiltonian. If the rate is high, one may have a higher chance of exploring hard-to-reach states (diabatic quantum computing). Adiabatic Quantum Computing (AQC) is therefore a type of quantum annealing and a way of solving for the groundstate of a particular Hamiltonian.

Typically, AQC is used for finding the groundstate of spin glasses (Ising model [153]). However, the same principles can be used to find the groundstate of chemistry Hamiltonians too. Typically, the quantum Hamiltonian consists of two non-commuting parts, say $\mathcal{H} = \mathcal{H}_A + \mathcal{H}_B$, where the groundstate of either part is efficiently solvable but not the groundstate of the sum of the two. The strategy for quantum annealing applied to quantum chemistry simulation is therefore as follows:

Initialize the simulator in the groundstate of $\mathcal{H}_A$. Next, evolve the system over Hamiltonian

$$\mathcal{H}(s) = \mathcal{H}_A + s\mathcal{H}_B \tag{5.6}$$

where $s = s(t)$ is a slowly increasing function going from 0 to 1 over a period of time $0 < t < T$. If the rate of change of $ds/dt)$ is slow enough as compared to the energy gap in the instantaneous energy spectrum of Hamiltonian $\mathcal{H}(s)$, the system stays in the instantaneous groundstate all the way until $s = 1$ and $\mathcal{H}(s) = \mathcal{H}_A + \mathcal{H}_B$, meaning that we find the groundstate of the total problem Hamiltonian.

The best strategy $s(t)$ for adiabatic quantum computing is to slow down near to a small energy gap in the spectrum and to speed up in places where the gap is large and the chance to jump out of the groundstate to higher excited states is small. Unfortunately, the structure of the instantaneous eigenspectrum of $\mathcal{H}(s)$ as a function of s is typically unknown or very hard to calculate classically. Therefore, it is often not possible to identify the location s' at which an anti-crossing occurs in the spectrum, so it is unknown where the adiabatic rate of change should slow down. Therefore the spline/strategy $s(t)$ which gives the best results, for a given $\mathcal{H}(s)$ without further information, is a linear one.

5.4.1 Digital annealing

Quantum annealing generally requires one to have access to hardware which directly can implement the problem Hamiltonian, including problem-specific connectivity requirements. This could be troublesome, as a fully programmable annealer with all-to-all connectivity is hard to construct.

An alternative method is to approximate the time-dependent annealing Hamiltonian evolution by a Suzuki-Trotter decomposition and apply each Trotter step using a set of gates. In that case, each Trotter step may have a different overall prefactor in order to make a Riemann approximation to the integral in Eq. 5.3, such that the overal circuit is of the form

$$
\begin{aligned}
U(T) &= e^{-i\int_0^T \mathcal{H}(s(t'))/\hbar \mathrm{d}t'} && (5.7)\\
&\approx e^{-i(T/p)\mathcal{H}_A/\hbar} e^{-i(T/p)\mathcal{H}_B s(T/p)/\hbar} && (5.8)\\
&\quad \times e^{-i(T/p)\mathcal{H}_A/\hbar} e^{-i(T/p)\mathcal{H}_B s(2T/p)/\hbar} \ldots && (5.9)\\
&\quad \times e^{-i(T/p)\mathcal{H}_A/\hbar} e^{-i(T/p)\mathcal{H}_B s(T)/\hbar} && (5.10)
\end{aligned}
$$

for p Trotter steps in the approximate Suzuki-Trotter decomposition. Note that Hamiltonian $\mathcal{H}_B$ is multiplied by a function $s(t)$ with the discrete timestep $\{T/p, 2T/p, ..., T$ as argument. In this way, a discretization of function $s(t)$ is performed alongside the digitization of time-dependent Hamiltonian evolution under Eq. 5.6

5.5 Variational Quantum Eigensolver

The variational quantum eigensolver (VQE), first introduced by Aspuru-Guzik in 2013 [154], is at the time of writing one of the most promising algorithms for simulating quantum chemistry on a Near-term Intermediate Scale Quantum (NISQ [155]) device. One of the problems with current hardware is that the coherence time and gate-depth of quantum circuits are very limited. Simulating exact dynamics and extracting useful information using the quantum phase estimation algorithm would require large circuits with many gates, requiring a per-gate fidelity much higher than currently achieved on all hardware realizations. In VQE, the coherence time requirement is drastically reduced by combing a quantum processing unit with a classical processing unit, computing the eigenvalues and eigenvectors of a Hamiltonian $\mathcal{H}$. By using a variational approach, this reduces the requirement of perfectly coherent evolution of the quantum state and makes more efficient use of the quantum resources. After its inception, quantum chemistry experiments on small-scale quantum hardware performed by Google [156] and IBM [157] have shown the success of this algorithm.

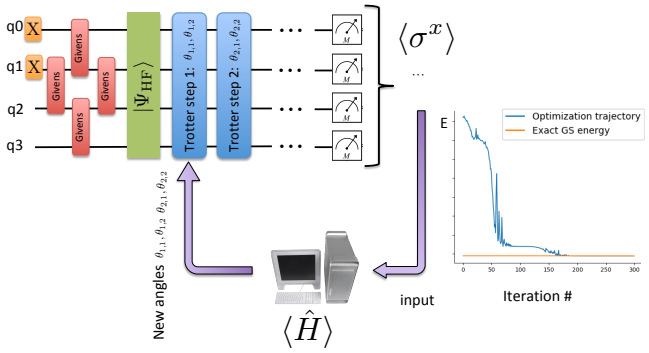

FIGURE 5.1: Schematic of the Variational Quantum Eigensolver classical optimization loop. The quantum circuit output is measured and a Hamiltonian averaging process feeds an expectation value for the energy into a classical computer. The classical optimization algorithm then suggests a new set of angles for the quantum circuit to run. This process is repeated until convergence of the groundstate energy as illustrated in the example optimization trajectory in the graph to the right.

The VQE works as follows [154]:

1. Transform the problem Hamiltonian to be simulated to a qubit Hamiltonian.
2. Pick an initial "trial wavefunction," or trial state, and encode it onto the quantum computer.
3. Estimate the energy of the trial state. This is done by measuring a sum of expectation values of Hamiltonian operators on the quantum state that was created in the previous step, in a process of 'Hamiltonian Averaging'.
4. Feed this energy to an optimizer that is run on a classical computer. The optimizer then generates a new set of control parameters that create a new trial wavefunction on the quantum computer with lower energy. Rinse and repeat until the energy converges to the lowest value; this final energy corresponds to the solution to the ground state energy for the problem Hamiltonian
5. (optional) Repeat steps 2-4 for Hamiltonians corresponding to different parameters of the physical system it aims to simulate.

5.6 Encoding & Basis choice

As we briefly mentioned in Section 5.3, for gate-based quantum computation it should be possible to map the problem one would like to solve to the qubit architecture available. In the case of quantum chemistry problems, antisymmetry of electrons must be enforced either in the solutions (a strategy called 'first quantization') or in the operators (second quantization). In Second-quantization, problems are governed by Fermionic Hamiltonians. Second-quantized Fock states can be constructed by applying creation operators to the vacuum state repeatedly. Creation and annihilation operators, familiar in the context of the iconic quantum harmonic oscillator, are thus fundamental to the quantum many-body theory and every many-body operator can be expressed in terms of them, including the Hamiltonian.

Typically, in computational chemistry for simulating single molecules, a Gaussian basis set is used and the Hamiltonian in this basis has the form [145]

$$\mathcal{H} = \sum_{p,q} h_{p,q} \hat{a}_p^\dagger \hat{a}_q + \frac{1}{2} \sum_{p,q,r,s} h_{p,q,r,s} \hat{a}_p^\dagger \hat{a}_q^\dagger \hat{a}_r \hat{a}_s \tag{5.11}$$

where $\{p, q, r, s\}$ are indices of electronic Gaussian orbitals. The first term includes the kinetic and nuclear potential terms, and the second refers to the electron-electron repulsion potential term. The total number of Hamiltonian terms scales polynomially, as $\mathcal{O}(N^4)$.

For periodic material chemistry simulation purposes, a more appropriate choice would be a basis set that assumes periodic boundary conditions rather than the spherical symmetry imposed on the Gaussian basis set. In Ref. [158], a plane wave dual basis is introduced in which the Hamiltonian has the following form:

$$\mathcal{H} = \sum_{p,q} T_{p,q} \hat{a}^\dagger \hat{a} + \sum_{p} U_p \hat{n}_p + \sum_{p,q} V_{p,q} \hat{n}_p \hat{n}_q, \tag{5.12}$$

where $\hat{a}$ are the annihilation operators, and $\hat{n} \equiv \hat{a}^\dagger \hat{a}$. This Hamiltonian is isospectral to a regular plane wave basis and therefore suffers no loss of accuracy with the normal plane wave basis; however, the dual form can be represented with only $\mathcal{O}(N^2)$ terms. This is advantageous to the Hamiltonian averaging process (3) in Section 5.5. From this point onwards, we will specifically use the dual plane wave basis.

Note that, in order to simulate a fermionic Hamiltonian on a qubit processor described by Pauli spin-1/2 operators, we need to perform a transformation between them such as the Jordan-Wigner transformation [159]. For a 1D-chain of qubits, this introduces strings of Pauli-spin operators, requiring long-range multi-qubit interactions or swapping protocols in the quantum simulation algorithm. In Section 5.7, we will detail more on this topic.

5.7 Connectivity & swap-network

One of the key issues with quantum simulation protocols is the mapping of the problem Hamiltonian to the simulator system Hamiltonian. For quantum chemistry problems in second quantization specifically, the Fermionic Hamiltonian describing the electron energies typically encompasses an 'all-to-all' type of connectivity. This is because all electron orbitals in principle interact with each other with a non-zero matrix-element.

Depending on the hardware being used for the simulator, this can pose a serious challenge. When each qubit describes the occupation of a certain (fixed) Fermionic mode, the Hamiltonian implementation will have to include physical interactions between each and every qubit in order to fully include all terms. However, not all platforms support 'all-to-all' qubit connectivity. On the contrary, most platforms with more than 10 qubits typically employ a rectangular grid structure, with each qubit connected to its nearest 4 neighbours.

In ion trap computing, 'all-to-all' connectivity may be achieved by actually moving atoms around and bringing two next to each other by manipulation with laser trapping beams. In superconducting qubit platforms, so-called `SWAP`-gate operations need to be performed to bring logical qubits next to each other for the nearest-neighbour gate interaction to be performed. The finite fidelity of such `SWAP` gates incurs errors in the algorithm. For the current state-of-the-art platforms, a comparison [160] shows that, while the ion trap chip performs consistently the SC hardware typically performs $20 - 50\%$ worse on a range of algorithm blocks.

It is clearly of paramount importance for the superconducting qubit platform, amongst others also limited to a fixed planar geometry with nearest-neighbour interactions, to improve

(1) SWAP gate fidelity and (2) devise optimal algorithm strategies making use of the strengths of the hardware implementation. We here focus on the latter approach.

One may ask, what is the minimal-depth of a quantum circuit that should be able to simulate all $N^2 - N$ two-body terms and N one-body terms (for example a Fermionic plane-wave dual basis Hamiltonian)? Assuming the gate architecture supports at most one-qubit and two-qubit gates, and gates can not be performed simultaneously on the same qubit, the minimal solution seems clear; each qubit would need to interact at least once with each other qubit, and therefore $N - 1$ layers are necessitated for the two-body terms, while all one-body terms can be included in a single layer of single-qubit rotations. The most compact representation of such a circuit would be the swap-network proposed in Ref. [161], depicted schematically in Figure 5.2

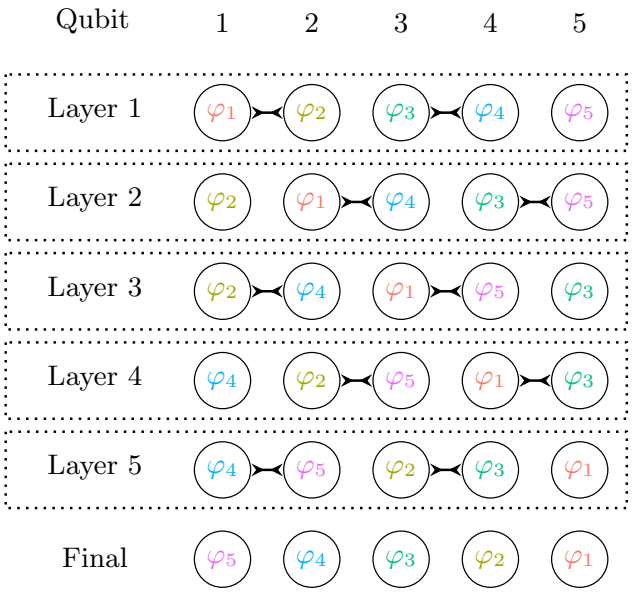

FIGURE 5.2: Schematic of the swap-network proposed in [161]

At first, all logical qubits are mapped directly to the physical qubits. In each step of the circuit, the relevant 2-body Hamiltonian term is applied as a 2-qubit gate operation, followed by a SWAP operation. This is repeated $N - 1$ times. We notice that, at some point in the swap network, a particular set of two logical qubits are neighbouring and the necessary gate operation is performed at that moment and location.

Note that this scheme only requires a linear array of qubits; in fact, even with access to 2D-array of qubits with greater connectivity, the swap network is still optimal. This, again, is because of the limitations of only having access to two-qubit gates.

5.8 Simulating Jellium on a small-scale quantum computer

We in this section summarize and combine strategies from Refs. [161] and [158] for a quantum simulation protocol of 'jellium'.

5.8.1 The jellium Hamiltonian & simulation requirements

The system of interest in this section is so-called jellium. It is defined as a system of electrons with a uniform electron density ρ and a homogeneous background charge such that the overall system is charge neutral [162]. We can model a finite version of this system as a system of η

electrons in a box with periodic boundary conditions, such that the Hamiltonian in the dual plane wave basis becomes

$$\hat{H} = \sum_p T_{p,p} \hat{a}_p^\dagger \hat{a}_p + \sum_{p \neq q} T_{p,q} \hat{a}_p^\dagger \hat{a}_q + \sum_{p \neq q} V_{p,q} \hat{n}_p \hat{n}_q \tag{5.13}$$

where T describes the electron kinetic energy and V the Coulombic electron-electron repulsion term. Note that we in principle can add local potentials of the form $U_p \hat{n}_p$, which means the total Hamiltonian could describe any periodic material chemistry. We will show later that this amounts to adding local Z rotations to the quantum simulation circuit, which is relatively trivial. The hard physics of material chemistry is therefore well-captured by the Jellium Hamiltonian and that makes it an extremely interesting problem to solve. In addition to chemistry, Jellium has been shown to be a good model for understanding high-temperature superconductivity.

While the ground state of jellium at high densities (metallic, rs 1 Bohr radii per particle) and at very low densities (insulating, rs 100 Bohr radii per particle) is well established, the precise phase diagram in the low to intermediate density regime is uncertain due to competing electronic and spin phases [163].

We can illustrate these regimes in a simple example. Let us diagonalize Hamiltonian Eq. 5.13 to find the groundstate energy of jellium as a function of the only variable, the electron density $\rho \propto 1/r_s$ with r_s a characteristic length scale.

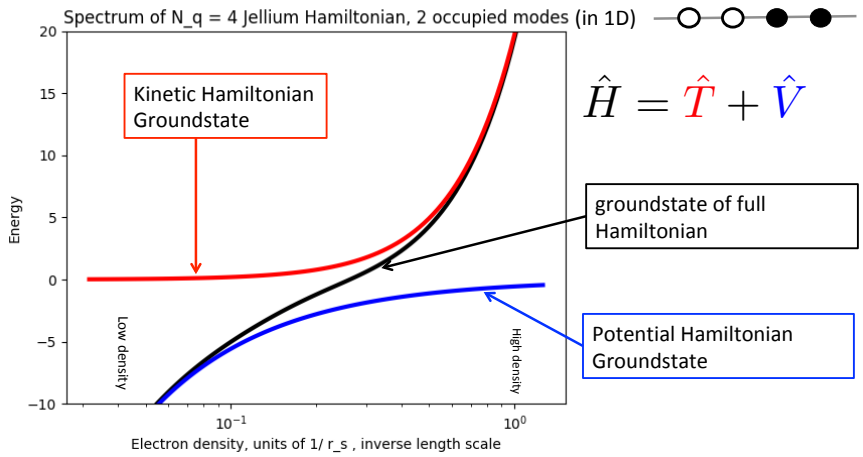

FIGURE 5.3: Ground state energy of a 1D Jellium Hamiltonian (black curve) with 4 plane waves at half-filling. Groundstate of only the kinetic part (red curve) and for only the electron repulsion part (blue) are shown for comparison.

In Figure 5.3 we find a clear confirmation of our previous statement: at low electron density, the complete Hamiltonian groundstate is clearly well approximated by the groundstate of just the potential operator. At high electron density, the complete Hamiltonian groundstate is closer approximated by the groundstate of the kinetic operator. In the intermediate density, $\rho \approx 0.03$, both the kinetic and potential contributions to the Hamiltonian appear to affect the groundstate physics.

Note that Hamiltonian Eq. 5.13 concerns at most two-body interactions. If we were to consider only a particular neighbouring pair of logical qubits, the Jordan-Wigner transformation [159] maps the Fermionic Hamiltonian directly to the Pauli-spin architecture of the qubits, meaning that we can intuitively replace annihilation operators $\hat{a}$ by Pauli spin operator σ_-, and number operator $\hat{n}$ by Pauli spin operator σ_Z.

In the Pauli basis $\{|00\rangle, |01\rangle, |10\rangle, |11\rangle\}$, we find that each unitary operation indicated by the black arrows in Figure 5.2 should be equal to

$$\texttt{FSIM} \equiv \begin{pmatrix} 1 & 0 & 0 & 0 \\ 0 & -i\sin[T_{pq}t] & \cos[T_{pq}t] & 0 \\ 0 & \cos[T_{pq}t] & -i\sin[T_{pq}t] & 0 \\ 0 & 0 & 0 & -e^{-iV_{pq}t} \end{pmatrix} \tag{5.14}$$

in order to implement the off-diagonal elements $T_{p,q}$ and $V_{p,q}$ in Hamiltonian Eq. 5.13. It should then be followed by local Z rotations for the diagonal terms $T_{p,p}$, all N of which can be applied in parallel after a full swap-network.

The above unitary can be constructed by applying a partial `SWAP` gate in conjunction with a partial `CPHASE` gate, both of which have some decompositions depending on the specific hardware architecture. Some hardware can implement these type of gates close to natively. It turns out a particularly promising architecture for this simulation would be the so-called 'g-mon' architecture. How does this gate emerge from a control pulse?

5.8.2 Gate synthesis: a g-mon case study

We have seen how quantum simulation on a gate-based quantum computer can be executed. We assumed access to a universal set of gates, capable of performing any operation on an input wavefunction, able to cover the entire Hilbert space given enough circuit depth and connectivity. How are these gates synthesized from hardware? In this section, we focus on a specific case of a superconducting qubit architecture with tunable gate coupling capability, to which we will refer as 'g-mon' architecture.

The Hamiltonian of a two-qubit chip looks like this:

$$\hat{\mathcal{H}}_{\text{2-qubit}}(t) = g(t)(\hat{a}_1^\dagger \hat{a}_2 + \hat{a}_2^\dagger \hat{a}_1) + \sum_1^2 \left[\frac{\eta_j}{2}\hat{n}_j(\hat{n}_j - 1) + \hat{a}_j^\dagger \hat{a}_j\right] \tag{5.15}$$

We now assume zero detuning and equal $\eta \equiv \eta_1 = \eta_2$. Assuming a cosine pulse profile for $g(t)$, i.e.

$$g(t) = \frac{g_0}{2}(1 - \cos[2\pi(t/T)]) \tag{5.16}$$

where T is the pulse time and g_0 is the maximum coupler bias strength.

The total evolution of the quantum system can be described by a (close-to-)unitary operation on the two qubits equal to

$$\hat{U} = e^{-i\int_0^\infty \hat{\mathcal{H}}(t)dt} \approx \begin{pmatrix} 1 & 0 & 0 & 0 \\ 0 & \cos[\theta] & -i\sin[\theta] & 0 \\ 0 & -i\sin[\theta] & \cos[\theta] & 0 \\ 0 & 0 & 0 & e^{i\phi} \end{pmatrix}, \tag{5.17}$$

where the matrix representation of the result is written in the basis $\{|00\rangle, |10\rangle, |01\rangle, |11\rangle\}$ with $\{0, 1\}$ indicating the occupation number of the qubit. We find a partial swap angle $\theta = g_0 T/2$ and an accumulated phase on the $|11\rangle$ state of $\phi \approx T g_0^2/\eta$. Clearly, the unitary performs a combination of two operations: a `SWAP`-gate operation between states $|10\rangle, |01\rangle$ and a `CPHASE` operation accumulating ϕ phase on the $|11\rangle$ state. The operation therefore synthesizes a gate with two angle-variables which the user can control.

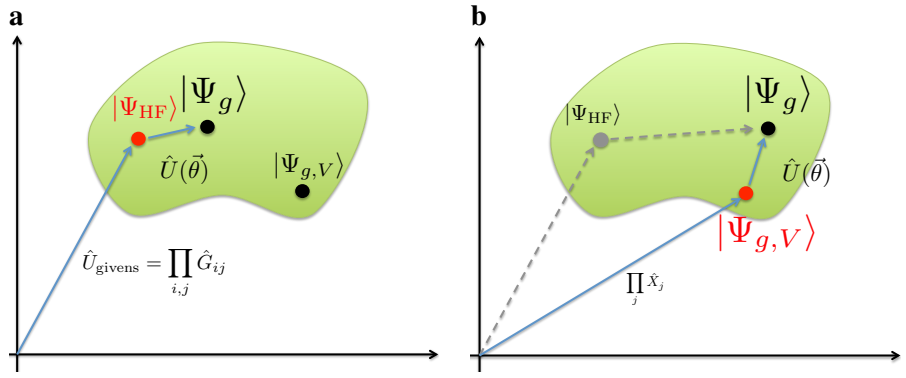

FIGURE 5.4: Schematic diagram illustrating the Hilbert space mapped to Euclidean space for ease of illustration. $|\Psi_g$ is the true groundstate of the chemistry problem Hamiltonian, while the green area around it illustrates a collection of states which are 'close' to the groundstate in terms of their electron configuration and/or energy. $|\Psi_{\mathrm{HF}}\rangle$ and $|\Psi_{g,V}\rangle$ are groundstates of the kinetic and repulsive potential operators in Hamiltonian Eq. 5.13, respectively. (a) Simulation strategy where $|\Psi_{\mathrm{HF}}\rangle$ is prepared and the quantum simulator applies a unitary $\hat{U}(\vec{\theta})$ to search for states close to it, hoping to finally reach the true groundstate $|\Psi_g\rangle$. (b) Similar simulation strategy but now $|\Psi_{g,V}\rangle$ is prepared using single bit-flips and subsequently, the quantum simulator applies a unitary $\hat{U}(\vec{\theta})$.

If we now choose these angles in a specific way, and combine the unitary operation with a full Fermionic swap operator,

$$\texttt{FSWAP} \equiv \begin{pmatrix} 1 & 0 & 0 & 0 \\ 0 & 0 & 1 & 0 \\ 0 & 1 & 0 & 0 \\ 0 & 0 & 0 & -1 \end{pmatrix}, \tag{5.18}$$

which swaps fermions with the correct Fermionic minus sign on the $|11\rangle$ state, the total operation defines a Fermionic simulation gate `FSIM`

$$\texttt{FSWAP} \cdot \hat{U}[\theta = T_{pq}t, \phi = -V_{pq}t] = \texttt{FSIM} \equiv \begin{pmatrix} 1 & 0 & 0 & 0 \\ 0 & -i\sin[T_{pq}t] & \cos[T_{pq}t] & 0 \\ 0 & \cos[T_{pq}t] & -i\sin[T_{pq}t] & 0 \\ 0 & 0 & 0 & -e^{-iV_{pq}t} \end{pmatrix} \tag{5.19}$$

which exactly performs the unitary operation necessary at every step in the swap-network of 5.7 for the simulation of a Jellium Hamiltonian in the dual form plane wave basis.

5.8.3 State preparation

One of the problems of solving for the groundstate of a quantum Hamiltonian using a minimization-search or annealing strategy is that the Hilbert space is *immense*. Searching this space one by one or even highly parallelized is not an effective strategy, and there are actually better ways to do it. It turns out that most states in the Hilbert space are not even close to the exact groundstate, in the sense that their energy is very different but also the configuration that these states describe do not obey physical laws such as particle conservation and the Pauli exclusion principle for fermions. Luckily, from classical computational chemistry methods,

there are states which can be numerically found in polynomial time on a classical computer, which have a close correspondence to the exact groundstate.

Why is it then, that we do not use the answers these methods give us? Are they not good enough? Yes, indeed they are not. Consider that the chemical reaction rate of many chemical processes can be predicted within an order of magnitude using the Eyring equation [164]

$$\text{Rate} \propto e^{-\Delta E/k_B T}. \tag{5.20}$$

where k_B is Boltzmann's constant, T is the temperature at which the reaction takes place, and ΔE is the energy barrier of the potential energy surface of a particular reaction.

Clearly, predicting the energy very accurately is required in order to predict the rate of a reaction, due to its exponential dependency on the potential difference. Often, a definition of 'chemical accuracy', amounting to 0.0016 Hartree, is used in order to quantify how accurate a chemistry simulation was.

To reach chemical accuracy, modern computational methods usually start with states close to the groundstate which are calculable in polynomial time and continue from there with a wide variety of methods. In quantum computing, it makes sense to make use of classically doable pre-computations and perform the hardest task, the capturing of strong electron correlations, on a quantum computer.

Let us consider an example applied to our Jellium simulation problem. In Figure 5.4a, we initialize the logical qubits in $|000...0\rangle$ and then apply the unitary circuit $\hat{U}_{\text{givens}}$. In [161], it is shown how a certain series of Givens rotations can decompose a transformation matrix defined by columns being the eigenvectors of the kinetic part of Jellium Hamiltonian Eq. 5.13. This means, the givens rotations can prepare an eigenstate of the kinetic part of the Jellium Hamiltonian, which is a good initial guess if that part contributes significantly to the total Hamiltonian. The diagonalization of Jellium Hamiltonian is never classically performed in the spin-basis; rather, it is the matrix of coefficients, $T_{p,q}$, with dimensions N instead of the humongous Hilbert dimension 2^N. [161] shows how such a circuit can prepare the groundstate in just depth $N/2 + 1$

Conversely, in Figure 5.4b, we again initialize the qubits in $|000...0\rangle$ but instead apply a specific combination of single-qubit bit-flips in order to prepare a groundstate of the repulsive part of Hamiltonian Eq. 5.13. This potential operator is diagonal with a convex structure to the diagonal function, meaning that a classical algorithm can efficiently find the lowest eigenvalue on the diagonal and associate it with a simple product state (meaning the eigenstate is also a basis state, for example $|01100010\rangle$). Hence, this state can be prepared using only single bitflips in depth 1.

5.8.4 Results 1: Trotterized Annealing

We here combine the ingredients from all previous sections, and simulate the groundstate energy of the jellium Hamiltonian Eq. 5.13 as a function of the electron density ρ. We assume 2-dimensional space with 2 basis functions per dimension for a total of 4 Fermionic plane wave modes. We assume half-filling, so two fermionic field modes are excited (can be viewed as 2 electrons in a 2D box of finite dimensions with periodic boundary conditions).

In our first attempt, we apply the Trotterized annealing strategy. The complete quantum circuit for simulating jellium chemistry with 4 qubits is schematically drawn in Figure 5.5.

First, all qubits are initialized in $|0\rangle$. Next, X-gates are applied to n_e qubits, where n_e is the desired number of electrons in the system. Then, an initial guess is prepared, in this case the Hartree-Fock state, by applying the appropriate preparation circuit (decomposed into a set of Givens rotations in this case). Next, a series of p Trotter steps are applied to the qubits, where for each Trotter step, the relevant Hamiltonian terms are applied using the fermionic

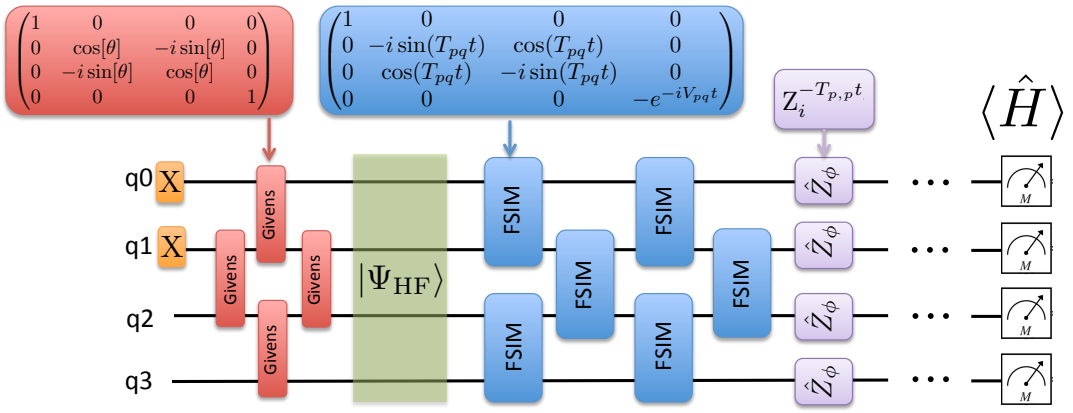

FIGURE 5.5: Schematic diagram of a quantum circuit for simulating Jellium on a 4-qubit quantum computer using the VQE paradigm.

simulation gate Eq. 5.19 and the local Z-gates. After the Trotter steps, the measurement phase consists of a Hamiltonian averaging procedure: the expectation value of the Hamiltonian for the output state is the final energy, and can be calculated as a sum over the expectation values of all operators inside. Because the operators need to be measured in different bases, they can not be measured simultaneously. Instead, the whole circuit is repeated many times until all N^2 terms in the Hamiltonian averaging process have been estimated. In our numerical simulation, this can be performed in a single run of the circuit as we have full access to the quantum wavefunction at the output port.

In the Trotterized annealing strategy, as detailed in Section 5.4.1, each trotter step applies the two parts of the jellium hamiltonian with different strengths. In Section 5.4 we argued that a linear schedule $s(t)$ would be most appropriate and in this case we approximate the linear ramp $s(t) = t/T$ with a 'stairs'-function, incrementing by T/p every trotter step.

In Figure 5.6a, we show the simulation results for jellium. We used the circuit in Figure 5.5 with 2 Trotter steps, for the annealing schedule initializing in the groundstate of the kinetic operator shown in black. For the green data points, we instead initialized the groundstate of the potential operator using single qubit rotations. The circuit output results are compared to the exact groundstate energies of the total Hamiltonian and the kinetic and potential sub-operators respectively.

We optimized the total annealing time T with a simple grid search. The necessity of this is clear from the following: slow enough annealing (large T) is guaranteed to end up in the groundstate of the final Hamiltonian according to the adiabatic theorem. But the Trotterization of the Hamiltonian evolution introduces Trotter errors which grow with the magnitude of the argument in exponential operators $e^{-i\mathcal{H}_A T/p/\hbar}$ (which means small T gives more accuracy). The tradeoff results in an optimal annealing time T depending on the details of the Hamiltonian and number of Trotter steps. The resulting optimal times T appears not be a smooth function of the density ρ for the case of the two Trotter steps applied here.

In Figure 5.6b, we show the relative error between the simulation results and the exact groundstate energies. For low electron density, the anneal starting from the groundstate of the potential operator performs several orders of magnitude better than the anneal starting from the kinetic operator. For high electron density, this is the opposite. The results can be explained by our argument in Section 5.8.1, that the density influences which Hamiltonian operator dominates. In the intermediate regime, both initialization methods have trouble annealing to the true groundstate. This could originate from instantaneous spectrum gap closing in the anneal, typical of a highly entangled final groundstate.

In the inset of Figure 5.6b, we illustrate the difference between the strategies portrayed

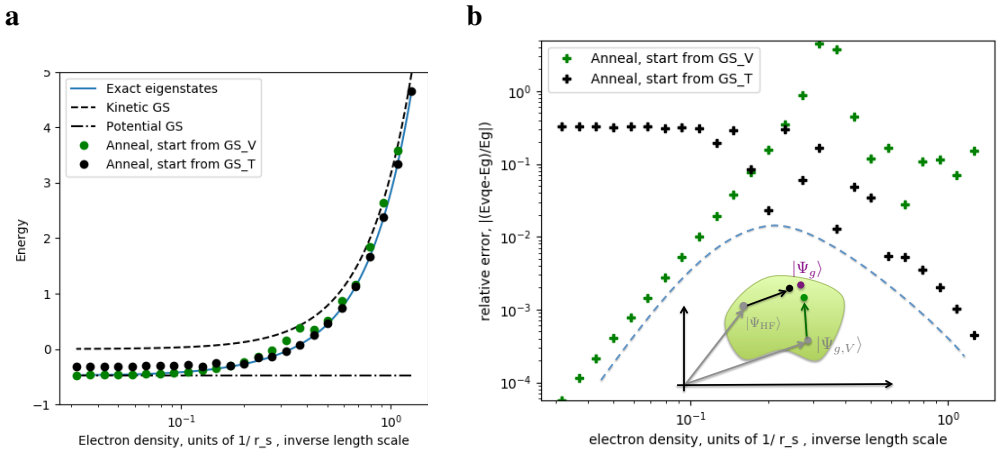

FIGURE 5.6: Jellium groundstate simulation for 2D jellium with 4 qubits assuming the availability of a universal set of gates. (a) Groundstate energy as a function of electron density. Full lines represent exact diagonalization results while discs represent Trotterized annealing simulation results. (b) Relative error between simulation results and exact diagonalization ground state energy. Blue dashed line indicates best results obtainable by choosing the annealing strategy based on the electron density regime. Inset: illustration of black and green strategies for the initial state preparation.

in the simulation results. The blue dashed line indicates the best strategy for Trotterized annealing: choose to start from the groundstate of the potential operator for the low density regime, and start from the groundstate of the kinetic operator for the high density regime. Still, in the intermediary regime the error is sometimes larger than 1%. This can likely be improved by increasing the number of Trotter steps which will increase the optimal total annealing time enabling better adiabaticity and thus resemblance to the true groundstate.

5.8.5 Results 2: VQE

For the Variational Quantum Eigensolver approach, we extend the strategy described in Section 5.4.1, the Trotterized annealing scheme. Indeed, the quantum circuit Figure 5.5 stays the same for this approach. For the initial angles in the VQE optimization loop, we choose the optimized annealing results from Section 5.8.4. Next, we perform feedback loop optimization on the circuit output Hamiltonian expectation value. The classical function optimizer we chose is the derivative-free heuristic Nelder-Mead downhill simplex method [165] over the multidimensional space defined by the Trotter angles. In this strategy, the circuit performs the following unitary operation:

$$\hat{U}_{\text{circuit}} = e^{\theta_{2,1} i \sum_{p,q} T_{p,q} \hat{a}_p^\dagger \hat{a}_q} e^{\theta_{2,2} i \sum_{p \neq q} V_{p,q} \hat{n}_p \hat{n}_q} e^{\theta_{1,1} i \sum_{p,q} T_{p,q} \hat{a}_p^\dagger \hat{a}_q} e^{\theta_{1,2} i \sum_{p \neq q} V_{p,q} \hat{n}_p \hat{n}_q} \quad (5.21)$$

where $\theta_{i,j}$ define the Trotter optimization angles. Each angle multiplies with the entire Hamiltonian sub-operators (kinetic and potential). This strategy therefore maintains the structure of the problem Hamiltonian in the circuit while allowing for (a)diabatic optimization.

In Figure 5.7, we show the simulation results for the VQE strategy detailed above. From the results, there is a clear improvement over just the annealing optimization strategy. In particular, regardless of whether the initial state was a groundstate of the kinetic or potential operator, the VQE converged to a fidelity to the exact groundstate over the entire range of the

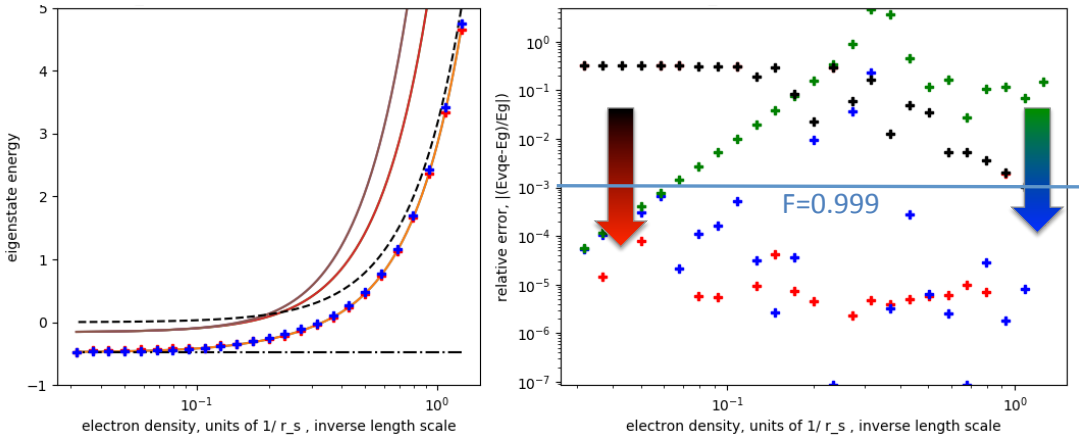

FIGURE 5.7: Simulation result of 2D jellium with 4-qubit architecture and Trotter depth $p = 2$, as a function of the electron density ρ. Left: Full lines depict the eigenvalue spectrum of the Hamiltonian. Blue data points started in the groundstate of the potential operator and Red data points started in the kinetic operator groundstate. Initial angles for the VQE were the end result of the annealing optimization strategy in Figure 5.6. Right: VQE relative errors of the data compared to the exact groundstate. The new VQE results are compared to the previous annealing optimzation results, and we compare to a fidelity of three 9's.

electron density we tested. This shows the flexibility of the optimization algorithm to find its way downhill in the energy landscape and its robustness against the specifics of initialization.

5.8.6 Results 3: Device-restricted angle recommendation

In Section 5.8.5 we showed promising results for simulating jellium on a low-depth quantum circuit. The classical optimization loop suggested angles for the circuit that would ultimately make the fidelity to the groundstate close to unity. In the simulation, we can select any angles for the `SWAP` and `CPHASE` gates we wish. However, we in this section would like to restrict ourselves to gate angles which can be performed by current hardware with high fidelity.

For specificity, we here consider the g-mon architecture and first analyze experimental data Figure 5.8 obtained by Andrew Dunsworth, graduate student at UCSB, USA (academic supervisor: John Martinis) on Google's quantum hardware in Santa Barbara, California. Figure 5.8 shows how there is a quadratic relationship between the amount of swap and the amount of phase accumulation on the $|11\rangle$ state for this 2-qubit gate pulse. We fitted the data to a quadratic curve satisfying approximately $\phi \approx 0.16\theta^2$

We next enforced this relationship on the classical optimization loop, allowing it to only pick sets of angles $\{\phi, \theta\}$ which satisfy this. Because the VQE optimization is then unlikely to lead to convergence to the exact groundstate, we now also allow each gate in Figure 5.5 to have their own pre-factor optimization angle, for a total of 32 angles over the 2 Trotter steps of the circuit. This in contrast to the previous VQE simulations in Section 5.8.5, where we enforced the Hamiltonian structure and had only 4 optimization angles in total.

Again, we compared performance between initializing the circuit in the groundstate of the kinetic or potential sub-operators of the total Hamiltonian. Depending on the electron density, these results would differ. In Figure 5.9 we plot the simulation results for the particular case of electron density $\rho = 4.3$ and also compare the convergence properties with the strategy detailed in Section 5.8.5. We notice up to an order of magnitude increase in the number of function calls, which can partially be explained by the increase in the dimensionality of the optimization problem due to the now free choice of each gate angle. For the other

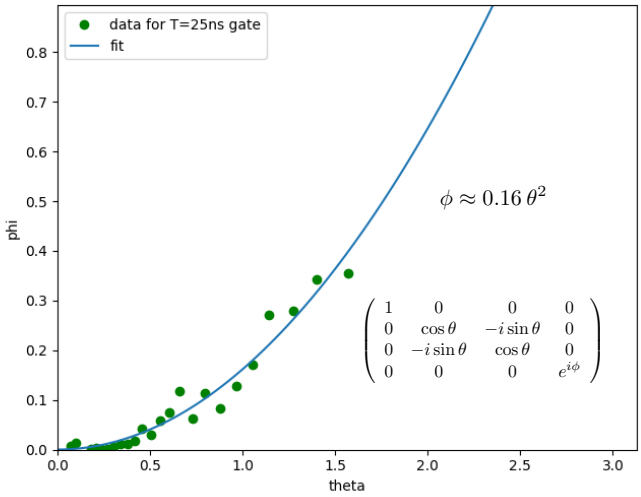

FIGURE 5.8: Relationship between SWAP-gate and CPHASE-gate angles for a coupler pulse with fixed length $T = 25$ ns and varying the coupler bias strength (maximum g_0 in Eq. 5.16). The data was obtained by Andrew Dunsworth, graduate student at UCSB.

part, we note that although we initialize the circuits faithfully to the groundstate of T or V respectively, the angle-restricted strategy employed here suffers from the inability to faithfully implement Trotterized annealing as an initial angle choice; rather, we initialized all angles at the midpoint of tested angles of the g-mon $T = 25$ ns dataset. This can be considered a rather random initialization, which also shows in the higher initial energy expectation value we find with this method.

5.9 Summary & Conclusions

In Section 5.8.5, we executed the VQE assuming no restrictions on the suggested gate angles. The number of angles in this strategy scales linearly in the number of Trotter steps and is independent of the number of basis functions chosen, meaning it is a scalable approach. In Section 5.8.6, we took into account the limitations of a particular hardware architecture, the g-mon platform, but allowed the classical optimizer to choose specific angles for each gate. This would scale with $\mathcal{O}(p \times N^2)$ where p are the number of Trotter steps and N is the number of qubits.

Both strategies have therefore their pros and cons; for future implementations of the VQE on g-mon architecture, a mixture of these strategies will be essential to achieve an efficient and accurate optimization result. It is paramount in the design phase to take into account the hardware limitations and structure, while simultaneously ensuring we make use of known strategies for more rapid convergence, such as clever initial states and initial angles.

In this project, we did not consider noise or imperfect gate fidelities. In practice, this will be one of the most important areas of research after optimizing the algorithm to the hardware. Recent developments in low-depth quantum circuit error mitigation show great promise in that regard but still lack widespread experimental implementation (see for instance Ref. [145] for a review of error-mitigation protocols).

Optimal use of classical pre-processing may help overcome most hurdles NISQ devices face in the near future, while hopefully exploiting the power of quantum hardware available today in order to achieve higher accuracy at larger system sizes than possible on current classical computational chemistry systems. Then, one can finally speak of *practical quantum supremacy* for quantum chemistry applications.

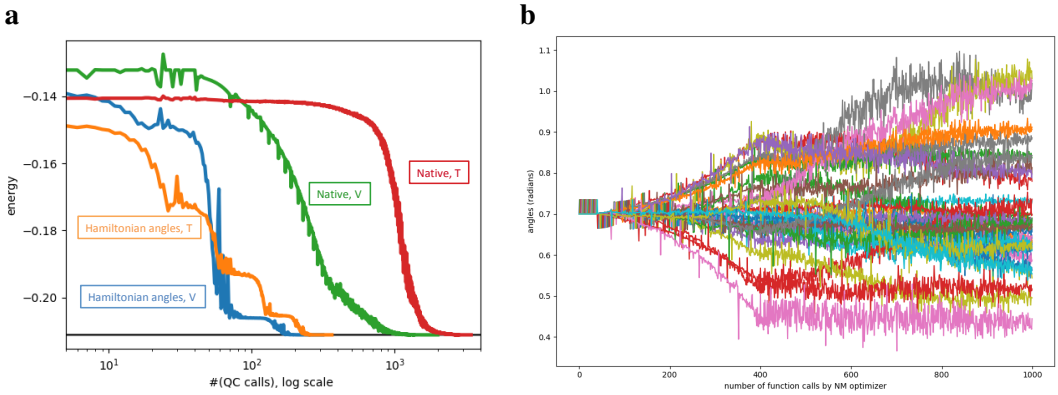

FIGURE 5.9: VQE simulation of 2D jellium on a 4-qubit g-mon architecture, for electron density $\rho = 4.3$. (a) VQE convergence comparison between free-angle VQE method starting in the groundstate of T and V, orange and blue full lines respectively, and VQE restricted to the theta-phi relationship in Figure 5.8. (b) Convergence of the angles which the classical optimizer algorithm suggests at every iteration number. Every FSIM-gate has a unique angle associated with it, in this case for 4 qubits there are $2 \times 4^2 = 32$ angles

Chapter 6

Summary & Outlook

In Chapter 2, we presented a photon scattering framework and applied the formalism to several example toy problems. We showed how the framework encapsulates most of the important assumptions and approximations one makes when performing quantum optics scattering calculations. In this way, we are able to focus on the physics rather than repeating the same mathematics over and over again. In just a few lines of derivations, we can analyze quite complex multi-emitter scattering situations and/or allow interactions between different excited or ground states within an emitter.

In the future, it may be possible to have a user-friendly Graphical User Interface (GUI) for either analytical or numerical calculations of the form presented here. In fact, the Author has taken steps to begin this process and the result will be available online, open-source and available to the quantum optics community and beyond. Ideally, the user would be able to add emitters, inter-and intra-emitter couplings, detunings, energy levels, decay channels and more. In this way, the user would be able to predict single-photon scattering results in a rapid design process. As a further augmentation, such a software would include a machine-learning based algorithm which aids in the design of a device with certain desired properties. Although the computational scaling is often more than manageable, the bottleneck is computing the inverse of a (potentially large) excited state Hamiltonian. For a large number of emitters or energy levels, this would entail a significant computational cost and reduce the number of design iterations one could process. This could be partially solved by applying the latest efficient Hamiltonian inversion algorithms.

Alongside the rapid technological developments in single-photon sources, waveguide photonics, and quantum optical hardware, theoretical scattering frameworks like the one we discussed will be most helpful in designing new experiments. The future of photonics is bright indeed.

In Chapter 3, we presented a novel quantum transducer concept based on semiconductor quantum dots (QDs) strongly coupled to a photonic waveguide. The device is capable of entanglement generation between a flying qubit (an optical photon) and a stationary qubit (a coherent two-level system). We calculated the success probability of photon-TLS entanglement and showed how the critical quantity affecting the performance is the TLS-QD coupling rate over the TLS transition frequency. For a single-QD system, we can still obtain a practical success probability. Exploiting photon-mediated interactions resulting in super/subradiant physics in a waveguide, we significantly enhance the coupling to the TLS by extending the effective lifetime of the matter excitation. Good result are expected for state-of-the-art photonic components available today. We numerically simulate the expected electrical coupling strength and the potential adverse effects of mode overlap with the system to be used for the transduction of a signal.

In Chapter 4, we proposed an alternative quantum transducer design based on a single QD coupled to a photonic cavity. We calculate details about the entanglement success probability and fidelity depending on dephasing effects and device imbalances on each arm of the interferometer setup. These results are an essential design guideline for a near-term experiment

for a quantum transducer device, regardless of the specific implementation. Whether the device is based on quantum dots in waveguides or cavity QED or something else again, the calculations we performed show how to deal with imbalances and how important dephasing effects are for the fidelity of entanglement.

Both these transducer proposal are promising candidates for the first experimental implementation of a quantum repeater or network node based on the superconducting qubit hardware platform. The ability to transfer quantum information optically over long distances is vital to the construction of a future quantum internet, one of the most ambitious applications of quantum information processing devices and protocols.

In Chapter 5, we briefly introduced the concept of quantum hardware simulation of quantum chemistry problems. More specifically, we step-by-step addressed all the ingredients necessary for a theoretical proposal for simulating a chemistry problem on specific quantum architectures. Specifically, we chose to simulate a material chemistry problem, where we are interested in the groundstate of a uniform electron gas coined 'jellium'. Being a system with periodic boundary conditions, we chose a plane-wave basis for the Hamiltonian. Specifically, there is a dual of the plane wave basis [158] which has significantly less terms and is isospectral to the regular plane wave basis. In the dual plane wave basis, the electron-electron repulsion operator is diagonal and the Hamiltonian contains at most two-body terms. This does two things: it drastically reduces the number of terms required in the Hamiltonian averaging process required for extracting an expectation value for the groundstate. It also enables a single Trotter step to be performed with gate depth N, where N is the number of qubits in a linear array. We initialize a good initial guess state on a quantum device, preparing the groundstate of part of the total Hamiltonian in order to start with an educated starting point. From there, we compared two related simulation algorithms: digitized annealing and the Variational Quantum Eigensolver. We show how the VQE can improve the final groundstate fidelity to the exact groundstate by orders of magnitude compared to a linear Trotterized annealing ramp, given limited quantum resources (a total gate depth of less than $3N$.

The future possibilities of quantum computing are far from endless. Quantum computing will very likely be used in parallel with classical computing and we here discussed an example of the symbiotic relation between the two. There are some specific tasks for which we expect quantum computing to be exceptionally efficient and good. Attempting to simulate such non-trivial quantum groundstates on a classical computer makes as much sense as processing classical 'big data' on a quantum computer: it does not.

To end on a positive note, there are a lot of indications and several supporting proofs that one of the most promising near-term applications of quantum computing is in simulating inherently quantum systems. It is hard to overstate the importance and impact of quantum chemistry simulation on society and daily life so far, using classical computing alone. From these clues, even though there are many challenges ahead, we expect a promising future for quantum information processing on quantum hardware.

Bibliography

[1] V. E. Elfving, S. Das, and A. S. Sørensen, "Enhancing quantum transduction via long-range waveguide mediated interactions between quantum emitters", ArXiv e-prints (2018).

[2] S. Das, V. E. Elfving, F. Reiter, and A. S. Sørensen, "Photon scattering from a system of multilevel quantum emitters. ii. application to emitters coupled to a one-dimensional waveguide", Phys. Rev. A **97**, 043838 (2018).

[3] S. Das, V. E. Elfving, S. Faez, and A. S. Sørensen, "Interfacing superconducting qubits and single optical photons using molecules in waveguides", Phys. Rev. Lett. **118**, 140501 (2017).

[4] S. Das, V. E. Elfving, F. Reiter, and A. S. Sørensen, "Photon scattering from a system of multilevel quantum emitters. i. formalism", Phys. Rev. A **97**, 043837 (2018).

[5] M. Hazewinkel, *Encyclopaedia of mathematics, supplement iii*, edited by M. Hazewinkel (Springer Netherlands, 2002).

[6] P. Zoller, T. Beth, D. Binosi, R. Blatt, H. Briegel, D. Bruss, T. Calarco, J. I. Cirac, D. Deutsch, J. Eisert, A. Ekert, C. Fabre, N. Gisin, P. Grangiere, M. Grassl, S. Haroche, A. Imamoglu, A. Karlson, J. Kempe, L. Kouwenhoven, S. Kröll, G. Leuchs, M. Lewenstein, D. Loss, N. Lütkenhaus, S. Massar, J. E. Mooij, M. B. Plenio, E. Polzik, S. Popescu, G. Rempe, A. Sergienko, D. Suter, J. Twamley, G. Wendin, R. Werner, A. Winter, J. Wrachtrup, and A. Zeilinger, "Quantum information processing and communication", The European Physical Journal D - Atomic, Molecular, Optical and Plasma Physics **36**, 203–228 (2005).

[7] M. A. Nielsen and I. L. Chuang, *Quantum computation and quantum information: 10th anniversary edition*, edited by C. U. Press, 10th (Cambridge University Press, New York, NY, USA, 2011).

[8] D. S. Abrams and S. Lloyd, "Simulation of many-body fermi systems on a universal quantum computer", Phys. Rev. Lett. **79**, 2586–2589 (1997).

[9] B. M. Boghosian and W. Taylor, "Simulating quantum mechanics on a quantum computer", Physica D: Nonlinear Phenomena **120**, Proceedings of the Fourth Workshop on Physics and Consumption, 30 –42 (1998).

[10] A. T. Sornborger and E. D. Stewart, "Higher-order methods for simulations on quantum computers", Phys. Rev. A **60**, 1956–1965 (1999).

[11] S. Wiesner, "Simulations of Many-Body Quantum Systems by a Quantum Computer", eprint arXiv:quant-ph/9603028 (1996).

[12] C. Zalka, "Grover's quantum searching algorithm is optimal", Phys. Rev. A **60**, 2746–2751 (1999).

[13] I. I. Manin, *Vychislimoe i nevychislimoe / iu.i. manin*, Russian, edited by. M. "Sov. radio ("Sov. radio," Moskva, 1980), 127 p. :

[14] R. P. Feynman, "Simulating physics with computers", International Journal of Theoretical Physics **21**, 467–488 (1982).

[15]D. P. DiVincenzo, "The physical implementation of quantum computation", Fortschritte der Physik **48**, 771–783 (2000).

[16]H. J. Kimble, "The quantum internet", Nature **453**, 1023 EP – (2008).

[17]M. K. Tey, Z. Chen, S. A. Aljunid, B. Chng, F. Huber, G. Maslennikov, and C. Kurtsiefer, "Strong interaction between light and a single trapped atom without the need for a cavity", Nature Physics **4**, 924 EP – (2008).

[18]J. L. O'Brien, A. Furusawa, and J. Vučković, "Photonic quantum technologies", Nature Photonics **3**, 687 EP – (2009).

[19]D. E. Chang, A. S. Sørensen, E. A. Demler, and M. D. Lukin, "A single-photon transistor using nanoscale surface plasmons", Nature Physics **3**, 807 EP – (2007).

[20]J. Hwang, M. Pototschnig, R. Lettow, G. Zumofen, A. Renn, S. Götzinger, and V. Sandoghdar, "A single-molecule optical transistor", Nature **460**, 76 EP – (2009).

[21]J. M. Raimond, M. Brune, and S. Haroche, "Manipulating quantum entanglement with atoms and photons in a cavity", Rev. Mod. Phys. **73**, 565–582 (2001).

[22]A. Reiserer and G. Rempe, "Cavity-based quantum networks with single atoms and optical photons", Rev. Mod. Phys. **87**, 1379–1418 (2015).

[23]C. Kurtsiefer, S. Mayer, P. Zarda, and H. Weinfurter, "Stable solid-state source of single photons", Phys. Rev. Lett. **85**, 290–293 (2000).

[24]R. Brouri, A. Beveratos, J.-P. Poizat, and P. Grangier, "Photon antibunching in the fluorescence of individual color centers in diamond", Opt. Lett. **25**, 1294–1296 (2000).

[25]Z. Yuan, B. E. Kardynal, R. M. Stevenson, A. J. Shields, C. J. Lobo, K. Cooper, N. S. Beattie, D. A. Ritchie, and M. Pepper, "Electrically driven single-photon source", Science **295**, 102–105 (2002).

[26]A. J. Shields, "Semiconductor quantum light sources", Nature Photonics **1**, 215 EP – (2007).

[27]J.-T. Shen and S. Fan, "Strongly correlated two-photon transport in a one-dimensional waveguide coupled to a two-level system", Phys. Rev. Lett. **98**, 153003 (2007).

[28]J. Majer, J. M. Chow, J. M. Gambetta, J. Koch, B. R. Johnson, J. A. Schreier, L. Frunzio, D. I. Schuster, A. A. Houck, A. Wallraff, A. Blais, M. H. Devoret, S. M. Girvin, and R. J. Schoelkopf, "Coupling superconducting qubits via a cavity bus", Nature **449**, 443 EP – (2007).

[29]K.-M. C. Fu, C. Santori, P. E. Barclay, I. Aharonovich, S. Prawer, N. Meyer, A. M. Holm, and R. G. Beausoleil, "Coupling of nitrogen-vacancy centers in diamond to a gap waveguide", Applied Physics Letters **93**, 234107 (2008).

[30], J. Twamley, and G. J. Milburn, "Giant kerr nonlinearities in circuit quantum electrodynamics", Phys. Rev. Lett. **103**, 150503 (2009).

[31]T. Shi and C. P. Sun, "Lehmann-symanzik-zimmermann reduction approach to multiphoton scattering in coupled-resonator arrays", Phys. Rev. B **79**, 205111 (2009).

[32]T. M. Babinec, B. J. M. Hausmann, M. Khan, Y. Zhang, J. R. Maze, P. R. Hemmer, and M. Lončar, "A diamond nanowire single-photon source", Nature Nanotechnology **5**, 195 EP – (2010).

[33]T. C. H. Liew and V. Savona, "Single photons from coupled quantum modes", Phys. Rev. Lett. **104**, 183601 (2010).

[34]T. Shi, S. Fan, and C. P. Sun, "Two-photon transport in a waveguide coupled to a cavity in a two-level system", Phys. Rev. A **84**, 063803 (2011).

[35]M. Bamba, I. Carusotto, and C. Ciuti, "Origin of strong photon antibunching in weakly nonlinear photonic molecules", Phys. Rev. A **83**, 021802 (2011).

[36]A. Majumdar, M. Bajcsy, A. Rundquist, "Loss-enabled sub-poissonian light generation in a bimodal nanocavity", Phys. Rev. Lett. **108**, 183601 (2012).

[37]T. Peyronel, O. Firstenberg, Q.-Y. Liang, S. Hofferberth, A. V. Gorshkov, T. Pohl, M. D. Lukin, and V. Vuletić, "Quantum nonlinear optics with single photons enabled by strongly interacting atoms", Nature **488**, 57 EP – (2012).

[38]A. F. van Loo, A. Fedorov, K. Lalumière, B. C. Sanders, A. Blais, and A. Wallraff, "Photon-mediated interactions between distant artificial atoms", Science **342**, 1494–1496 (2013).

[39]T. Shi and S. Fan, "Two-photon transport through a waveguide coupling to a whispering-gallery resonator containing an atom and photon-blockade effect", Phys. Rev. A **87**, 063818 (2013).

[40]S. Baur, D. Tiarks, G. Rempe, and S. Dürr, "Single-photon switch based on rydberg blockade", Phys. Rev. Lett. **112**, 073901 (2014).

[41]A. Reiserer, N. Kalb, G. Rempe, and S. Ritter, "A quantum gate between a flying optical photon and a single trapped atom", Nature **508**, 237 EP – (2014).

[42]V. Giesz, N. Somaschi, G. Hornecker, T. Grange, B. Reznychenko, L. De Santis, J. Demory, C. Gomez, I. Sagnes, A. Lemaître, O. Krebs, N. D. Lanzillotti-Kimura, L. Lanco, A. Auffeves, and P. Senellart, "Coherent manipulation of a solid-state artificial atom with few photons", Nature Communications **7**, 11986 EP – (2016).

[43]A. Goban, C. L. Hung, S. P. Yu, J. D. Hood, J. A. Muniz, J. H. Lee, M. J. Martin, A. C. McClung, K. S. Choi, D. E. Chang, O. Painter, and H. J. Kimble, "Atom–light interactions in photonic crystals", Nature Communications **5**, 3808 EP – (2014).

[44]P. Lodahl, S. Mahmoodian, and S. Stobbe, "Interfacing single photons and single quantum dots with photonic nanostructures", Rev. Mod. Phys. **87**, 347–400 (2015).

[45]K. Inomata, Z. Lin, K. Koshino, W. D. Oliver, J.-S. Tsai, T. Yamamoto, and Y. Nakamura, "Single microwave-photon detector using an artificial lambda-type three-level system", Nature Communications **7**, 12303 EP – (2016).

[46]P. Solano, J. A. Grover, J. E. Hoffman, S. Ravets, F. K. Fatemi, L. A. Orozco, and S. L. Rolston, *Chapter seven - optical nanofibers: a new platform for quantum optics*, edited by E. Arimondo, C. C. Lin, and S. F. Yelin, Vol. 66, Advances In Atomic, Molecular, and Optical Physics (Academic Press, 2017), pp. 439 –505.

[47]T. G. Tiecke, J. D. Thompson, N. P. de Leon, L. R. Liu, V. Vuletić, and M. D. Lukin, "Nanophotonic quantum phase switch with a single atom", Nature **508**, 241 EP – (2014).

[48]I. Shomroni, S. Rosenblum, Y. Lovsky, O. Bechler, G. Guendelman, and B. Dayan, "All-optical routing of single photons by a one-atom switch controlled by a single photon", Science **345**, 903–906 (2014).

[49]N. V. Corzo, B. Gouraud, A. Chandra, A. Goban, A. S. Sheremet, D. V. Kupriyanov, and J. Laurat, "Large bragg reflection from one-dimensional chains of trapped atoms near a nanoscale waveguide", Phys. Rev. Lett. **117**, 133603 (2016).

[50]H. L. Sørensen, J.-B. Béguin, K. W. Kluge, I. Iakoupov, A. S. Sørensen, J. H. Müller, E. S. Polzik, and J. Appel, "Coherent backscattering of light off one-dimensional atomic strings", Phys. Rev. Lett. **117**, 133604 (2016).

[51]R. Mitsch, C. Sayrin, B. Albrecht, P. Schneeweiss, and A. Rauschenbeutel, "Quantum state-controlled directional spontaneous emission of photons into a nanophotonic waveguide", Nature Communications **5**, 5713 EP – (2014).

[52]C. Sayrin, C. Junge, R. Mitsch, B. Albrecht, D. O'Shea, P. Schneeweiss, J. Volz, and A. Rauschenbeutel, "Nanophotonic optical isolator controlled by the internal state of cold atoms", Phys. Rev. X **5**, 041036 (2015).

[53]A. Javadi, I. Söllner, M. Arcari, S. L. Hansen, L. Midolo, S. Mahmoodian, G Kiršanskė, T. Pregnolato, E. H. Lee, J. D. Song, S. Stobbe, and P. Lodahl, "Single-photon non-linear optics with a quantum dot in a waveguide", Nature Communications **6**, 8655 EP – (2015).

[54]A. Sipahigil, R. E. Evans, D. D. Sukachev, M. J. Burek, J. Borregaard, M. K. Bhaskar, C. T. Nguyen, J. L. Pacheco, H. A. Atikian, C. Meuwly, R. M. Camacho, F. Jelezko, E. Bielejec, H. Park, M. Lončar, and M. D. Lukin, "An integrated diamond nanophotonics platform for quantum-optical networks", Science **354**, 847–850 (2016).

[55]P. Solano, P. Barberis-Blostein, F. K. Fatemi, L. A. Orozco, and S. L. Rolston, "Super-radiance reveals infinite-range dipole interactions through a nanofiber", Nature Communications **8**, 1857 (2017).

[56]J.-T. Shen and S. Fan, "Coherent single photon transport in a one-dimensional waveguide coupled with superconducting quantum bits", Phys. Rev. Lett. **95**, 213001 (2005).

[57]V. I. Yudson and P. Reineker, "Multiphoton scattering in a one-dimensional waveguide with resonant atoms", Phys. Rev. A **78**, 052713 (2008).

[58]D Witthaut and A. S. Sørensen, "Photon scattering by a three-level emitter in a one-dimensional waveguide", New Journal of Physics **12**, 043052 (2010).

[59]H. Zheng, D. J. Gauthier, and H. U. Baranger, "Waveguide qed: many-body bound-state effects in coherent and fock-state scattering from a two-level system", Phys. Rev. A **82**, 063816 (2010).

[60]J.-Q. Liao and C. K. Law, "Correlated two-photon transport in a one-dimensional waveguide side-coupled to a nonlinear cavity", Phys. Rev. A **82**, 053836 (2010).

[61]I. H. Deutsch, R. J. C. Spreeuw, S. L. Rolston, and W. D. Phillips, "Photonic band gaps in optical lattices", Phys. Rev. A **52**, 1394–1410 (1995).

[62]D. E. Chang, L Jiang, A. V. Gorshkov, and H. J. Kimble, "Cavity qed with atomic mirrors", New Journal of Physics **14**, 063003 (2012).

[63]S. Fan, and J.-T. Shen, "Input-output formalism for few-photon transport in one-dimensional nanophotonic waveguides coupled to a qubit", Phys. Rev. A **82**, 063821 (2010).

[64]K. Lalumière, B. C. Sanders, A. F. van Loo, A. Fedorov, A. Wallraff, and A. Blais, "Input-output theory for waveguide qed with an ensemble of inhomogeneous atoms", Phys. Rev. A **88**, 043806 (2013).

[65]H. Zheng, D. J. Gauthier, and H. U. Baranger, "Cavity-free photon blockade induced by many-body bound states", Phys. Rev. Lett. **107**, 223601 (2011).

[66]D. Roy, "Two-photon scattering by a driven three-level emitter in a one-dimensional waveguide and electromagnetically induced transparency", Phys. Rev. Lett. **106**, 053601 (2011).

[67]M. Laakso and M. Pletyukhov, "Scattering of two photons from two distant qubits: exact solution", Phys. Rev. Lett. **113**, 183601 (2014).

[68]M. V. Gustafsson, T. Aref, A. F. Kockum, M. K. Ekström, G. Johansson, and P. Delsing, "Propagating phonons coupled to an artificial atom", Science **346**, 207–211 (2014).

[69]A. Roulet and V. Scarani, "Solving the scattering of n photons on a two-level atom without computation", New Journal of Physics **18**, 093035 (2016).

[70] V. A. Pivovarov, A. S. Sheremet, L. V. Gerasimov, V. M. Porozova, N. V. Corzo, J. Laurat, and D. V. Kupriyanov, "Light scattering from an atomic array trapped near a one-dimensional nanoscale waveguide: a microscopic approach", Phys. Rev. A **97**, 023827 (2018).

[71] A. F. Kockum, G. Johansson, and F. Nori, "Decoherence-free interaction between giant atoms in waveguide quantum electrodynamics", Phys. Rev. Lett. **120**, 140404 (2018).

[72] T. Caneva, M. T. Manzoni, T. Shi, J. S. Douglas, J. I. Cirac, and D. E. Chang, "Quantum dynamics of propagating photons with strong interactions: a generalized input-output formalism", New Journal of Physics **17**, 113001 (2015).

[73] T. Shi, D. E. Chang, and J. I. Cirac, "Multiphoton-scattering theory and generalized master equations", Phys. Rev. A **92**, 053834 (2015).

[74] F. Reiter and A. S. Sørensen, "Effective operator formalism for open quantum systems", Phys. Rev. A **85**, 032111 (2012).

[75] J. Dalibard, Y. Castin, and K. Mølmer, "Wave-function approach to dissipative processes in quantum optics", Phys. Rev. Lett. **68**, 580–583 (1992).

[76] P. Lodahl, S. Mahmoodian, S. Stobbe, A. Rauschenbeutel, P. Schneeweiss, J. Volz, H. Pichler, and P. Zoller, "Chiral quantum optics", Nature **541**, 473 EP – (2017).

[77] A. Frisk Kockum, P. Delsing, and G. Johansson, "Designing frequency-dependent relaxation rates and lamb shifts for a giant artificial atom", Phys. Rev. A **90**, 013837 (2014).

[78] P. Solano, J. A. Grover, Y. Xu, P. Barberis-Blostein, J. N. Munday, L. A. Orozco, W. D. Phillips, and S. L. Rolston, "Alignment-dependent decay rate of an atomic dipole near an optical nanofiber", ArXiv e-prints (2017).

[79] L. Novotny and B. Hecht, *Principles of nano-optics* (Cambridge University Press, 2006).

[80] F. Le Kien, S. D. Gupta, K. P. Nayak, and K. Hakuta, "Nanofiber-mediated radiative transfer between two distant atoms", Phys. Rev. A **72**, 063815 (2005).

[81] J. T. Shen and S. Fan, "Coherent photon transport from spontaneous emission in one-dimensional waveguides", Opt. Lett. **30**, 2001–2003 (2005).

[82] L. Zhou, Z. R. Gong, Y.-x. Liu, C. P. Sun, and F. Nori, "Controllable scattering of a single photon inside a one-dimensional resonator waveguide", Phys. Rev. Lett. **101**, 100501 (2008).

[83] J. Kim, O. Benson, H. Kan, and Y. Yamamoto, "A single-photon turnstile device", Nature **397**, 500 EP – (1999).

[84] B. Dayan, A. S. Parkins, T. Aoki, E. P. Ostby, K. J. Vahala, and H. J. Kimble, "A photon turnstile dynamically regulated by one atom", Science **319**, 1062–1065 (2008).

[85] M. T. Manzoni, F. Reiter, J. M. Taylor, and A. S. Sørensen, "Single-photon transistor based on superconducting systems", Phys. Rev. B **89**, 180502 (2014).

[86] O. Kyriienko and A. S. Sørensen, "Continuous-wave single-photon transistor based on a superconducting circuit", Phys. Rev. Lett. **117**, 140503 (2016).

[87] A. Gonzalez-Tudela, D. Martin-Cano, E. Moreno, L. Martin-Moreno, C. Tejedor, and F. J. Garcia-Vidal, "Entanglement of two qubits mediated by one-dimensional plasmonic waveguides", Phys. Rev. Lett. **106**, 020501 (2011).

[88] X. Wu, J.-D. Bancal, M. McKague, and V. Scarani, "Device-independent parallel self-testing of two singlets", Phys. Rev. A **93**, 062121 (2016).

[89] R. H. Dicke, "Coherence in spontaneous radiation processes", Phys. Rev. **93**, 99–110 (1954).

[90]M. O. Scully, E. S. Fry, C. H. R. Ooi, and K. Wódkiewicz, "Directed spontaneous emission from an extended ensemble of n atoms: timing is everything", Phys. Rev. Lett. **96**, 010501 (2006).

[91]S. Das, G. S. Agarwal, and M. O. Scully, "Quantum interferences in cooperative dicke emission from spatial variation of the laser phase", Phys. Rev. Lett. **101**, 153601 (2008).

[92]E. A. Sete and S. Das, "Quantum interference in timed dicke basis and its effect on bipartite entanglement", Phys. Rev. A **83**, 042301 (2011).

[93]M.-T. Cheng, J. Xu, and G. S. Agarwal, "Waveguide transport mediated by strong coupling with atoms", Phys. Rev. A **95**, 053807 (2017).

[94]H.-J. Briegel, W. Dür, J. I. Cirac, and P. Zoller, "Quantum repeaters: the role of imperfect local operations in quantum communication", Phys. Rev. Lett. **81**, 5932–5935 (1998).

[95]S. Pirandola, J. Eisert, C. Weedbrook, A. Furusawa, and S. L. Braunstein, "Advances in quantum teleportation", Nature Photonics **9**, 641 EP – (2015).

[96]H.-K. Lo, M. Curty, and K. Tamaki, "Secure quantum key distribution", Nature Photonics **8**, 595 EP – (2014).

[97]E. Togan, Y. Chu, A. S. Trifonov, L. Jiang, J. Maze, L. Childress, M. V. G. Dutt, A. S. Sørensen, P. R. Hemmer, A. S. Zibrov, and M. D. Lukin, "Quantum entanglement between an optical photon and a solid-state spin qubit", Nature **466**, 730 EP – (2010).

[98]L. K. Grover, "Quantum Telecomputation", eprint arXiv:quant-ph/9704012 (1997).

[99]T. Pellizzari, "Quantum networking with optical fibres", Phys. Rev. Lett. **79**, 5242–5245 (1997).

[100]K. Zhang, F. Bariani, Y. Dong, W. Zhang, and P. Meystre, "Proposal for an optomechanical microwave sensor at the subphoton level", Phys. Rev. Lett. **114**, 113601 (2015).

[101]J. A. Sedlacek, A. Schwettmann, H. Kübler, R. Löw, T. Pfau, and J. P. Shaffer, "Microwave electrometry with rydberg atoms in a vapour cell using bright atomic resonances", Nature Physics **8**, 819 EP – (2012).

[102]V. Giovannetti, S. Lloyd, and L. Maccone, "Advances in quantum metrology", Nature Photonics **5**, 222 EP – (2011).

[103]K. Stannigel, P. Rabl, A. S. Sørensen, P. Zoller, and M. D. Lukin, "Optomechanical transducers for long-distance quantum communication", Phys. Rev. Lett. **105**, 220501 (2010).

[104]S. Barzanjeh, M. Abdi, G. J. Milburn, P. Tombesi, and D. Vitali, "Reversible optical-to-microwave quantum interface", Phys. Rev. Lett. **109**, 130503 (2012).

[105]J. Bochmann, A. Vainsencher, D. D. Awschalom, and A. N. Cleland, "Nanomechanical coupling between microwave and optical photons", Nature Physics **9**, 712 EP – (2013).

[106]R. W. Andrews, R. W. Peterson, T. P. Purdy, K. Cicak, R. W. Simmonds, C. A. Regal, and K. W. Lehnert, "Bidirectional and efficient conversion between microwave and optical light", Nature Physics **10**, 321 EP – (2014).

[107]T. Bagci, A. Simonsen, S. Schmid, L. G. Villanueva, E. Zeuthen, J. Appel, J. M. Taylor, A. Sørensen, K. Usami, A. Schliesser, and E. S. Polzik, "Optical detection of radio waves through a nanomechanical transducer", Nature **507**, 81 EP – (2014).

[108]A. Rueda, F. Sedlmeir, M. C. Collodo, U. Vogl, B. Stiller, G. Schunk, D. V. Strekalov, C. Marquardt, J. M. Fink, O. Painter, G. Leuchs, and H. G. L. Schwefel, "Efficient microwave to optical photon conversion: an electro-optical realization", Optica **3**, 597–604 (2016).

[109]M. Tsang, "Cavity quantum electro-optics. ii. input-output relations between traveling optical and microwave fields", Phys. Rev. A **84**, 043845 (2011).

[110]M. Hafezi, Z. Kim, S. L. Rolston, L. A. Orozco, B. L. Lev, and J. M. Taylor, "Atomic interface between microwave and optical photons", Phys. Rev. A **85**, 020302 (2012).

[111]L. A. Williamson, Y.-H. Chen, and J. J. Longdell, "Magneto-optic modulator with unit quantum efficiency", Phys. Rev. Lett. **113**, 203601 (2014).

[112]A. S. Sørensen, C. H. van der Wal, L. I. Childress, and M. D. Lukin, "Capacitive coupling of atomic systems to mesoscopic conductors", Phys. Rev. Lett. **92**, 063601 (2004).

[113]D. Marcos, M. Wubs, J. M. Taylor, R. Aguado, M. D. Lukin, and A. S. Sørensen, "Coupling nitrogen-vacancy centers in diamond to superconducting flux qubits", Phys. Rev. Lett. **105**, 210501 (2010).

[114]A. Sipahigil, M. L. Goldman, E. Togan, Y. Chu, M. Markham, D. J. Twitchen, A. S. Zibrov, A. Kubanek, and M. D. Lukin, "Quantum interference of single photons from remote nitrogen-vacancy centers in diamond", Phys. Rev. Lett. **108**, 143601 (2012).

[115]A. André, D. DeMille, J. M. Doyle, M. D. Lukin, S. E. Maxwell, P. Rabl, R. J. Schoelkopf, and P. Zoller, "A coherent all-electrical interface between polar molecules and mesoscopic superconducting resonators", Nature Physics **2**, 636 EP – (2006).

[116]L. R. Testardi, "Destruction of superconductivity by laser light", Phys. Rev. B **4**, 2189–2196 (1971).

[117]A. V. Kuhlmann, J. H. Prechtel, J. Houel, A. Ludwig, D. Reuter, A. D. Wieck, and R. J. Warburton, "Transform-limited single photons from a single quantum dot", Nature Communications **6**, 8204 EP – (2015).

[118]M. Arcari, I. Söllner, A. Javadi, S. Lindskov Hansen, S. Mahmoodian, J. Liu, H. Thyrrestrup, E. H. Lee, J. D. Song, S. Stobbe, and P. Lodahl, "Near-unity coupling efficiency of a quantum emitter to a photonic crystal waveguide", Phys. Rev. Lett. **113**, 093603 (2014).

[119]Y. Tsuchimoto, P. Knüppel, A. Delteil, Z. Sun, M. Kroner, "Proposal for a quantum interface between photonic and superconducting qubits", Phys. Rev. B **96**, 165312 (2017).

[120]M. O. Scully, "Single photon subradiance: quantum control of spontaneous emission and ultrafast readout", Phys. Rev. Lett. **115**, 243602 (2015).

[121]M. Gross and S. Haroche, "Superradiance: an essay on the theory of collective spontaneous emission", Physics Reports **93**, 301 –396 (1982).

[122]W. Guerin, M. O. Araújo, and R. Kaiser, "Subradiance in a large cloud of cold atoms", Phys. Rev. Lett. **116**, 083601 (2016).

[123]V Bouchiat, D Vion, P Joyez, D Esteve, and M. H. Devoret, "Quantum coherence with a single cooper pair", Physica Scripta **1998**, 165 (1998).

[124]Y. Nakamura, Y. A. Pashkin, and J. S. Tsai, "Coherent control of macroscopic quantum states in a single-cooper-pair box", Nature **398**, 786 EP – (1999).

[125]M. H. Devoret and R. J. Schoelkopf, "Superconducting circuits for quantum information: an outlook", Science **339**, 1169–1174 (2013).

[126]F. Jelezko, T. Gaebel, I. Popa, A. Gruber, and J. Wrachtrup, "Observation of coherent oscillations in a single electron spin", Phys. Rev. Lett. **92**, 076401 (2004).

[127]N. Samkharadze, G. Zheng, N. Kalhor, D. Brousse, A. Sammak, U. C. Mendes, A. Blais, G. Scappucci, and L. M. K. Vandersypen, "Strong spin-photon coupling in silicon", Science **359**, 1123–1127 (2018).

[128]A. Stockklauser, P. Scarlino, J. V. Koski, S. Gasparinetti, C. K. Andersen, C. Reichl, W. Wegscheider, T. Ihn, K. Ensslin, and A. Wallraff, "Strong coupling cavity qed with gate-defined double quantum dots enabled by a high impedance resonator", Phys. Rev. X **7**, 011030 (2017).

[129]X. Mi, J. V. Cady, D. M. Zajac, P. W. Deelman, and J. R. Petta, "Strong coupling of a single electron in silicon to a microwave photon", Science **355**, 156–158 (2017).

[130]P. W. Fry, I. E. Itskevich, D. J. Mowbray, M. S. Skolnick, J. J. Finley, J. A. Barker, E. P. O'Reilly, L. R. Wilson, I. A. Larkin, P. A. Maksym, M. Hopkinson, M. Al-Khafaji, J. P. R. David, A. G. Cullis, G. Hill, and J. C. Clark, "Inverted electron-hole alignment in inas-gaas self-assembled quantum dots", Phys. Rev. Lett. **84**, 733–736 (2000).

[131]V. S. C. Manga Rao and S. Hughes, "Single quantum-dot purcell factor and beta-factor in a photonic crystal waveguide", Phys. Rev. B **75**, 205437 (2007).

[132]T. Ba Hoang, J. Beetz, L. Midolo, M. Skacel, M. Lermer, M. Kamp, S. HÃ¶fling, L. Balet, N. Chauvin, and A. Fiore, "Enhanced spontaneous emission from quantum dots in short photonic crystal waveguides", Applied Physics Letters **100**, 061122 (2012).

[133]C. Cabrillo, J. I. Cirac, P. García-Fernández, and P. Zoller, "Creation of entangled states of distant atoms by interference", Phys. Rev. A **59**, 1025–1033 (1999).

[134]A. A. Houck, J. Koch, M. H. Devoret, S. M. Girvin, and R. J. Schoelkopf, "Life after charge noise: recent results with transmon qubits", Quantum Information Processing **8**, 105–115 (2009).

[135]D. E. Aspnes, S. M. Kelso, R. A. Logan, and R. Bhat, "Optical properties of alxga(1-x) as", Journal of Applied Physics **60**, 754–767 (1986).

[136]A. D. Rakić, "Algorithm for the determination of intrinsic optical constants of metal films: application to aluminum", Appl. Opt. **34**, 4755–4767 (1995).

[137]Kavokin, Alexey, *Microcavities*, edited by O. U. Press (Oxford University Press, 2011).

[138]R Miller, T. E. Northup, K. M. Birnbaum, A Boca, A. D. Boozer, and H. J. Kimble, "Trapped atoms in cavity qed: coupling quantized light and matter", Journal of Physics B: Atomic, Molecular and Optical Physics **38**, S551 (2005).

[139]H. J. Kimble, "Strong interactions of single atoms and photons in cavity qed", Physica Scripta **1998**, 127 (1998).

[140]M. Nomura, N. Kumagai, S. Iwamoto, Y. Ota, and Y. Arakawa, "Laser oscillation in a strongly coupled single-quantum-dot–nanocavity system", Nature Physics **6**, 279 EP – (2010).

[141]Z Blanco-Garcia, "Quantum control of the states of light in a mach-zehnder interferometer", Journal of Physics: Conference Series **839**, 012021 (2017).

[142]H. P. Seigneur, M. N. Leuenberger, and W. V. Schoenfeld, "Single-photon mach–zehnder interferometer for quantum networks based on the single-photon faraday effect", Journal of Applied Physics **104**, 014307 (2008).

[143]M. Körber, O. Morin, S. Langenfeld, A. Neuzner, S. Ritter, and G. Rempe, "Decoherence-protected memory for a single-photon qubit", Nature Photonics **12**, 18–21 (2018).

[144]M. Born and R. Oppenheimer, "Zur quantentheorie der molekeln", Annalen der Physik **389**, 457–484 (1927).

[145]S. McArdle, S. Endo, A. Aspuru-Guzik, S. Benjamin, and X. Yuan, "Quantum computational chemistry", ArXiv e-prints (2018).

[146]E. Schrödinger, "An undulatory theory of the mechanics of atoms and molecules", Phys. Rev. **28**, 1049–1070 (1926).

[147]G. J. Milburn, "Quantum optical fredkin gate", Phys. Rev. Lett. **62**, 2124–2127 (1989).

[148]J. J. Pla, K. Y. Tan, J. P. Dehollain, W. H. Lim, J. J. L. Morton, F. A. Zwanenburg, D. N. Jamieson, A. S. Dzurak, and A. Morello, "High-fidelity readout and control of a nuclear spin qubit in silicon", Nature **496**, 334 EP – (2013).

[149] A. İmamoğlu, D. D. Awschalom, G. Burkard, D. P. DiVincenzo, D. Loss, M. Sherwin, and A. Small, "Quantum information processing using quantum dot spins and cavity qed", Phys. Rev. Lett. **83**, 4204–4207 (1999).

[150] M. H. Devoret, A. Wallraff, and J. M. Martinis, "Superconducting Qubits: A Short Review", eprint arXiv:cond-mat/0411174 (2004).

[151] T. Kadowaki and H. Nishimori, "Quantum annealing in the transverse ising model", Phys. Rev. E **58**, 5355–5363 (1998).

[152] M. Born and V. Fock, "Beweis des adiabatensatzes", Zeitschrift für Physik **51**, 165–180 (1928).

[153] E. Ising, "Beitrag zur theorie des ferromagnetismus", Zeitschrift für Physik **31**, 253–258 (1925).

[154] A. Peruzzo, J. McClean, P. Shadbolt, M.-H. Yung, X.-Q. Zhou, P. J. Love, A. Aspuru-Guzik, and J. L. O'Brien, "A variational eigenvalue solver on a photonic quantum processor", Nature Communications **5**, 4213 EP – (2014).

[155] J. Preskill, "Quantum Computing in the NISQ era and beyond", Quantum **2**, 79 (2018).

[156] P. J. J. O'Malley, R. Babbush, I. D. Kivlichan, J. Romero, J. R. McClean, R. Barends, J. Kelly, P. Roushan, A. Tranter, N. Ding, B. Campbell, Y. Chen, Z. Chen, B. Chiaro, A. Dunsworth, A. G. Fowler, E. Jeffrey, E. Lucero, A. Megrant, J. Y. Mutus, M. Neeley, C. Neill, C. Quintana, D. Sank, A. Vainsencher, J. Wenner, T. C. White, P. V. Coveney, P. J. Love, H. Neven, A. Aspuru-Guzik, and J. M. Martinis, "Scalable quantum simulation of molecular energies", Phys. Rev. X **6**, 031007 (2016).

[157] A. Kandala, A. Mezzacapo, K. Temme, M. Takita, M. Brink, J. M. Chow, and J. M. Gambetta, "Hardware-efficient variational quantum eigensolver for small molecules and quantum magnets", Nature **549**, 242 EP – (2017).

[158] R. Babbush, N. Wiebe, J. McClean, J. McClain, H. Neven, and G. K.-L. Chan, "Low-depth quantum simulation of materials", Phys. Rev. X **8**, 011044 (2018).

[159] P. Jordan and E. Wigner, "Über das paulische äquivalenzverbot", Zeitschrift für Physik **47**, 631–651 (1928).

[160] N. M. Linke, D. Maslov, M. Roetteler, S. Debnath, C. Figgatt, K. A. Landsman, K. Wright, and C. Monroe, "Experimental comparison of two quantum computing architectures", Proceedings of the National Academy of Sciences **114**, 3305–3310 (2017).

[161] I. D. Kivlichan, J. McClean, N. Wiebe, C. Gidney, A. Aspuru-Guzik, G. K.-L. Chan, and R. Babbush, "Quantum simulation of electronic structure with linear depth and connectivity", Phys. Rev. Lett. **120**, 110501 (2018).

[162] G. Giuliani, G. Vignale, and C. U. Press, *Quantum theory of the electron liquid*, edited by C. U. Press, Masters Series in Physics and Astronomy (Cambridge University Press, 2005).

[163] D. M. Ceperley and B. J. Alder, "Ground state of the electron gas by a stochastic method", Phys. Rev. Lett. **45**, 566–569 (1980).

[164] H. Eyring, "The activated complex in chemical reactions", The Journal of Chemical Physics **3**, 107–115 (1935).

[165] J. A. Nelder and R. Mead, "A simplex method for function minimization", The Computer Journal **7**, 308–313 (1965).